MHD
POWER GENERATION

RESEARCH, DEVELOPMENT,
AND ENGINEERING

Quarterly Progress Report
June 1977

The Montana Energy and MHD Research and Development Institute, Inc.

Post Office Box 3809
Butte, Montana 59701

energy

PLEASE RETURN

MHD
POWER GENERATION

RESEARCH, DEVELOPMENT,
AND ENGINEERING

Quarterly Progress Report
June 1977

THE MONTANA ENERGY AND MHD
RESEARCH AND DEVELOPMENT INSTITUTE, INC.
P. O. Box 3809
Butte, Montana   59701

PREPARED FOR THE UNITED STATES
ENERGY RESEARCH AND DEVELOPMENT ADMINISTRATION

Contract No. EF-77-C-01-2524

TABLE OF CONTENTS

REPORT INTRODUCTION

During the fall of 1974, a major portion of Montana's scientific community formed a task force to initiate and aggressively pursue a broad-based program of research, development, and engineering in the field of open-cycle magnetohydrodynamics (MHD). This effort was based on the firm belief that MHD technology, although still early in its development and not fully proved as a practical generator of electric power, is the only non-nuclear, central station electric power generation technology with significant potential for greatly improved fuel efficiency and direct operation with coal. MHD also offers lower environmental impact and a reduced pollution signature. Associated with this high efficiency is the reduced consumption of water--a factor of importance to the semi-arid western regions.

This task force was incorporated into the Montana Energy and MHD Research and Development Institute. MERDI is a not-for-profit Montana corporation with team members drawn from the research faculties of the Montana College of Mineral Science and Technology (MCMS&T) in Butte, Montana, and the Montana State University (MSU) in Bozeman, Montana.

With the able and generously provided assistance and advice of the MHD research and development staff of Avco Everett Research Laboratory in Everett, Massachusetts, Institute researchers formulated a broad scope research proposal to address the key technical problems currently recognized for MHD technology at both fundamental and practical levels. The Institute prepared a complete, unsolicited proposal that included a section on the design and construction of major MHD experimental facilities (Combustion Test Facilities, Engineering Test Facility). In November 1974, this proposal was submitted to the Office of Coal Research, now the Fossil Energy Program, U.S. Energy Research and Development Administration (ERDA).

Following an intensive and critical review of our proposal, ERDA awarded MERDI a contract in March 1975 for a portion of the MHD supporting science and technology tasks submitted in the original proposal. Work was divided among researchers at our performing elements (MCMS&T and MSU) on the basis of primary specialization and expertise. MCMS&T was assigned tasks relating to coal fuel supply, characterization, preparation, and handling--as well as MHD materials engineering. MSU tasks are related to science, heat transfer and mechanical engineering, and chemical and chemical engineering aspects of MHD technology. MERDI assumed responsibility for overall program management and leadership of an interdisciplinary team conducting environmental and site selection studies of future MHD central station power plants.

CURRENT PROGRAM

Deliverables due under all tasks of the contract have been submitted to ERDA-FE/MHD including a CDIF operations management plan and a CDIF staffing plan which should serve as base data for an operating contract.

A plan showing the staff required to support the materials evaluation and chemical analysis effort for the CDIF was prepared and submitted to ERDA with the overall CDIF package. A document showing the need for centralized management of materials evaluation in the MHD program was prepared and submitted for ERDA utilization.

MHD research program directions at the Montana College of Mineral Science and Technology and Montana State University have been modified to meet more fully MHD development requirements as presented by ERDA and by MERDI in-house personnel. Cooperative exchange of technical samples and information between tasks at the Montana schools and MERDI is greatly expanding the technical output and relevance of the technical data produced. Efforts are being made to expand this technical cooperation to other MHD contractors and government research facilities.

Final disposition of the audit of the MSU subcontract 77-002 has been delayed pending receipt of a final report of the audit performed by HEW last quarter of all other MSU federal contracts. Upon receipt of this report, MERDI's audit will be forwarded for final determination to the contracting officer.

An audit of MERDI's procurement procedures was conducted by ERDA's procurement operation. A final report of this audit has not been received yet.

TASK A
Characterization of Coal for Open-Cycle MHD Power Generation Systems
F. Diebold

ABSTRACT

Work during the third quarter (15 March, 1977 to 10 June, 1977) has involved the following categories: sulfur method development, ARL emission direct reader standardization, photographic emission liquid method development, and flameless atomic absorption metal analysis method development.

The indirect atomic absorption method for determining sulfur content has been plagued with matrix interference problems from samples generated via acid-bomb digestion. The initial data from the X-ray fluorescence procedure indicates a significant decrease in sulfur content when the coal is ashed.

The poor detection limits and precision of metal concentration data generated on the ARL emission direct reader had indicated optical alignment problems. The total optical realignment, including selection of more sensitive lines for the metals, has been completed.

The photographic emission spectrographic analysis of solutions, generated via acid-bomb digestion of the coal, indicates that synthetic standards are appropriate for generating working curves.

Initial work on establishing the flameless atomic absorption procedures for selected trace metals in the coal indicates the presence of matrix effects.

I.   OBJECTIVE AND SCOPE OF WORK

The primary objective of this program is the detailed character-ization of typical Fort Union region coal to assess its applicability to performance in direct, coal-fired MHD electrical generation systems. Accomplishment of this objective requires the selection of specific coal seams for study and development. It also necessitates a progressive sampling technique that permits three-dimensional chemical mapping of the seam as well as the development of suitable sample preparation and sample analysis techniques. Resultant data will be compared and correlated with information obtained from a literature search and the mining companies. The goal is to provide the MHD process designer with the most comprehensive fuel engineering information available. The coal properties to be determined are as follows:

1) Btu, percent moisture, volatile matter, fixed carbon, ash, S, H, C, O, N, Cl, and F content;

2) Major inorganic constituents of the coal ash: Al, Ca, Fe, K, Mg, Na, Si, and Ti; and

3)   Trace elements of the coal ash: Ag, As, B, Ba, Be, Cd, Co, Cr, Cs, Cu, Ga, Hg, La, Li, Mn, Ni, P, Pb, Rb, Sb, Se, Sn, Sr, U, V, Zn, and Zr.

A secondary project objective involves a careful examination of potential environmental problems caused by the inorganic constituents of the coal. Special consideration will be given to the effects that each inorganic element has on air, soil, and water problems. This study will be coordinated closely with the work of the MERDI environmental engineer as well as federal and state officials. It also will include a review of pertinent literature.

The analytical data generated by this work will be of immediate use in the interpretation of corrosion studies involving MHD preheater materials and experiments on coal drying. Coal properties certainly will affect the drying mechanics of western coals. Therefore, it will be important to ascertain the magnitude of coal property changes, such as Btu content, caused by drying and grinding coal. The data from the corrosion study of preheater materials eventually must be interpreted in terms of the actual eastern Montana coal properties having the greatest potential for use in MHD power generation.

II.   SUMMARY OF PROGRESS TO DATE

The development of analytical procedures for determining sulfur content has involved an investigation of the indirect atomic absorption (AA) in solutions generated by acid-bomb digestion of the coal samples. It appears that the use of sodium and potassium hydroxide to adjust the pH of the solutions creates a significant matrix problem. Simultaneously with this effort, the ARL X-ray fluorescence quantometer has been pressed into service. The initial sulfur data on this instrument indicates a significant loss of sulfur upon ashing the coal samples prior to analysis.

Work on establishing flameless AA procedures for trace metals has begun. The preliminary data indicate that careful attention to potential matrix effects will be necessary.

The poor precision and detection limits of data generated with the ARL emission direct reader has been traced to poor optical alignment of the primary and secondary slits. The spectrometer has been reworked completely, and new, more sensitive analytical lines (including an internal standard) have been chosen.

The work on establishing the photographic emission spectrographic procedure for trace metals in solutions generated by acid-bomb digestion of the coal samples has indicated that synthetic standards can be used to establish the working curves.

III. DETAILED DESCRIPTION OF TECHNICAL PROGRESS

A.   Sulfur Method Development

1. Work Accomplished

4

The work on sulfur method development encompassed a) further investigation of the ASTM gravimetric and the indirect AA procedures utilizing solutions generated via acid-bomb digestion of the coal samples, and b) the establishment of an X-ray fluorescence working curve utilizing solid coal samples.

The investigation of the ASTM gravimetric procedure for the acid-bomb coal digestion solutions has involved an attempt to solve the problem of obtaining a sodium nitrate precipitate by evaporating the solution prior to adding the aqueous solution of barium chloride. The high concentration of nitrate is due to the use of nitric acid for oxidizing the organic phase of the coal sample during its acid-bomb digestion. Investigation of different oxidizing agents has not been pursued. Rather, the use of a mixture of sodium and potassium hydroxide, instead of just sodium hydroxide, for pH adjustment of the acid-bomb solution has proved successful in eliminating the formation of the precipitate. The data generated via this ASTM gravimetric analysis of sulfur in acid-bomb digestion solutions are presented in Table 1.

The investigation of an indirect AA procedure for sulfur analysis in acid-bomb digestion solutions has indicated a significant matrix effect. This matrix effect appears to be due to the high concentration of sodium and potassium.

The third line of investigation has been to initiate the establishment of an X-ray fluorescence technique using the ARL X-ray fluorescence quantometer. A working curve has been generated with synthetic standards composed of sodium sulfate and boric acid. These reagents are mixed in the appropriate proportions and pressed into a pellet. The pellet diameter is 1.125 inches, and the pressure exerted during pellet formation is 15,000 psi. There was no significant difference between the calibration curve generated with pellets containing 7g and those containing 3g of sodium sulfate plus boric acid. Calibration curves were generated for sample pellets suspended on thick and thin mylar film. In addition, integration periods of one and two minutes were used. The characteristics of these calibration curves are presented in Table 2.

Two coal samples were prepared, and using the appropriate calibration curves, the sulfur content was determined. These data are presented in Table 3.

To ascertain the loss of sulfur when the coal is ashed, the following data were generated. One of our laboratory reference coals (LRC II) and one of the coal samples supplied to us by the United States Geological Survey of Denver, Colorado (USGS #D163516) were ashed for eight hours at 500°C, followed by eight hours at 700°C. The sulfur contents of these ashed samples, as determined by X-ray fluorescence, are presented in Table 4.

2. Discussion

The replacement of a portion of the sodium hydroxide with potassium hydroxide to adjust the pH of the acid-bomb digestion

samples prior to precipitatation of barium sulfate has successfully
eliminated the precipitation of sodium nitrate. Because the
gravimetric method is quite time-consuming, we were hopeful that
the indirect AA method would result in valid data; thus, it has
been somewhat disappointing to observe the apparent interference
of the sodium and potassium.

The poor precision of the ASTM gravimetric data generated with
solutions prepared in the small (30 ml) capacity Parr acid digestion
bombs is unexplained at this time. The predicted precision, due
to weighing errors associated with the relatively small masses of
coal (0.1g) and small masses of $BaSO_4$ precipitate (0.01g) in the
small bombs, would indicate relatively poor precision; i.e., ±0.03
weight percent for the small bomb and ±0.003 weight percent for
the large bomb data. But this is a small fraction of the ±42.1
percent relative standard deviation associated with the small
bomb experimental data. Additionally, the percent recovery of
the two standards is in contradiction to the poor precision. It
is assumed that the poor precision of the large (300 ml/capacity)
bomb data is due to the variable loss of sulfur in the vapor
during the 120°C to 150°C eight-hour digestion of the coal sample.
We plan to alter the gasket assembly for the teflon lid in an
attempt to improve the precision of the data. As noted in earlier
reports, the reason for designing these large bombs is to increase
the amount of coal sample digested and thereby increase the
detectability of the trace metals.

The initial effort in establishing the X-ray fluorescence
procedure for total sulfur in the coal has yielded encouraging
results but also has indicated the existence of a few problems.
It is encouraging that the range of linearity of the working curve
encompasses the expected sulfur concentration in eastern Montana
coal. Even though the characteristics of the working curve appear
to change from day to day (Table 2), the linearity of the curve
is indicated by the correlation coefficients. A greater similarity
in these working curves is expected with an altered sample prepar-
ation procedure.

The X-ray fluorescence data for LRC II in Table 2 include
data generated via the ASTM gravimetric acid-digestion bomb
procedure (Table 1). It should be noted that even though there
did not appear to be an effect on the standards, the ratio of coal
to boric acid seems to affect the data from the coal samples. This
is interpreted as a matrix problem that can be resolved with
appropriate sample preparation. In addition, it has been observed
that the position of the pellet in the sample holder has a
significant effect upon the data. This, too, is a problem that
may be solved by appropriate sample preparation.

It should be pointed out that the precision of the X-ray
fluorescence data is approximately 30 percent relative standard
deviation, whereas that of the ASTM gravimetric acid-digestion
bomb data is 42 percent. Since the precision of the X-ray
fluorescence data incorporates the significant effect of the
variable position of the pellet in the sample holder, there seems
to be only a minor effect attributable to sampling error. Therefore,

6

it does not seem probable that the sampling error is a significant contribution to the precision associated with the ASTM gravimetric. The poor precision of the ASTM gravimetric data appears to be due to the variable loss of sulfur in the gas phase from the acid-digestion bombs.

Sulfur content in the ash of the USGS #D163516 sample, as reported by the USGS, is 10 percent by weight. This value was determined via X-ray fluorescence analysis of a sample of coal ash fused with tetraborate. Our X-ray fluorescence value on the same coal ash mixed with boric acid (used as a binder) is 21.3 ± 3.2 weight percent sulfur. This discrepancy has not been investigated yet, but it could be related to differences in the ashing conditions. The difference in weight percent sulfur in the LRC II coal and LRC II ash, as determined by X-ray fluorescence, is calculated by converting the coal data, via percent ash, to that expected in the ash. This expected value (56.7 percent), which is calculated on the assumption that no loss of sulfur will occur during ashing, then is compared to that experimentally determined to be in the ash. The expected value of 56.7 percent sulfur is contrasted to the experimental value of 21.3 percent sulfur. The experimental value obviously depends upon the ashing conditions, and our ashing is done at a lower temperature than that of the USGS.

B. ARL Direct Reader Emission Spectrographic Method Development

1. Work Accomplished

During this last quarter, data generated on coal standards and synthetic standards have shown poor precision and detection limits. After solving a number of electronic problems associated with the recording console, we concluded that the alignment of the primary and secondary slits were at fault. A considerable amount of time has been expended recently in aligning the optic system of the spectrometer.

2. Discussion

The data that has been generated on the old ARL emission direct reader has been a constant source of disappointment, especially after the expenditure of a considerable amount of funds for an ARL technician to bring the instrument on-line. Subsequently, we have had to spend a considerable amount of time to overcome electronic problems associated with the recording console. The major electronic problem was solved by replacing the strip chart recorder with an electronic digital readout which was designed orginally to be used on the NSL densitometer for reading the JACO emission plates and film.

After apparently overcoming the electronic problems, the poor detection limits indicated that the optical system of the spectrometer was out of alignment. We recently have finished approximately three weeks' work realigning the primary and the secondary slits. It was observed that many of the secondary slits were not set on the lines as reported in the company literature.

Subsequent to this realignment, the initial data indicated a considerable improvement in the detection limits.

C. Photographic Emission Spectrographic Method Development

1. Work Accomplished

The work during this quarter has involved investigation of the acid-digestion bomb technique for preparing solutions and an examination of the emulsion calibration (H & D) curve.

A new analytical function for the H & D curve has been established. This function, relating intensity to percent transmittance, is that of an arc expressed as a straight line. This straight line closely fits the experimental data, especially near the lower and higher ranges of percent transmittance.

The investigation of acid-digestion bomb techniques involved a comparison of the intensities of the major and selected minor elements in five coal samples prepared via high temperature ash (HTA), low temperature ash (LTA), and acid-digestion bomb (ADB) to the intensities generated by arcing whole coal samples. The only intensities that appear to have been changed significantly from that observed in the whole coal samples is that of silicon in samples prepared via ADB. To further investigate this apparent loss, a time-burn of the ADB was performed. The variation of the intensities of all elements as a function of time were not significantly different from that of samples prepared via HTA and LTA and that of whole coal samples. Additionally, the ADB solutions were allowed to evaporate in the electrodes at room temperature instead of under the influence of the 100 watt bulb placed six inches from the electrode. No difference in the silicon intensity of the high or room temperature electrode was observed; i.e., in both cases, the silicon intensity was significantly lower than that observed in arcing whole coal.

2. Discussion

The possible loss of silicon during the ADB sample preparation procedure is considered to be caused by either a matrix effect, loss of silicontetrafluoride from the ADB's teflon liner during digestion of the coal sample with hydrofluoric acid at 130°C or loss of silicontetrafluoride during evaporation at approximately 80-90°C in the electrode cavity. It was thought that the solution was being absorbed partially by the graphite electrode; thus, a portion of the solution components were being arced with graphite (i.e., at a higher temperature than the non-absorbed portion). The evidence of the time-burn did not indicate that such a phenomenon was occurring. Evaporation of the solution in the electrode cavity at room temperature did not indicate that the volatilization of silicontetrafluoride is the reason for the significant decrease in intensity of the silicon emission in the arc. We have not investigated yet the possible loss of silicontetrafluoride from the bomb. As noted above, the design of a new

8

gasket for the teflon liner of the bombs may not only stop the apparent loss of sulfur but also the loss of silicon.

We have compared various sample preparation techniques for the emission spectrograph. This comparison is based upon the magnitude of matrix problems, the observed sensitivity, the possibility of the sample being representative, the amount of time involved, and the number of possible error sources. Because of the investigation yet to be performed with ADB, this comparison is not complete, but it would appear that one of the largest factors in favor of HTA and ADB is the possibility of using synthetic standards. Closely associated with this same point is the consideration of the characteristics of the analytical working curves, such as how well a straight line represents the experimental data. It is apparent to us that our use of the USGS coal samples as standards affects the accuracy of the working curves for the cases in which we are not using HTA (the USGS method of preparing samples for analysis). Thus, the possibility of using synthetic standards becomes an important factor in selecting a sample preparation technique.

D. Routine Analysis of Coal Samples

1. Work Accomplished

A tentative agreement has been worked out with the Western Energy Company to pursue a sample program. This will involve the comparison of three sampling techniques based on their respective capability of yielding analytical data that is representative of the Rosebud coal seam. The three sampling techniques are channel sampling, tipple sampling, and core sampling.

2. Discussion

Western Energy personnel have agreed verbally to supply tipple samples and a portion from core samples taken earlier. We will be taking the channel samples over a period of time. The data generated by these three sampling techniques will be used to construct chemical maps of the coal seam, thereby allowing a comparison of the relative degree to which these three sampling techniques are capable of characterizing coal seams.

E. Work Forecast

1. Sulfur Method Development

A limited amount of effort will be expended in investigating the apparent matrix interference of sodium and potassium upon the indirect AA procedure for sulfur in the acid-digestion bomb solutions. Additionally, a new gasket will be designed for the teflon liners of the acid-digestion bombs, and the precision of the ASTM gravimetric acid-digestion bomb data will be investigated.

9

An investigation of alterations to the present X-ray fluorescence sample preparation technique will be undertaken. In addition, an effort will be made to understand the discrepancy between ours and the USGS weight percent sulfur data in the coal ash. Upon eventual establishment of the X-ray fluorescence procedure, data will be generated on existing Dietz No. 2 and Rosebud coal samples.

2. ARL Direct Reader Emission Spectrographic Method Development

The appropriate working curves will be prepared. Concentration data then will be generated for those elements presently programmed on the recording console and those elements detectable in the Dietz No. 2 and Rosebud coal samples on hand.

3. Photographic Emission Spectrographic Method Development

We intend to pursue the investigation of the apparent loss of silicon from the ADB solutions. Closely associated with this study is the investigation of the use of synthetic standards to establish the analytical working curve for ADB solutions. Both investigations will be approached by experimentally determining the percent recovery of spikes into the ADB solutions and analyzing the coal (via AA) before digestion, the solutions before evaporation in the electrodes, and the residue obtained from evaporation.

4. Routine Analysis of Coal Samples

The coal sampling program will be initiated early in the next quarter. We plan to make as many sampling trips and obtain as many samples as our analytical capability will allow.

IV. CONCLUSIONS

The most appropriate sample preparation technique involves the use of the acid-digestion bomb. This decision is based on the possibility of aliquots of the solution being used in other aspects of the overall analytical scheme. It still is obvious to us that a multi-element analytical method is the most appropriate technique; thus, the plasma source direct-reader emission spectrograph, utilizing solutions generated in the acid-digestion bomb, should be coupled with a flameless atomic absorption spectrometer as the combined analytical approach in characterizing coals for MHD power generation.

TASK ___A___

MAJOR MILESTONES

1. Sulfur Method Development
   Establishment of ASTM Procedure
   Establishment of AA Procedure
   Establishment of X-ray Fluorescence
   Procedure

2. Chlorine Method Development
   Establishment of AA Procedure
   Data Generation & Comparison with
   SIE and ASTM Procedures

3. Atomic Absorption (Flame) Analysis
   Generation of Data for ARL Quantom-
   eter Standards

4. ARL Direct Reader Emission Spectro-
   graphic Analysis
   Establishment of Procedures for
   Trace Metals
   Establishment of Procedures for
   Major Metals
   Generation of Data and Interpretation

5. Photographic Emission Spectrographic
   Analysis
   Establishment of Procedure for Trace
   Metals (solid samples)
   Establishment of Procedure for Major
   Metals (solutions)
   Establishment of Procedure for Trace
   Metals (solutions)

6. Ultimate Analysis--Establish Procedure

7. Routine Analysis of Coal Samples

8. Analytical Services to other MHD
   Tasks

9. Literature Study: Toxic Metals--
   Environment Interaction

1977

O N D J F M A M J J A S

PROGRESS

TASK ___A___ (cont.)

MAJOR MILESTONES

X-ray Fluorescence Analysis of Trace
Metals

  Set up of Apparatus
  Analytical Method Development
  Data Generation & Interpretation

Flameless Atomic Absorption

Analysis of Trace Metals
  Set up of Apparatus
  Analytical Method Development of
    Trace Metals of Relatively Low
    Concentration
  Data Generation & Interpretation

1977

PROGRESS

12

TABLE 1
ASTM Gravimetric-Acid Bomb Digestion

	Weight % Sulfur	
Coal Sample	Large Bombs	Small Bombs
LRC II	1.36 ± 0.71 ($\pm 52.3\%$)	3.28 ± 1.38 ($\pm 42.1\%$)
Sulfosalicylic acid standard (0.8%)	0.6989	0.76
Na_2SO_4 standard (1.000%)		1.016

TABLE 2
Characteristics of Calibration Curves

Integration Period	Slope	Intercept	Correlation Coefficient
1 Minute			
Thick Film	1.912	-0.201	0.9834
Thin Film	0.128	-0.00137	0.9905
2 Minutes			
Thick Film	0.879	-0.00286	0.97716
Thin Film	.0923	-0.0252	0.9882

TABLE 3
Weight Percent S in Coal - X-ray Fluorescence

(1 Minute Integration)

Coal Sample	Coal/Boric Acid	Weight % S
LRC II	1/9	2.576 ± 0.695 (±27%)
	0.5/9.5	1.582 ± 0.792 (±50%)
USGS #D163516	0.5/9.5	4.972 ± 1.530 (±30%)

(2 Minute Integration)

LRC II	1/9	2.056 ± 0.130 (±6%)
	0.5/9.5	0.787 ± 0.262 (±33%)
USGS #D163516	0.5/9.5	3.742 ± 0.783 (±21%)

TABLE 4
Weight Percent S in Coal Ash - X-ray Fluorescence

(1 Minute Integration)

Coal Sample	Ash/Boric Acid	% Ash	Weight Percent S
LRC II	0.3/9.7	8.89 ± 1.38	9.196 ± 1.461 (±16%)
USGS #D163516	0.4/9.6	8.77	21.559 ± 4.088 (±18%)

(2 Minute Integration)

LRC II	0.3/9.7	8.89 ± 1.38	8.286 ± 1.521 (±18%)
USGS #D163516		8.77	21.011 ± 4.01 (±19%)

TASK B
Corrosion Studies of MHD Preheater Materials
W. Callister

ABSTRACT

A new corrosion-testing technique was attempted in which the cylindrical refractory specimen is translated up and down in a vertical manner so that a portion of the specimen dips into and out of the slag bath. No excessive slag-line corrosion was observed for this technique; however, corrosion was not uniform along the length of the corroded region, decreasing linearly with specimen length from the slag-air interface. Possible explanations for slag-line corrosion for the rotating rod tests are offered, and future experiments should ascertain which, if any, of these proposed explanations are valid. It is felt that all three of the corrosion techniques which have been used (static, rotating rod, and dipping) should be continued to clarify the corrosion mechanisms involved. Stress computations to produce anticipated maximum preheater creep rates were made for the dense and polycrystalline alumina by extrapolation of data which recently appeared in the literature.

I. OBJECTIVE AND SCOPE OF WORK

The primary objective of this task is to characterize the behavior of potential MHD preheater materials under the following conditions: a) in gaseous atmospheres simulating the MHD preheater environment, b) at elevated temperatures to 3100°F (1700°C), c) for exposure periods up to 500 hours, and d) while being exposed to a slag that contains potassium.

Experimental systems will be constructed to permit dynamic or static corrosion tests at temperatures up to 3100°F and for periods of time up to 500 hours. The design will include the capability of passing the desired gas mixture into the furnace chamber containing the slag-immersed sample. Gaseous environments will include air and a simulated combustion atmosphere whose composition will be in accord with NBS computations for air combustion of seeded coal.

Synthetic slags and seed-slags will be prepared. Initial tests will begin with a simple four-component slag to provide very basic engineering data. Further tests will employ more complex systems to include the addition of a potassium seed. These compositions will be representative of slags resulting from the combustion of typical coals found in the United States. The slag compositions appearing in the preheater region may be quite different than the starting coal slag. Therefore, synthetic slags will be prepared to duplicate compositions of condensed products resulting from the combustion of coal at the University of Tennessee Space Institute's MHD combustion facility.

During corrosion tests, the slag will be sampled periodically to determine compositional changes (especially in potassium content) and changes caused by the dissolution of refractory constituents.

The candidate materials to be tested will be high purity, single crystal or dense polycrystalline materials to include Al_2O_3 and MgO. Prior to exposure, sample materials will be characterized with respect to chemical composition, microstructure, density, and open porosity.

After the high temperature exposure to the slag, the refractory samples will be recovered and dimensional changes recorded. Metallographic and microprobe investigations will be made so that corrosion mechanisms may be ascertained.

During this past quarter our efforts have been devoted to (1) assessing the relative merits of rotating rod and "dipping" corrosion tests; (2) making preparations to conduct corrosion tests in simulated combustion atmospheres; (3) polishing and photographing the microstructure of corroded specimens; and (4) designing the apparatus and making computations for creep-corrosion tests.

II. SUMMARY OF PROGRESS TO DATE

Several "dipping" corrosion tests were conducted in which the specimen was translated vertically into and out of the slag bath. Because of distinct differences in the corrosion behavior observed in this test and that observed in rotating rod tests, we are conducting an evaluation of the relative merits of each test type. This also has led to some insights into corrosion mechanisms, which also are being investigated.

The two high-temperature furnaces to be used for corrosion tests in a simulated combustion atmosphere are operable, and work is nearly complete on the system to produce this simulated atmosphere.

Sections of several corroded specimens were polished and photomicrographed. Our imporved polishing technique now produces satisfactory surfaces for examination. This work was performed in anticipation of EDAX SEM microstructural examination.

Some effort has been devoted to designing an apparatus for making creep tests in conjunction with corrosion by slags and slag-seeds. We have computed the magnitude of stress necessary to produce the minimum anticiapted allowable creep rate on dense and polycrystalline alumina at several temperatures.

III. DETAILED DESCRIPTION OF TECHNICAL PROGRESS

A. Work Accomplished

The problems that we have had with the two graphite element furnaces to be used to make corrosion tests in simulated combustion atmospheres seem to be resolved. A programmer previously was constructed to heat

and cool one furnace at a controlled rate, and a second programmer has been constructed for the other furnace.

Some improvements have been made on the combustion atmosphere system; the flow meters have been calibrated; and the water pick-up system is in the process of being calibrated.

There have been some changes in the technique used in preparing slags and slag-seeds. Rather than melting or fritting the constituents in a sillimanite crucible in a gas-fired furnace prior to a corrosion run, the slag is melted directly in the Pt-Rh crucible which is to be used for the test. This process is carried out in several identical steps in which only a fraction of the total amount of constituents is added and then melted. This minimizes the frothing problem and reduces or totally eliminates impurity contamination and alteration of the slag composition. The same procedure is used by the NBS for preparation of their synthetic slags.

We feel that one necessary means of examining corrosion and slag penetration into the ceramic materials is with the scanning electron microscope used in conjunction with energy dispersive X-ray analysis (EDAX). Before examination, specimens must be polished. If they are porous, they first must be impregnated with a material to prevent grain pull-out during polishing. Corroded specimens of fully dense alumina and also several commercial materials have been vacuum-impregnated, when necessary, with an epoxy before polishing. Our polishing technique has been improved so it now seems satisfactory for this type of examination. Because some grain pull-out was evident in the porous materials, we are in the process of improving the epoxy impregnation technique.

Figures 1a, 1b, and 1c are photomicrographs of a magnesia-chrome material with about 15 percent open porosity which was corroded at 1450°C for 72 hours. The micrographs were taken, respectively, at the center of the specimen, at a position somewhat removed from the specimen-slag interface, and right at this interface. Some slag penetration is evident from the latter two micrographs.

Several dipping tests were made on the dense, polycrystalline alumina, with significantly different corrosion behavior than was observed for the rotating rod tests. First of all, there was no excessive slag-line corrosion. Second, the corrosion along the length of the specimen was not uniform; the diameter of the sample increased almost linearly from the top to the bottom of the specimen region which dipped into and out of the slag. We feel that these results provide some insight into the mechanisms of corrosion, as discussed in the following section.

During this period, personnel working on the task attended three conferences, and a paper on our corrosion results was delivered at each conference: "Conference on High Temperature Sciences Related to Open-Cycle, Coal-Fired MHD Systems" at ANL; the 79th Annual Meeting of the American Ceramic Society in Chicago; and the 16th Symposium on Engineering Aspects of MHD in Pittsburgh.

When the hiring freeze was lifted, two new technicians were hired, one as a replacement and the other to fill a new position.

B. Discussion

1. Creep Tests

In a previous report,[1] the expected stress levels and cyclic temperature ranges were tabulated for four different positions along the preheater length; this is repeated in Table I. Data was taken from <u>Open Cycle MHD Power Generation</u>[2] by Heywood and Womack for two possible situations for which the maximum temperature at the top of the preheater is either 1700°C or 1600°C, for a maximum temperature difference of 750°C between top and bottom positions, and assuming a linear dependence of temperature on position along the preheater length. The stress levels presented were calculated assuming a closed basket-weave stacking of refractory bricks and a specific packing volume (brick volume divided by total matrix volume) of 0.5 and neglecting thermal stresses. Heywood and Womack quote a maximum allowable creep rate of 10^{-4} percent per hour.

Most of our slag corrosion work to date has been conducted on a fully dense and polycrystalline alumina, and it seems reasonable that this material would be a prime candidate upon which to initiate the creep-corrosion studies. A recent paper[3] presented the results of a creep study on this same material at temperatures between 1600°C and 1700°C. Creep rates measured were in the range of 10^{-6} to 10^{-7} sec^{-1}, and materials with two different grain sizes were tested. One material was coarsed-grained with an average grain size between 64 and 66 microns. The other material had a medium grain size very close to that of the medium-grained material.

Data on both materials were extrapolated to determine the stress level necessary to give the anticipated minimum allowable creep rate of 10^{-4} percent per hour (3×10^{-10} sec^{-1}) at several different temperatures. These extrapolations assumed a steady-state creep rate dependence on temperature and stress according to

$$\dot{\varepsilon} = K\sigma^n \exp{-Q/RT}$$

in which $\dot{\varepsilon}$ is the steady-state creep rate, K is a constant, σ is the stress, n is the stress exponent, Q is an activation energy, and R and T are the gas constant and absolute temperature, respectively. It was determined that n and Q were different for these two materials.

The extrapolated data to give an $\dot{\varepsilon}$ of 3×10^{-10} sec^{-1} is presented in Table II, from which it may be noted that at the higher temperatures, the difference in stress level for the two materials is approximately a factor of 100. Cannon and Sherby, authors of the aforementioned article, proposed that different creep mechanisms could account for the behavior. We recognize that the extrapolations into lower stress and temperature regimes are extreme and that other creep mechanisms may be operative. Nonetheless,

we have made a rough estimate as to the expected stress to give the maximum allowable creep rate for the previously described preheater.

Upon comparison of the data in Tables I and II, it may be noted that a preheater designed for a maximum preheat temperature of 1700°C might encounter difficulties with the medium-grained alumina near the top of the preheater. This medium-grained material is marginal in its ability to sustain the stresses imposed by that mass of material above it in the column and still maintain a creep rate of less than 3×10^{-10} sec^{-1}. It appears that the medium-grained material is satisfactory at lower temperatures, and the coarse-grained material is good at all temperatures for both preheater designs. Again, thermal stresses have been neglected in these computations; their contribution to creep is not known.

2. Corrosion Tests

Thus far in our investigation, three types of corrosion tests have been employed to assess the corrosion behavior of potential preheater materials. These tests are 1) a static test in which a cylindrical rod specimen is immersed in a slag bath with no forced motion of the liquid slag; any fluid motion is a result only of natural convection effects; 2) a rotating rod test in which a cylindrical specimen of $\frac{1}{2}$-inch diameter is rotated in the bath at a angular velocity of 25 rpm; and 3) a "dipping" test in which a specimen of the same size and geometry is moved up and down so that the lower extremity of the specimen moves alternately into and out of the liquid slag. This motion occurs at a rate of 25 cycles per minute, and the shear flow rate of slag in contact with the specimen interface is the same for 2 and 3 if the diameter is $\frac{1}{2}$ inch. These last two techniques are dynamic tests in which fluid motion is created by movement of the specimen; it is termed forced convection.

The results of the few static corrosion tests indicate essentially uniform corrosion along the length of that portion of the specimen which was immersed. The shape of most corroded rotating rod specimens is shown in Figure 2. That portion of the specimen which is at the slag-air interface generally experiences the greatest amount of corrosion; this phenomenon is called "necking." The remainder of the immersed region exhibits essentially uniform corrosion, while the bottom face most often corrodes more at the edges than at the center. Corrosion rates for this test type are computed away from the neck where corrosion is uniform. Not all specimens tested using the rotating rod technique experienced slag-line corrosion. Most, but not all, dense alumina samples corroded this way; as for the commercial materials, some did and some did not.

The appearance of a specimen which has experienced corrosion from the dipping test is represented in Figure 3. No extreme corrosion is observed at the slag-air interface. The greatest corrosion, however, is at this point, and the diameter increases

approximately linearly with length to that portion of the sample which remains in the slag. For this test, corrosion is measured as the total volume of sample removed in that specimen region which translates into and out of the slag.

There are different corrosion mechanisms which may be distinguished by a rate-controlling or slow step in a series of reactions which may occur in sequence. It is possible that this step might be the diffusion of sample material which has dissolved into the slag away from the slag-sample interface or it may be the actual reaction of the dissolution process by which some type of chemical reaction occurs. It also is possible that both steps could occur at comparable rates and be rate-controlling.

Reactions between refractory ceramics and various slag types have been treated in a number of papers in the literature.[4-12] Most of them have assumed that the rate of corrosion is controlled by the diffusion of dissolved species away from the interface through a slag boundary layer of thickness δ. A second important parameter is the diffusion coefficient, D, of species across this layer.

A mathematical treatment, which is presented and discussed in several of the references cited above, permits computation of δ and D from experimentally measurable variables.

A ceramic material is brought into contact with a semi-infinite bath of slag with concentration C_∞ of the diffusing species. The concentration of this species in the specimen is C_o; the initial concentration profile is shown in Figure 4.

After having been submerged for some finite time period, the profile will appear as shown in Figure 5, which shows several distinct regions. The undissolved sample exists for $x > X_1$; the concentration C_i exists at $x = X_2$ and is the concentration of the diffusing species at the liquidus line on the phase diagram for all of the constituents in the slag. For $x > X_3$, the concentration in the slag is C_∞. The dissolving sample species diffuses through the boundary layer, down the concentration gradient, and into the slag.

Application of appropriate boundary conditions to the solution of Fick's second law yields the following:

$$C(x,t) - C_\infty = \frac{(C_i - C_\infty)\,\mathrm{erfc}\left[\dfrac{x}{2(Dt)^{1/2}}\right]}{\mathrm{erfc}\left[\dfrac{X_2}{2(Dt)^{1/2}}\right]}$$

20

Combining treatments in References 5 and 10 leads to the following result:

$$\alpha^2 = \frac{-\nu^{1/2}J}{2V_A^* t^{5/2}\omega^{3/2}}$$

for which $\alpha = \dfrac{X_2}{2(Dt)^{\frac{1}{2}}}$;

ν = the kinematic viscosity;

J = flux of diffusing species;

V_A^* = the partial volume;

t = time; and

ω = angular velocity of slag past the slag-sample interface.

All of these parameters are known or can be measured; hence, D may be computed. Once D is known, the boundary layer thickness may be computed from

$$\delta = 2^{2/3}D^{1/3}\nu^{1/6}\omega^{-\frac{1}{2}}$$

and C_i from

$$\pi^{\frac{1}{2}}\alpha\;\text{erfc}(\alpha)\;\exp(\alpha^2) = \frac{-V_A^*(C_i-C_\infty)}{(1-V_A^* C_i)}$$

Or if the phase diagram is known, as would be the case for simple systems, C_i may be read directly from the phase diagram.

The values of some of the parameters given above will depend on the type of corrosion test. Diffusion coefficients may be obtained from both static and dynamic tests, but for the static test, C_i and the density of the slag must be known. For dynamic tests, the viscosity of the slag must be known, but C_i need not be known and may be calculated. Both static and dynamic tests should be performed for short time periods so the semi-infinite conditions in the slag may be maintained.

To confirm that corrosion is diffusion-controlled, the corrosion rate should be varied with ω, where ω is the angular velocity of a rotating rod test. A linear plot of corrosion rate versus $\omega^{-\frac{1}{2}}$ should result from the data since the diffusion rate would be proportional to the boundary layer thickness, which in turn is inversely proportional to the square root of angular velocity.

For chemically controlled corrosion, this relationship would not hold (rate of attack would be independent of angular velocity), and variation of other parameters such as surface area (porosity, specimen size) and grain size should produce changes in corrosion rate.

The necking phenomenon which occurs in the rotating rod tests, thus far, has been an experimental liability insofar as the rate of alteration of slag composition is increased. Some specimens have completely necked off and fallen into the bath, thus invalidating that particular test. However, understanding this phenomenon may give rise to further insights into the processes involved in dissolution of refractories.

Several possible reasons for necking are

1) Enhanced fluid flow at the slag surface due to convection because of thermal and/or density gradients or to rotation of the rod specimen;

2) Increased chemical activity of the slag species because of the presence of oxygen at this interface; and

3) Depletion of dissolving species due to surface energy effects.

The first possibility is unlikely to be a significant contributing factor since necking has not occurred in all of the rotating tests performed. Ordinarily, the appearance of necking, or lack of it, is consistent for a particular refractory type.

The influence of the second reason (above) will be investigated in the near future when the simulated combustion atmosphere rotating rod corrosion tests begin. This atmosphere is much more reducing and contains less oxygen than does an air atmosphere.

The third possibility relates to the segregation of certain slag species at the slag-air-sample interface (the position where necking occurs) in order to minimize the surface energy at this position (according to the Gibbs absorption isotherm.) This effect possibly could increase the concentration gradient for the diffusing species at the slag line with respect to other regions. If diffusion through the boundary layer is rate-controlling, the rate of diffusion and subsequent corrosion could be enhanced by the concentration gradient alteration. Thus, there would be more rapid corrosion and necking at the slag-sample-air interface position.

The observation that some refractory types exhibit slag-line corrosion while others do not lends credence to this postulation. The surface energy and preferential segregation of slag species due to interfacial energies undoubtedly will vary with refractory composition.

We propose that all three types of corrosion tests (static, rotating rod, and dipping) be continued in order to investigate the mechanisms which are responsible for corrosion and necking. Static tests may be used to determine diffusion coefficients. Rotating rod tests provide data which is useful for both boundary layer thickness and diffusion computations. Dipping tests will be used for assessing the corrosion resistance of the various refractories since corrosion is perhaps the easiest measure with this technique and possibly may be monitored on a continuous basis.

C.   Work Forecast

During the ensuing quarter, we plan to start operating the simulated combustion atmosphere systems and to begin corrosion tests in them.

Corrosion tests will continue using the three different techniques in an effort to understand the mechanisms of corrosion and the necking phenomenon as outlined in this report.

We will continue to examine materials before and after corrosion, with emphasis on using the scanning electron microscope with EDAX accessory.

Components for the apparatus for conducting the creep-corrosion tests will be ordered.

IV. CONCLUSIONS

The following conclusions were derived from this quarter's work.

1) For specimens which were corroded using the dipping test, the corrosion interface was distinctly different from that observed for the rotating rod tests. There was no excessive slag-line corrosion (or necking) of the dip-tested specimens. Instead, they were tapered so the diameter increased with position in going from the top to the bottom of the specimen region which was immersed in the slag.

2) Several possible explanations are offered for slag-line corrosion from the rotating-rod tests, and future tests are outlined to ascertain which explanations are valid.

3) All three corrosion techniques (static, rotating rod, and dipping) can contribute insight and information concerning the mechanisms of corrosion, and all should be used.

TASK ___ B

MAJOR MILESTONES

1. Sample Procurement

2. Corrosion Tests
   a) Continue Tests on Polycrystalline Materials in Air & Synthetic Slag and Seed
   b) Perform Corrosion Tests on Commercial Materials
   c) Test Polycrystalline Materials in Montana Slag and Seed
   d) Check-out Simulated Combustion Atmosphere in Furnaces at High Temperatures
   e) Test Polycrystalline Materials in Simulated Combustion Atmosphere
   f) Examine Idiosyncrasies in Corrosion Dependence on Atmosphere
   g) Test Single Crystals
   h) Perform Tests in High Speed Compositions

3. Sample Characterization (Microprobe, SEM, Chemical, Microstructure)

4. Creep
   a) Design Apparatus
   b) Order Components
   c) Assembly and Check-out

1977

PROGRESS

O N D J F M A M J J A S

24

TABLE I
Cyclic Temperature Ranges and Anticipated Stress Levels (Neglecting Thermal Stresses) for a Regenerative Preheater Employing a Brick Checkerwork (Data taken from Reference 2 assuming a linear variation of temperature with preheater height.)

Position From Bottom of Matrix (m)	Temperature on Basis of 1700°C		Temperature on Basis of 1600°C		Compressive Stress	
	Max (°C)	Min (°C)	Max (°C)	Min (°C)	PSI	MPa
38.5 (Top)	1700	1620	1600	1520	0	0
30.8	1570	1485	1470	1385	41.6	0.29
25.7	1485	1395	1385	1295	69.2	0.48
12.8	1265	1175	1165	1075	138.6	0.96
0 (Bottom)	1050	950	950	850	207.8	1.43

TABLE II
Tabulation of Extrapolated Stress Values to Produce a
Creep Rate of $3 \times 10^{-10} Sec^{-1}$ for Fully Dense and
Polycrystalline Alumina of Two Different Grain Sizes
(Extrapolations from data in Reference 3.)

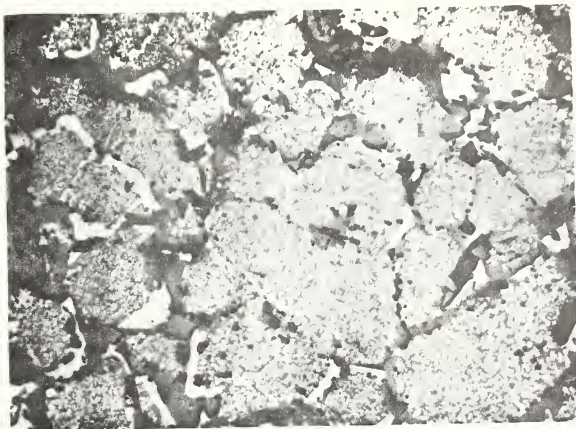| T(°C)	Stress, Medium Grain (18-19μ)		Stress, Coarse Grain (64-66μ)	
	Psi	MPa	Psi	MPa
1700	2.6	0.018	323	2.23
1650	5.6	0.039	462	3.19
1600	13.0	0.090	670	4.62
1550	31.2	0.22	994	6.85
1500	79.0	0.54	1506	10.4
1450	211	1.45	2339	16.1
1400	597	4.12	3728	25.7
1350	1803	12.4	6117	42.2
1300	5841	40.3	10356	71.4
1250	20436	140.9	18150	125.1
1200	77847	536.8	33046	227.9

Figure 1a. Photomicrograph of a commercial magnesia-chrome refractory which was corroded in a coal slag, taken near the center of the ½ inch diameter specimen. Magnification = 240X.
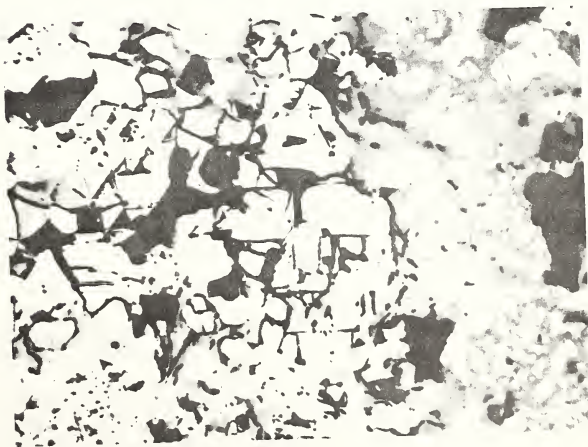

Figure 1b. Photomicrograph of same specimen as in Figure 1a at a region near to the slag-sample interface. Magnification = 240X.
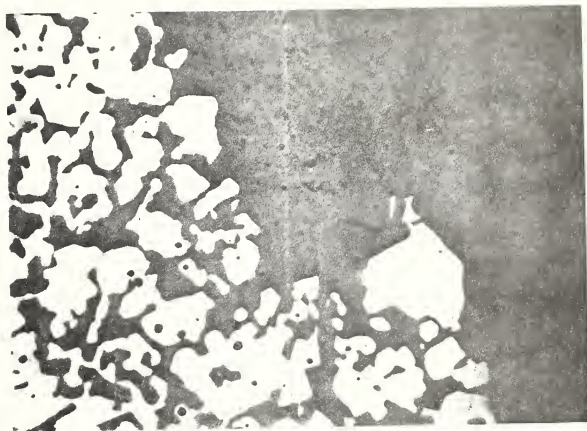
Figure 1c. Photomicrograph of same specimen as in Figure 1a at
the slag-sample interface.
Magnification = 240X.

UNCORRODED REGION

SLAG-LINE REGION (NECKING)

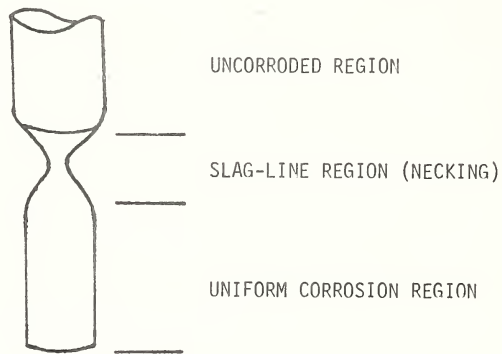UNIFORM CORROSION REGION

Figure 2.   Corrosion profile of a typical specimen which has been
            corroded in a rotating rod test, and which has experienced
            slag-line corrosion or necking.

UNCORRODED REGION
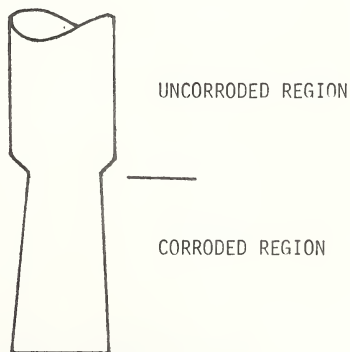
CORRODED REGION

Figure 3.   Corrosion profile of a typical specimen which has been
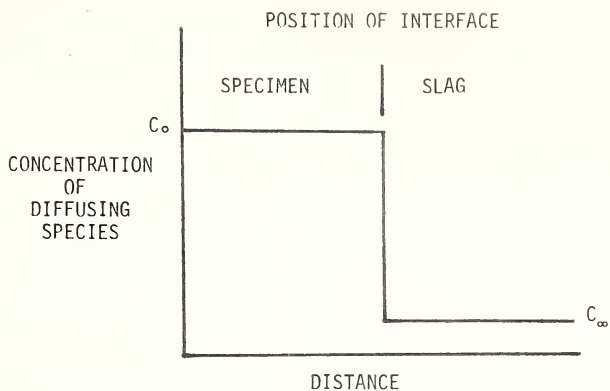   corroded in a dipping test.

Figure 4. Concentration profile of diffusing (specimen) species at the initiation of a corrosion run.
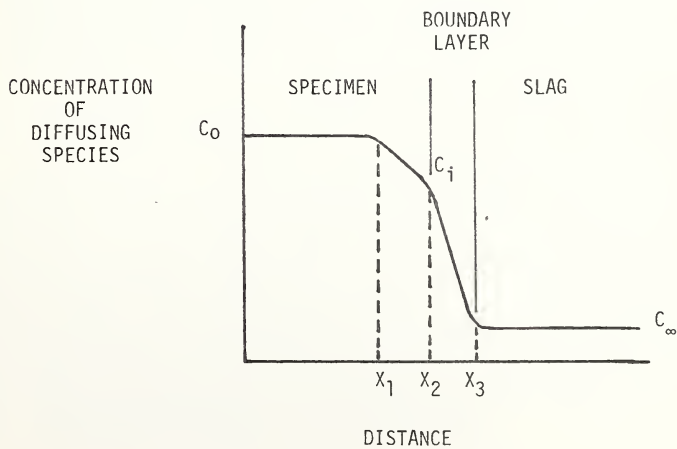

Figure 5. Concentration profile of diffusing species during a corrosion run.

TASK C
Preparation of Coals for Utilization in Direct Coal-Fired MHD Generation
G. Ziesing

ABSTRACT

Accomplishments during this quarter include the following:
1) measurements of oxygen uptake by 14 x 35 mesh Rosebud coal;
2) flotation tests for separation of ash minerals from coal;
3) determination of Btu losses due to drying; 4) identification
of low-boiling organic compounds which are volatilized during
drying; and 5) construction of a six-inch fluidization column.

The rate at which oxygen is consumed by a bed of dried Rosebud
coal at 30°C was found to vary directly as the 0.82 power of the
influent oxygen concentration and inversely as the 0.4 power of
the exposure time. The total oxygen uptake varied directly with
the entering oxygen concentration and ranged from 0.2 to 0.6 grams
O_2 per gram of dry coal. The oxygen consumed by the coal is
thought to form acidic polar groups rather than gaseous oxides.

Flotation of Rosebud coal was extremely difficult and
required extraordinary amounts of fuel oil and frother. The
extremely high surface area of the coal appears to absorb these
surfactants, rendering flotation difficult.

Ash rejection from coal ground to 89 percent passing 37
micrometers was only 2.5 ash percentage points. Drying Rosebud
coal at 105°C results in a measured Btu loss ranging from 4 to 8
percent. Eight low-boiling organic compounds were identified as
effluents evolved during coal-drying at 105°C. Assembly of
components for a six-inch coal fluidization column was initiated
during this quarter.

I. OBJECTIVE AND SCOPE OF WORK

Rosebud seam coal (Colstrip, Montana) has been designated as a potential
MHD reference coal to fuel prototype MHD combustors. Associated with the
utilization of this coal in an MHD power generation facility are potential
problem areas in coal preparation. These include the phenomena of coal dust
pyrophoricity and explosivity, the reactivity of hot processed coal upon
exposure to 'inertized' atmospheres containing variable amounts of oxygen
and water vapor, and the efficacy of beneficiating the candidate coal for
possible removal of slag-forming minerals ahead of combustion. In addition,
fluidization drying of Rosebud coal is a potential processing method about
which very little information is available. The collection of information
in the aforementioned areas is the objective of this continuing research
task. The scope of this work is outlined below.

A. Stability of Processed Rosebud Coal and Derived Coal Dusts

Processed Rosebud coal has been observed in vendor drying tests to abstract oxygen and moisture from the atmosphere after drying, to ignite (when hot) upon contact with ambient air, to exhibit potential for explosion or autoignition, and to self-heat in storage after discharge from a dryer. To characterize certain of these effects, work has been initiated to 1) measure the explosion severity, ignition sensitivity, and index of explosibility for Rosebud coal dust, and 2) measure the uptake of oxygen and water vapor from a synthesized gas by sized fractions of coal relative to oxygen concentration, humidity, and coal temperature. A collateral study will measure and identify non-aqueous volatiles associated with demoisturizing Rosebud coal in the temperature range up to 400°F.

B. Coal Beneficiation

The rejection of slag-forming minerals from Rosebud coal before combustion would decrease sensible heat losses from the combustion train. To examine this processing alternative, a program has been initiated to identify the type and amount of the major mineral components in a selected sample of Rosebud coal and to determine the relationship between size reduction and mineral liberation. Washability curves for sink-float separation in heavy liquids will be constructed, and the applicability of froth flotation and electrostatic methods for separating coal will be evaluated.

C. Fluidized Drying

Fluidization was found to be a viable processing alternative for drying Rosebud coal to low moisture levels. While vendor fluid bed drying tests demonstrated the feasibility of the drying method, the tests did not shed much light on the behavior of Rosebud coal in a fluidized state, on the influence of processing variables, or on the heat and mass transfer phenomena associated with drying. To obtain engineering data of this nature, a program has been initiated to construct a two-foot diameter fluid bed dryer and associated equipment. The work during this contract period will concern the design, construction and assembly of the fluid bed drying facility and initial shake-down testing.

II. SUMMARY OF PROGRESS TO DATE

Work completed to date includes 1) a test program to measure the ignition and explosion characteristics of Rosebud coal dust; 2) a mineragraphic examination of ashed coal residues; 3) a sink-float evaluation of fine coal fractions (-8 to -100 mesh); and 4) flotation tests on wet-ground coal. Work currently in progress includes sink-float tests on coarse coal fractions (-1½" to -8 mesh); pilot-scale tabling tests to evaluate the separability of ash minerals in a conventional coal cleaning unit; collection and identification of organic volatile losses; and construction of a six-inch diameter fluidization column. This quarterly report discusses the progress on the oxygen sorption study, the flotation test work, the work on organic volatile matter, and the status of the fluid bed drying study.

III. DETAILED DESCRIPTION OF TECHNICAL PROGRESS

A. Oxidation of Dried Rosebud Coal

1. Work Accomplished

The sorption, or uptake, of oxygen by dried Rosebud coal was examined in a series of experiments performed in a flow apparatus illustrated in Figure 1. A sample (250 grams) of vacuum-dried coal is placed in the chromatographic column under a blanket of flowing nitrogen. Following sample emplacement, the column and gas heater are raised to the desired test temperature. During this heating period, nitrogen is passed continuously through the coal column. When the coal sample reaches operating temperature, oxygen is bled into the system and proportioned to give the desired oxygen concentration at a total gas flow of 300 cc/min. The effluent gas stream from the coal column is cooled to less than 40°C and passed into a sample chamber containing an electrolytic oxygen sensor. The experiment is continued until the effluent and influent oxygen concentrations are equal, or nearly so.

The sorption of oxygen by the coal sample is calculated from Equation 1:

$$Q = \Sigma[V_i \ (f_i - f_o) \ \frac{(1 - f_i)}{(1 - f_o)}] \ \Delta t \tag{1}$$

where Q = cc oxygen consumed by the coal sample;

V_i = gas flowrate entering coal column, cc/min.;

f_i = volume fraction of oxygen in entering gas stream;

f_o = volume fraction of oxygen in leaving gas stream; and

t = time, minutes.

Equation 1 implicitly assumes that nitrogen does not react with the coal. A set of experimental data illustrating the affinity of oxygen for Rosebud coal at 30°C (86°F) over a range of oxygen concentrations from 9 to 33 volume percent is summarized in Table 1.

2. Discussion

The time dependency of the effluent oxygen concentration is shown graphically in Figure 2. Figure 3 is a plot of the specific oxygen consumption (C cc/gram dry coal) against oxidation time (t) taken from Table 1. The same data, when plotted in Figure 4 on log-log coordinates, yield straight lines during the initial period of oxygen exposure (up to about 12 minutes). During this period, the specific oxygen consumption, C, varies as a power function of the oxidation time, t; that is, as

$$C = b \ t^m. \tag{2}$$

For initial oxygen levels from 13.5 to 33 volume percent, m was found to be constant at 0.59 and at 0.56 for the 9 volume percent level. When intercept b (in Equation 2) is plotted against f_i, the oxygen concentration entering the coal column, on log-log coordinates (Figure 5), a linear relation is obtained; viz.,

$$b = 0.045 \ f_i^{0.827}. \tag{3}$$

Substituting for b and m in Equation 2 yields

$$C = 0.45 \ f_i^{0.827} \ t^{0.59}, \tag{4}$$

which correlates with the data in Table 1 for oxidation periods up to 12 minutes. Upon differentiating Equation 4, the rate of specific oxygen uptake varies approximately as the 0.8 power of the initial oxygen concentration and inversely as the 0.4 power of the oxidation time. The power dependency of the oxygen concentration compares with 0.7 found by Porter and Ralston,[1] 0.6 found by Schmidt and Eider,[2] and 0.5 reported by Winmill[3] for bituminous coals. Figures 6 and 7 are plots of C vs. $t^{0.59}$ (Equation 4) and dC/dt vs. $t^{-0.41}$ (Equation 5), respectively, for coal exposure times from 2 to 10 minutes and initial oxygen concentrations from 5 to 20 volume percent.

$$\frac{dC}{dt} = 0.02655 \ f_i^{0.827} \ t^{-0.41} \tag{5}$$

The uptake of oxygen by Rosebud coal (Figure 3) is observed to approach a limiting value, C_L, which depends upon the initial concentration of oxygen in the entering gas stream, f_i. The relationship between these parameters is summarized in Table 2 and is shown graphically in Figure 8.

Based on the correlation in Figure 8, C_L varies linearly with f_i, i.e.,

$$C_L = 0.133 \ f_i, \tag{6}$$

for initial oxygen levels up to about 21 volume percent. Above 21 percent oxygen, the rate of uptake decreases with f_i to a constant value of 0.056. Comparing C at 10 minutes to C_L shows that from 70 to 80 percent of the total oxygen uptake occurred within 10 minutes after initiation of the experiment.

From previous work,[4] Rosebud coal was found to have a BET-equation surface area of 3.7 square meters per gram. The coal surface area based on oxygen uptake, assuming an atomic radius of 0.74 Angstroms, is shown in Table 3. Column 3 reports the grams of oxygen consumed per gram of coal; column 4 reports the equivalent surface area per gram of coal based on the observed oxygen uptake; and the last column indicates the

ratio of the equivalent oxygen surface to the BET-equation surface based on nitrogen adsorption.

The equivalent surface area of Rosebud Coal based on the observed oxygen uptake is 8.5 to 25.5 times as great as the BET-equation surface area. This difference suggests that oxygen combines with the coal to form a reaction product. If the oxidation of Rosebud coal is represented by

$$CH_{0.7} + 1.175 \ O_2 \rightarrow CO_2\uparrow + 0.35 \ H_2O, \tag{7}$$
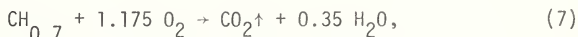
2.96 grams of oxygen should be consumed per gram of coal. The measured uptake of oxygen (Column 3 of Table 3) ranges from 0.2 to about 0.6 grams of oxygen per gram of coal, suggesting that oxygen combines with the coal to form acidic polar groups rather than gaseous oxides. Orsat analysis of samples of the column off-gas, taken 5 minutes after initiation of the experiment, failed to reveal carbon dioxide as a gas constiutent. Additional work is required to confirm this observation.

The oxygen sorption data reported above are dependent upon the past history of the coal sample and upon the stability of the electrolytic oxygen sensor. At no time during sample preparation was the coal excluded from contact with air although the coal samples were dehydrated under vacuum and flushed with nitrogen after emplacement in the column. Preparing the oxygen electrode and maintaining calibration during the course of an experiment was particularly troublesome.

B. Separation of Ash Minerals by Flotation

    1. Work Accomplished

The objective of this study is to examine the feasibility of separating ash minerals from Rosebud coal by froth flotation using fuel oil and pine oil as collector and frother, respectively. This simple reagent scheme should float the bulk of the coal, leaving the ash minerals as tailings. As discussed in the last quarterly report, about 70 percent of the ash minerals are locked in the coal as grains smaller than about 300 micrometers. To liberate these fine particles, the coal was ground to a size that would pass 100 mesh (150 micrometers).

A total of 50 flotation tests were performed and 28 were recorded. The effect of fuel oil level on flotation response is shown in Table 4 for a constant grinding time of 20 minutes (100% -100 mesh, 75% -400 mesh). Table 5 compares the effect of grinding time and fuel oil level, while Table 6 compares the effect of grinding time, fuel oil level, and pine oil level. All flotation tests were performed with 13 percent solids in Butte tap water in an Agitair flotation cell operating at 1100 rpm. No pH modifiers were utilized. Each test was performed on 200 grams (wet) of -6 mesh coal ground wet in a 10-inch steel laboratory ball mill.

    2. Discussion

The flotation results presented in Tables 4, 5, and 6 are not encouraging because of the extraordinary amounts of fuel oil and pine

oil required to promote coal flotation. This result was unexpected and departs significantly from the flotation behavior of eastern coals.

Table 4 compares the flotation response for additions of fuel oil (F.O.) ranging from none to 82 lb/ton at a constant pine oil (P.O.) addition of 9.3 lb/ton and constant grinding time. Over this range of fuel oil additions, the weight yield (Column 7) varied from 46 percent for pine oil alone to 81 percent for 82 lb/ton fuel oil. The separation efficiency, which is defined as coal recovery minus ash recovery with respect to the float product, varied from 3.2 percent for Test 10 (no F.O.) to 23 percent for Test 3 (66 lb/ton F.O.). The ash content of the float coal varied from 8.2 to 10.5 percent, the latter representing the effect of no fuel oil addition.

Increasing the fineness of the ground coal, shown in Table 5, did not result in satisfactory yields when the fuel oil level was either low (16.4 lb/ton) or high (82 lb/ton). Actually, flotation response became poorer with finer grinding at the higher fuel oil level, suggesting that over-grinding is detrimental to flotation. Coal ground for 35 minutes gave a particle size analysis such that 100 percent of the coal passed 105 micrometers and 88 percent passed 37 micrometers. Although liberation of ash minerals is estimated to be from 60 to 70 percent complete at this grind, the ash content of the float coal is higher than for the tests conducted using a 20-minute coarser grind.

The data in Table 6 clearly demonstrate that pine oil has the most significant effect on flotation response. In these tests, flotation response is compared for 20- and 35-minute grinds at equal fuel oil and pine oil levels although the pine oil level is 50 to 100 percent higher than in previous tests. For example, by comparing Test 23 at 13.9 lb/ton P.O. with Tests 1, 2, and 28 at 9.3 lb/ton P.O., Test 23 gave 13 percent greater yield and coal recovery than Tests 1, 2, and 28 at comparable ash contents. The effect of pine oil was even more significant at the 35-minute grind, as seen by comparing Tests 19 and 16. Table 6 also shows that there was very little difference in flotation response with grinding time, provided the fuel oil and pine oil levels were at least 30 lb/ton and 18.5/ton, respectively. Grinding the coal more than 20 minutes produced no significant improvement in ash content of the float coal.

The high levels of fuel oil and pine oil required to induce satisfactory flotation of Rosebud coal are believed to be related to the extremely high surface area (3.7 square meters/gram) of the coal and the oxidized condition of the coal surface. The coal acts much like activated carbon in its ability to absorb hydrocarbon surfactants and oils. Also, surface oxidation of the coal probably rendered the surface highly water-avid due to the presence of acid polar groups. Although we did not investigate control of the flotation pulp pH, that variable may be quite important. Based on the results collected so far, Rosebud coal is characterized as being very difficult to float and requiring very high levels of frother and collector to achieve adequate yields. The ash content of the float coal is reduced only 2.5 to 2.7 ash percentage points by flotation treatment.

C.   Organic Volatile Matter

     1.   Work Accomplished

          Replicated Btu analyses were made for samples of Rosebud coal
     before and after drying. One sample, which was sealed in a mason jar
     for over one year, showed a decrease in Btu value from 10,971 Btu/lb
     to 10,527 Btu/lb (dry basis) when dried at 105°C for three hours. This
     represents a loss of 4.1 percent of the heat content of the original
     sample. Another sample taken recently from Colstrip showed a decrease
     in Btu value from 11,815 Btu/lb to 10,879 Btu/lb when dried at 105°C
     for three hours. This represents a loss of 8 percent of the original
     heat content. These Btu values are the averages of eight analyses for
     each sample with a standard deviation of ±89 Btu/lb (±0.8 percent).

          Coal samples were heated in a tube furnace immersed in a fluidized
     bath at 90°C ± 2°C. Off-gases were collected in a slush bath at -22°C.
     The collected organic matter (plus water) was injected into a OV-101
     gas chromatographic column which separated the constituents prior to
     their detection by a flame ionization detector. The detector signal,
     plotted in Figure 9, shows at least 16 organic compounds which were
     evolved during the drying period. These have not been identified at
     this time.

          Isolation and identification of low-boiling volatiles has begun.
     Eight hydrocarbons have been identified (Table 7). Quantification of
     these compounds is awaiting the determination of response factors on
     the gas chromatograph. An experiment using liquid chromatography with
     a fluorescent detector gave results that confirm the presence of poly-
     nucleated aromatic compounds. This data has not been interpreted
     completely.

     2.   Discussion

          The heat loss on drying Rosebud coal appears to range from 4 to
     8 percent and represents a real loss, not a loss due to variations in
     the analytical method. Various low-boiling volatiles, which are evolved
     from Rosebud coal under moderate drying conditions (105°C), have been
     identified although their amounts await quantification. These organics
     may represent a source of air pollution.

D.   Fluid Bed Drying Study

     1.   Work Accomplished

          For reasons discussed in previous quarterly reports, the fluid
     bed drying study has not progressed according to the work plan. The
     principal investigator had planned to construct a two-foot diameter
     fluidization column on-campus. Siting problems led to the abandonment
     of this idea. Following the May ERDA review visitation, we began to
     construct a six-inch fluidiz ion column, and progress has been rapid
     since this decision point.

2.   Discussion

Equipment that has been purchased or encumbered since May includes a Chromalox indirect gas heater and proportional controller, a bag house with compressor and exhaust fan, a supply fan, flow meters, thermocouples, pressure gauges, and a cyclone. The fluidization column and supporting structure is being fabricated locally. A multi-channel recorder and coal feeder with controller were purchased last August. The experimental fluid bed is located in the basement of Montana Tech's Metallurgy Building, where it will occupy about 250 square feet of floor area. Material handling and disposal and coal dust will present problems. Advertisements have been placed for a three-quarter time project engineer and a full-time technician.

E.   Work Forecast

Additional tests will measure oxygen uptake at elevated temperatures to 175°C (350°F) and in the presence of water vapor.

The effect of pH, pine oil level, and promoter type will be examined during the next quarter to seek improved coal-ash mineral separations.

Quantification of the organic volatiles will be made during the next quarter.

Work will continue on the assembly and erection of the fluidization column and associated hardware. Completion is expected by September.

IV. CONCLUSIONS

The abstraction of atmospheric oxygen by Rosebud coal depends upon the oxygen concentration, time of exposure, and temperature. At 30°C, the amount of oxygen which reacts with the coal is only 20 percent of the stoichiometric amount required to initiate combustion. There does not appear to be any combustion hazard associated with storing 'dried' Rosebud coal at ambient temperature and oxygen levels.

Flotation of Rosebud coal does not appear to be a feasible method for rejecting ash minerals. Reagent consumption is extremely high and uneconomic.

Drying Rosebud coal leads to a significant loss in Btu value, ranging from 4 to 8 percent. This loss is associated with the removal of low molecular weight organic volatiles.

TASK ___C___

MAJOR MILESTONES

A. Stability of Processed Rosebud Coal and Dervied Coal Dust
1. Pyrophoricity Vendor Tests
2. Coal Stability Tests
   a. Apparatus assembly
   b. Completion of tests
   c. Completion of data analysis
3. Organic Volatile Losses
   a. Completion of literature study
   b. Apparatus set-up
   c. Procedure development
   d. Data collection & evaluation

B. Coal Beneficiation
1. Mineragraphic Analysis
2. Completion of Heavy Liquid Tests
3. Completion of Flotation Tests
4. Completion of Electrostatic Tests
5. Completion of Evaluation

C. Fluid-Bed Drying
1. Completion of Design and Parts Purchase
2. Completion of Fluid-bed Fabrication
3. Completion of Dryer Erection at MRC
4. Completion of Shakedown Tests

1977

O N D J F M A M J J A S

PROGRESS

39

TABLE 1

Oxygen Sorption Data; 14x35 Mesh Rosebud Coal at 30°C

Oxidation Time, Min.

	2.5	5	7.5	10	12.5	15	17.5	20	22.5	25	27.5	30	35	40	45	50	55	60
f_i = 8.8% O_2																		
f_o, %		1.1		3.0		6.25		7.72		8.25		8.48		8.70		8.73		8.75
Q, cc	113		207		266		292		302		308		313		314		314	
cc/gm	0.45		0.83		1.07		1.17		1.21		1.24		1.26		1.26		1.26	
f_i = 13.3% O_2																		
f_o, %		1.25		3.05		10.5		12.5		12.7		13.0		13.2		13.25		
Q, cc	163		309		400		425		435		441		446		446		–	–
cc/gm	0.66		1.24		1.61		1.71		1.75		1.77		1.79		1.79			–
f_i = 20% O_2																		
f_o, %		1.52		4.25		13.75		17.35		18.4		18.8		19.35		19.65		19.75
Q, cc	233		444		584		668		699		720		744		751		755	
cc/gm	.93		1.78		2.37		2.68		2.81		2.89		2.99		3.02		3.03	
f_i = 25% O_2																		
f_o, %		1.75		5.4		18.4		23		24.5		24.8		25				
Q, cc	274		524		691		752		771		766		779		–			
cc/gm	1.10		2.10		2.78		3.02		3.09		3.12		3.13					
f_i = 30% O_2																		
f_o, %		1.8		7.4		23.0		28.0		28.5		29.5					
Q, cc	308		588		771		835		860		875		–		–			
cc/gm	1.24		2.36		3.10		3.35		3.45		3.51						
f_i = 33% O_2																		
f_o, %		2.3		23.0		78.8		30.0		30.8		31.9	32				
Q, cc	399		688		785		848		894		923	942	–			–	–
cc/gm	1.6		2.76		3.15		3.40		3.59		3.71	3.78					

40

TABLE 2
Limiting Values of Specific Oxygen Consumption at 30°C

f_i, Entering O_2 Conc., %	C_L, Limiting O_2 Uptake, cc/gm
9	1.26
13.5	1.78
20	3.03
25	3.13
30	3.53
33	3.63

TABLE 3
Oxygen Uptake and Equivalent Surface Coverage at 30°C

f_i, %	C_L, cc O_2/gm	gm O_2^*/gm	cm^2 O_2^*/gm	A/A_{BET}
9	1.26	0.19	3.1×10^5	8.5
13.5	1.78	0.27	4.5×10^5	12.1
20	3.03	0.46	7.6×10^5	20.5
25	3.13	0.47	7.8×10^5	21.1
30	3.53	0.53	8.8×10^5	23.7
33	3.63	0.57	9.4×10^5	25.5

*Corrected to STP

TABLE 4
Flotation Response for Various Fuel Oil Levels:
20 Minute Grinding Time

| Test | lb/Ton | | % Ash | | | % Yield | % Recovery | | % Eff. |
	F.O.	P.O.	Head	Conc.	Tail		Coal	Ash	
10	None	9.3	11.2	10.5	11.8	45.5	45.9	42.7	3.2
9	4.1	9.3	10.4	8.7	13.8	67.0	68.3	56.0	12.3
7,8	8.2	9.3	10.2	8.4	14.7	71.5	73.0	58.9	14.1
6	16.4	9.3	11.4	8.8	17.2	70.0	71.9	54.0	17.9
5	32.8	9.3	10.2	8.7	14.3	74.6	75.8	63.6	12.2
4	49.2	9.3	11.0	8.9	18.4	77.6	79.5	62.8	16.7
3	65.6	9.3	11.5	9.1	21.1	80.1	82.2	63.4	22.9
1,2,28	82	9.3	10.7	8.2	21.6	81.1	83.4	62.1	21.3

TABLE 5

Flotation Response for Various Grinding Times and Fuel Oil Levels

Test	Grind Min.	lb/Ton		lb/Ton			% Yield	% Recovery		% Eff.
		F.O.	P.O.	Head	Conc.	Tail		Coal	Ash	
6	20[1]	16.4	9.3	11.4	8.8	17.2	70.0	71.9	54.0	17.9
11	25	16.4	9.3	12.6	9.2	15.6	47.0	48.8	34.4	14.4
12	30	16.4	9.3	13.0	9.4	17.2	53.5	55.8	38.7	17.1
13	35[2]	16.4	9.3	12.6	9.4	16.7	56.7	58.7	42.5	16.2
1,2,28	20	82	9.3	10.7	8.2	21.6	81.1	83.4	62.1	21.3
14	25	82	9.3	11.4	8.8	16.5	66.3	68.3	51.3	17.0
15	30	82	9.3	11.3	8.7	14.8	57.9	59.5	44.6	14.9
16	35	82	9.3	11.8	8.9	16.1	59.8	61.7	45.1	16.6
18	35	123	9.3	11.3	8.8	14.9	57.7	59.4	44.5	14.9

(1) 100%-100, 75%-400

(2) 100%-150, 89%-400

TABLE 6
Flotation Response for Various Grinding Times, Fuel Oil, and Pine Oil Levels

Test	Grind Min.	lb/Ton F.O.	lb/Ton P.O.	Head	lb/Ton Conc.	lb/Ton Tail	% Yield	% Recovery Coal	% Recovery Ash	% Eff.
23	20	82	13.9	10.9	8.3	39.2	91.5	94.2	69.7	24.5
19	35	82	13.9	11.1	8.5	45.4	93.0	95.7	71.4	29.3
24	20	82	18.5	10.6	8.5	64.6	96.2	98.5	77.1	21.4
17	35	82	18.5	12.4	10.1	63.0	95.5	98.2	78.0	20.2
25	20	32.8	18.5	10.9	8.7	70.3	96.3	98.8	76.9	21.9
20	35	32.8	18.5	12.0	4.9	46.1	94.1	96.4	77.3	19.1
26	20	16.4	18.5	11.0	8.5	54.4	94.6	97.3	73.1	21.5
21	35	16.4	18.5	13.6	11.1	26.7	84.1	86.6	68.8	17.8

TABLE 7
Identified Organics Volatilized from
Rosebud Coal During Drying

n. hexane

cyclohexane

n. heptane

2, 2 dimethyl butane

(2, 2, 4) ? trimethyl pentane

2 methyl or 3 methyl pentane

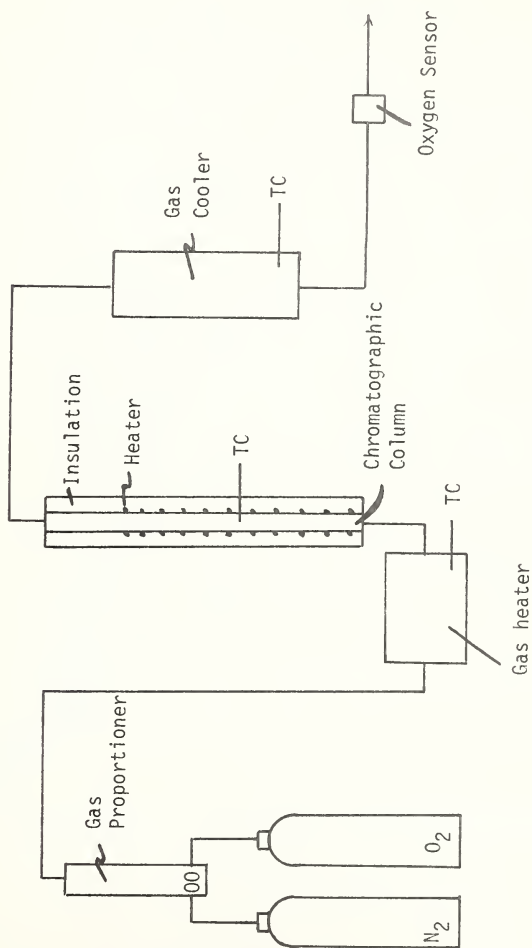methyl cyclohexane

cyclohexene

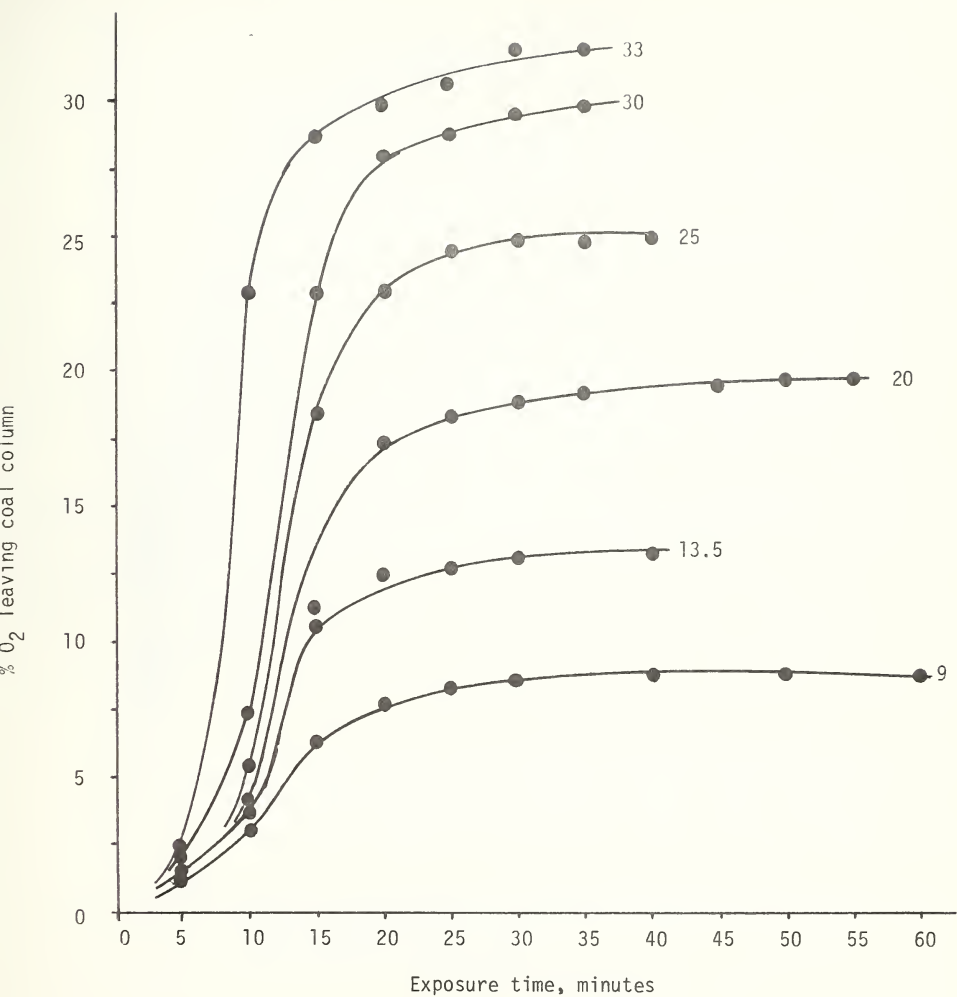Figure 1. Flow apparatus for measuring oxygen uptake.

Figure 2. Oxygen concentration in coal column off-gas vs exposure time.
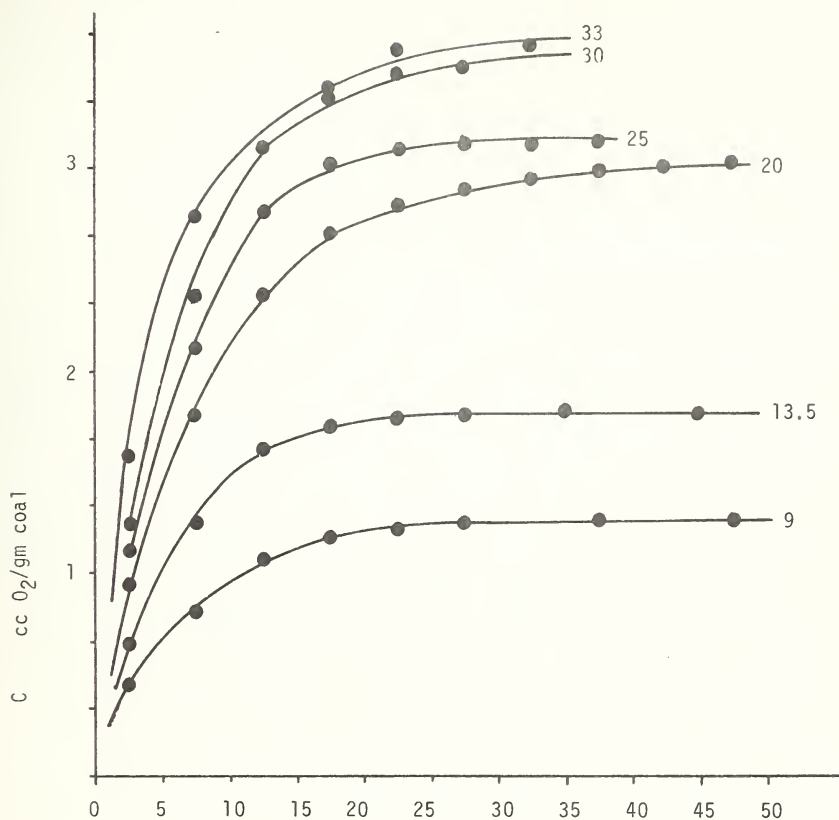
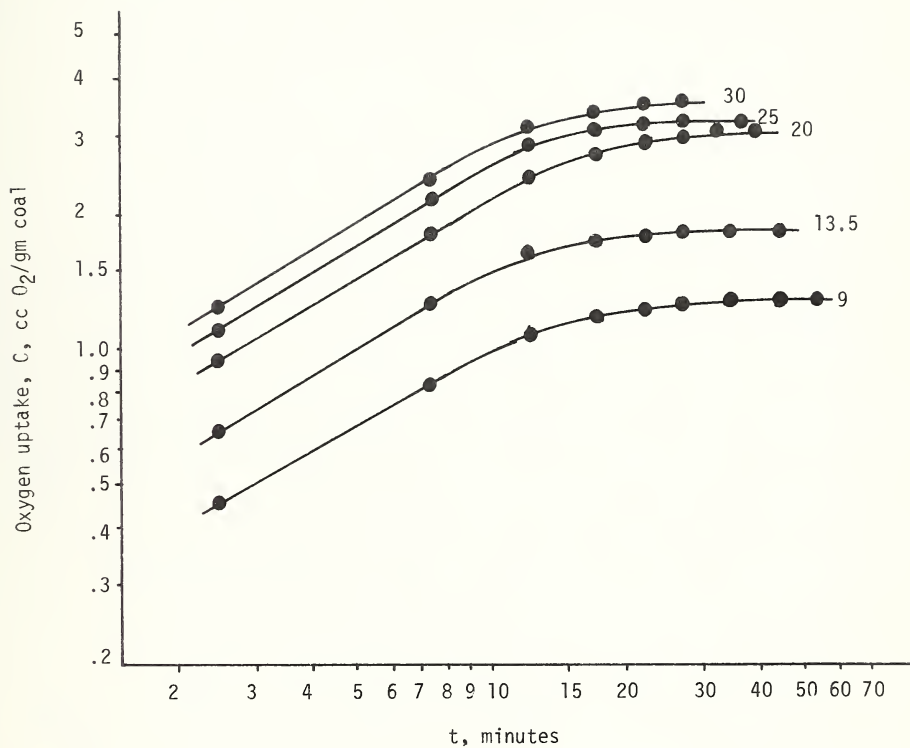Figure 3. Specific oxygen uptake C vs exposure time t for various inlet oxygen concentrations.

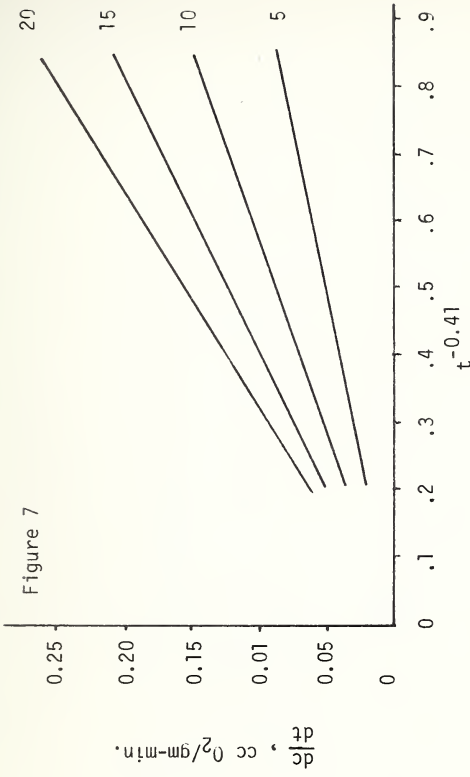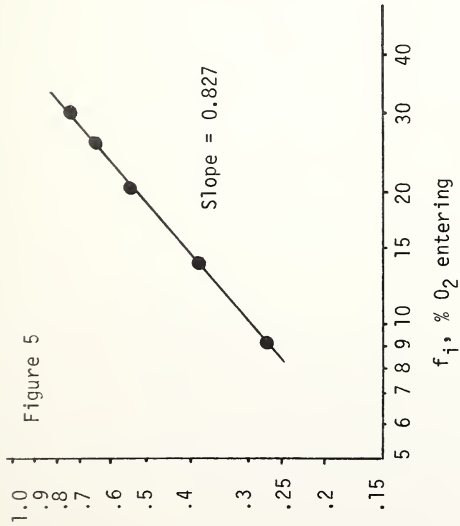Figure 4. Log-log plot of specific oxygen uptake C vs exposure time, t, for various inlet oxygen concentrations.

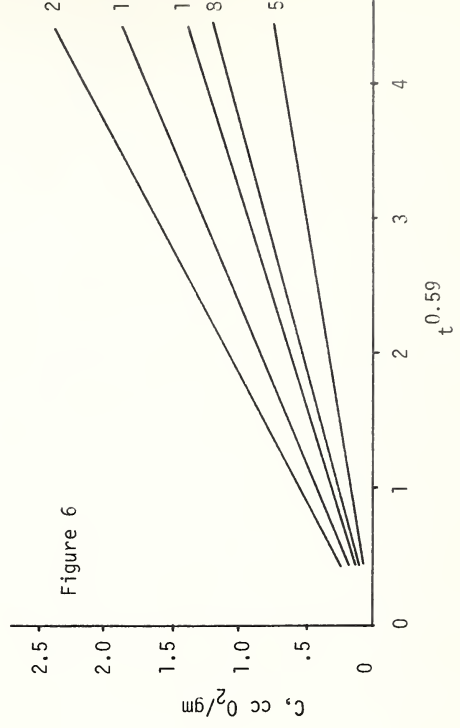Figure 5. Plot of constant b in equation 2 vs f_i, % O_2 entering coal column.

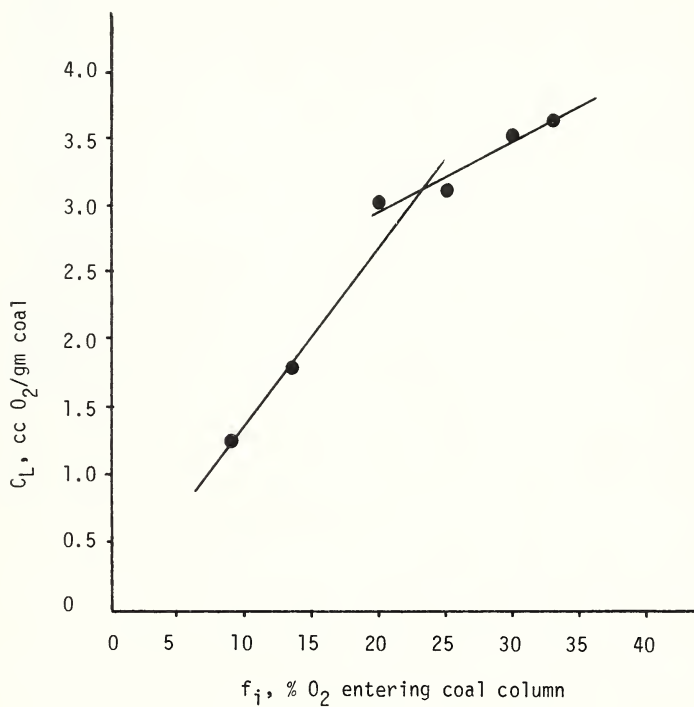Figure 6. Plot of equation 4.
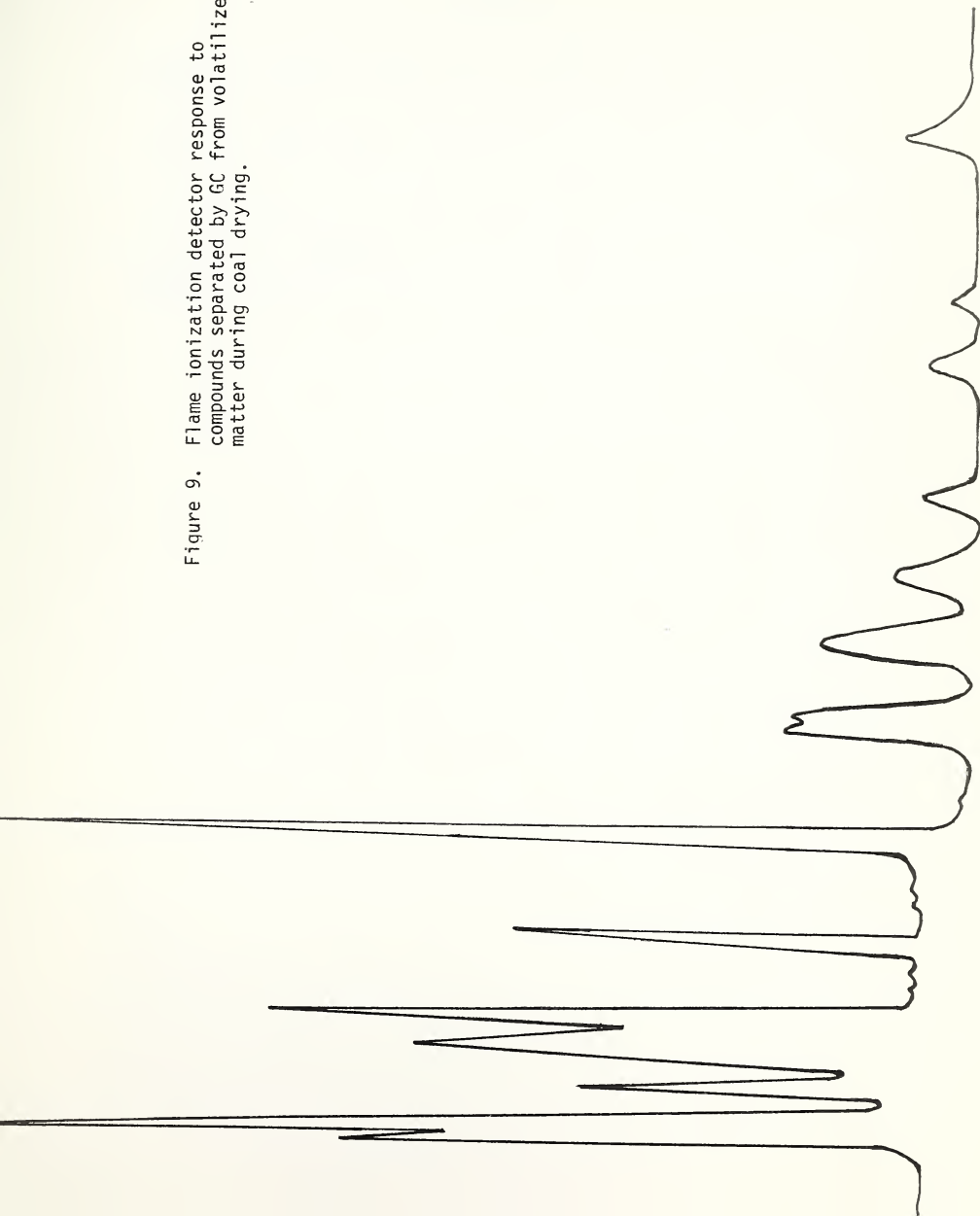
Figure 7. Plot of equation 5.

Figure 8. Limiting oxygen uptake, C_2 ccO_2/gm, vs entering oxygen concentration, f_i.

Figure 9. Flame ionization detector response to compounds separated by GC from volatilized matter during coal drying.

REFERENCES

1. Porter, H. C. and D. C. Ralston, "A Study of the Oxidation of Coal," USBM Tech Paper 65, 1914.

2. Schmidt, L. D. and J. L. Elder, "Atmospheric Oxidation of Coal at Moderate Temperatures," I & EC, Vol. 32, #2, pp. 249-256, 1940.

3. Windmill, T. F., "The Absorption of Oxygen by Coal," Trans. Institute of Mining Engineers, Vol. 46, pp. 563-578, 1913-14.

4. Preparation of Rosebud Coal for Utilization in Direct Coal-Fired MHD Generation, Final Report; pp. 2-12; Contract E(49-18)-1811, MERDI, December 1976.

TASK E
Slag Flow and NO_x Kinetics:
Moderate Temperature Slag Flow Facility (MTSFF)
H. W. Townes and T. C. Reihman

ABSTRACT

The primary objective of this task is to determine the deposition rate of solids on the flow passages of high temperature air preheaters operating on the combustion products of a coal-fired MHD system. Secondary objectives include the determination of the corrosion rate of materials, analytical simulation of the deposition process, and simulation of the operation of full-scale heat exchangers.

During this reporting period, three tasks have been completed. The pressure drop characteristics of the cold clean core of the MTSFF have been determined. A parametric study of MHD air preheaters has been performed. A model of the MTSFF core and insulation has been used to study their thermal interactions.

I. OBJECTIVE AND SCOPE OF WORK

The objective of this program is to determine the operational characteristics of a high-temperature packed-bed regenerative heat exchanger for a coal-fired open-cycle MHD system. There is considerable information on the operation of regenerative heat exchangers at temperatures up to 4200°F, but all experience to date has utilized clean fuels such as natural gas. The present work concentrates on the effects that coal slag and MHD seed material have on the performance of regenerative packed-bed heat exchangers. Anticipated effects include the deposition of coal slag and seed material on the heat exchanger surfaces, the subsequent transport along the surfaces, the obstruction of the passages, the chemical interaction with the heat exchanger material, and changes in the friction and heat transfer coefficients of the heat exchanger flow passages.

An experimental facility, the moderate temperature slag flow facility (MTSFF), is being built and will be operated to study the effects that typical open-cycle MHD channel-exit flows will have on the high-temperature air preheater. The test core of the MTSFF consists of typical MHD air preheater ceramic bricks. Instrumentation and in situ optical diagnostics for the MTSFF will include a laser Doppler anemometer system for determining gas stream velocities and turbulence properties within the MTSFF and an optical spectroscopy system for determining the chemical composition and concentrations of the various combustion products within the MTSFF. Emphasis will be placed on monitoring the NO_x concentrations. A data acquisition and control system will be utilized to record gas flow rates, pressures, compositions, and velocity data, as well as temperatures at approximately two hundred (200) locations.

The effects of the coal slag and MHD seed material on the heat exchanger performance and NO_x kinetics will be determined over a wide range of operational parameters, principally temperature limits of the bed material and flow velocities for the combustion gas and for the air to be heated. The experimental system has been sized so that the above temperatures and velocities can be achieved with a circular flow passage from 0.25 to 1.5 inches in diameter. Initially, natural gas will be used as the fuel. Coal ash will be added to simulate the combustion products of coal firing. The amounts of coal ash added to the combustion gas will simulate the full range that can be expected from the burning of various coals with zero to 95 percent ash removal. The influence of particle size and residence time in the combustor also will be determined. At a later date, it may be desirable to add an actual coal combustion unit to the apparatus.

The overall program consists of analytical as well as experimental work. Analytical studies have been conducted to size the MTSFF, to determine the geometry of the cored ceramic brick, and to determine the ranges of the variables in the experimental program. Current effort is directed toward studies of the transient response of the entire MTSFF during start-up and cooldown, toward predictions of the slag deposition rates on the heat exchanger surfaces, and toward development of sets of operational test conditions (flow rates and temperature profiles) representing several maximum stress levels in the ceramic bricks.

II. SUMMARY OF PROGRESS TO DATE

Progress has been made during the last quarter in three areas. The major portion of the moderate temperature slag flow facility (MTSFF) has been completed. The ceramic core is in place, and the combustor has been tested. In addition, pressure drop tests of the cold clean core have been run using the data acquisition and control system (DACS).

A thorough parametric study of heat exchangers, which will satisfy the operating conditions of the ECAS[1] Open-Cycle MHD Base Case One, has been completed. Plots are presented which show the effects of parametric variations on heat exchanger mass and operational characteristics.

The model of the MTSFF core and insulation thermal interaction has been completed. This thermal model has been used to understand better the effects of the small size of the MTSFF on its thermal behavior.

III. DETAILED DESCRIPTION OF TECHNICAL PROGRESS

A. Pressure Drop Studies on MTSFF Core

1. Work Accomplished

Part of the baseline data necessary for the MTSFF first core is the pressure drop behavior prior to heat up of the core. This data provides information on the roughness of the flow holes and on the pseudo-roughness due to misalignment of the cored bricks.

The pressure drop characteristics of three separate flow holes in the 6-hole ring of the 19-hole MTSFF first core were measured. A

static pressure probe was inserted four feet from the bottom (entrance) of the core. This corresponds to 64 diameters, and entrance effects should not influence the pressure drop measurements. A pressure probe was inserted one foot into the top of the heat exchanger core for measurement of both static pressure and total head. Using this probe, the centerline velocity in the flow holes was determined. From the two static probes, the pressure drop through the core was found. The flow rate was measured with the orifice flowmeter in the inlet air line of the MTSFF. The data acquisition and control system for the MTSFF was used for all data acquisition and reduction.

Analysis of the pressure drop data initially showed pressure drops lower than that predicted for smooth tubes when using the flow-meter data for flow rates. This, of course, is not possible. When comparing the metered flow with the flow determined from the velocity data in the individual holes, it was found that there was an appreciable leakage flow through parallel paths in the spaces between the MTSFF insulation and containment layers.

A computer code was developed to analyze the effect of this leakage on the pressure drop characteristics of the core. The model assumed that the leakage occurred through the gaps between the three-inch-thick bricks. Thus, there were 75 leakage slots over the 19-foot length of the core. The leakage through each slot was assumed to be by laminar flow, so that the leakage rate was proportional to the pressure difference across the slot. The axial pressure drop in any segment was due to turbulent flow at a flow rate equal to the entering flow rate minus the sum of the leakage flows to that point. The friction factor was assumed to follow a relation of the form $f = C/(Re)^{.25}$, where C has a value of 0.316 for smooth tubes. By an iterative procedure, the code based on this model computed the value of C and leakage slot thickness that corresponded to the measured pressure drop and total leakage flow. The value of C and slot thickness were assumed to be the same for each axial segment and leakage slot, respectively.

2. Discussion

The results show that the characteristics of the three individual channels are slightly different. This indicates that the leakage slots and the brick misalignment may differ from flow hole to flow hole. The same probes were used for all three flow holes. Two sets of experimental runs with separate probe insertions were made for each hole. The data from the same hole agree well with one another, but there is a measurable variation in the flow characteristics between the holes. The total leakage is 32 percent of the entering flow; at the other extreme, the leakage is 40 percent of the entering flow. There is also a slight Reynolds number dependence on the leakage rates, varying from an average of about 34 percent at a Reynolds number of 5000 to about 37 percent at a Reynolds number of 10,000. The slot thickness required to yield the measured leakages was found to be typically 0.007 inches.

The values of C required to produce the measured core pressure drop depend somewhat on the Reynolds number but more strongly on the specific hole investigated. At a Reynolds number of 8000, the values for the extreme holes were 0.325 and 0.360. This corresponds to increases above smooth behavior of about 3 percent and 14 percent, respectively. For one hole, the typical variation was from 0.325 at a Reynolds number of 5000 to 0.348 at a Reynolds number of 10,000. Comparison of the percent increases observed in this study to Nikuradse's[5] sand grain roughness data in the same Reynolds number range gives an equivalent sand grain relative roughness of about 0.012, which corresponds to an equivalent sand grain roughness of about 0.009 inches for the 3/4 inch flow channels.

B.   Thermal Interaction of the MTSFF Core and Insulation

1.   Work Accomplished

Because the MTSFF uses a single core brick for the slag deposition and thermal experiments, it is necessary to know the interaction between this rather small core and the surrounding insulation. Knowledge of the extent of this interaction will allow a better correlation between the characteristics of the MTSFF and full-scale air preheaters. The following discussion summarizes briefly the full study which is contained in Reference 2.

2.   Discussion

To reduce heat losses from the MTSFF, approximately twenty-one inches of insulation surrounds the MTSFF core. The containment tube, which is made of Harbison-Walker Guidon, is the first layer of insulation with successive layers of John's Manville insulating firebrick. It is necessary, on start-up, to bring this insulation layer up to a cyclic equilibrium temperature profile. In addition, during cycling of the core, some heat will be transferred between the core and the surrounding insulation. The study[2] concerned itself with two aspects of this thermal interaction problem: first, the time necessary to reach a cyclic equilibrium condition, and second, the degree of thermal interaction between the core and the insulation at cyclic equilibrium conditions.

For the purpose of this study, the time to reach cyclic equilibrium operation was defined as the time at which the net amounts of energy transferred during successive reheat and blowdown cycles between the gas and the core were within five percent. The difference between these energy transfers represents heat loss to the environment and energy necessary to bring the insulation up to a cyclic equilibrium temperature profile. As can be seen in Figure 1, after approximately ninety hours of real-time simulation, cyclic equilibrium operation is not reached. It is apparent from this figure that the time to reach the cyclic equilibrium condition is relatively long. Because of the long time involved, it was concluded that the MTSFF probably will be operated only occasionally in the cyclic equilibrium mode.

The degree of thermal interaction between the core and the containment tube is shown in Figure 2. At the top (high temperature) end of the bed, the containment tube temperature closely follows that of the core. Consequently, there is a rather large amount of heat transfer between the core and the containment tube, effectively increasing the thermal mass of the core. The degree of interaction is shown by the heat transfer ratios in Figure 3.

C. Parametric Study of Heat Exchangers

1. Work Accomplished

In the course of selecting the operating conditions for the MTSFF, it became evident that detailed thermal-hydraulic design information on cored-brick regenerative heat exchangers was not available. Therefore, an investigation was undertaken to obtain this information. An iterative design method was developed in which the geometry and the operational parameters were adjusted systematically until the specified heat exchanger performance was achieved. The lumped-mass model code, described in previous reports,[3] was the primary analytical tool in this work.

Over two hundred sets of design specifications have been developed which satisfy the criteria of the ECAS[1] Open-Cycle MHD Base Case 1. These design specifications were developed for two maximum thermally-induced stress levels, three flow-hole diameters, three ratios of hole spacing to diameter, three total cycle times, four ratios of number of reheat to number of blowdown heat exchangers, and three values of wall roughness. Of these designs, those exhibiting blowdown exit temperature droops of over 100 K were discarded. Of the remaining designs, the ones exhibiting lower ceramic mass requirements were identified.

The MTSFF geometry also was studied for a range of flow rates and for a range of total cycle times. The variations in average blowdown and reheat exit temperatures, the maximum thermal stress, and the maximum base ceramic temperature were determined.

Thermal hydraulic design specifications have been developed for over 200 heat exchanger systems satisfying the ECAS[1] Open-Cycle MHD Base Case 1 conditions. These design specifications were developed for the following conditions:

- Maximum tensile stress levels of 13.8 and 34.5 MPa;

- Flow hole diameters of 19, 38, and 51 mm;

- Flow hole spacing to diameter ratios of 1.2, 1.4, and 1.6;

- Total cycle times of 1000, 2000, and 3000 sec;

- Ratio of number of reheat to number of blowdown heat exchangers in system of 4/6, 5/5, 6/4, and 6/3; and

•   Wall roughness equivalent sand grain heights of 0,
        0.102, and 0.254 mm.

The procedure used was to select the flow hole diameter, flow
hole spacing to diameter ratio, total cycle time, ratio of reheat to
blowdown heat exchangers, wall roughness, and thermal stress level for
which the design specifications leading to the ECAS Open-Cycle MHD
Base Case 1 conditions were to be determined. A trial bed length and
reheat inlet velocity (the only two remaining independent variables)
were selected. The lumped-mass code[5] then was run to determine the
thermal-hydraulic characteristics of that heat exchanger system and
for two slightly different (typically five percent offsets in length
and reheat inlet velocity) heat exchanger systems. Then, by a Newton-
Raphson iterative technique, the precise values of length and inlet
velocity to produce the required blowdown exit temperature and thermal
stress level were found. These then were input to a check run, and
another iteration round was performed if necessary. Designs that
exhibited blowdown exit temperature droop of over 100 K were discarded.

2.   Discussion

The results of the ECAS design study are presented primarily in
graphical form. Three types of plots were developed. In the first
type, shown in Figure 4, the length and the inlet velocities required
to meet the ECAS[1] Open-Cycle MHD Base Case 1 specifications were
plotted versus the ratio of reheat to blowdown heat exchangers in the
system for fixed diameter, fixed spacing to diameter ratio and fixed
stress level, and for three values of total cycle time. Nine plots of
this type, representing 84 specific heat exchanger designs and each
satisfying the 100 K droop limitation, were developed.

The second type of plot is shown in Figure 5. The total ceramic
mass for a heat exchanger system (reheat heat exchangers + blowdown
heat exchangers + 2) is shown as a function of the ratio of reheat to
blowdown heat exchangers for fixed diameter and fixed stress level
with the total cycle time and spacing to diameter ratio as parameters.
The total ceramic mass required is related strongly to the air pre-
heater costs. At an assumed cost of 50¢ per pound of ceramic, a total
ceramic mass of 20 x 10^6 Kg for a 2000 MWe power plant represents a
ceramic cost of about $11 per installed KWe.

The third series of plots, shown in Figures 6 and 7, indicates
the sensitivity of the average blowdown exit temperature and the
maximum thermal stress to the reheat inlet velocity for fixed length,
fixed spacing to diameter ratio, and fixed total cycle time and ratio
of reheat to blowdown heat exchangers with the diameter as a parameter.
In other plots (see Figure 4), each of the parameters fixed here is
taken, in turn, as the variable. The extension of the results into
the region where excessive blowdown exit temperature droop exists is
shown as dashed lines.

Typical simulation results for the MTSFF are shown in Figure 8.
The average blowdown exit temperature, the maximum and average reheat
exit temperature, the maximum ceramic base temperature, and the maximum

thermal stress are shown as a function of the total cycle time. Other results[4] in this series show the variations with reheat inlet velocity and the ratio of blowdown to reheat mass flow rate. This information is necessary in selecting safe operating conditions for the MTSFF.

Additional details on the ECAS design study and the MTSFF performance study are found in the recently completed M.S. thesis by G. A. Upshaw.[4] The major conclusions of his work are listed below:

a) ECAS Base Case 1 conditions can be attained for a variety of cored ceramic brick heat exchanger designs;

b) Lower D, lower S/D, lower total cycle time, lower NR/NB ratio, or higher thermal stress limits result in lower ceramic mass;

c) Changes in Item b parameters to reduce mass are limited severely by the maximum blowdown exit temperature droop criterion. Low ceramic mass designs are associated with high blowdown temperature droop;

d) Changes in Item b parameters to reduce mass also are limited by potential plugging of smaller diameter holes, manufacturing difficulties for small diameter, small S/D ceramic bricks, increased valve operation frequency at lower cycle times, or instability of bricks at high thermal stress levels; and

e) Variations in tube roughness do little to affect the total ceramic mass; instead, they alter the length and diameter of the bed while maintaining nearly constant total mass values.

D.   Work Forecast

1.   Pressure Drop Studies on MTSFF Core

Overall pressure drop measurements will be made throughout the test program in the MTSFF and will be used to monitor the deposition rate of the slag on the tube walls. Detailed pressure drop and leakage studies like those reported here will be made at intervals throughout the test program to give an indication of the flow hole surface and leakage characteristics of the MTSFF core.

2.   Thermal Interaction of the MTSFF Core and Insulation

The two effects which were discussed previously are a result of the small size of the MTSFF. The time required to reach cyclic equilibrium and the thermal interaction between the core and the containment tube cannot be avoided in an experiment of this size. Further work will be done to determine the influence these effects will have on the slag deposition rates and the relationship between experiments done in the MTSFF and full-scale heat exchangers. Work on a more detailed model is in progress.

3. Design of Coal-Fired Cored-Brick Regenerative Heat Exchanger

The designs completed to date show that the blowdown exit temperature droop is an important constraint on acceptable air preheater designs. Both the temperature droop and the ceramic mass requirements are reduced for lower cycle times. The design work will be extended to total cycle times of 500 seconds during the next reporting period.

IV. CONCLUSIONS

Three major tasks have been completed. The MTSFF clean-core pressure drop studies have identified parallel leakage paths and have yielded an estimate of the clean flow passage surface roughness. The parametric study of air preheaters has identified typical operating conditions which are used in the MTSFF test plans. The MTSFF core-insulation study has shown a larger interaction than anticipated, indicating the need for a more detailed study.

3. Design of Coal-Fired Cored-Brick Regenerative Heat Exchanger

The designs completed to date show that the blowdown exit temperature droop is an important constraint on acceptable air preheater designs. Both the temperature droop and the ceramic mass requirements are reduced for lower cycle times. The design work will be extended to total cycle times of 500 seconds during the next reporting period.

IV. CONCLUSIONS

Three major tasks have been completed. The MTSFF clean-core pressure drop studies have identified parallel leakage paths and have yielded an estimate of the clean flow passage surface roughness. The parametric study of air preheaters has identified typical operating conditions which are used in the MTSFF test plans. The MTSFF core-insulation study has shown a larger interaction than anticipated, indicating the need for a more detailed study.

DIVISION OF MAGNETOHYDRODYNAMICS
MONTHLY PROJECT MANAGEMENT STATUS REPORT

FOSSIL ENERGY

REPORT DATE _____

CONTRACT/PROJECT		
CDIF Project Management Support and Related MHD Dev. Effort		77-002
CONTRACT NO.	VENDOR	Task E - Slag Flow and NO_x Kinetics
EF-77-C-01-2524	Montana State University	
		SCHEDULE
		Moderate Temperature Slag Flow Facility

TASK E

MAJOR MILESTONES AND DECISION POINTS	YEAR	1977												VARIANCE
	MONTH	O	N	D	J	F	M	A	M	J	J	A	S	

COMPLETE MTSFF STARTUP AND CHECKOUT RUNS

COMPLETE CLEAN AIR STUDIES

COMPLETE EXAMINATION OF CERAMIC CORE AFTER CLEAN AIR STUDIES

COMPLETE FIRST SET OF SLAG FLOW STUDIES

MODIFY MTSFF FOR 2600°F BOTTOM END TEMPERATURE AND INSTALL NEW CORE

STATUS DATE
SCHEDULE PLAN
PROGRESS
STATUS DATE

CONTRACT/PROJECT
CDIF Project Management Support and Related MHD Dev. Effort

CONTRACT NO.   VENDOR
EF-77-C-01-2524   Montana State University

Task E - cont. Page 2

FOSSIL ENERGY

| TASK E | YEAR | 1977 | | | | | | | | | | | | VARIANCE |
| | MONTH | O N D J F M A M J J A S | |

MAJOR MILESTONES AND
DECISION POINTS

CORRELATE MODEL PREDICTIONS
OF SLAG DEPOSITIONS AND HEAT
TRANSFER RATES WITH RESULTS
OF FIRST SLAG FLOW TESTS

BEGIN INSPECTION AND STUDY OF
CERAMIC-SLAG INTERACTIONS FOR
SLAG FLOW RUNS

STATUS DATE _____ △
SCHEDULE PLAN ▷
PROGRESS ▬▬▷

STATUS
DATE

ADMINISTRATIVELY CONFIDENTIAL

VARIANCE OR PROBLEM FLAG IN RIGHT COLUMN ◇
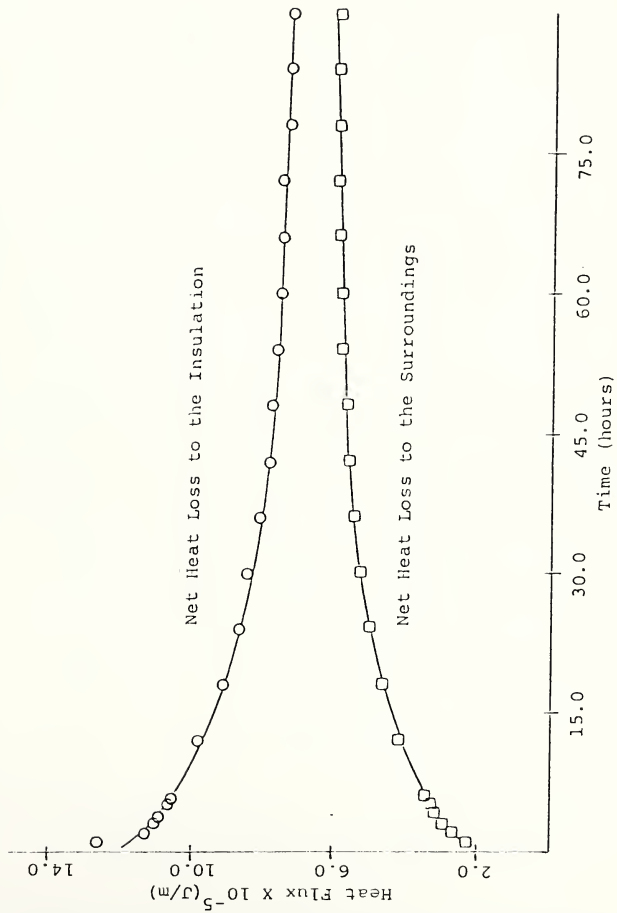
Figure 1.--Heat flux approach to steady state

Net Heat Loss to the Insulation

Net Heat Loss to the Surroundings

Time (hours)

Heat Flux X 10⁻⁵(J/m)
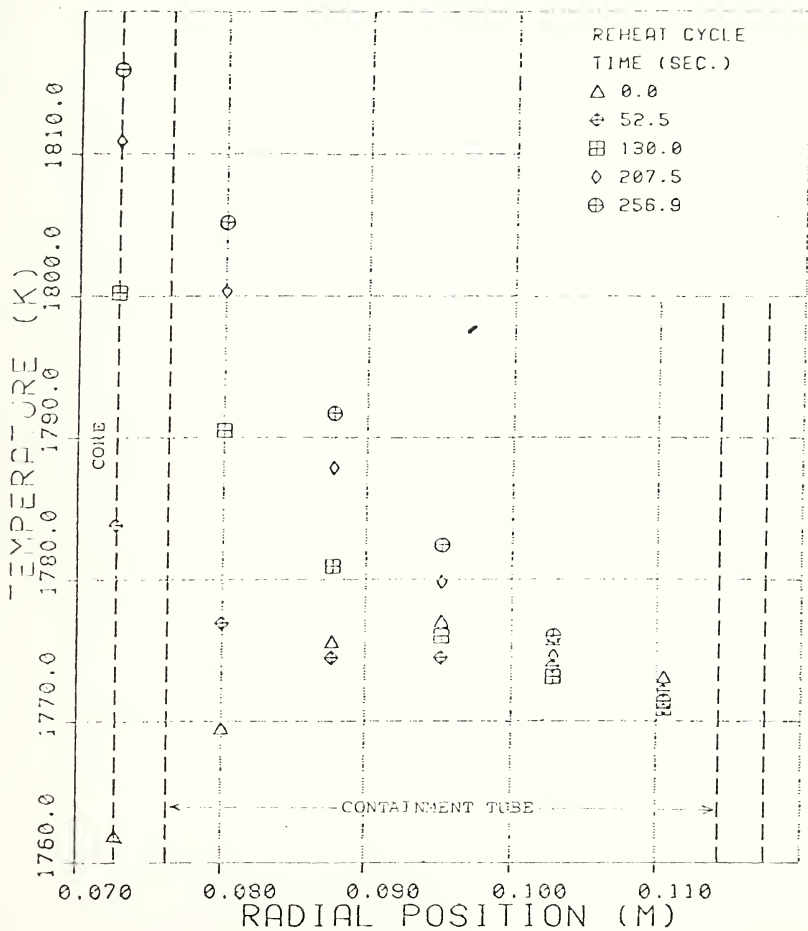
Figure 2.--Temperature of the core and containment tube during a cyclic
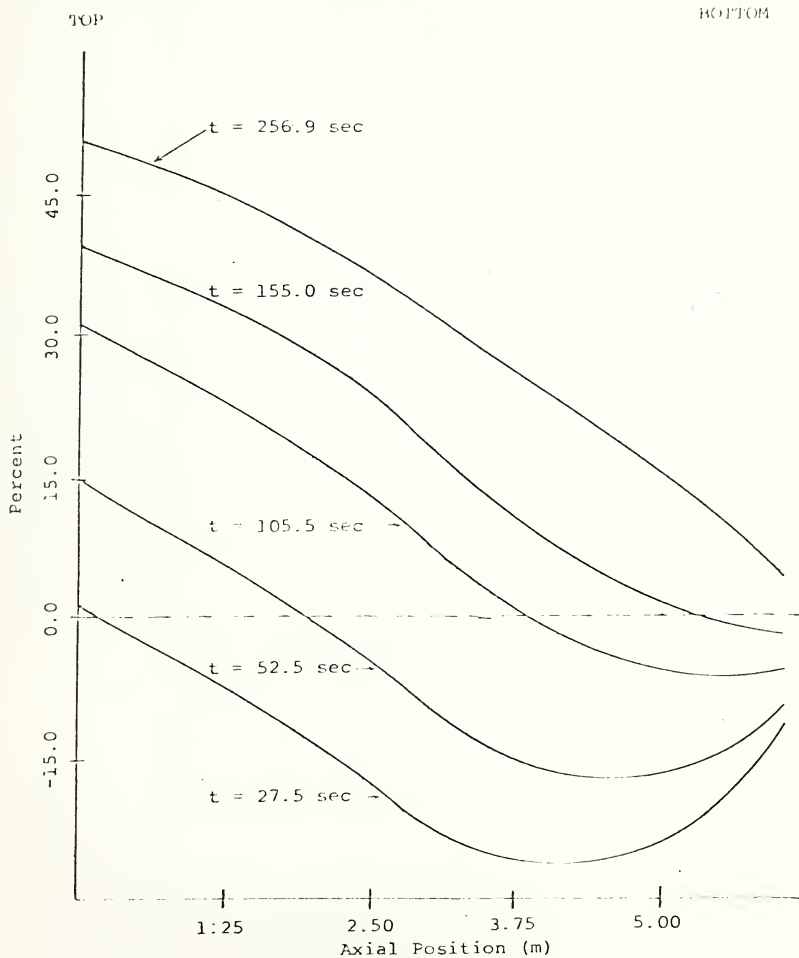equilibrium reheat cycle axial position 2.7 cm from bed top

Figure 3.--Percentage of gas to core heat transferred from core to
        containment tube during a cyclic equilibrium reheat cycle
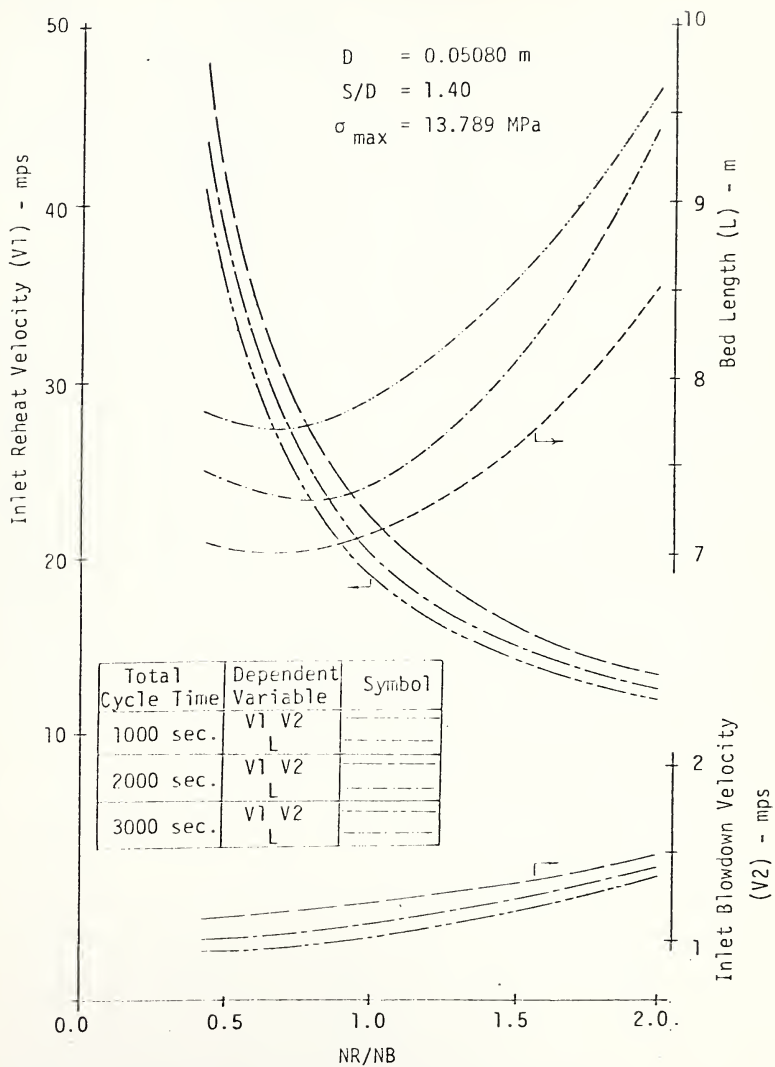
Figure 4.--Length and inlet velocities required to meet ECAS Open-Cycle MHD Base Case 1 specifications
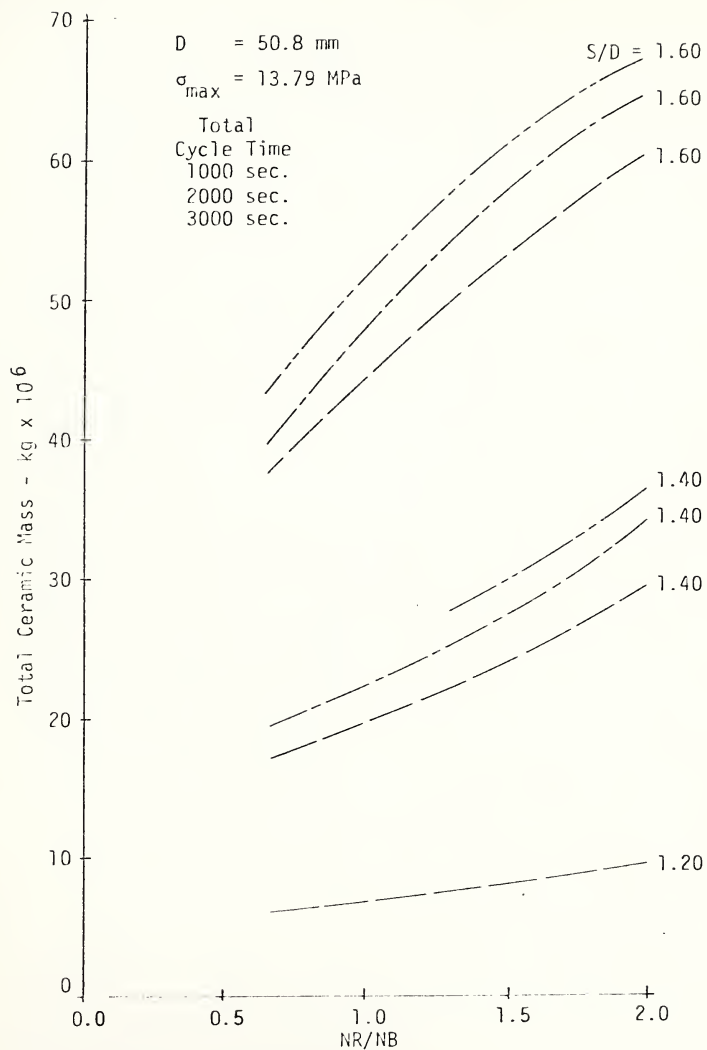
Figure 5.--Total mass of cored ceramic brick required for
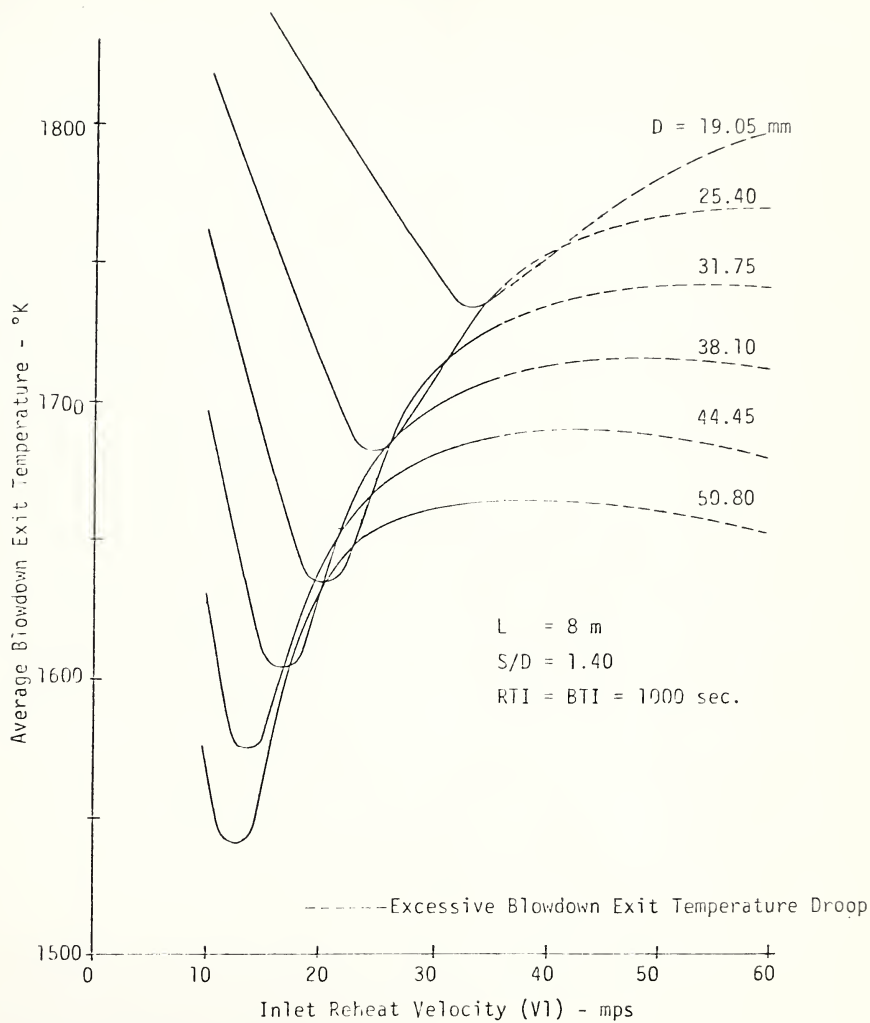ECAS Open-Cycle MHD Base Case 1 air preheater
system designs

Figure 6.--Sensitivity of average blowdown exit temperature
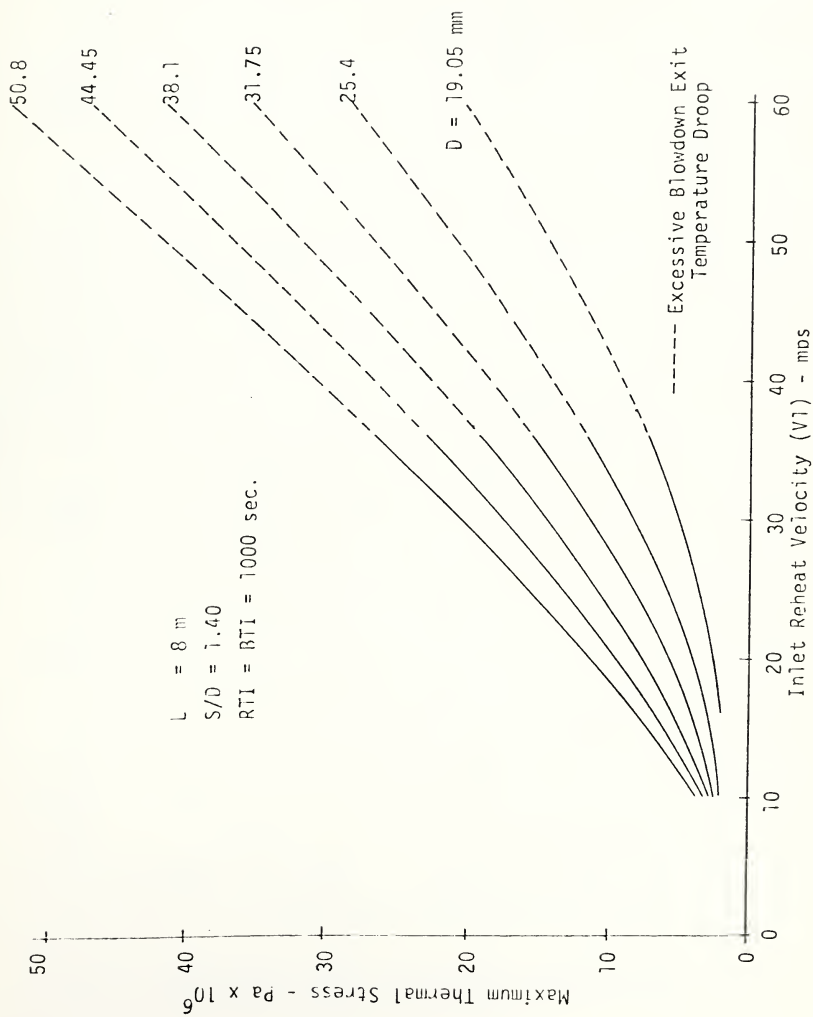to inlet gas velocity and flow hole diameter

Figure 7.--Sensitivity of maximum thermal stress to inlet gas velocity and flow hole diameter
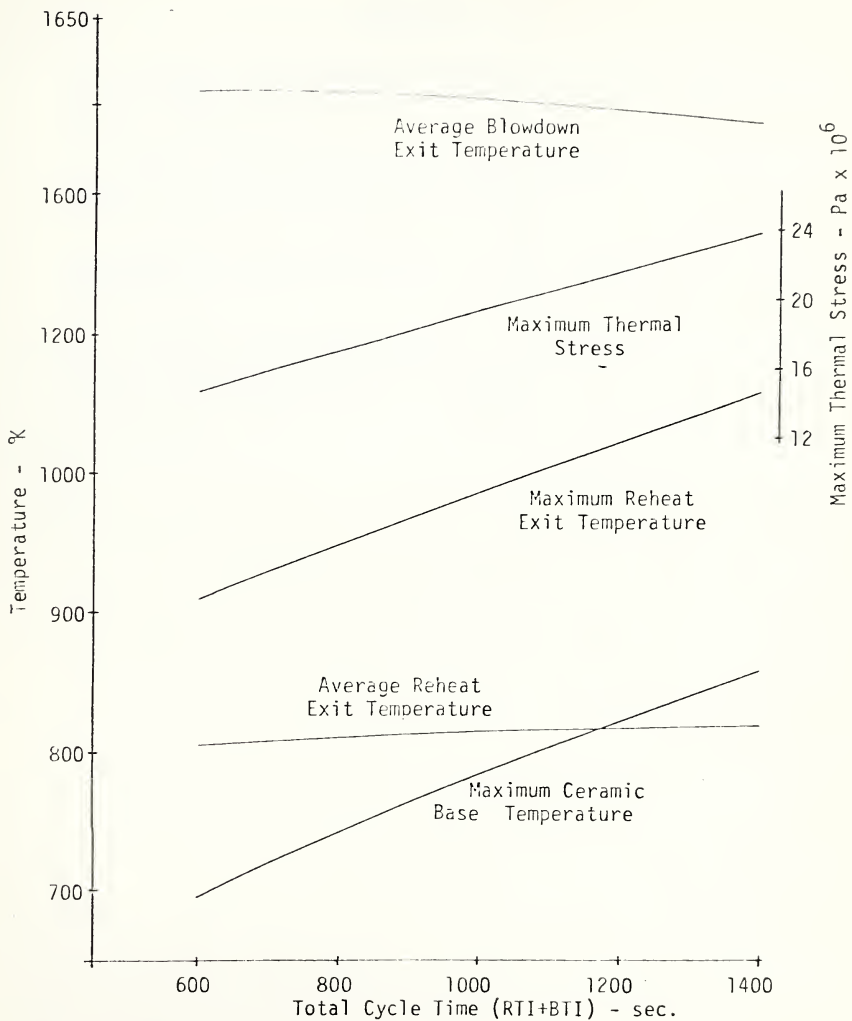
70

Figure 8.--Variation in MTSFF equilibrium conditions for variation in total cycle time

REFERENCES

1. J. C. Corman, et al., "Energy Conversion Alternatives Study--General Electric Phase I Final Report," Lewis Research Center NASA, ERDA, NSF, NASA-CR 134948, 1976.

2. T. A. Ameel, "Thermal Simulation of an Experimental High-Temperature Fixed-Bed Cored-Brick Regenerative Air Preheater," Unpublished M.S. Thesis, Montana State University, Bozeman, 1977.

3. T. C. Reihman, H. W. Townes, and C. J. Mozer, "Thermal Analysis Techniques for Regenerative Heat Exchanger Simulation," ASME Paper 76-WA/HT-7, 1976.

4. G. A. Upshaw, "A Simulation Approach to the Thermal-hydraulic Design of Cored Ceramic Brick Regenerative Heat Exchangers," Unpublished M.S. Thesis, Montana State University, Bozeman, 1977.

5. J. Nikuradse, "Laws of Flow in Rough Pipes," NACA TM 1292 (1950).

TASK F
Slag-Seed Equilibria and Separations Related to the MHD System
R. Woodriff, R. Howald, J. Amend, I. Eliezer, and N. Eliezer

ABSTRACT

Measurements of potassium vapor pressures over the potassium oxide-silicon oxide system were concluded. Measurements of potassium vapor pressures over slags and seeded slags were continued. Measurements of potassium vapor pressures over the ternary system potassium oxide-silicon oxide-aluminum oxide were initiated. The thermodynamic analysis of the results together with literature data has led to a phase diagram of the potassium oxide-silicon oxide system and a preliminary phase diagram of part of the $K_2O-SiO_2-Al_2O_3$ system.

I. OBJECTIVE AND SCOPE OF WORK

The main purpose of this work is to provide the physicochemical information required for the incorporation of a seed separation and recovery process in the MHD system. Therefore, the objectives of the work are as follows:

1.   The experimental determination of the vapor pressure of potassium, seed compounds, and other elements and compounds over coal slag; and

2.   The thermodynamic analysis of the equilibria in the vaporization and condensation sequences in the above systems under the MHD conditions of operation.

Thus, the scope of work includes species other than seed compounds.

The first objective is to be accomplished by use of the Woodriff furnace, which was originally developed at Montana State University for atomic absorption analysis. The vapor pressure of the relevant elements and compounds will be measured by heating them in cells located in the furnace near the optical path, then monitoring the escaping vapor by atomic absorption spectroscopy. Modifications must be made in the furnace to provide isothermal or increasing-thermal gradient operation, to permit measurements unperturbed by vapor condensation, to obtain reproducible response curves for the vapors measured, and to measure, simultaneously, the vapor pressures of the elements and compounds or mixtures. This last task necessitates the development of appropriate optics and electronics for use with a direct reader.

The scope of the experimental work will include synthesis or preparation of the relevant pure compounds, preparation of "Knudsen" cells of various materials and designs, preparation of double-window hollow-cathode lamps, and conversion of a Jaco polychromator to permit integrated atomic absorption measurements.

The second objective will be accomplished, mainly, by developing and applying appropriate computer programs that will utilize the experimental data obtained on site and also data available in the literature or supplied by other investigators. These computer programs will assist in obtaining the thermodynamic parameters, equilibrium constants, and phase diagrams of the systems in question over a range of slag compositions and temperatures expected in MHD operation. This work includes a thorough literature search, the critical evaluation of the experimental research, and the development of reliable extrapolation or estimation techniques whenever necessary.

II. SUMMARY OF PROGRESS TO DATE

A paper summarizing the vapor pressure measurement technique developed for this project was prepared and submitted for publication.

The experimental work on the potassium oxide-silica system was completed and the results, together with a thermodynamic analysis of the system, were presented at the April Argonne MHD Symposium and will be published in the proceedings of the conference.

The work with slags was continued, and potassium vapor pressures were measured over several slag and seeded slag samples.

Work was initiated on the silica-alumina-potassium oxide system, and potassium vapor pressures were measured over several synthetic samples.

The data acquisition system developed for this project was presented at the Stanford MHD workshop in May. Work on the system this quarter was concerned mainly with replication of instrumentation modules to allow the operation of three data-acquisition channels.

The theoretical work this quarter involved work on the mechanism of diffusion of potassium through graphite, inclusion of the thermodynamic properties of $K_2Si_4O_9$ and $K_2Si_2O_5$ in the analysis of the silica-potassium oxide system, and a preliminary analysis of the alumina-silica-potassium oxide ternary system.

III. DETAILED DESCRIPTION OF TECHNICAL PROGRESS

A. Vapor Pressure Measurements

During this period, potassium vapor pressures were measured over several slag and seeded slag samples and over three synthetic SiO_2-Al_2O_3-K_2O samples.

Results for the slags are summarized in Figures 1, 2, and 3. In Figure 1, results are shown for an Avco slag sample, the composition of which is given in Table I. Experimental results are for the original composition and for a seeded sample containing 17 percent K_2O. This sample was prepared by adding the calculated amount of $KHCO_3$ to the slag, grinding to achieve intimate mixing and heating at 660°C for six hours. The lines calculated for both of these compositions and for an additional one higher in potassium are shown in Figure 1.

Figure 2 shows results for Rosebud coal ash at the original and two seeded compositions. These samples were obtained from Dr. R. Pollina; their preparation procedure and compositions are reported in Reference 1.

In Figure 3, results are shown for two seed/slag deposits obtained from Fluidyne Engineering Corporation. The compositions of these samples are shown in Tables II and III. A least-squares treatment of the potassium pressures for slag 83 gives a heat of vaporization of 85 Kcal/mol. A heat value at least as good can be calculated from the mole fraction of $KO_{.5}$ present, giving our best estimate of the potassium pressure for this sample:

$$P_K = 2.69 \times 10^6 \times e^{-86.4/RT} \text{ atm.} \tag{1}$$

If the value $X_{KO_{.5}} = .347$ which we have calculated for sample #78 is correct, the corresponding expression for that slag is

$$P_K = 4.48 \times 10^5 \times e^{-82.4/RT} \text{ atm.} \tag{2}$$

If it actually has a lower potassium content, as indicated by the reported total value of over 100 percent, the calculated line will fit the data even better.

$K_2O\text{-}Al_2O_3\text{-}SiO_2$ samples were prepared from SiO_2, Al_2O_3 and $KHCO_3$ ground together thoroughly and heated for six hours at 660°C. When put in the furnace at around 1500°C, it took up to four hours for these samples to reach a constant absorbance. Results for three samples are shown in Figure 4.

A paper summarizing the vapor pressure measurement technique developed for this project was submitted for publication.[2] It evaluates the capabilities of the technique and analyzes the vapor loss mechanisms in the furnace.

B. Data Acquisition System

The work this quarter was concerned principally with replication of the instrumentation modules developed previously. By the end of June, we expect to have enough modules on hand for three data acquisition channels.

At the MHD workshop on optical diagnostics held at Stanford in May, a paper was presented describing our data acquisition system.[3] It appears that the MHD group at Mississippi State is working on modeling the combustion system and downstream flow, and the group is very interested in obtaining a working system for installation on their apparatus. The problems of high background (both emission and absorption) which our system handles well are common to both our work and theirs. We presently are carrying on correspondence regarding this work and may submit a proposal to ERDA for MSU to fabricate and deliver a working system to this group.

C. Thermodynamic Analysis

The theoretical work this quarter centered primarily on calculation of the vapor pressure results for the $KO_{.5}-SiO_2$ system. The initial calculation was completed in time for presentation at the Argonne meeting in April. A copy of that paper is included as Appendix B in this report. The calculations were continued in May to include the thermodynamic properties of both $K_2Si_4O_9$ and $K_2Si_2O_5$, and the calculated phase diagram is given in Figure 5. One additional refinement loop through the calculations is required, and then the results will be submitted for publication. This calculation has been delayed until next quarter in order to devote time to the two major areas described below--the mechanism for the diffusion of potassium through graphite and a preliminary analysis of the $KO_{.5}-AlO_{1.5}-SiO_2$ ternary system.

A number of experiments on the motions of potassium atoms within the Woodriff furnace were performed during this quarter. They provided experimental confirmation of the predicted (exponential or hyperbolic sine) steady-state distribution of potassium in the graphite tube. In addition, the temperature dependence of the diffusion process through the graphite walls was obtained. A paper on this material has been submitted for publication.[4] The general agreement between the activation energy for this diffusion process and the heat of vaporization of potassium from graphite clearly indicates that the rate-limiting process in this diffusion is transfer from one graphite grain to the next rather than motion of the potassium atoms within a layer in the grain. A paper supporting this conclusion is being prepared.[5]

The ERDA panel, which reviewed the MSU/MHD program in May, suggested that Task F concentrate on the $KO_{.5}-AlO_{1.5}-SiO_2$ ternary system to further evaluate our experimental technique for vapor pressure measurements. We believe that our results for the $KO_{.5}-SiO_2$ system (see the Argonne paper attached) and on slags show conclusively that our procedures give good vapor pressure data, particularly in the ranges of $KO_{.5}$ mole fractions of most interest to MHD. However, we agree that additional experimental data and a full theoretical analysis are needed for this important ternary system. As mentioned above, three low silica ternary samples have been tested experimentally, and a preliminary analysis has been made of the thermodynamic data available for sanidine, leucite, and kaliophilite. Values are available for these three solids in Bulletin 1259 of the U.S. Geological Survey (1968). However, it is widely recognized that there are substantial errors in the enthalpy values for the aluminum compounds listed there. The major cause of these discrepancies is in the values used for the enthalpies of Gibbsite, γ-alumina, and $AlCl_3 \cdot CH_2O$ used by workers using HF calorimetry. Therefore, we have recalculated the heat of formation of leucite and kaliophilite from the original data, and the results are shown in Table IV.

The original calculation of Barony and Adami for leucite was based on $AlCl_3-CH_2O$ instead of gibbsite; this seems to be less accurate even after recalculation by Thompson.[6] Thompson's calculation for kaliophilite, -- 506.870, is in excellent agreement with ours, and we have used his values

for further calculations. We have not performed the similar calculation for sanidine since the correction has been made by Chatterjee and Johannes.[7] These heat values should be valid within $\pm$ 1 kcal mol^{-1}. Good entropy and heat capacity data are available for all three of these compounds, and we have used these for our preliminary calculations with only one exception. We have increased S_{298} for sanidine to 54.56 from the value 53.26, reported by Chatterjee and Johannes, in order to avoid disproportionation of sanidine into cristobalite and leucite at 1200 K and above. A computer listing of the resulting calculations of high temperature enthalpy, free energy function, and heat capacity for these three materials is included in Appendix A.

With these values (together with our earlier values) for cristobalite, mullite, corundum, β-alumina, and $KAlO_2$, it is possible to calculate the activity of $KO_{.5}$ and the potassium pressure at a particular temperature for a set of coexisting solid phases, stable or metastable. Figure 6 shows a preliminary diagram for the calculated equilibria of three solid phases at 1500 K.

We have examined three separate high-alumina compositions in molybdenum cells in our furnace. In all these samples, a substantial amount of $KO_{.5}$ first is vaporized, but stable plateau pressure readings are obtained eventually. The effects of metastability are clear, since different plateaus can be reached from a particular sample. More work is needed to establish conclusively the phases present in particular runs, but the tentative assignments shown in Table V are sufficient to show that the Woodriff furnace does give good pressure measurements for these samples. When the assignments are confirmed, the thermodynamic values for the solid phases can be adjusted to give even better agreement. Work with samples in this composition region is continuing. We also are preparing samples higher in silica, which will be partially or completely liquid at the experimental temperatures. The liquid phase helps in reaching equilibrium, and we expect to get as good or better vapor pressure data for these additional samples. This data is less essential to the thermodynamic treatment of the ternary system since there already is a substantial body of equilibrium data on solubilities in the liquid phase.

In addition to the major theoretical efforts outlined above, there were two substantial theoretical achievements during this quarter. Using the thermal diffusivity data of Bates, we demonstrated that the Redlich-Kister equations can be used to represent transport data on slags in cases where one composition is varied, keeping the relative amounts of the other components constant. We hope to use our computer to store coefficients representing various measured properties for a large number of different slags. We also have calculated properties of two additional gas phase potassium species, $K_2CO_3(g)$ and $K_2O(g)$, based upon the recent measurements of Simmons, Towden, and Ehlert.[8]

IV. CONCLUSIONS

Substantial progress has been made in generating experimental vapor pressure data. Instrumentation for data acquisition will allow three-channel operation by the end of the next quarter. The thermodynamic analysis methods are proving very productive, not only for thermodynamic but also for transport properties.

DIVISION OF MAGNETOHYDRODYNAMICS

MONTHLY PROJECT MANAGEMENT STATUS REPORT

REPORT DATE _____

CONTRACT/PROJECT

CDIF Project Management Support and Related MHD Dev. Effort

CONTRACT NO.   VENDOR
EF-77-C-01-2524   Montana State University

FOSSIL ENERGY

77-002   SCHEDULE

Task F - Slag Seed Equilibria and Separations Related to the MHD System

TASK F

YEAR   1977
MONTH   O N D J F M A M J J A S

MAJOR MILESTONES AND DECISION POINTS   VARIANCE

COMPLETE CHECKOUT OF DIGITAL ABSORBANCE READOUT

COMPLETE CHECKOUT OF THREE-COMPONENT COMPUTER PROGRAM

COMPLETE BACKGROUND CORRECTIONS CIRCUITRY

COMPLETE CHECKOUT OF NOBLE METAL FURNACE

COMPLETE ANALYSIS OF TWO LITERATURE BINARY SYSTEMS

STATUS DATE
SCHEDULE PLAN
PROGRESS

STATUS DATE

VARIANCE OR PROBLEM FLAG IN RIGHT COLUMN

ADMINISTRATIVELY CONFIDENTIAL

DIVISION OF MAGNETOHYDRODYNAMICS
MONTHLY PROJECT MANAGEMENT STATUS REPORT

REPORT DATE _____

CONTRACT/PROJECT
CDIF Project Management Support and Related MHD Dev. Effort

CONTRACT NO.   VENDOR
EF-77-C-01-2524   Montana State University

77-002   SCHEDULE

Task F - cont. Page 3

FOSSIL ENERGY

TASK F

	YEAR		1977												VARIANCE
	MONTH	O	N	D	J	F	M	A	M	J	J	A	S	

MAJOR MILESTONES AND
DECISION POINTS

COMPLETE ANALYSIS OF
MEASURED AND LITERATURE
TERNARY SYSTEMS

STATUS DATE _____

SCHEDULE PLAN △▷   STATUS DATE

PROGRESS ◆▶

ADMINISTRATIVELY CONFIDENTIAL

VARIANCE OR PROBLEM FLAG IN RIGHT COLUMN ◇

81

TABLE I.--Composition of Avco Slag

P_2O_5	0.58
SiO_2	42.11
Fe_2O_3	18.91
Al_2O_3	23.63
TiO_2	1.38
CaO	6.00
MgO	1.35
SO_3	2.20
K_2O	2.08
Na_2O	1.61
Undetermined	0.15

TABLE II.--Composition of Slag #78

(as determined by Coors Spectrochemical Laboratory)

Element	Percent
Aluminum (Al_2O_3)	$10.6 \pm .3$
Antimony	<0.003
Arsenic	<0.01
Barium	0.1
Beryllium	<0.001
Bismuth	<0.005
Boron	<0.003
Cadmium	<0.05
Calcium (CaO)	$10.2 \pm .3$
Chromium	<0.003
Cobalt	<0.01
Copper	0.003
Gallium	<0.007
Germanium	<0.005
Indium	<0.005
Iron (Fe_2O_3)	$2.0 \pm .2$
Lead	<0.009
Magnesium	2.0
Manganese	0.2
Molybdenum	<0.01
Nickel	<0.01
Phosphorus	<0.3
Silicon (SiO_2)	$49.2 \pm .3$

TABLE II.--(continued)

Element	Percent
Silver	<0.001
Strontium	0.5
Tin	<0.003
Titanium	0.3
Vanadium	0.005
Zinc	<0.08
Zirconium	0.01
Sodium (Na_2O)	$1.0 \pm .1$
Cesium	<0.001
Lithium	0.005
Potassium (K_2O)	$34.0 \pm .3$
Rubidium	0.02
Sulfur	0.39

TABLE III.--Composition of Slag #83
(as determined by Coors Spectrochemical Laboratory)

Element	Percent
Aluminum	7.5 ± 0.8
Antimony	<0.003
Arsenic	<0.01
Barium	0.2
Beryllium	<0.001
Bismuth	<0.005
Boron	<0.003
Cadmium	<0.05
Calcium	4.3 ± 0.5
Chromium	0.3
Cobalt	<0.01
Copper	0.002
Gallium	<0.005
Germanium	<0.005
Indium	<0.005
Lead	<0.08
Magnesium	11 ± 1.0
Manganese	0.1
Molybdenum	<0.01
Nickel	<0.01
Phosphorus	<0.3
Silicon	17 ± 1.0
Silver	<0.001
Strontium	0.02

TABLE III.--(continued)

Element	Percent
Tin	<0.003
Titanium	0.3
Vanadium	0.02
Zinc	<0.08
Zirconium	0.01
Sodium	0.9
Cesium	<0.001
Lithium	0.001
Potassium	18 ± 1.0
Rubidium	0.001
Ferrous	0.20 ± 0.02
Ferric	2.6 ± 0.3

TABLE IV.--Heats of Formation of Leucite and Kaliophilite

Compound	ΔH_f^0 Reported	Reference	ΔH_f^0 Recalculated
$KAlSi_2O_6$ (c, leucite)	-----------	Krocek, Ann. Rep. Dir. Geophys. Laboratory, paper 1215 (1953)	-726.320
$\gamma-Al_2O_3$	-394.95	Yokokawa and Kleppa, J. Phys. Chem. 68 3246 (1964)	
$KAlSi_2O_6$ (c, leucite)	-721.630	Barony and Adami, U.S. Bureau Mines, R.I. 6873	-726.210
$KAlSiO_4$ (c, leucite)	-503.800		-506.753
$Al(OH)_3$ (c, gibbsite)	-309.325	Hemingway and Robie, and Gross, Christie and Heyman, cited by Thompson (ref. 6)	

TABLE V.--Comparison of Observed and Calculated Potassium Pressures and Phase Assignments for the K_2O-SiO_2-Al_2O_3 System

Sample	Run	Observed K Pressure Corrected to 1500 K	Tentative Phase Assignment	Calculated K Pressure at 1500 K
1	1	1.7×10^{-7}	corundum, β-alumina, kaliophilite	1.5×10^{-7}
1	2	1.3×10^{-6}	leucite, β-alumina, kaliophilite	3.4×10^{-7}
2	1	1.3×10^{-6}	leucite, β-alumina, kaliophilite	3.4×10^{-7}
2	2	1.1×10^{-7}	corundum, leucite, mullite	1.1×10^{-7}
3	1	1.1×10^{-7}	corundum, leucite, mullite	1.1×10^{-7}

Figure 1.--Avco coal ash feedstock
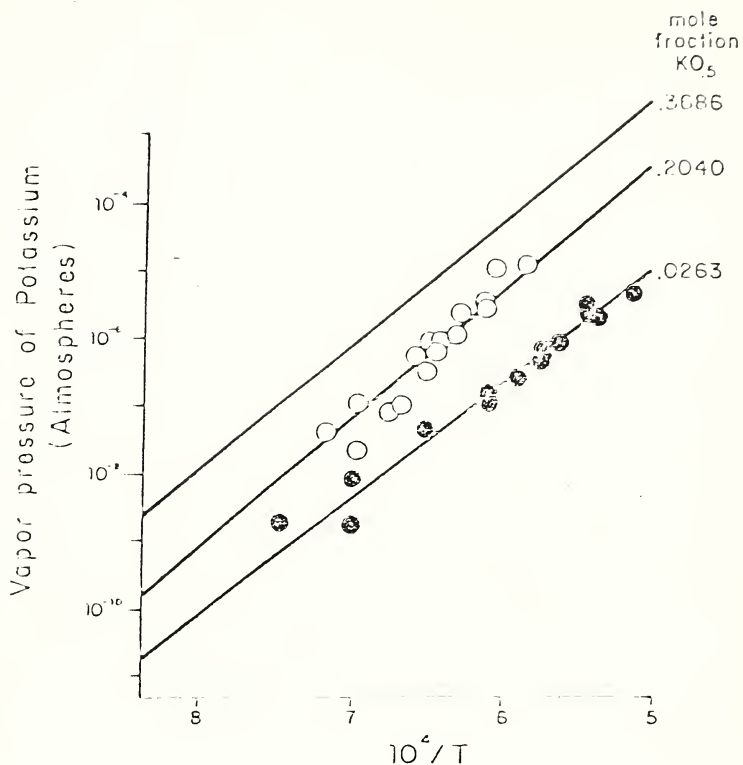
Solid lines calculated using Redlich-Kister equation with the constants:-

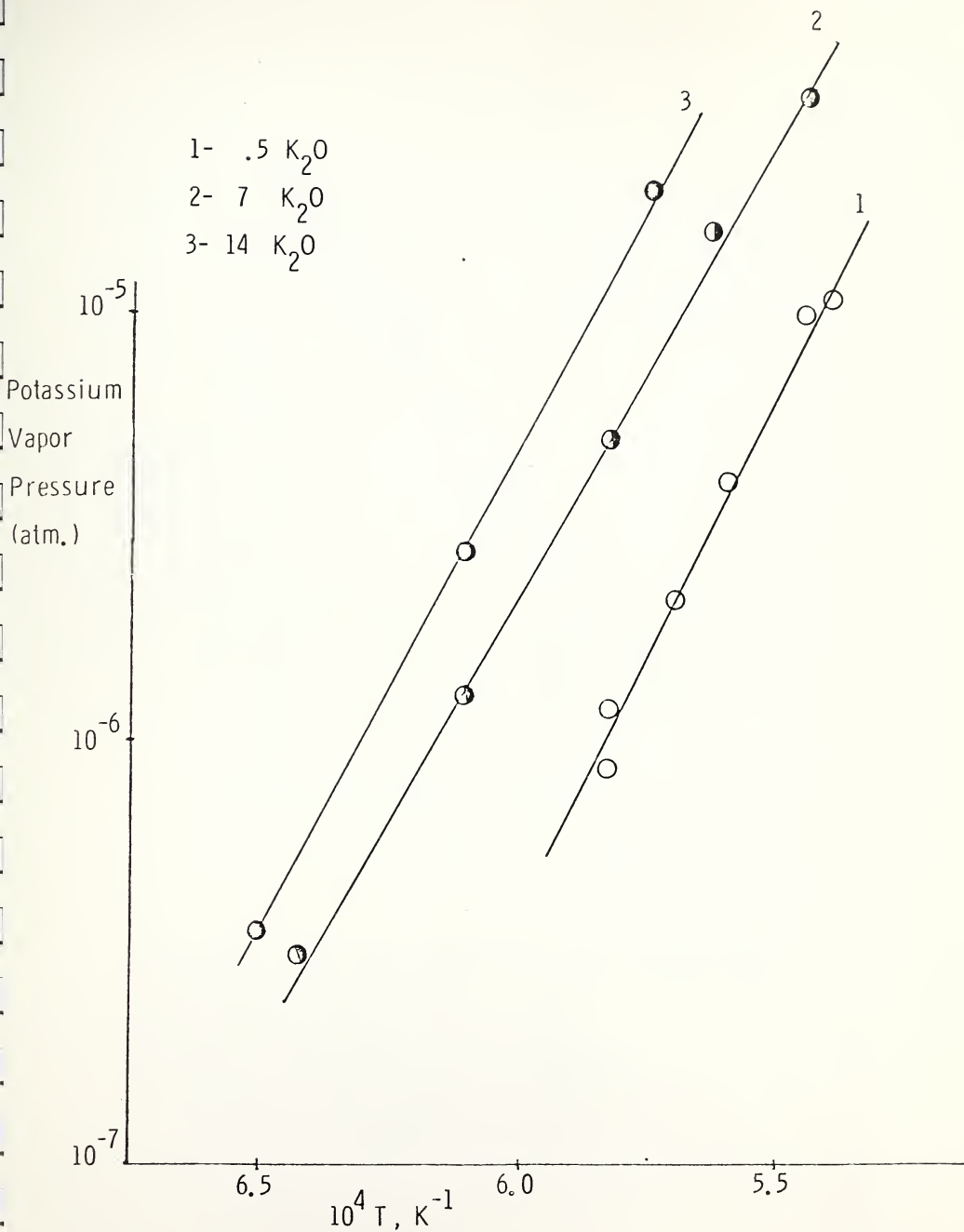|	$\log \gamma_{1000}$	enthalpy
A	-16.742	-98700
B	- 8.616	-57000
C	- 1.0756	0

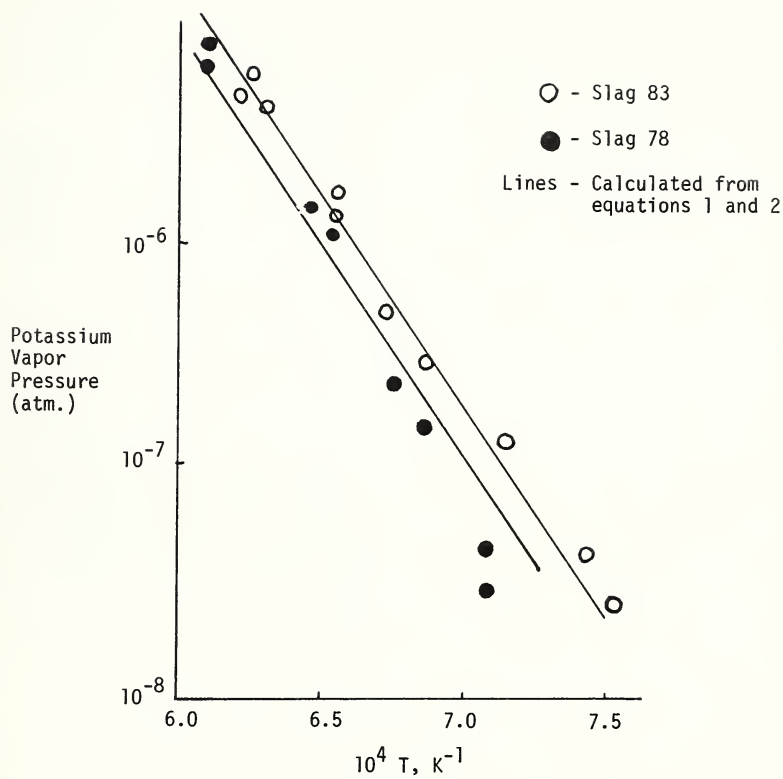Figure 2.--Potassium vapor pressure over Rosebud coal fly ash
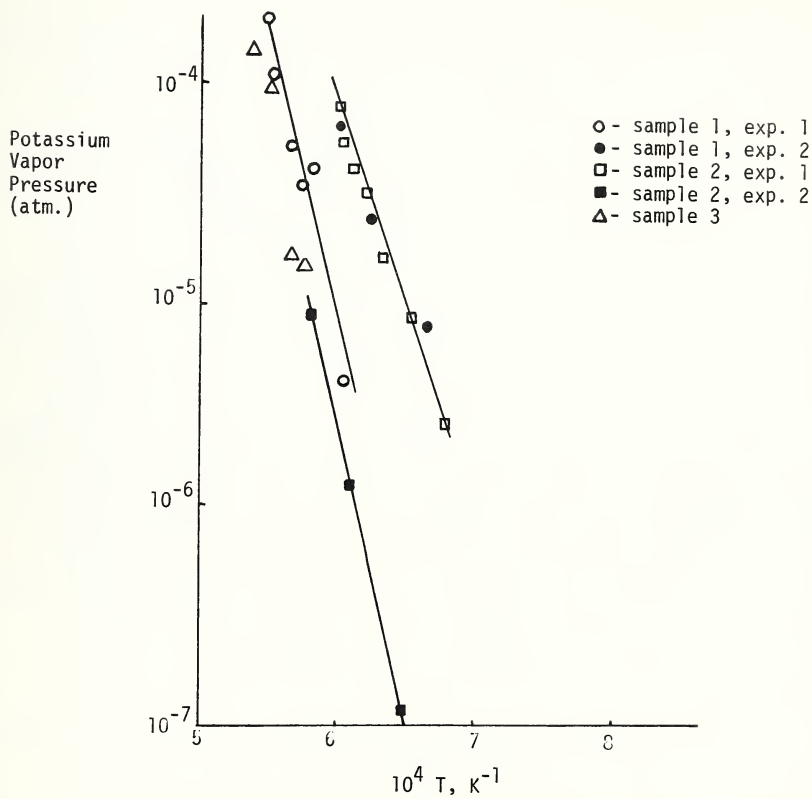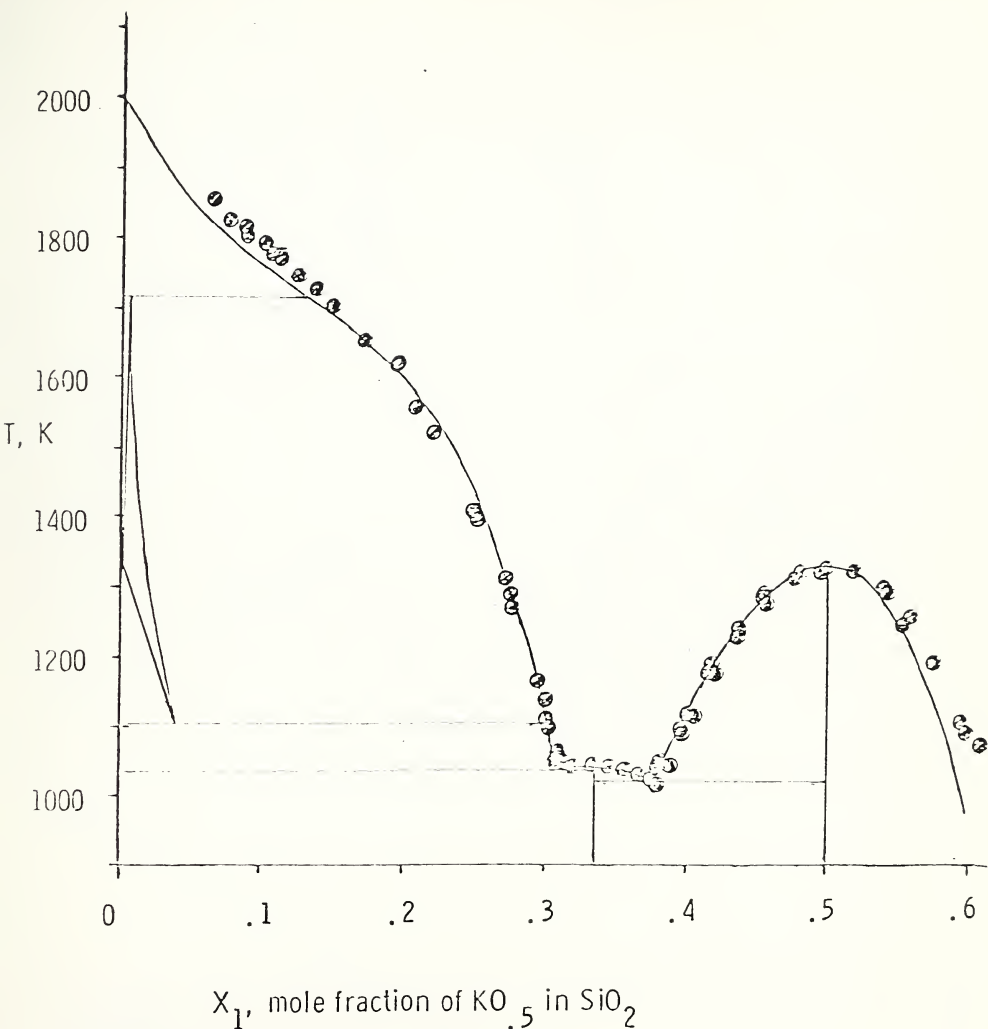
Figure 3.--Potassium vapor pressure over Fluidyne slags

Figure 4.--Potassium vapor pressure over SiO_2-Al_2O_3-K_2O samples

The circles are experimental points of Kracek et al. (1937)

Figure 5.--Computer calculated phase diagram for the $KO_{.5}-SiO_2$ system

93

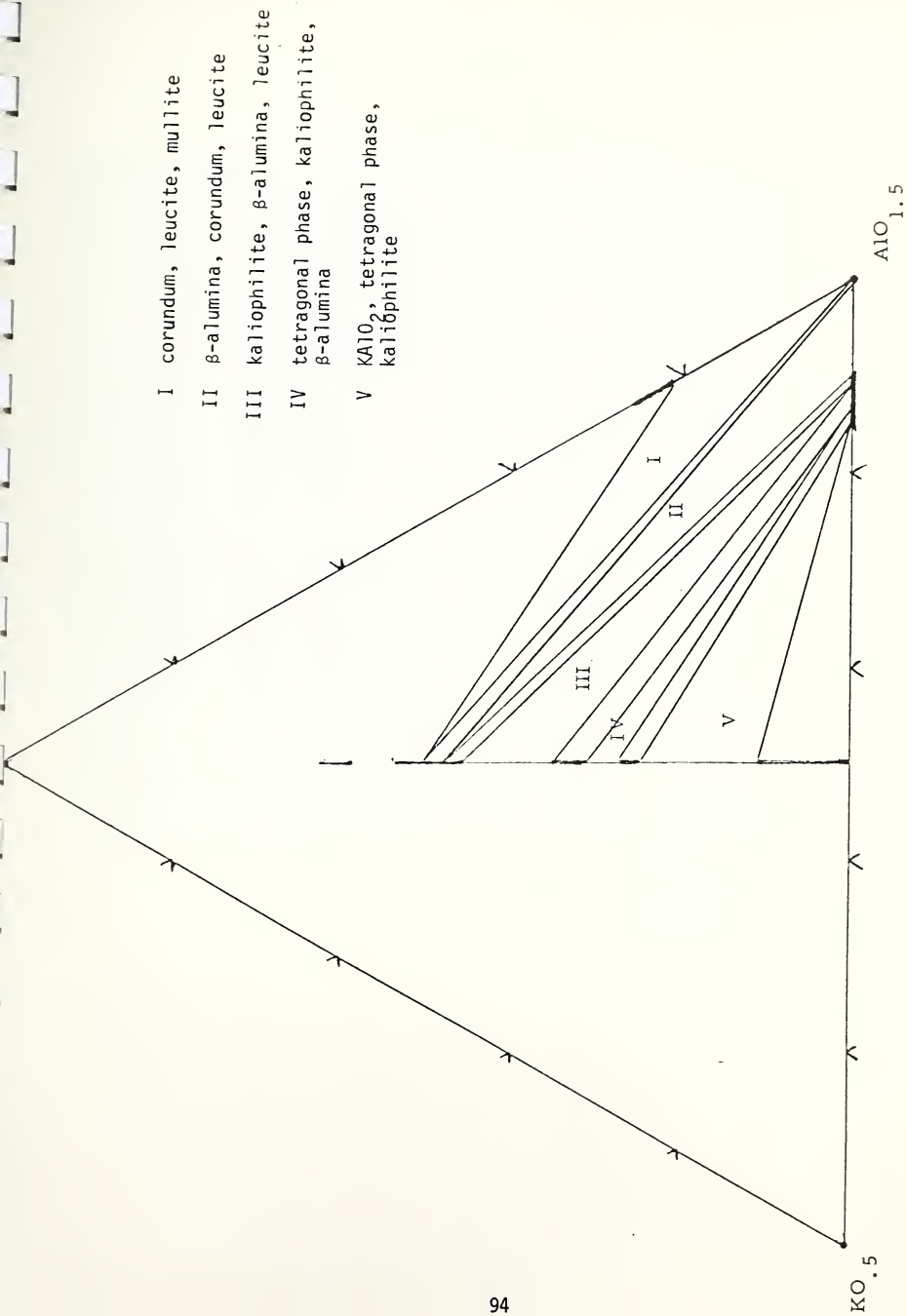I   corundum, leucite, mullite

II β-alumina, corundum, leucite

III kaliophilite, β-alumina, leucite

IV tetragonal phase, kaliophilite, β-alumina

V   KAlO₂, tetragonal phase, kaliophilite

Figure 6.--Regions of three coexisting solid phases at 1500 K

KO.5

AlO₁.₅

```
KALS1308 (C, SANIDI
OMPONENT   1 OF PHASE  3 HO298 IS  -945686.0000   46960.0000
T1000.000 HO = -898736.00000 AND PHI IS   85.379990 CP=   75.50000
T1037.000 HO = -895985.62500 AND PHI IS   87.102676 CP=   75.87000
T1000.000 HO = -898786.00000 AND PHI IS   85.379990 CP=   75.50000
T1050.000 HO = -894998.50000 AND PHI IS   87.701950 CP=   76.00000
T1100.000 HO = -891186.00000 AND PHI IS   89.977371 CP=   76.50000
T1150.000 HO = -887348.50000 AND PHI IS   92.246100 CP=   77.00000
T1200.000 HO = -883486.00000 AND PHI IS   94.388762 CP=   77.50000
T1250.000 HO = -879598.50000 AND PHI IS   96.575894 CP=   78.00000
T1300.000 HO = -875686.00060 AND PHI IS   98.618698 CP=   78.50000
T1350.000 HO = -871748.50000 AND PHI IS  100.648335 CP=   79.00000
T1400.000 HO = -867786.00000 AND PHI IS  102.676956 CP=   79.50000
T1450.000 HO = -863798.50000 AND PHI IS  104.643265 CP=   80.00000
T1500.000 HO = -859786.00000 AND PHI IS  106.571289 CP=   80.50000
T1550.000 HO = -855748.50000 AND PHI IS  108.461502 CP=   81.00000
T1600.000 HO = -851686.00000 AND PHI IS  110.315247 CP=   81.50000
T1650.000 HO = -847598.50000 AND PHI IS  112.133789 CP=   82.00000
T1700.000 HO = -843486.00000 AND PHI IS  113.918488 CP=   82.50000
T1750.000 HO = -839348.50000 AND PHI IS  115.670532 CP=   83.00000
T1800.000 HO = -835186.00000 AND PHI IS  117.391113 CP=   83.50000
T1850.000 HO = -830998.50000 AND PHI IS  119.081421 CP=   84.00000
KALS1206 (C, LEUCIT
OMPONENT   2 OF PHASE  3 HO298 IS  -726210.0000   37930.0000
T1000.000 HO = -688280.00000 AND PHI IS   68.569992 CP=   56.50000
T1037.000 HO = -686187.37500 AND PHI IS   69.960175 CP=   56.61618
T1000.000 HO = -688280.00000 AND PHI IS   68.569992 CP=   56.50000
T1050.000 HO = -685451.06250 AND PHI IS   70.442429 CP=   56.65700
T1100.000 HO = -682614.31250 AND PHI IS   72.267303 CP=   56.81400
T1150.000 HO = -679769.68750 AND PHI IS   74.045776 CP=   56.97099
T1200.000 HO = -676917.18750 AND PHI IS   75.779327 CP=   57.12801
T1250.000 HO = -674056.87500 AND PHI IS   77.469437 CP=   57.28500
T1300.000 HO = -671188.68750 AND PHI IS   79.117691 CP=   57.44200
T1350.090 HO = -668312.68750 AND PHI IS   80.725693 CP=   57.59900
T1400.000 HO = -665428.81250 AND PHI IS   82.294998 CP=   57.75600
T1450.000 HO = -662537.06250 AND PHI IS   83.827255 CP=   57.91299
T1500.000 HO = -659637.50000 AND PHI IS   85.323959 CP=   58.07001
T1550.000 HO = -656730.06250 AND PHI IS   86.786514 CP=   58.22701
T1600.000 HO = -653814.81250 AND PHI IS   88.216400 CP=   58.38400
T1650.000 HO = -650891.68750 AND PHI IS   89.614883 CP=   58.54100
T1700.000 HO = -647960.68750 AND PHI IS   90.983307 CP=   58.69800
T1750.000 HO = -645021.87500 AND PHI IS   92.322811 CP=   58.85500
```

```
T1800.000 HO = -642075.18750 AND PHI IS  93.6:4720 CP=   59.61199
T1850.000 HO = -639120.68750 AND PHI IS  94.919998 CP=   59.16901
CO2 (G)
OMPONENT   4 OF PHASE  3 HO298 IS   -94051.0000    7984.0000
T1000.000 HO =  -86067.00000 AND PHI IS  56.358994 CP=   12.98061
T1037.000 HO =  -85584.81250 AND PHI IS  56.652328 CP=   13.08341
T1000.000 HO =  -86067.00000 AND PHI IS  56.358994 CP=   12.98061
T1050.000 HO =  -85414.56250 AND PHI IS  56.754425 CP=   13.11798
T1100.000 HO =  -84755.43750 AND PHI IS  57.142365 CP=   13.24395
T1150.000 HO =  -84090.25000 AND PHI IS  57.522720 CP=   13.35964
T1200.000 HO =  -83419.62500 AND PHI IS  57.895523 CP=   13.46603
T1250.000 HO =  -82743.81250 AND PHI IS  58.261017 CP=   13.56401
T1300.000 HO =  -82063.31250 AND PHI IS  58.619278 CP=   13.65440
T1350.000 HO =  -81378.43750 AND PHI IS  58.970413 CP=   13.73791
T1400.000 HO =  -80689.68750 AND PHI IS  59.314651 CP=   13.81524
T1450.000 HO =  -79997.06250 AND PHI IS  59.652191 CP=   13.88694
T1500.000 HO =  -79301.00000 AND PHI IS  59.983170 CP=   13.95354
T1550.000 HO =  -78601.81250 AND PHI IS  60.307890 CP=   14.01552
T1600.000 HO =  -77899.50000 AND PHI IS  60.626251 CP=   14.07331
T1650.000 HO =  -77194.50000 AND PHI IS  60.938797 CP=   14.12729
T1700.000 HO =  -76486.81250 AND PHI IS  61.245499 CP=   14.17777
T1750.000 HO =  -75776.81250 AND PHI IS  61.546585 CP=   14.22511
T1800.000 HO =  -75064.31250 AND PHI IS  61.842270 CP=   14.26953
T1850.000 HO =  -74349.87500 AND PHI IS  62.132645 CP=   14.31133
KALSIO4 (S) KALIOPH
OMPONENT   3 OF PHASE  3 HO298 IS  -506870.0000   27100.0000
T1000.000 HO = -479770.00000 AND PHI IS  49.609985 CP=   42.50000
T1037.000 HO = -478197.50000 AND PHI IS  50.604599 CP=   42.50000
T1000.000 HO = -479770.00000 AND PHI IS  49.609985 CP=   42.50000
T1050.000 HO = -477645.00000 AND PHI IS  50.950241 CP=   42.50000
T1100.000 HO = -475520.00000 AND PHI IS  52.260681 CP=   42.50000
T1150.000 HO = -473395.00000 AND PHI IS  53.541168 CP=   42.50000
T1200.000 HO = -471270.00000 AND PHI IS  54.791977 CP=   42.50000
T1250.000 HO = -469145.00000 AND PHI IS  56.013580 CP=   42.50000
T1300.000 HO = -467020.00000 AND PHI IS  57.206619 CP=   42.50000
T1350.000 HO = -464895.00000 AND PHI IS  58.371857 CP=   42.50000
T1400.000 HO = -462770.00000 AND PHI IS  59.510040 CP=   42.50000
T1450.000 HO = -460645.00000 AND PHI IS  60.622116 CP=   42.50000
T1500.000 HO = -458520.00000 AND PHI IS  61.708923 CP=   42.50000
T1550.000 HO = -456395.00000 AND PHI IS  62.771317 CP=   42.50000
T1600.000 HO = -454270.00000 AND PHI IS  63.810150 CP=   42.50000
T1650.000 HO = -452145.00000 AND PHI IS  64.826263 CP=   42.50000
T1700.000 HO = -450020.00000 AND PHI IS  65.820511 CP=   42.50000
T1750.000 HO = -447895.00000 AND PHI IS  66.793655 CP=   42.50000
T1800.000 HO = -445770.00000 AND PHI IS  67.746475 CP=   42.50000
T1850.000 HO = -443645.00000 AND PHI IS  68.679718 CP=   42.50000
```

REFERENCES

1. R. J. Pollina and R. Larsen, "Electrical Conductivity of a Montana Coal Ash," MHD Symposium, Argonne National Laboratory, April 1977.

2. M. Marinkovic and R. Woodriff, "A New Technique for Vapor Pressure Measurements of Potassium over Coal Slags Applicable to MHD Problems," submitted to the "Review of Scientific Instruments."

3. J. R. Amend, "An Integrating Three-Phase Background-Corrected Data Acquisition System for Atomic Absorption Spectroscopy," Workshop on Diagnostics for Combustion MHD, Stanford, May 1977.

4. R. Woodriff, M. Marinkovic, R. Howald, and I. Eliezer, "Sample Loss Mechanism in a Constant Temperature Graphite Furnace," submitted to Anal. Chem.

5. I. Eliezer, R. A. Howald, and M. Marinkovic, "Mechanism for the Diffusion of Potassium Atoms through Graphite," to be submitted to J. Phys. Chem.

6. A. B. Thompson, contrib. Mineral. Petrol. 48, 123 (1974).

7. Chatterjee and Johannes, contrib. Mineral. Petrol. 48, 89 (1974).

8. Simmons, Towden, and Ehlert, J. Phys. Chem. 81, 706 (1977).
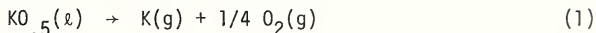
APPENDIX B

VAPOR PRESSURE MEASUREMENT STUDIES ON SLAG-SEED COMPONENT EQUILIBRIA: THE SILICA-POTASSIUM OXIDE SYSTEM*

Naomi Eliezer, R. A. Howald, M. Marinkovic and I. Eliezer
Department of Chemistry, Montana State University
Bozeman, Montana

ABSTRACT

Potassium oxide vaporizes from solutions in SiO_2 primarily according to the equation:

$$KO_{.5}(\ell) \rightarrow K(g) + 1/4\ O_2(g) \tag{1}$$

We have studied this equilibrium using atomic absorption in the Woodriff constant temperature graphite furnace to measure the absorbance of the steady state distribution of potassium atoms. The potassium atoms were introduced at the center of the furnace by diffusion through a small orifice in sample cells which we developed for vapor pressure measurements. These cells are made of molybdenum or platinum. We have shown both experimentally and theoretically that at a particular temperature, the absorbance we measure is proportional to the rate of diffusion of potassium atoms from the vapor pressure sample cells. For a particular cell with a particular orifice, there is a temperature dependent conversion factor between absorbance and pressure which we evaluated from measurements with potassium aluminate standards in the cells.

It was possible to measure the pressure of potassium atoms over a sufficient range of temperature to obtain the heat of vaporization. The Redlich-kister coefficients for the enthalpy of mixing of liquid $KO_{.5}$ and SiO_2: A = -98.7, B = -57 kcal mol^{-1}, were obtained from this data and estimates for the thermodynamic properties of $KO_{.5}$ (liquid), literature data on the enthalpy of glasses, the temperature dependence of rate of vaporization, and the variation of the activity of SiO_2 with temperature.

Redlich-Kister coefficients for log $\gamma_{KO_{.5}}$ were obtained from the concentration dependence of the vapor pressure of potassium over the $KO_{.5}$-SiO_2 samples: A = -10.5729, B = -6.5935, and C = -1.0756 at 1500 K. From these values, together with the enthalpy coefficients above, activities of both $KO_{.5}$ and SiO_2 can be calculated over a wide range of temperatures and compositions.

INTRODUCTION

We have developed a new method of measuring the vapor pressure of samples at high temperatures applicable to the measurement of potassium pressures in equilibrium with slag-like materials. We have used the pressure of β-alumina in equilibrium with corundum in the $KO_{.5}$-$AlO_{1.5}$ system [1] to calibrate the apparatus, and we have applied it to the system $KO_{.5}$-SiO_2. This system was chosen because of its similarity to seeded slags, because some equilibrium thermodynamic measurements are available for comparison [1-3], and because there appears to be a need for additional experimental data to establish the way in which activities vary with temperature and composition in the system.

The samples are placed in molybdenum or platinum cells with a small drilled hole through which vapors can diffuse at high temperatures. These cells are inserted into the center of an electrically heated graphite tube furnace in an atmosphere of argon (Woodriff furnace), and the relative amount of potassium atoms in the graphite tube is measured by atomic absorption. The measured absorbance normally increases within 5 to 15 minutes to a steady-state value, where the rate of diffusion out of the cell equals the rate at which potassium atoms leave through the ends and walls of the graphite tube. For a particular sample cell, the steady-state absorbance is proportional to the pressure of potassium atoms inside the cell. There is, however, a substantial exponential temperature dependence for the proportionality constant:

$$P = c_{cell} \, e^{-39/RT} \quad \text{(absorbance)} \tag{2}$$

The value of 39 kcal mol^{-1} is the average obtained with two separate graphite tubes with cells filled with a mixture of corundum and potassium β-alumina. The equilibrium vapor pressures for this system are known from the work of Plante et al. [1].

Equation 2 also fits the temperature dependence observed in a second graphite tube furnace. The agreement between the data in the different furnaces is a clear indication that the value 39 Kcal mol^{-1}, depends more on the nature of the potassium-graphite interaction (diffusion coefficients and the equilibrium constant for compound formation) than on the geometry of a particular Woodriff furnace.

EXPERIMENTAL

1. Preparation and Analysis of Samples

Samples in the system $KO_{.5}$-$AlO_{1.5}$ were prepared by grinding together and then heating weighed amounts of Al_2O_3 and $KHCO_3$ in covered platinum crucibles in a gas furnace. The temperature was gradually increased to around 1000°C during 1 to 4 hours, then to 1000-1100°C where it was kept for 8-12 hours, and finally to 1250°C for another 8-12 hours. About 600 mg for each sample were prepared.

$KO_{.5}$-$SiO_{.2}$ samples were prepared by grinding mixtures of potassium silicate and either potassium bicarbonate or silica, heating to 630-650°C for about 5 hours, grinding again, and storing in a desiccator. The potassium content of samples was determined by dissolving them and measuring potassium concentration in the solutions using the Varian Atomic Absorption Spectrophotometer, model 1100.

2. Potassium Vapor Pressure Measurements

These measurements were carried out by atomic absorption using a graphite furnace. The essential features of the furnace are described in [4], and its modifications for vapor pressure measurements are reported in [5]. The temperature of the area where the sample is introduced was measured by optical pyrometer. The sample cells were made of platinum or molybdenum. Molybdenum has sufficient strength at high temperatures to allow the use of cells with a screw closure. Molybdenum has a tendency to stick, and to

prevent sealing the cell into the furnace, the pedestal on which the molybdenum cells sit was rotated during the time the cell was in the furnace. With the molybdenum cells, different tops with different hole sizes could be screwed onto the base holding any particular sample. However, for loading platinum cups, the bottom was sawed off, the sample was introduced, and the bottom was welded back on.

Calibration was carried out for each cup, before and several times between measurements. A $KO_{.5}$-$AlO_{1.5}$ sample was put in the furnace and plateau transmittance values were recorded. The same procedure was followed for measurements of $KO_{.5}$-SiO_2 samples.

Two different procedures were used in collecting data, with one furnace each sample was measured at a series of temperatures once it was inserted into the furnace. In the other furnace, the usual procedure was to adjust the furnace temperature and then take readings on a series of samples. Both procedures gave accurate vapor pressures and no distinction is made between them in the analysis of the data.

RESULTS

In analyzing a two component system like $KO_{.5}$-SiO_2, it is desirable to have enthalpy data available as well as activity data. However, there are no good measurements of the high temperature enthalpies or heat capacities of liquid potassium silicates, and even the heats of fusion of potassium silicates are not well established. The enthalpies at 25°C for two potassium silicate glasses have been measured [6] and reported [7], although the details [8] were apparently never published. These values can be combined with our selected values for liquid $KO_{.5}$ and SiO_2 at 25°C to obtain Redlich-Kister coefficients [9,10] (A = -90,000, B = -68,000 cal mol^{-1}) for the enthalpy at 298 K. The values at high temperatures should be similar; in fact, this is confirmed by measurements on the temperature dependence of activity coefficients.
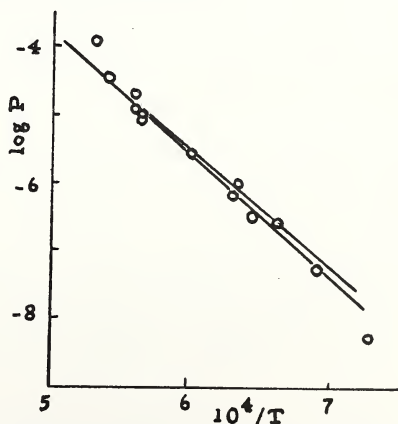

Figure 1.--Observed and calculated pressures for the sample with $X_{KO_{.5}}$ = .14440.

It is hard to obtain accurate vapor pressure measurements on a $KO_{.5}$-SiO_2 liquid of a particular composition over a wide temperature range because at low temperatures, the liquids are quite viscous. They may be present as a homogeneous glass, but is is also possible to have a liquid saturated with a solid such as tridymite or even an intermediate non-equilibrium state. This is illustrated by the calculated lines in Figure 1 for a sample with the overall composition $X_{KO_{.5}}$ = .1444. If the lower temperature values are included in a least squares analysis, the apparent heat of vaporization is low, and if they are omitted, one is left with a temperature range of only 111°. We have omitted points at temperatures where a solid would be present at equilibrium from the initial treatment of the data. This leaves five samples for which the measurements span a temperature range of at least 200°. One of these (X = .4719) is in error for reasons considered below and must be dropped from consideration. Table 1 shows the values for $\overline{H}_1$ calculated from our data. These values correspond to Redlich-Kister values of A = -140 and B = -14 kcal mol^{-1}.

TABLE 1.--Partial Molal Enthalpy of $KO_{.5}$ from ℓnP vs. 1/T.

X	$\overline{H}_1$
.21537	-86.8
.28548	-67.3
.33497	-63.5
.34025	-67.1

One can supplement our values with others from the literature, but there are problems in all these cases. The latest NBS measurements [11] have not been published yet. The available values [1] have been analyzed without any allowance for a composition dependence of the heat of vaporization. Preston and Turner [12] have accurately measured the rate of evaporation of potassium oxide from $KO_{.5}$-SiO_2 glasses over a wide temperature range, but the heats of vaporization which they found are too low to correspond to the process:

$$KO_{.5} \text{ (soln)} \rightarrow K(g) + 1/4\ O_2 \text{ (g)} \qquad (3)$$
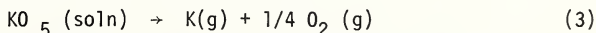
The most reasonable interpretation of their data is that they were measuring evaporation by the process:

$$KO_{.5} \text{ (soln)} + 1/2\ H_2O \text{ (g)} \rightarrow KOH \text{ (g)} \qquad (4)$$
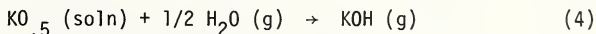
Using values selected for the thermodynamic properties of KOH(g) [13] gives $\overline{H}_1$ values consistent with ours and with the one average value in [1]. These values correspond to Redlich-Kister coefficients of A = -104,000 and B = -33,000. A combined least squares treatment of our values and those in [12] gives A = -125,000, B = -13,000 cal mol^{-1}.

It is clear from these determinations, summarized in Table 2, that A is around -100,000 cal mol^{-1}, but the value for B is not fixed very closely. A good value for B can be obtained, however, from the temperature dependence of $\log \gamma_2$. $\log \gamma_2$ is known at several temperatures and compositions from

the phase diagram measurements. [2] We have selected T = 1784 K, X = .102, K = .94293, log γ_2 = .0212, because we have a substantial amount of vapor pressure data at this temperature. The other point selected is T = 1150 K, X = .293, K = .76281, log γ_2 = .0330. Using our values for log γ_1 as function of composition at 1784 K, one can get log γ_2 ~ -0.1 at X = .293, T = 1784 K by a Gibbs-Duhem integration. This corresponds to a value of $\overline{H}_2$ = 600 + 400 cal mol^{-1} for X = .293. This establishes the equation: $A - 1.628B = 7000 \pm 5000$. The linear combination orthogonal to this is A + .5470B which sum is approximately -130000 (Table 2). This gives A = -98000, B = -58000 cal mol^{-1}. Once enthalpy values are chosen, we have considerably more data on log γ_1 and a better value can be obtained for log γ_2 and $\overline{H}_2$. This process converges in two steps to the final Redlich-Kister values, A = -97600, B = -57000.

Every measured potassium pressure can be converted to an activity of $KO_{.5}$ by assuming the $P_{O_2} = 1/4\ P_K$ and dividing $P_K P_{O_2}^{1/4} = .707\ P_K^{5/4}$ by the corresponding product of the pressures in equilibrium with pure liquid $KO_{.5}$ at the experimental temperature. Pure liquid $KO_{.5}$ cannot be prepared and handled at these temperatures, so the thermodynamic properties assigned to it cannot be checked experimentally. Table 3 shows the values selected for liquid $KO_{.5}$ along with ones for SiO_2 selected to fit the JANAF [14] values, and values for various solids considered later in this paper.

TABLE 2.--Redlich-Kister Coefficients for Enthalpy in the $KO_{.5}-SiO_2$ System.

	A	B	A + .547B
our data	-140	-14	-148
rate of vaporization [12]	-104	-33	-122
joint least squares	-125	-13	-132
enthalpy of glasses, 25°C [6-8]	- 90	-68	-127
selected, including log γ_2 data	- 98.7	-57	-130

TABLE 3.--Thermodynamic Properties for the Pure Materials

	H°_{298}	H°_{1000}	Φ°_{1000}		c_p equation	
	kcal mol^{-1}			a	$b\times10^3$	$c\times10^6$
$KO_{.5}(s)$	-43.2	- 37.2	10.09	9.097	.96	
$KO_{.5}(\ell)$	-36.506	- 27.944	23.57	11.45	1.8	
$SiO_2(\ell)$	-216.01	-205.01	18.20277	16.61	3.2268	1.2384
$K_2Si_4O_9(c)$	-1062.124	-1005.366	90.5716	85.081	9.0876	-3.1173

The calculated activities can be divided by the mole fractions to get activity coefficients at the experimental temperature, and these values can be corrected to a standard temperature of 1500 K using the equation:

$$d \log \gamma_1 / d (1/T) = - \overline{H}_1 / 4.575428 \qquad (5)$$

and values of $\overline{H}_1$ from the Redlich-Kister equation:

$$\overline{H}_1 = (1-x)^2 [-97600 - 57000 (-1 + 4X)] \qquad (6)$$

The values of $\log \gamma_1$ corrected to 1500 K are plotted in Figure 2. Compositions which would have solid present at equilibrium appear twice in Figure 2, as diamonds assuming a non-equilibrium glass of the stoichiometric composition and as squares for the equilibrium liquid composition from the phase diagram of Kracek et al. [2]. Most of these points are closer to the line when the equilibrium liquid assumption is used, but for some, the stoichiometric glass is clearly a better approximation. A choice has been made for each point, and the corresponding square or diamond is shown in solid black. An increased experimental scatter for points at mole fractions above 0.4 is clearly evident in Figure 2. This is probably related to the problems of maintaining a uniform known composition when the vapor pressure of $KO_{.5}$ is relatively high. The effect is most pronounced at lower temperatures and higher $KO_{.5}$ concentrations and is sufficient to prevent an accurate determination of the heat of vaporization of $KO_{.5}$ from the sample at X = .4719 with our apparatus.

The points in Figure 2 were fitted well by the Redlich-Kister coefficients A = -10.5729, B = -6.5935, and C = -1.0756. The solid line in Figure 2 is calculated from these values. From the activities of $KO_{.5}$ and SiO_2 along the liquidus curve for tridymite, we can evaluate the Redlich-Kister coefficients for solid tridymite. Similarly, from the liquidus curve for $K_4Si_4O_9$, we can evaluate the thermodynamic properties of this solid (Table 3). From these parameters it is possible to calculate a phase diagram for the $KO_{.5}-SiO_2$ system. Also the equilibrium vapor pressure of potassium over a $KO_{.5}-SiO_2$ liquid can be calculated as a function of temperature and composition. The solid lines in Figure 1 were calculated in this way.
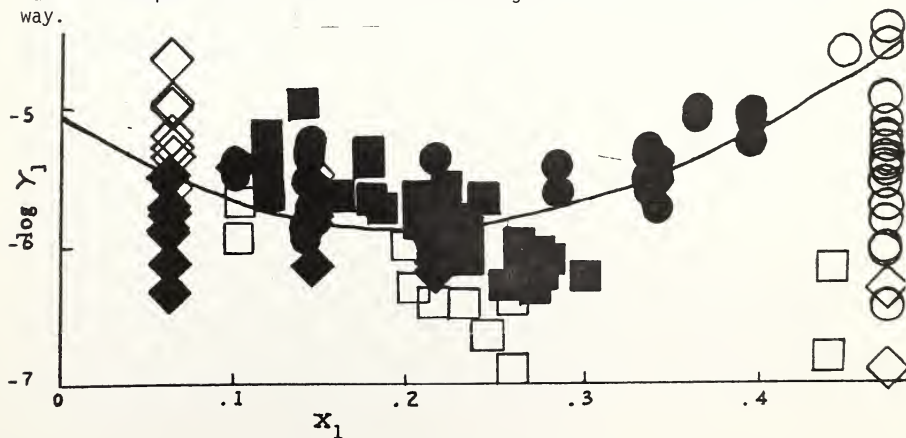

Figure 2.--Log γ_1 vs mole fraction

REFERENCES

[1] E. R. Plante, C. D. Olson, and T. Negas, Sixth International Conference on MHD Electrical Power Generation, Vol. II, 211 (1975).

[2] F. E. Kracek, N. L. Bowen, and G. W. Morey, J. Phys. Chem., 41, 1183 (1937).

[3] R. J. Callow, Trans. Farad. Soc., 46, 663 (1950).

[4] R. Woodriff, Applied Spectroscopy, 28, 413 (1974).

[5] R. Woodriff, M. Marinkovic, and J. Amend, These proceedings.

[6] Kracek, Neuvonen, Burley and Gordon, Ann. Rept. Director of the Geophysical Laboratory, Geophisical Lab. Paper 1215, 69 (1953).

[7] K. K. Kelley, Bureau of Mines, Report of Investigations 5901, 1 (1962).

[8] F. C. Kracek and K. J. Neuvonen, Am. J. Science, 250A, 293 (1952).

[9] R. A. Howald and I. Eliezer, Metallurgical Trans., 8B, 190 (1977).

[10] O. Redlich, A. T. Kister, and C. D. Turnquist, Chem. Eng. Progr., Symp. Ser., 48 no. 2, 49 (1952).

[11] E. R. Plante, Private Communication.

[12] E. Preston and W. E. S. Turner, J. Soc. Glass Technology, 27, 122 (1933).

[13] I. Eliezer and R. A. Howald, J. Chem. Phys., 65 3053 (1976).

[14] JANAF Thermochemical Tables, Nat. Stand. Ref. Data Ser. Nat. Bur. Stand. 37 (1971).

TASK G1
Slag Physical Properties:
Properties of Current Carriers
V. H. Schmidt, S. N. Sharma, and S. Snyder

ABSTRACT

Hall effect apparatus tests were made at room temperature using a commercially available Hall generator chip. The apparatus worked very well. The measured Hall voltage agreed with the rated value, and we observed Hall voltages as low as 3 nV. An attempt to measure the Hall mobility in solid coal slag at 925°C also was made. Excessive noise and drift, which may have originated in the contacts to the sample, made it impossible to measure any Hall voltage, but we were able to establish an upper limit of 0.01 cm^2/volt-sec for the Hall mobility. The Robinson NMR spectrometer was improved and was used in conjunction with a signal averager to search for the Al^{27} NMR signal at room temperature in slag from Montana Rosebud coal. A good signal was observed after annealing the sample. A second NMR spectrometer has been built which appears to have higher sensitivity, but it has not been tested yet with a coal slag sample.

I. OBJECTIVE AND SCOPE OF WORK

The concentrations and mobilities of current carriers in coal slag and seed-slag mixtures are to be determined using Hall mobility and NMR (nuclear magnetic resonance) measurements. Initial measurements will be made at temperatures up to 1600°C, with an eventual goal of 2200°C. The Hall mobility work will begin with a continuation of apparatus check-out, followed by measurements on slag and seed-slag samples. Some design and construction of the NMR apparatus must precede apparatus check-out and sample measurements.

Hall mobility and NMR methods also will be used to examine the nature of conduction processes in certain ceramic materials used or planned for use in MHD channels.

The slags to be examined will be mostly from Western and especially Montana coals. The seed compounds will be potassium carbonate and potassium sulfate. Provision will be made for control of partial pressure of oxygen to maintain reasonable constancy of seed-slag composition during a given run. The ceramics to be tested will be mainly those in which the conduction mechanism at high temperature is in doubt.

II. SUMMARY OF PROGRESS TO DATE

The electronics and experimental procedure were checked out using a commercial Hall generator chip. A test on Rosebud slag at 925°C was made.

The Robinson NMR (nuclear magnetic resonance) spectrometer was improved, and another cw (continuous wave) spectrometer was built. The Al^{27} NMR

signal was observed at room temperature in a slag sample made from Rosebud coal ash.

III. DETAILED DESCRIPTION OF TECHNICAL PROGRESS

A. Hall Mobility

The aim of this experiment is to determine, from Hall mobility measurements, the nature of electrical conductivity in seeded coal slags. Specifically, the aim is to determine whether the current is electronic or ionic. The sample must be large enough so that the crucible and electrode insulators will not be corroded away during the course of a run. Considerable additional space is needed for the heater and thermal insulation. To accommodate the space needed for this apparatus, a large magnet is required. An ac electromagnet of the necessary size would require too much power. Accordingly, a dc electromagnet with a 5-inch gap and a maximum field of 12,000 gauss is being used. The construction and test results of the heater and thermal insulation have been described in previous reports.

To obtain the best possible signal/noise ratio, we are using an ac electric field perpendicular to the dc magnetic field; the Hall field should appear in the third perpendicular direction at the same ac frequency. The ac applied field is supplied by a Princeton Applied Research Model HR-8 Lock-in Amplifier stepped up by a transformer. Because of unavoidable misalignment of the Hall electrodes, an ac signal appears at these electrodes even in the absence of a dc magnetic field. We have provided a bucking circuit with coarse and fine amplitude and phase adjustments to cancel out this spurious ac signal. The desired signal, plus any uncancelled spurious signal, then is fed into the HR-8 pre-amplifier. After amplification, this signal is multiplied electronically by the signal from the HR-8 audio oscillator, and the product signal is run through a low-pass filter. Only signals and noise within a very narrow band near the oscillator frequency produce a dc component in the product signal; noise at all other frequencies is rejected. This dc output is displayed by a chart recorder.

Success in measuring a Hall voltage, using a commercial integrated circuit chip with a Hall generator, gave us confidence in our experimental procedure. The Hall voltage generated by the chip was proportional to the dc output of the lock-in amplifier, which was displayed on a chart recorder. When the magnetic field was reversed, the dc output was shifted above or below a base or reference line, depending on the direction of the field. By varying the magnitude of the magnetic or applied electric field, a proportionate change in the magnitude of the Hall voltage was recorded. We were successful in measuring a Hall voltage as small as 3 nV, with a signal/noise ratio of 2.

Next, we tried to measure the Hall coefficient of a solid sample of Rosebud slag at a temperature of 925°C. Our sample has dimensions of 0.85 cm x 0.27 cm x 0.13 cm and is attached to nickel wire electrodes with silver paint. The assembly was suspended in the alumina crucible inside the furnace.

106

Because of the high resistance of slag[1] (for our sample, $R \sim 1.18$ MΩ at 925°C) and the low impedance of the balance circuit, only a small fraction of any Hall voltage would have appeared at the preamplifier of the lock-in. Hence, our signal-to-noise ratio was not very good, and we observed no Hall voltage. We were able to conclude, however, that the maximum mobility at 925°C was $\mu_{max} = 0.01$ cm^2/volt-sec if electronic conductivity primarily by one carrier (electrons or holes) is assumed. This maximum mobility is lower than almost all mobilities reported[2] in oxides such as Fe_2O_3, so it seems likely that conduction in this slag is primarily ionic at 925°C.

A new balance circuit was designed and built to improve the signal-to-noise ratio. In the new circuit, one of the Hall terminals is connected directly to the "A" terminal of the high impedance preamplifier, thus eliminating electrical loading of the sample. The capacitive impedance to ground of the coaxial cable from the Hall contact to the "A" terminal is compensated by a variable capacitor between the signal generator and the Hall contact. A voltage obtained from a potentiometer is fed into the "B" terminal. For the "A minus B" mode of operation, adjustments of these phase and amplitude controls allow any misalignment voltage to be nulled out so that the dc output of the lock-in is then zero in the absence of a Hall signal.

Difficulty was encountered in doing the experiment with this balance circuit because the balance point of the circuit constantly drifted. This made it impossible to establish a stable base line on the chart recorder, especially in the sensitivity range required by the experiment. The cause of this drift is not known. Possibly, the silver paint connecting the electrodes to the slag sample evaporates slowly and consequently changes the contact resistance. It also may be that temperature fluctuations in the furnace caused the resistance of the sample to vary continuously. Based on Pollina's[1] work, a temperature change of 1 K will produce a 1.44 percent change in the sample resistance.

The furnace was improved by adding clamps to hold the lid down tightly. This maintained the argon atmosphere better and prevented the Grafoil insulation from burning.

B.   Nuclear Magnetic Resonance

We have chosen the Al^{27} nuclear isotope as the NMR probe for the initial study of coal slag because Al_2O_3 constitutes about 20 percent of the slag, and Al^{27} is a good NMR nucleus. Using the Robinson spectrometer, the Varian magnet, and a Northern Scientific NS-575 Signal Averager, we have succeeded in seeing the Al^{27} resonance in Al_2O_3 in an annealed sample of coal slag at room temperature. However, the signal to noise ratio (S/N) is poor. The S/N even in pure Al_2O_3 powder is not very high,[3] and we have only 20 percent Al_2O_3 in the sample. In addition, the presence of para-magnetic iron ions may be responsible for broadening the resonance and reducing the S/N.

Thus, we feel a more sensitive spectrometer is needed. We have designed another spectrometer which has been completed and presently is being optimized using some other samples. We also intend to modify our fixed frequency (14 MHz) Pulse NMR "Spin-Lock" Spectrometer to a lower frequency to suit the magnetic field available to us.

C.   Work Forecast

Hall effect studies of solid slag samples will continue. Platinum paint may be used instead of silver paint to cement the sample to the electrodes since the vapor pressure of platinum at high temperatures is lower than that of silver. This may eliminate the drift problem. Tests on liquid slag samples will be made. Initially, the tests will be on unseeded slag because it is less corrosive to the ceramic crucible and insulating tubes surrounding the electrodes. These tests will be made at temperatures just above the melting point of the slag. We also will begin tests on solid pellets of Fe_2O_3, which we already have prepared.

In the NMR studies, once we observe an Al^{27} signal in slag of S/N = 10 or more, we plan to follow it as a function of temperature at intervals of 100°C. We shall use a quartz crucible in our preliminary experiments.

We shall be making T_1 (nuclear spin-lattice relaxation time) measurements using the pulsed spectrometer to obtain information on diffusion processes in the slag. As a first step, we plan to study the slag in the solid state just below the melting point. These experiments should give information regarding the conduction and diffusion mechanism which should be valuable for coal-fired MHD power plants.

We are planning to study the seeded slag as well. We will choose seed-containing nuclei which provide relatively large NMR signals. The most commonly used seed, so far, is K_2CO_3, but potassium is not very suitable for NMR studies. We may try Na_2CO_3 in place of K_2CO_3 because the chemical properties are almost the same, and Na^{23} is a good NMR nucleus.

IV.   CONCLUSIONS

We were successful in measuring the Hall voltage of a semiconductor chip at room temperature, indicating that the electronics worked well. However, our first attempts to observe the Hall effect in solid slag at high temperatures failed. Deterioration of the sample contacts due to the high temperature must be overcome in order to improve the accuracy of our measurements. With improved accuracy, we should be able to measure any Hall mobility within the usual range for electronic semiconductors. Absence of a measurable Hall mobility then would strongly indicate predominantly ionic conductivity. With our present accuracy, we can state only that it appears likely that ionic conduction predominates in Rosebud slag at 925°C.

Our ability to obtain a good Al^{27} NMR signal from slag at room temperature makes us optimistic about being able to observe this signal at high temperature. The Boltzmann factor will tend to reduce the signal in inverse proportion to the absolute temperature, but the increased ionic motion at high temperature is expected to narrow the line and make it easier to observe.

FOSSIL ENERGY

CONTRACT/PROJECT

CDIF Project Management Support and Related MHD Dev. Effort

CONTRACT NO. EF-77-C-01-2524

VENDOR Montana State University

REPORT DATE

77-002 **SCHEDULE**

Task G1 - Slag Physical Properties:

Properties of Current Carriers

TASK G1

YEAR		1977										
MONTH	O	N	D	J	F	M	A	M	J	J	A	S

MAJOR MILESTONES AND DECISION POINTS

VARIANCE

COMPLETION OF NMR DESIGN

COMPLETION OF NMR CONSTRUCTION

COMPLETION OF NMR CHECKOUT

PARTIAL COMPLETION OF HALL MOBILITY MEASUREMENTS

PARTIAL COMPLETION OF NMR MEASUREMENTS

STATUS DATE

SCHEDULE PLAN

PROGRESS

STATUS DATE

REFERENCES

1. R. J. Pollina, MSU/MHD Quarterly Report, October-December 1976.

2. H. J. van Daal and A. J. Bosman, Phys. Rev. 158, 736 (1967).

3. R. V. Pound, Phys. Rev. 79, 685 (1950).

TASK G2
Physical Properties of Coal Slag: Thermionic Emission

G. Lapeyre and J. Anderson

ABSTRACT

Work has continued on the investigation of the thermionic
emission properties of coal slag. A number of synthetic slag
samples containing varying amounts of potassium oxide were
obtained, and tests were performed on one of these to determine
its behavior when heated in a vacuum. The Auger Electron Spec-
troscopy unit was delivered; the necessary peripheral apparatus
was constructed; and the instrument was checked out for proper
operation. The Auger system was tested successfully on a sample
of stainless steel, and tests were begun on slag samples.

I. OBJECTIVE AND SCOPE OF WORK

The objective of this project is to determine the thermionic emission
properties (e.g., thermionic work function) of coal slag, including slag-
seed mixtures. Evaluation of the need for thermionic emission data on
electrode materials will be made in the context of clean electrodes in hot-
wall, coal-fired channels, and exploratory measurements will be made.

Initial measurements will be performed on synthetic slags of various
compositions at temperatures both below and above the temperature at which
the slag is liquid.

Since the actual surface composition is of paramount importance in
determining the work function and the thermionic emission, in situ surface
analysis will be carried out by Auger electron spectroscopy. Materials
desorbing and evaporating from the surface will be determined by mass
spectrometry.

II. SUMMARY OF PROGRESS TO DATE

For work on potassium-containing synthetic slags, we obtained twenty
samples from the Bureau of Standards containing a systematically varying
amount of potassium oxide. One of these samples, designated K 510, was
prepared and loaded into the measurement apparatus. Heating tests were run
to determine if it was possible to prepare a well-behaved sample geometry
and, if possible, measure the thermionic emission from the slag. Some
difficulty was experienced in producing a uniform layer on the platinum
holder, and the preparation of a suitable slag sample may be more of a
problem than in earlier experiments on slags which did not contain potassium.
Upon arrival of the Auger Electron Spectroscopy (AES) apparatus, the tests
were put aside to set up the AES apparatus. The necessary peripheral
instrumentation was assembled (high voltage ramp, modulation, and detection
units), and the instrument was tested by taking a spectrum of stainless
steel, whose Auger spectrum is well known. The correct elements were
observed in the stainless steel sample, so the Auger technique was tested
on a piece of K 214[1] synthetic slag.

In these first slag tests, carbon and oxygen were identified clearly; iron may have been detected, but it will require additional runs with a better signal-to-noise ratio to bring out the ion spectrum. These tests are now in progress.

III. DETAILED DESCRIPTION OF TECHNICAL PROGRESS

To obtain large thermionic emission from the slag, it generally is assumed that it is necessary to have a substantial surface concentration of potassium, which lowers the work function. To study the effect of potassium on the thermionic emission, we have obtained twenty samples of synthetic slag from the National Bureau of Standards. These samples contain the oxides of aluminum, silicon, calcium, iron, and magnesium in varying amounts and potassium oxide, which varies systematically in concentrations from zero to 30 percent by weight.

A critical part of the experiments is to establish a sample configuration suitable for the experiments. It must be possible to heat the slag sample uniformly; physically, it must have a flat surface in order to position the anode close by. In addition, it should not flow or move about when heated to the point where it is quite fluid. A thin flat slag sample resting on a flat platinum sheet and heated from underneath worked well in earlier experiments with slags not containing potassium. Some heating experiments were performed to see if the configuration worked as well with potassium-containing slag. These tests were on synthetic slag designated K 510, which contains SiO_2, Al_2O_3, Fe_3O_4, CaO, MgO, and K_2O in the proportions (by weight percent) of 32, 12, 12, 16, 8, and 20, respectively. Some difficulties were experienced in making a good sample. However, before the tests could be completed, the Auger electron spectroscopy system arrived. The heating tests then were suspended, and the balance of the time, up to the present, has been employed in setting the Auger system into operation and testing it.

The first test on the Auger system was on a sample of stainless steel, which contained a number of elements which are discerned easily in an Auger spectrum. Figure 1 shows such a spectrum; peaks corresponding to sulfur, carbon, chromium, oxygen, and iron are evident. To clarify the meaning of the spectrum, it is appropriate to explain briefly the principles of Auger electron spectroscopy.[2,3] If an electron is ejected from an inner shell of an atom, the excited atom can decay in such a manner that it emits a second electron from the atom at an energy characteristic of that shell. This phenomenon is called the Auger effect, and the emitted electron is called an Auger electron. Since the shell energies vary from element to element, one can, in principle, identify the atom by measuring the kinetic energy of the Auger electrons. The inner-shell hole is created by bombarding the sample with a beam of electrons (the primary beam) at an energy of about 3000 eV. The primary beam current is about 50 microamperes; when the beam strikes the sample, various scattering processes produce a current of secondary electrons, also measured in microamperes. Since the current of Auger electrons is less than a nanoampere, the instrumental problem is separately detecting the Auger electrons in the midst of a much larger current of secondaries. This separation is accomplished by the following means: A metallic plate (the collector) is placed near the sample so as to collect all the emitted electrons; a grid then is interposed between the

sample and the collector and biased negatively to a retarding potential -
E_0. Only those electrons with energy greater than E_0 (in electron volts)
can pass to the collector, so that the total collected current I_0 is given
by

$$I_0 = \int_{E_0}^{\infty} N(E)dE \qquad (1)$$

where $N(E)$ is the relative number of electrons of energy E. The bias on
the grid then is modulated sinusoidally at a frequency ω, and standard
lock-in techniques are used to measure $\frac{dI}{dt}$, which is proportional to $N(E)$.
As E_0 (with the superimposed modulation) is increased through the energy
corresponding to the characteristic Auger energies, a peak will appear in
the spectrum. Experimentally, the peak is quite small, so the current is
generally differentiated once more by measuring the component of collected
current which varies sinusoidally at a frequency 2ω, twice the modulation
frequency, giving $\frac{dN(E)}{dE}$. The spectrum shown in Figure 1 exemplifies the
results, and from the characteristic energies at which the peaks appear,
the element can be identified. For instance, the peak at approximately 510
volts is due to the decay of a hole created in the K-shell of an oxygen
atom.

Preliminary spectra were taken on a sample of K 214 synthetic slag,
which had been used previously for the thermionic emission experiments.
Oxygen was identified, as well as a small peak probably due to iron. The
largest peak in the spectrum occurred at a measured retarding potential of
about 280 volts. This peak was probably due to carbon, whose Auger signal
should appear at 272 volts; however, it may be the 291 volt calcium peak.
The retarding potentials are measured with an ordinary voltmeter, and it
will require more exact measurements, as well as tests on known calcium and
carbon samples, to decide between the two. If the 280 volt peak is due to
carbon, the carbon may have been deposited on the surface in the form of
carbon monoxide or hydrocarbon from the background gases in the vacuum
chamber. The largest peaks for silicon and aluminum lie below 100 volts, a
region difficult to analyze in Auger spectra due to the rapidly changing
background in the spectra (see Figure 1). As a result, we have not yet
identified these two elements in the slag. Further improvements on experi-
mental technique, particularly improving the signal-to-noise ratio, should
make it possible to detect silicon and aluminum easily.

During the next quarter, we will continue to work on the Auger spectro-
scopy system to optimize its sensitivity. Further tests will be run on
synthetic slags, both at room temperatures and at elevated temperatures.
The heating tests on the potassium-containing slags will be resumed; when
a satisfactory method of sample preparation is determined, we will proceed
with the thermionic emission measurements again.

IV. CONCLUSIONS

Initial tests with potassium-containing slag indicate that such slag may be more difficult to handle than those we have worked with previously. Additional experiments should clarify the issue and indicate the best way to prepare a suitable sample. The Auger system performed about as expected, judging from the spectrum taken from a stainless steel sample. Tests also show that Auger spectroscopy on slag can be done; however, additional effort to improve the signal-to-noise ratio is necessary.

CONTRACT/PROJECT

CDIF Project Management Support and MHD Related Dev. Effort

77-002 SCHEDULE

CONTRACT NO.
EF-77-C-01-2524

VENDOR
Montana State University

Task G2 - Physical Properties of

Coal Slag: Thermionic Emission

FOSSIL ENERGY

TASK G2

YEAR 1977
MONTH O N D J F M A M J J A S

VARIANCE

MAJOR MILESTONES AND DECISION POINTS	
COMPLETION OF AUGER SYSTEM TEST	
COMPLETION OF FIRST AUGER TESTS ON HEATED SYNTHETIC SLAG	
COMPLETION OF FIRST THERM-IONIC EMISSION MEASUREMENTS ON SYNTHETIC SLAG WITH SURFACE CHARACTERIZATION	
REVIEW OF PRELIMINARY RESULTS	
COMPLETE CLEAN ELECTRODE EVALUATION	

STATUS DATE

SCHEDULE PLAN

PROGRESS

STATUS DATE

ADMINISTRATIVELY CONFIDENTIAL

VARIANCE OR PROBLEM FLAG IN RIGHT COLUMN

115

MONTHLY PROJECT MANAGEMENT STATUS REPORT

FOSSIL ENERGY

CONTRACT/PROJECT
CDIF Project Management Support and Related MHD Dev. Effort

77-002 SCHEDULE

CONTRACT NO. EF-77-C-01-2524

VENDOR Montana State University

Task G2 - cont. Page 2

	YEAR	1977												VARIANCE
TASK G2	MONTH	O	N	D	J	F	M	A	M	J	J	A	S	

MAJOR MILESTONES AND DECISION POINTS

INITIATION OF THERMIONIC EMISSION MEASUREMENTS ON SYNTHETIC SLAG WITH ADDED POTASSIUM

COMPLETION OF AUGER TESTS ON SYNTHETIC SLAG

COMPLETION OF THERMIONIC EMISSION MEASUREMENTS ON SYNTHETIC SLAG AND SELECTED ELECTRODE MATERIALS

STATUS DATE
SCHEDULE PLAN
PROGRESS
STATUS DATE

ADMINISTRATIVELY CONFIDENTIAL

VARIANCE OR PROBLEM FLAG IN RIGHT COLUMN

116
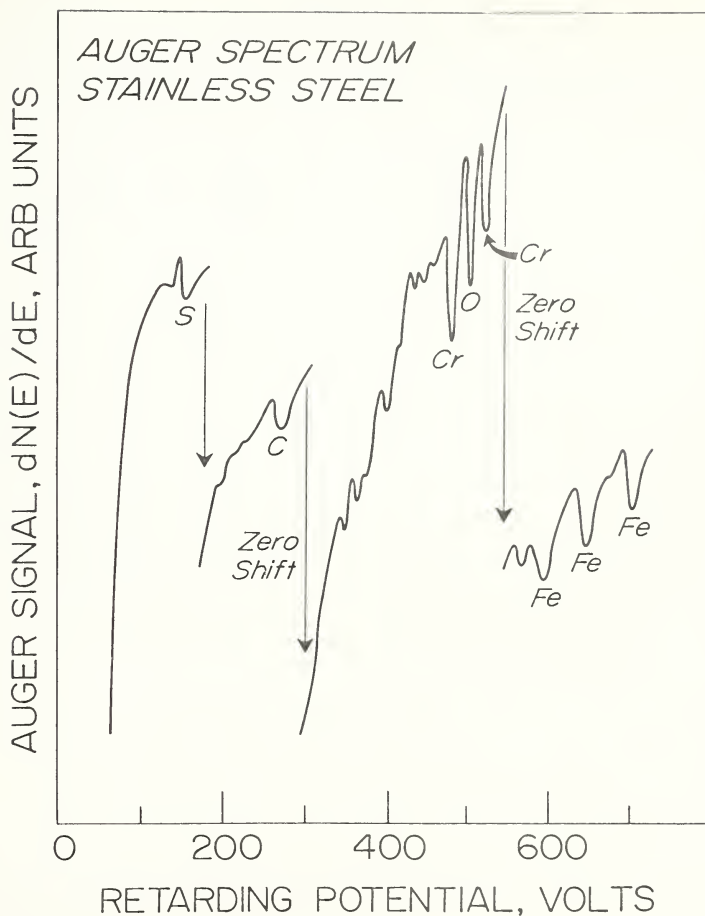
Figure 1.--Auger spectrum of a sample of stainless steel, showing
signal peaks due to the elements normally found on the
surface of stainless steel: sulfur, carbon, oxygen,
chromium, and iron

REFERENCES

1. K214 synthetic slag has the following components by weight percent: SiO_2 - 37.6%; Al_2O_3 - 31.9%; Fe_3O_4 - 19.98%; CaO - 10.53%.

2. P. W. Palmberg and T. N. Rhodin, "Auger Electron Spectroscopy from fcc Metal Surfaces," J. Appl. Phys. __39__ 2425 (1967).

3. D. F. Stein, R. E. Weber, and P. W. Palmberg, "Auger Electron Spectroscopy of Metal Surfaces," J. Metals, __23__ 39 (1971).

TASK G3
Slag Physical Properties:
Electrical and Thermal Conductivity
R. Pollina

ABSTRACT

Work this quarter centered around improving and modifying
the experimental systems presently being used and expanding
our capability to measure the electrical conductivity above
1450°C and at lower oxygen pressures than in the past. A
thermal conductivity system was delivered and partially installed
this quarter. Experimental work to date is summarized in a
paper presented this past quarter which is appended to this
report. The electrical conductivity of seeded Rosebud ash as
a function of seed content shows regular behavior.

I. OBJECTIVE AND SCOPE OF WORK

The objectives of this task are to determine the electrical and ther-
mal conductivities of unseeded and seeded coal slags under isothermal
conditions. The electrical conductivity measurements will be determined by
the NBS four-lead technique up to 1450°C and by a two-lead technique at
higher temperatures. The thermal conductivity measurements will be made
below the slag softening point using a cut bar conduction system.

II. SUMMARY OF PROGRESS TO DATE

Much rebuilding, improving, and installing of equipment took place
this past quarter to expand and improve our capabilities. A heat exchanger
and time-temperature-programmable temperature controller was designed and
constructed in-house for the high-temperature graphite tube furnace. A new
$MoSi_2$ furnace is nearing the final stage of construction and should be
operable this coming quarter. The atmosphere control system was expanded
to include $CO-CO_2$ gas mixing which enables us to obtain oxygen partial
pressures as low as 10^{-10} atm. The thermal conductivity system was received
and installed, and a manually operated power supply was constructed for it,
pending arrival of a temperature control system.

The electrical conductivity of seeded Rosebud ash, when plotted iso-
thermally as a function of seed content, shows regular behavior which is
encouraging for future theoretical analysis of ash conductivity. We have
included in this report a copy of a paper presented at the MHD Basic Science
Conference at Argonne National Laboratory on April 4-6, 1977. It summarizes
our results so far.

III. DETAILED DESCRIPTION OF TECHNICAL PROGRESS

A number of experimental systems have been developed or improved upon
this past quarter. The graphite tube furnace is operable again now that a
heat exchanger was installed in the furnace cooling line. This was necessary

because local water is too dirty to run directly through the furnace and power supply, and filtered water requires a new filter every one to five days, depending upon the type of filtration used. This was impractical since most high-temperature experiments last 3 to 10 days and would have to be interrupted for filter changes.

A temperature programmer was designed and constructed in-house. It consists of an electro-mechanical voltage ramp generator with switch-selectable slopes and periods to automatically raise and lower furnace temperature at any desired rate. Its voltage source for the ramp signal is stable to better than one microvolt (or 0.16 K with a type B thermocouple) and ramp linearity is better than 1/2 percent.

Because of the high demand on the SiC furnace, a $MoSi_2$ furnace is being constructed in-house for use to 1750 K and should be in the testing stage in early June. Several power supplies will be jury-rigged in order to operate the furnace.

The atmosphere control system, constructed to study low-iron Rosebud slags, is more than adequate for its purpose. However, high-iron slags have an extremely high sensitivity to oxygen partial pressure and require much lower oxygen pressures than heretofore needed. The present system is an air-argon gas mixing system. This past quarter, we have added a $CO-CO_2$ gas mixing system for lower oxygen pressures than those obtainable with an air-argon system. During construction of the new $CO-CO_2$ system, we found that the commercially available "calibrated" rotameters are not calibrated well. In some cases, the flow rate behavior bore no relationship to the manufacturer's calibration curve. Therefore, we recalibrated all our rotameters to eliminate this source of error.

The oxygen partial pressure of a $CO-CO_2$ equilibrium mixture as a function of temperature is given by Muan and Osborn.[1] With this new gas mixing system added to the air-argon system, we have the following capabilities:

P_{O_2}	Mixture	T range
0.17	air	all
10^{-1} to 10^{-3}	air-argon	all
10^{-4}	$CO-CO_2$	1550 - 2000 K
10^{-6}	$CO-CO_2$	1400 - 2000 K
10^{-8}	$CO-CO_2$	1300 - 1900 K
10^{-10}	$CO-CO_2$	1200 - 1700 K

The thermal conductivity system was installed this month, and a manually-operated power supply was constructed for it. The temperature controllers will be delivered next quarter. Some difficulty has been encountered in preparing and annealing vitreous samples of coal slag for the thermal conductivity system. The smallest sample advisable for the system is a cylinder 2.5 cm in diameter and 1-2 cm thick. Some additional work is necessary to determine a suitable annealing for these samples since they fracture while being machined to proper size.

Continuing our study of the seed dependence of the electrical conductivity of Rosebud coal ash, Figure 1 shows isotherms of the conductivity as a function of added K_2CO_3 for temperatures from 1000 K to 1667 K. The temperature dependence of the electrical conductivity of seeded Rosebud ash has been presented previously,[2] but Figure 1 illustrates its seed concentration dependence in a better way. All isotherms exhibit approximately a linear behavior in conductivity as a function of K_2CO_3 seed additions up to 20 percent K_2CO_3. Above this seed concentration, the behavior changes drastically, indicating a possible change in chemistry of the system. We shall investigate this effect in further detail in the future.

In Figure 1, we also can see a continual flattening of the isotherms as higher temperatures are approached. This gradual loss of sensitivity of electrical conductivity to seed content at higher temperature may indicate a gradual increase of the electronic contribution to the conductivity. If so, then at 1667 K ($10^4/T = 6$), where the electrical conductivity is independent of seed content up to 20 percent K_2CO_3, the conductivity may be predominantly electronic. This is one possible explanation of the effect, but more must be known about the charge carrier and diffusion rates.

There is little change in the slopes of isotherms at $10^4/T = 8, 9, 10$ below 20 percent K_2CO_3. Above these temperatures, the slopes gradually flatten and coincide with the softening of the crystal. In Figure 2, we show the X-ray pattern obtained from four samples of Rosebud bottom ash; all are of the same composition but with different heat treatments. This sequence shows the onset of the crystallization of anorthite from Rosebud ash. Near 1378°C (1651 K), we first noticed the growth of an anorthite peak which is more pronounced at 1265°C. The sample, slow-cooled from 1450°C (1773 K), exhibited a strong anorthite spectrum since it had more time to anneal but it also showed unidentified peaks. These are marked with little checkmarks above them. If we consider this Rosebud ash sample as comprised only of CaO, Al_2O_3, and SiO_2, then the composition falls in the anorthite region of the phase diagram at these temperatures.[3]

This past quarter, a paper was presented at the MHD conference held at Argonne Laboratory which summarized our work to that time. The paper is included as an appendix to this report and will be published in the conference proceedings which should appear shortly.

IV. CONCLUSIONS

None.

DIVISION OF MAGNETOHYDRODYNAMICS
MONTHLY PROJECT MANAGEMENT STATUS REPORT

REPORT DATE: _____

CONTRACT/PROJECT
CDIF Project Management Support and Related MHD Dev. Effort

CONTRACT NO.	VENDOR
EF-77-C-01-2524	Montana State University

77-002   SCHEDULE
Task G3 - Slag Physical Properties:
Electrical and Thermal Conductivity

FOSSIL ENERGY

	YEAR		1977	
	MONTH	O N D J F M A M J J A S		VARIANCE

TASK G3

MAJOR MILESTONES AND
DECISION POINTS

COMPLETE DESIGN OF DATA
ACQUISITION SYSTEM

COMPLETE MULTIPLE SAMPLE
TRIALS OF ELECTRICAL
CONDUCTIVITY SYSTEM

COMPLETE CONSTRUCTION OF
CUT BAR CONDUCTIVE SYSTEM

PERFORM ELECTRICAL CONDUC-
TIVITY MEASUREMENTS ON A
CONSIDERABLE NUMBER OF SLAG
SAMPLES

DETERMINE THE THERMAL
CONDUCTIVITY OF SEVERAL COAL
SLAG SAMPLES

STATUS DATE _____ ^
SCHEDULE PLAN _____   STATUS
PROGRESS _____   DATE

ADMINISTRATIVELY CONFIDENTIAL

VARIANCE OR PROBLEM FLAG IN RIGHT COLUMN ◇

122
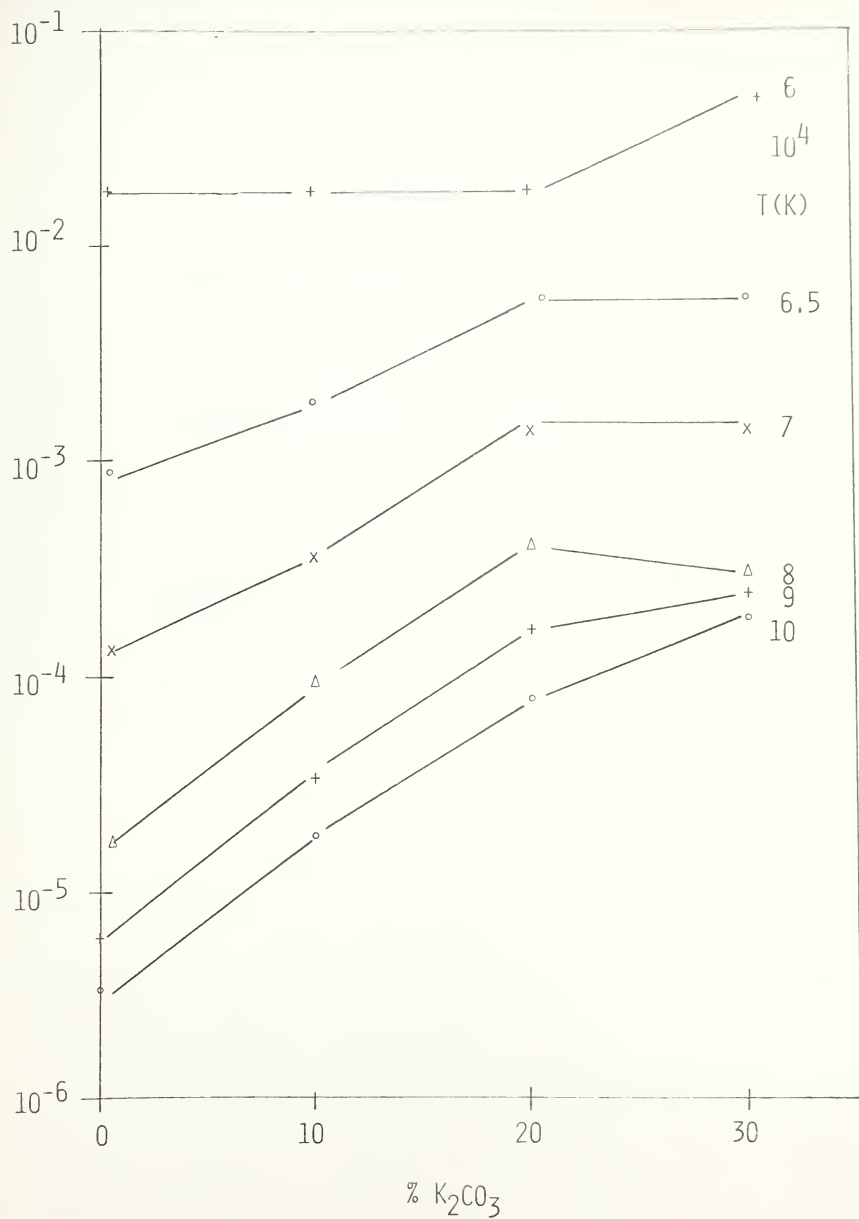
Figure 1.--K_2CO_3 dependence of the conductivity of Rosebud ash

123

quenched from 1403° C

quenched from 1378° C

quenched from 1265° C

1450° C to 50° C
in 12 hours

Figure 2.--Crystallization of anorthite from Rosebud ash

REFERENCES

1. A. Muan and E. F. Osborn, "Phase Equilibria Among Oxides in Steel-making," Addison-Wesley, Reading, Massachusetts, 1965.

2. Annual Progress Report, MSU/MHD-76-ARI, 1976.FY 1976.

3. E. Levin, C. Robbins, and H. McMurdie, "Phase Diagrams for Ceramists," American Ceramic Society, Third Edition, 1964.

ELECTRICAL CONDUCTIVITY OF A MONTANA COAL ASH[†][*]

R. Pollina and R. Larsen
Montana State University
Bozeman, Montana

In this report we present preliminary electrical conductivity studies of a typical Montana coal ash (as obtained from the power plant) with and without the additions of potassium seed, iron oxide, and alumina. The addition of alumina did not significantly lower the electrical conductivity at high temperature. This result may prove to be important for electrode replenishment if a more favorable chemical environment at the electrode-slag interface is ever necessary.

The conductivity of Rosebud ash was found to be only weakly dependent upon oxygen partial pressure. Graded samples of bottom ash with additions of K_2CO_3 were studied to determine the effect of potassium seed addition on the conductivity of Montana coal ash. Large additions (up to 30%) of K_2CO_3 produce only small changes in the electrical conductivity at high temperatures but important and substantial changes at temperatures below approximately 1550 K.

INTRODUCTION

In an MHD generator channel the conductivity of the slag layer adhering to the walls of the generator must be in a range appropriate for the slag to act as a good conductor for the generator output current and yet must be low enough to prevent shorting of the axially directed Hall current. The mathematical analysis of this balance in seemingly opposing demands upon the slag conductivity has already been carried out [1]. However, yet to be determined is the criterion by which we judge the suitability of a given slag with respect to its electrical conductivity. The ultimate goal of this project is to satisfy demands of the designers for data necessary in modeling the output of the channel and to predict empirically the behavior of slag under any constraints which might occur when larger scale projects such as the CDIF become operational.

EXPERIMENTAL TECHNIQUE

The coal ash used in our experiments is from the Rosebud seam and was obtained from a local power company [2]. The combustor temperature was approximately 1900 K [3] and bottom and fly ash were supplied from the combustor and the base of the stack respectively. The samples were received in the form of powder, and each was homogenized and melted in alumina or platinum crucibles in air at 1700-1750 K for 1 to 36 hours and then air quenched. Corrosion of alumina crucibles was generally not observable until the seed content was increased. Above 10% K_2CO_3 a changeover to platinum crucibles was necessary.

The bottom and fly ash compositions were essentially the same except for slightly higher concentrations of sulphur, potassium, and calcium in the bottom ash as seen in an intensity analysis [4] of the proton induced x-ray spectrum (PIX) of each sample.

Below 1800 K, samples were contained in alumina boats of 99.8% purity [5] (interior dimensions 25 x 4 x 4 mm.) and the conductivity was measured using the conventional 4-lead technique to separate polarization effects

from the true conductivity. Pulverized samples were placed in a crucible into which four leads had been suspended. A type B thermocouple (platinum-6% rhodium vs platinum-30% rhodium), which was checked periodically at the gold point, monitored the temperature.

The furnace was used with a controlled atmosphere for which a gas scrubbing system had been constructed [6]. Normally air and argon were mixed for the sample environment.

In a measurement, samples were raised to the maximum temperature of the run, and data was taken from the highest temperature downwards. After a run, the ceramic boats developed a web of cracks indicating that the slag had a lower thermal expansion than alumina. During or after a run, the platinum leads were sometimes eroded away. This always occurred at the outer or current carrying leads. Both these effects will be investigated further in the future.

Multiple tests of the electrical conductivity of Rosebud coal ash were run in air (oxygen partial pressure of 0.17 atm). To eliminate effects due to thermal cycling, two samples of Rosebud bottom ash with identical thermal history were measured twice giving each repetition of each sample the same thermal cycle. The conductivity is quite reproducible both between samples and between runs, indicating that conductivity measurements on coal slag are quite reliable.

RESULTS AND DISCUSSION

In Figure 1 we present results of a study of Rosebud coal ash conductivity at three different oxygen pressures as indicated in the figure. The solid line is drawn through the 10^{-3} atm data points. Here, as in all conductivity figures, the log of the conductivity in $(ohm-cm)^{-1}$ is plotted as a function of $10^4/T(K)$. The top scale shows the corresponding Kelvin temperatures. Two regions of instability are noticeable. They are characterized by a sharp change in the electrical conductivity accompanied by long relaxation times. The first instability occurs at a reduced temperature of $6.1 K^{-1}$ and the second at $7.15 K^{-1}$. These instabilities regularly appear in the Rosebud ash and generally occur at $6.2 \pm 0.2 K^{-1}$ (1615 K) and $7.2 \pm 0.2 K^{-1}$ (1390 K). They may be due to the mode of devitrification taking place within the sample. It is difficult to be more specific at present because of the large number of compounds which may crystallize at these temperatures from such a complex medium.

To determine the effect of a thermal cycling change on the conductivity behavior, a sample of bottom ash with the same thermal history was studied by changing the initial temperature of the run from 1725 K to 1825 K. Departures of the two curves from one another occurred only in the instability regions mentioned above. The higher temperature sample exhibited conductivity which is smoother but the instabilities evidenced themselves as longer equilibrium times necessary to obtain data at the instability temperatures. The dashed line in this figure is taken from data on Montana coal ash published by Bates [7]. It is in excellent agreement with our own data except for some deviation below 1100 K. A comparison of the chemical compositions of our own Rosebud bottom ash and the Battelle sample designated SMF-O is contained in Table 1 [8]. SMF-O appears to be substantially more silica rich and alumina poor than our Rosebud ash.

Figure 1. Rosebud ash conductivity at varying oxygen pressure.

Table 1

The Compositions of MHD-12 and Two Montana Coal Ashes.

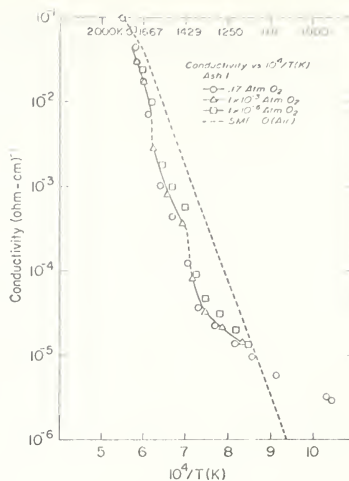|	Rosebud Ash	MHD-12	SMF-0
SiO_2	40.34%	50%	47
Al_2O_3	24.6	21	20.7
CaO	18.9	1	21.9
MgO	5.8	5	6.6
Fe_2O_3	4.4	14	5.0
K_2O	0.53	1	0.43
Na_2O	0.46	--	0.40
SO_3	0.28	2	--
TiO_2	--	--	1.0
P_2O_5	--	--	0.39

On completion of the controlled atmosphere system, a test was made of the efficacy of the system using a sample (MHD-12) obtained from, and previously characterized by, the National Bureau of Standards. It was felt that this would make an ideal "standard" with which to evaluate our system. Our results give good agreement with those of NBS [9] considering the presumably different thermal treatments the sample received, small thermocouple differences, and errors in determining sample geometry. These results serve to demonstrate the kind of reliability and reproducibility one can expect in the conductivity even between different laboratories. These results justify the conclusion that electrical conductivity measurements in the laboratory, can contribute significant and meaningful data relating to the behavior of slag in an MHD generator. What needs to be known is the sort of changes in composition the ash may be expected to undergo under MHD conditions so that the slag compositions studied in the laboratory will be similar to those of the wall condensate and will therefore yield data for engineering design calculations. The behavior of Rosebud bottom ash conductivity with varying oxygen pressure is quite different from MHD-12. Not only does the conductivity have a greatly reduced sensitivity to the oxygen pressure, as indicated in Figure 1, but the effect of reducing the oxygen content is reversed. Since the primary effect of the presence of oxygen on the electrical conductivity is through the Fe^{2+}/Fe^{3+} ratio, the reduced sensitivity shown in Figure 1 follows from the lower iron oxide content for the Montana coal. The difference in magnitudes of the conductivities of MHD-12 and Rosebud ash (labeled 5C) is shown in Figure 2. These differences are probably attributable to the reduced iron oxide content of Rosebud ash. Not enough information is available at present to say just how the Rosebud samples studied here relate to

the overall spectrum of compositions expected from the Rosebud seam. However, similarity of Rosebud ash in an oxygen environment to MHD-12 in an oxygen free environment should mean that Rosebud ash with its apparently "absent" oxygen-dependent conducting mode (presumably $Fe^{2+} - Fe^{3+}$ charge transfer) has a conductivity mechanism similar to MHD-12 in an oxygen free environment where that mode is quenched.

Two samples of iron enriched Rosebud ash were prepared by mixing the natural coal ash with 5% and 10% Fe_2O_3 to give total Fe_2O_3 concentrations of 9.2% and 14% respectively. The conductivity data (in air, 0.17 atm. O_2) for the two enriched samples and for the natural ash are shown in Figure 3. At temperatures below 1600 K and especially below 1450 K additional iron enhances the conductivity substantially. It has been noted by Bates [10] that the log of the electrical conductivity at both 1667 K and 1250 K appears to decrease approximately linearly with a decrease in the percentage of Fe_2O_3. Our data for the iron enriched samples are in good agreement with Bates' observation on the effect of Fe_2O_3 concentration at 1250 K, but the correlation is very poor at the 1667 K isotherm where no significant differences in conductivity between the three samples were observed. Data taken at other oxygen partial pressures (not shown) exhibit substantial sensitivity of conductivity to oxygen for the two enriched samples and indicate that 5% Fe_2O_3 content is the approximate cut-off in iron concentration. Below this iron ox content, pressure does not appear to significantly affect slag conductivity. Iron content in coal slags is a sensitive composition variable at temperatures below 1600 K, and oxygen partial pressure is a sensitive variable at iron concentrations above 5% Fe_2O_3. These effects would have considerable practical significance in an MHD generator utilizing iron containing electrodes, even if low iron coals were used as fuel.

Figure 4 displays the electrical conductivity data for Rosebud coal ash (Ash 1) with graded additions (10,20,30%) of K_2CO_3 as seed. The corresponding potassium content of these samples is 7,14,21% K_2O. Below approxmately 1540K there is a strong dependence of the conductivity on potassium content. This dependence increases with decreasing temperature. The potassium concentration dependence of conductivity above 1540K is weak and somewhat erratic in that different runs will shift the curves. This is exemplified by the behavior of the 10% sample above 1650K which has a slightly lower conductivity than Ash 1 in this run, but higher in another run. Much practical importance is placed on the strong low-temperature dependence of conductivity on potassium content since channel wall temperatures may be in this temperature region. All four of the samples displayed here were prepared simultaneously in platinum crucibles so their thermal history is similar.

Figure 5 shows some interesting results obtained by measuring the conductivity of Rosebud bottom ash with 20% alumina enrichment and with both 20% alumina and 20% K_2CO_3 enrichment. On removing the latter two samples from the sample holder after the experiments had terminated, no noticeable corrosion of the alumina boats was observed. This is in sharp contrast to earlier runs with seeded slag in which substantial corrosion was observed for the high seed concentration (20-30% K_2CO_3) slags. This corrosion inhibition effect gives added weight to the arguments of those who favor electrode replenishment. Several items are to be considered in Figure 5. The sample of 80% ash and 20% alumina (----) illustrates the mild sensitivity of slag conductivity and alumina content. This is to be expected since alumina is an insulator and hence would not contribute charge carriers. Fe_2O_3 and CaO

would appear to supply the major contribution to the slag conductivity though
we have not looked at CaO yet. It is interesting to note that below 1400 K
alumina actually enhances the conductivity. Of equal interest is the fact
that above 1667 K slag conductivity is virtually independent of the addi-
tives as was seen in Figure 4 above 1550 K. The 80% ash and 20% K_2CO_3 line
(- .- .) is taken from the data of Figure 4 and is merely repeated here for
comparison. Again we note that the enhancement of conductivity contributed by
the addition of 20% K_2CO_3 (14% K_2O equivalent) appears to be significant only
below 1667 K and therefore would matter little in a hot wall channel.
Finally, we look at the sample 60% ash and 20% each of Al_2O_3 and K_2CO_3. This
sample was prepared because of the observed substantial decrease in corro-
siveness on adding alumina. It was then decided to find out if this decreased
corrosiveness was maintained in the presence of seeded slag, and indeed it was.
The alumina addition decreases the conductivity of a seeded slag but the de-
crease is only significant below 1250 K, where replenishment is unnecessary.
This led us to the conclusion that electrode replenishment cannot be ruled
out on the grounds that replenishment lowers the slag conductivity.

<div align="center">REFERENCES</div>

[1] Design Considerations for Coal Fired MHD Generator Ducts, R.J. Rosa,
     Fifth International Conference on MHD Electrical Power Generation,
     Munich, 1971.
[2] Montana Power Company, Corette Plant, Billinga, Montana.
[3] Montana Power Company, Private Communication.
[4] This work was done by W. Beezhold and R. Burghard using the MSU ion beam
     facility.
[5] McDanel Refractories, Beaver Falls, Pennsylvania.
[6] MSU/MHD Energy Research Office, Quarterly Report IV, Task G1, Montana
     State University, Bozeman, Montana, April, 1976.
[7] Final Progress Report on Properties of Molten Coal Slags Relating to
     Open Cycle MHD, Battelle, Pacific Northwest Laboratories, Richland, WA,
     December, 1975, BNWL-B-466.
[8] The data on Rosebud ash was supplied by W. Seymour, MERDI, and that on
     MHD-12 by W.R. Hosler, NBS. SMF-0 is a sample of Montana coal ash
     studied at Battelle, Pacific Northwest Laboratories. The data included
     here is from Reference 1.
[9] HPR Frederikse and W.R. Hosler, J. Am. Ceram. Soc. 56, 418 (1973).
[10] Progress Report No. 1 on Properties of Molten Coal Slags Related to
     Open Cycle MHD. Battelle, Pacific Northwest Laboratories, Richland,
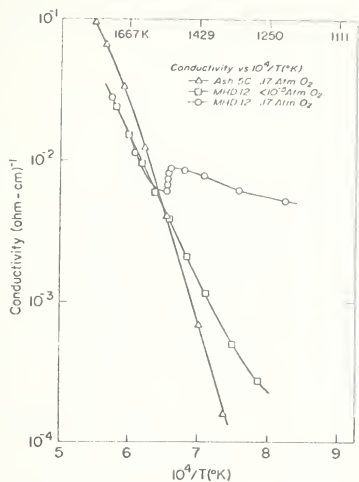   WA, February, 1975.

Figure 2. Comparison of Rosebud
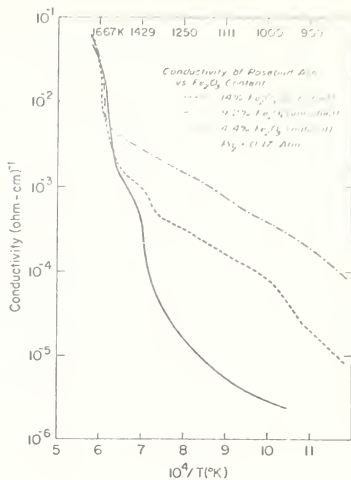ash with MHD-12.

Figure 3. Rosebud ash conductivity
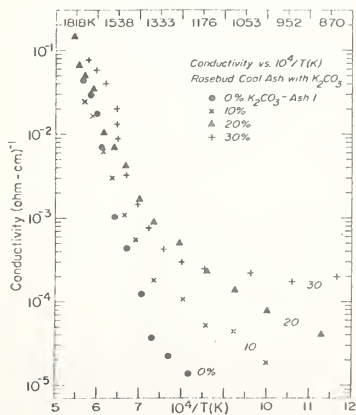for varying iron oxide
content

Figure 4. Effect of seed on Rosebud
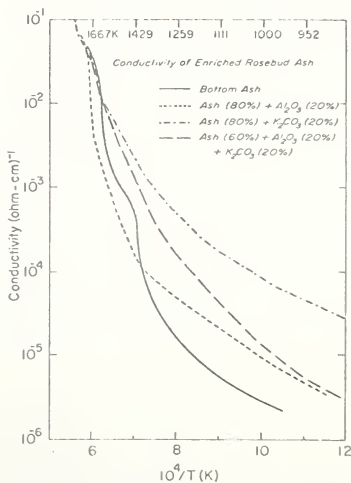ash conductivity.

Figure 5. Effect of alumina enrich-
ment on seeded & unseeded
Rosebud ash.

131

TASK H1
MHD Systems Instrumentation and Data Acquisition
R. Johnson and T. Robles

ABSTRACT

Modification of the computer programs for simulating the steady-state and non-steady-state operation of the MHD channel has been completed. These programs provide the capability to evaluate the behavior of MHD channels operating under normal or abnormal conditions. The computer codes were utilized to simulate the CDIF and ETF channels. The result of a preliminary simulation of the CDIF channel was delivered to MERDI in April. Partial results of the ETF channel simulation are presented in this report. Work on the steam plant and air preheater simulation and the data flow simulation model is in progress.

I. OBJECTIVE AND SCOPE OF WORK

The work to be performed is in the general area of MHD systems, instrumentation, and controls and consists of two general parts:

A. The systems analysis and computer simulation of a time-dependent, one-dimensional model of a complete MHD/steam power plant to include combustor, nozzle, channel, diffuser, high-temperature air preheater, heat-exchanger array, inverters and steam plant. The simulation program should provide the capability to evaluate the sensitivity of a combined-cycle MHD/steam power plant to changes in operating conditions which may be induced both internally and externally. In particular, the effects of load variations due to fault conditions, changes in fuel and seed-flow rate, internally-simulated arcing conditions, and variable air-preheat heat-exchanger configurations should be eventually treatable by the program.

B. The continued development of a data flow and control simulation program for the study of the data processing requirements of a MHD/steam power plant. The program should allow for the introduction of various instrumentation configurations and complements, choice of control algorithms, and variation of operational loading scenario.

II. SUMMARY OF PROGRESS TO DATE

During this quarter, the following work was performed:

A. Time dependent and steady-state computer models for MHD channel simulation were completed;

B. Simulation codes for steady-state and time-dependent CDIF models were delivered to MERDI;

C.   Documentation of the computer codes was completed;

D.   Coding of air preheater and steam plant dynamic models was completed;

E.   A technical paper on the heat capacitor was presented at the 16th MHD Symposium;[13] and

F.   Work on the data flow simulation model continued.

III. DETAILED DESCRIPTION OF TECHNICAL PROGRESS

A. Time-Dependent and Steady-State Computer Models

Modification of the computer program for simulating MHD channels was completed this quarter. Coding has been modularized so that the collection of programs will be more versatile in its application to different configurations and requirements.

A code for simulating the CDIF channel was completed, and test runs were made using the incomplete data provided to us. A copy of the codes and the results of a preliminary simulation of the CDIF channel were delivered to MERDI in April. The steady-state cooling system model for the CDIF channel was included in the steady-state computer code.

The operation of the time-dependent model requires that the steady-state model be completed first in order to provide a set of initial and boundary conditions for the time-dependent program. Simulation with the ETF steady-state model was completed; partial results are shown in Figures 1 through 5. The ETF generator is the Faraday type operating under subsonic conditions. The generator is connected to a set of inverters (one inverter per electrode pair) that transform d-c to a-c power.

The variations of the area, velocity, and Mach number within the designed MHD channel are shown in Figure 1. The combustion gas from the combustor is accelerated from 36 m/sec to 768 m/sec in a .57 meter-long nozzle. The area ratio required to accelerate the flow is approximately 16.4. The Mach number of the flow through the channel is fairly constant at Mach 0.8.

The variations of the gas temperature, pressures, and mass density are shown in Figure 2. The magnitude of the combustion pressure and temperature (5 atma., 2810 K) assumed is comparable to that required in a base-load plant.

The electric field distribution is shown in Figure 3. The maximum axial field is approximately 32 volts/cm, which is within the limitations imposed by axial breakdown. The maximum transverse current density is approximately 1.1 amperes/sq. cm. (Figure 4). The electrode current and inverter (terminal) voltage distributions also are shown in Figure 4. The magnetic field, electrical conductivity, and Hall parameter distributions are shown in Figure 5. The maximum magnetic field is 6 Tesla. The complete results of the ETF simulation will be reported during next quarter.

The initial and boundary conditions needed in the simulation with the ETF time-dependent model will be obtained from the results of the steady-state simulation of the ETF model. The simulation studies with the time-dependent model will be conducted during next quarter.

A copy of the computer codes for simulating the steady-state and non-steady-state operation of the CDIF channel was delivered to MERDI in April. Preliminary results of the simulation, using the incomplete data provided to us, were included.

The documentation of the computer codes was completed this quarter (see Appendix A). A copy will be sent to MERDI soon.

B. Steam Plant and Air Preheater Dynamic Model

Simulation with the steam plant and air preheater dynamic model was completed this quarter. The simulation runs enabled us to study the response to step changes in inlet gas temperatures and mass flow rate. The effect of the gas temperature variation at the heat exchanger exit (due to cycling) on the steam plant response is being studied also. These studies will provide the information needed for instrumentation, data acquisition, and control requirements of the system. The results will be reported next quarter.

A technical paper on the heat capacitor for MHD air preheater systems was presented at the 16th Symposium on the Engineering Aspects of Magnetohydrodynamics at Pittsburgh, Pennsylvania. The heat capacitor combined with a reduced number of phased regenerative heat exchangers appears promising for reducing temperature ripple at the high-temperature air preheater output.

C. Data Flow Simulation Model

The data flow simulation model and computer program, as originally coded, assumed that all data would be input to a single computer for subsequent data reduction and control algorithm computation. Although this information still is of great interest in studies of the total processing requirements for acquiring system data and controlling an MHD plant, microprocessors probably will be used on many system components for individual control and status monitoring functions.

The data flow simulation program is being modified to permit the study of individual distributed data acquisition and control by microprocessors. The particular components chosen initially for such treatments are those with slow dynamics or limited processing requirements: the coal feed system, the air preheat-heat capacitor system, the steam turbine throttle systems, and the electrode voltage-consolidation-inverter system. The latter system may have a processor speed requirement in excess of currently available microprocessor capability, but it is being studied to establish the necessary requirements. Detailed results of this work will be presented in the next quarterly report.

IV. CONCLUSIONS

The modularized computer programs provide the user with flexibility in simulating MHD channels of any size. Minor changes may be made in user-supplied subroutines without affecting the program structure. The steady-state program can be used not only for designing linear MHD channels but also for conducting parametric studies of the MHD channel that is designed.

The simulation program will provide the capability to study the sensitivity of MHD channels to changes in operating conditions. The information obtained from these studies is needed for specifying MHD system instrumentation and data acquisition requirements.

REPORT DATE

77-002   SCHEDULE

CONTRACT/PROJECT

CDIF Project Management Support and Related MHD Dev. Effort

CONTRACT NO. | VENDOR
EF-77-C-01-2524 | Montana State University

Task H1 - MHD Systems Instrumentation and Data Acquisition

FOSSIL ENERGY

TASK H1

| YEAR MONTH | O N D J F M A M J J A S | VARIAN |

MAJOR MILESTONES AND DECISION POINTS

EXTENSION OF TIME-DEPENDENT MODELS FOR ETF AND BL PLANT CONFIGURATION

REFINEMENT OF TIME-DEPENDENT MODELS

EXTENSION OF THE DATA FLOW SIMULATION MODEL TO INCLUDE THE COMPUTATION REQUIRE-MENTS FOR CONTROL

DEVELOP TIME-DEPENDENT MODEL FOR THE CDIF MHD CHANNEL (NOZZLE, GENERATOR, AND DIFFUSER)

STATUS DATE

SCHEDULE PLAN

PROGRESS

STATUS DATE

VARIANCE OR PROBLEM FLAG IN RIGHT COLUMN

136

CONTRACT/PROJECT

CDIF Project Management Support and Related MHD Dev. Effort

CONTRACT NO. EF-77-C-01-2524

VENDOR Montana State University

FOSSIL ENERGY

SCHEDULE

Task H1 - cont. Page 2

TASK H1

YEAR MONTH	O N D J F M A M J J A S

MAJOR MILESTONES AND DECISION POINTS

VARIAN

DEVELOP STEADY-STATE MODEL FOR THE COOLING SYSTEM OF THE CDIF TEST TRAIN TO INCLUDE NOZZLE, GENERATOR, AND DIFFUSER

COMPLETE THE DOCUMENTATION FOR ITEMS 4 AND 5 ABOVE

STATUS DATE

SCHEDULE PLAN ⟶ STATUS DATE

PROGRESS ⟶

VARIANCE OR PROBLEM FLAG IN RIGHT COLUMN ∨
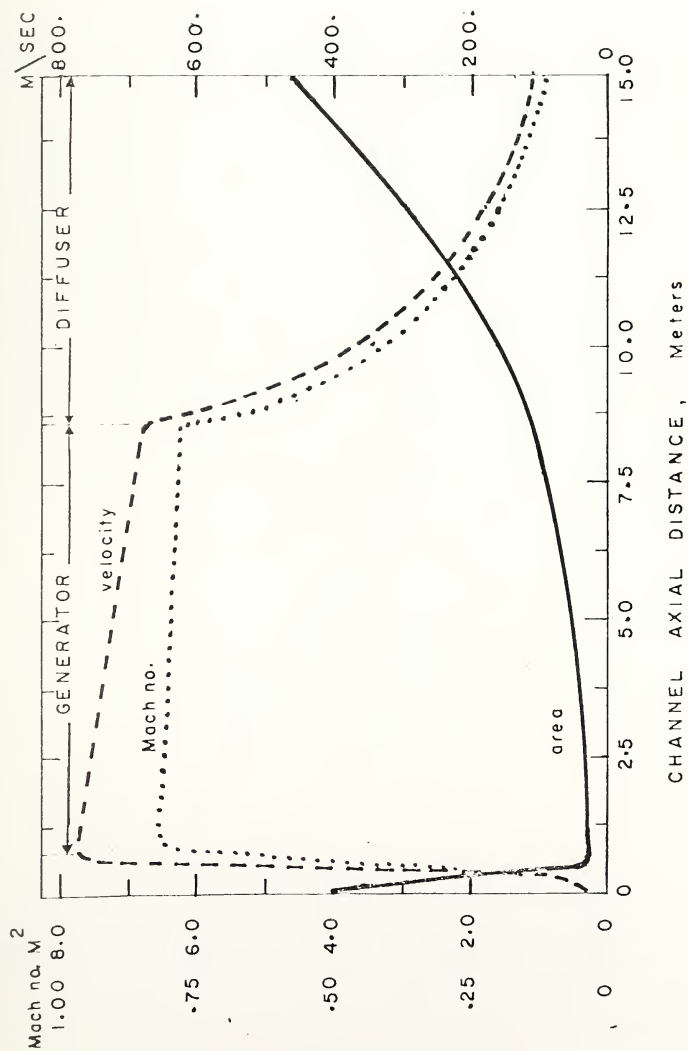
Figure 1.—Variation of flow properties within the MHD channel
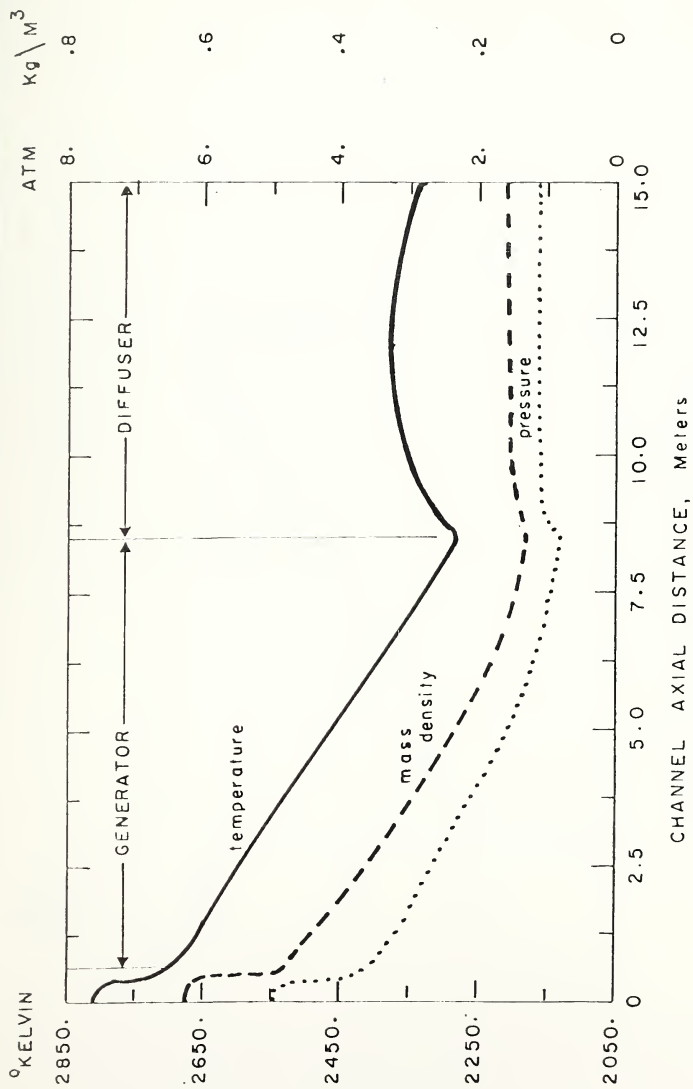
Figure 2.--Variation of temperature, mass density and pressure within the MHD channel

139
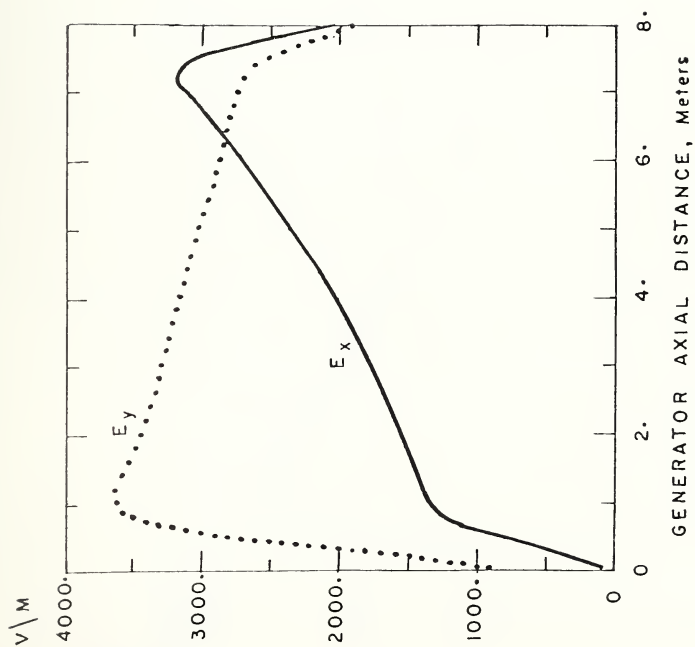
Figure 3.--Electric field distribution
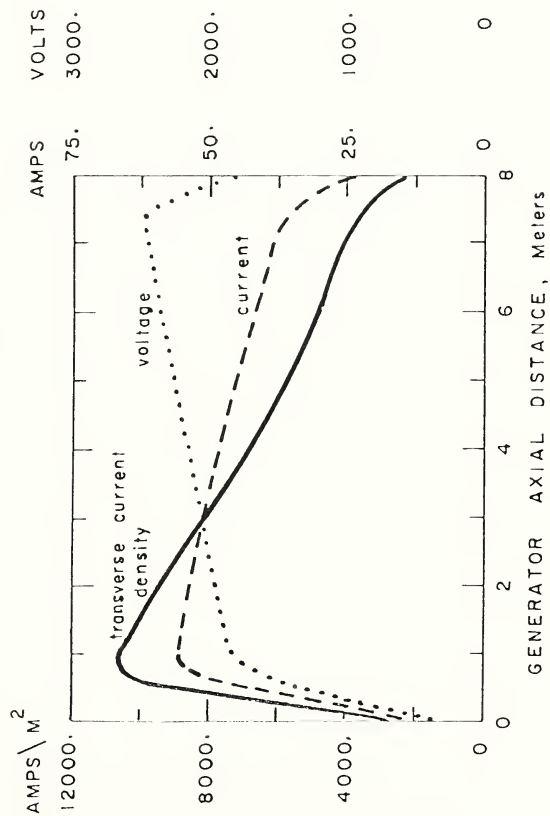
Figure 4.--Transverse current density, electrode current and terminal voltage distributions
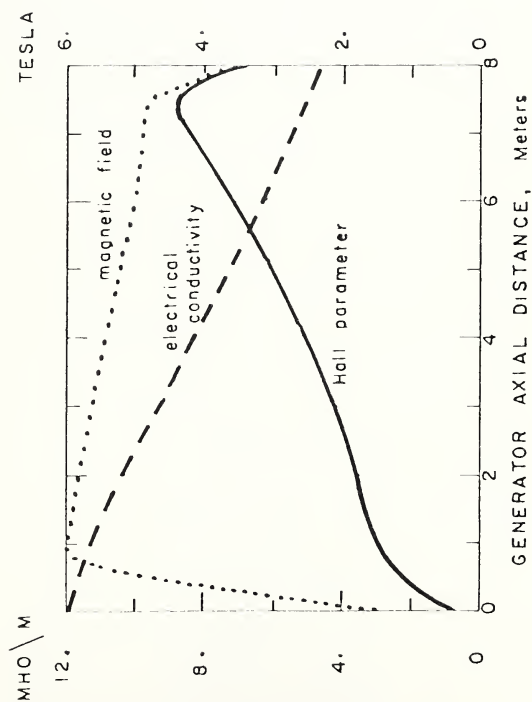
Figure 5.--Magnetic field, electrical conductivity and Hall parameter distributions

FORTRAN IV COMPUTER PROGRAMS FOR THE ANALYSIS
OF QUASI ONE-DIMENSIONAL MHD FLOW PROBLEMS

I. Program MHDAV

This program is used for designing linear MHD generators or analyzing the steady-state flow in the magnetohydrodynamic channel (nozzle, generator, diffuser) based on the quasi one-dimensional steady-state MHD equations. In the design mode, the MHD generator may be a Faraday or diagonally-connected generator operating with a constant or variable flow velocity. In the analysis mode, the program is suitable for conducting parametric studies of a designed MHD generator operating under various combustion conditions or load conditions.

The MHD equations are:

CONTINUITY Equation

$$\rho u A = w \tag{1}$$

MOMENTUM Equation

$$\rho u \frac{du}{dx} + \frac{dp}{dx} = (J \times B)_x - F \tag{2}$$

ENERGY Equation

$$\rho u \frac{dh}{dx} + \rho u^2 \frac{du}{dx} = (J \cdot E) - G \tag{3}$$

STATE Equation

$$\rho = \frac{.120268 \times 10^{-3} \, pM}{T} \tag{4}$$

where

A	=	cross-sectional area of the channel at x
F	=	friction term[1]
G	=	heat transfer term[1]
h	=	gas enthalpy
M	=	gas molecular weight
p	=	gas pressure
T	=	gas temperature
u	=	gas velocity
W	=	gas mass flow rate
JxB	=	Lorentz force
J·E	=	electrical power density

143

x = distance along the channel

ρ = gas mass density

The equations for the electrical properties of the flow are[1]

a. Faraday generator

$Jx = 0$ axial current density   (5)

$Jy = \sigma u B(1-K)$ transverse current density   (6)

$Ex = \beta u B(1-K)$ axial electric field   (7)

$Ey = KuB$ transverse electric field   (8)

$J \cdot E = -K(1-K)\sigma u^2 B^2$ electrical power density   (9)

$JxB = -\sigma u B^2(1-K)$ Lorentz force   (10)

b. Cross-connected generator

$Jx = \sigma u B(I^*(1+\alpha\beta) - \alpha)/(1+\alpha^2)$ (11)

$Jy = -\sigma u B(1+I^*(\alpha-\beta))/(1+\alpha^2)$ (12)

$Ex = -uB[(\alpha+\beta) - I^*(1+\beta^2)]/(1+\alpha^2)$ (13)

$Ey = \alpha u B[(\alpha+\beta) - (1+\beta^2)I^*]/(1+\alpha^2)$ (14)

$J \cdot E = -\sigma u^2 B^2(I^*(\alpha+\beta) - I^{*2}(1+\beta^2))/(1+\alpha^2)$ (15)

$JxB = -\sigma u B^2(1+I^*(\alpha-\beta))/(1+\alpha^2)$ (16)

where I = $A(Jx-\alpha Jy)$; I^* = $I/(A\sigma u B)$

K =   load factor   = $\dfrac{Ey}{uB}$ (Faraday generator)

β =   Hall parameter

α =   cross-connection parameter

σ =   electrical conductivity

I =   load current

I^* =   dimensionless load current

B =   magnetic field.

The effect of finite segmentation of the electrodes may be included with the introduction of correction factors derived by Dzung[2] and Witalis.[3] The terminal voltages are modified by the electrode voltage and boundary

layer voltage drops. The calculations of the heat transfer (G) and friction (F) effects are based on the work of Knudsen and Katz[4], Teno[5], and Bartz.[6]

Design Mode:

Equations (1) through (3) are transformed into two simultaneous differential equations with temperature (T) and channel cross-sectional area (A) as dependent variables:

$$\frac{dT}{dx} = \frac{1}{\rho u C_p} \left[(J \cdot E) - G - \rho u^2 \frac{du}{dx} \right] - \frac{C_T}{C_p} \left[(J \times B) - F - \rho u \frac{du}{dx} \right] \qquad (17)$$

$$\frac{dA}{dx} = \frac{-A}{p} \left[(J \times B)_x - F - \rho u \frac{du}{dx} \right] + \frac{A}{T} \frac{dt}{dx} - \frac{A}{u} \frac{dT}{dx} - \frac{A}{u} \frac{du}{dx} \qquad (18)$$

The velocity variation in the MHD generator conforms to the following relation[7]:

$$\frac{d}{dx} \left(\frac{u^2}{2} \right) = \frac{c}{\rho} \cdot \frac{dp}{dx}$$

where c is a numerical constant.

Analysis Mode:

Equations (1) through (3) are transformed into two simultaneous differential equations with temperature (T) and velocity (u) as dependent variables:

$$\frac{dT}{dx} = \frac{T(\rho u^2 - p)}{u[\rho^2 u^2 (C_p T + C_T p) - \rho p (C_p T + u^2)]} \left[(J \cdot E) - G + \right.$$

$$\frac{\rho u^3 (\rho C_T - 1)}{\rho u^2 - p} \cdot \frac{p}{A} \frac{dA}{dx} - \frac{(u^2 - C_T p)}{\rho u^2 - p} \cdot \rho u \left. ((J \times B) - F) \right] \qquad (19)$$

$$\frac{du}{dx} = \frac{u}{\rho u^2 - p} \left[\frac{p}{A} \frac{dA}{dx} - \frac{p}{T} \frac{dT}{dx} + (J \times B)_x - F \right] \qquad (20)$$

where C_p = gas specific heat, constant pressure

C_T = gas specific heat, constant temperature

<u>Computer Program</u>

The program was written in Fortran IV language for processing in a SEL 32/55 computer. It consists of a main program, nine subroutine subprograms (4 are user-supplied subprograms) and one function subprogram. The interconnection flow chart is shown in Figure 1. The main program provides input/output functions and control of the solution. The flow chart for the main program is shown in Figure 2.

<u>Control Variables</u>:

       IDS -- program usage control variable
            0 -- design mode
            1 -- analysis mode

       ISG -- segmentation effects control variable
             0 -- segmentation effects are included
             1 -- segmentation effects are neglected

       ITYPE -- generator type control variable
              0 -- diagonal or cross-connected generator
              1 -- Faraday generator

       IF1 -- load control variable for a Faraday generator
             0 -- load factor is specified
             1 -- terminal voltage across each electrode pair is specified
             2 -- load resistance across each electrode pair is specified

       IA -- area control variable (may be modified by the user)
            0 -- Read AR(I)
            1 -- AR=f(x) (in subroutine area)

       IFREQN � frequency of intermediate printout. Solutions are
       IFREQG ⟩ printed at t=0 and after every IFREQ steps (N-nozzle,
       IFREQD ⎦ G-generator, D-diffuser)

<u>List of Variables</u>

AA   =   channel aspect ratio (channel width/channel height)

ALPHA   =   numerical constant that determines the gas velocity profile in the MHD generator (design mode)

$$\frac{d}{dx}(u^2/2) = ALPHA \cdot \frac{dp/dx}{\rho}$$

AR   =   channel cross-sectional area

A1
A2   =   constants reserved for subroutine AREA
C

C5   =   electrode pitch, m

C7   =   friction coefficient, nozzle

C8	=	friction coefficient, generator
C9	=	friction coefficient, diffuser
C10 C11 C12	=	empirical coefficients in turbulent heat transfer correlation for channel walls (nozzle, generator, diffuser)
C13	=	wall emissivity, nozzle
C14	=	wall emissivity, generator
C15	=	wall emissivity, diffuser
DELTA	=	Carbon/hydrogen mole ratio of the fuel
DUCT	=	length of the nozzle and generator
DX	=	integration step size
DX1	=	integration step size, nozzle
DX2	=	integration step size, generator
DX3	=	integration step size, diffuser
DY	=	(dy/dx) where y is the state variable
E	=	stagnation internal energy density
ERV	=	terminal voltage or load resistance (Faraday)
FACT	=	factor by which step size is reduced
ICT	=	step counter
IPR	=	state variable identifier
NA	=	size of array
NAME	=	type of generator (Faraday or diagonal), or channel section (nozzle or diffuser), or program identifier
NC	=	step size reduction counter
NO	=	number of first order differential equations (=2)
NP	=	total number of variables (y)
NPR	=	number of variables (y) to be printed
P	=	pressure
PHI	=	fuel mixture ratio (PHI<1 -- fuel rich)
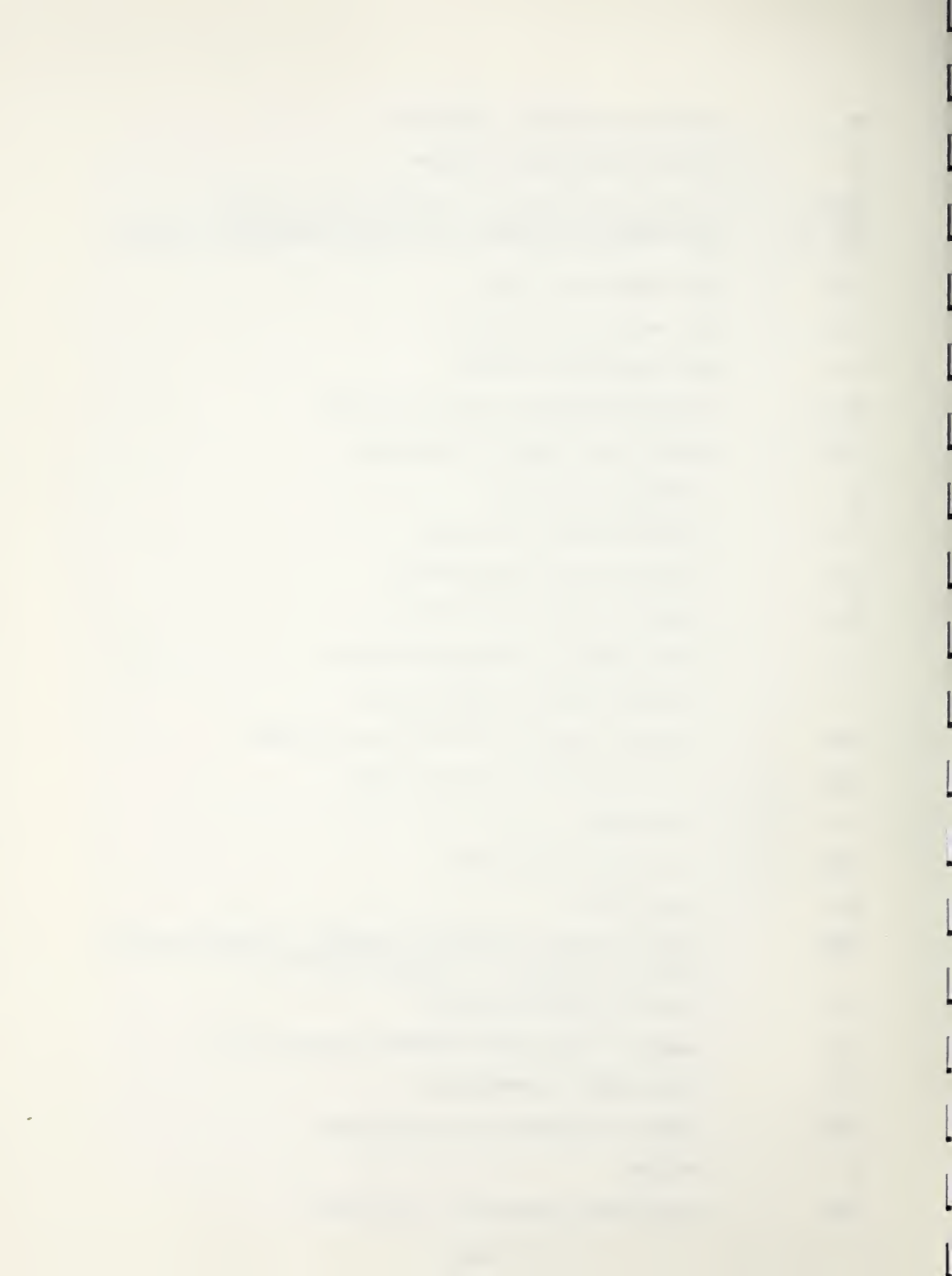
PSI	=	N_2/O_2 mole ratio of the combustion air
PLOSS	=	power dissipated in the electrodes
P1	=	water pressure at the channel cooling tubes inlet
Q	=	seed concentration, mole % K
RHO	=	mass density
S	=	constant reserve for subroutine AREA
TW1	=	wall temperature, nozzle
TW2	=	wall temperature, generator
TW3	=	wall temperature, diffuser
T1	=	water temperature, channel cooling tubes inlet
VD	=	voltage drop across the electrodes and the boundary layer
X	=	distance into the channel
XC	=	combustor length
XF	=	upper limit of integration
XI	=	$4 \cdot DELTA/(4 \cdot DELTA+1)$
XKY	=	cross-connection angle (diagonal generator), inlet
XKZ	=	generator cross-connection parameter at location x
XNOZ	=	length of nozzle
Y(1)	=	gas temperature
Y(2)	=	gas velocity
Y(3)	=	channel cross-sectional area
Y(4)	=	gas mass density
Y(5)	=	electric power density
Y(6)	=	Lorentz force
Y(7)	=	heat transfer term
Y(8)	=	friction term
Y(9)	=	gas specific heat, constant pressure
Y(10)	=	gas specific heat, constant temperature
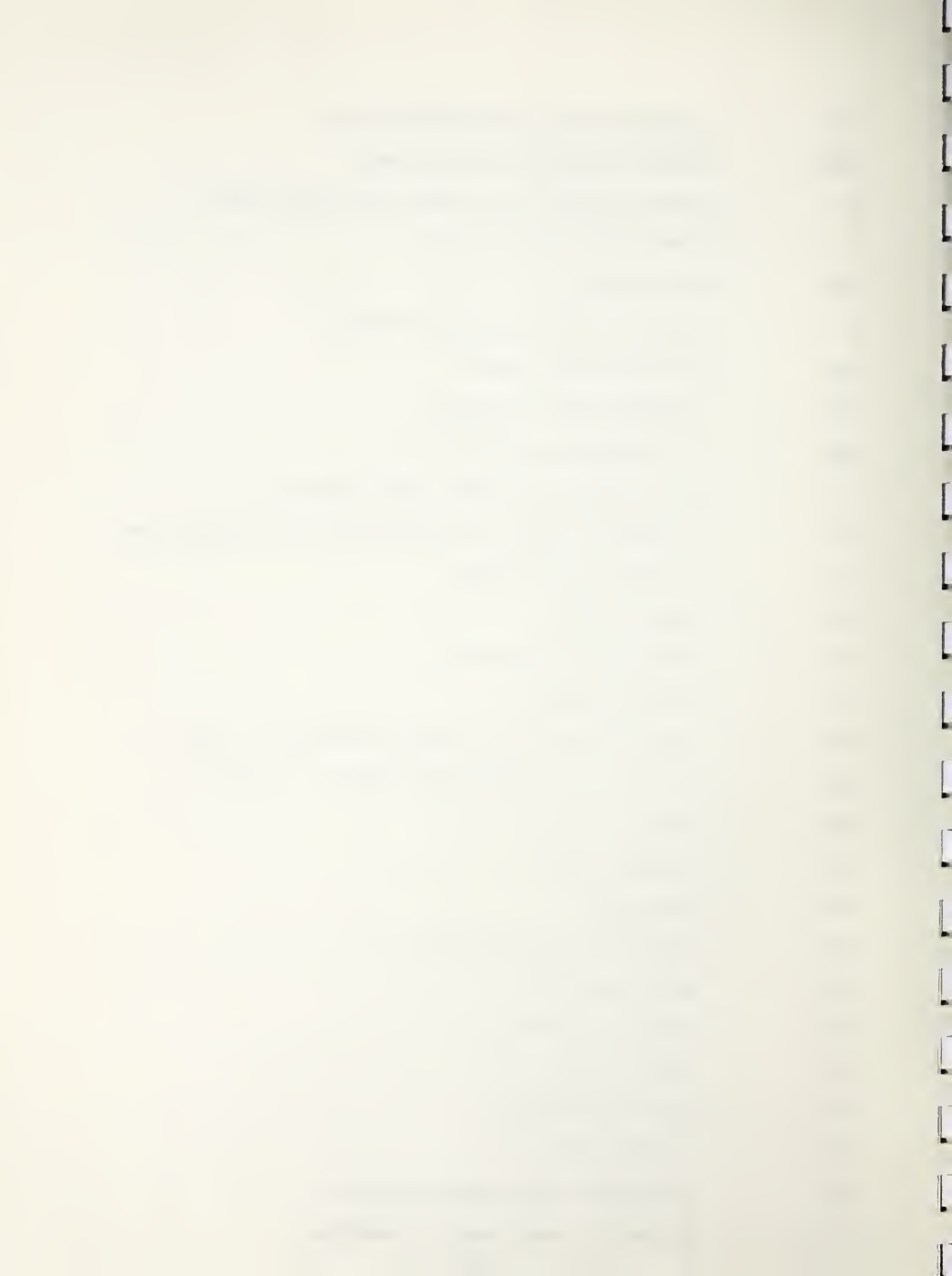
Y(11)	=	gas pressure
Y(12)	=	(design mode - du/dx); (analysis mode - dA/dx)
Y(13)	=	Hall parameter
Y(14)	=	electrical conductivity, mho
Y(15)	=	axial electric field, diagonal generator, v/m
Y(16)	=	axial electric field, (open circuit), diagonal generator
Y(17)	=	axial current density, amperes/m^2
Y(18)	=	transverse electric field
Y(19)	=	heat loss to the channel walls, Joules/sec
Y(20)	=	electrical power output, Joules/sec
Y(21)	=	load factor
Y(22)	=	isotropic efficiency, diagonal generator
Y(23)	=	electrode current (Faraday generator), amperes
Y(24)	=	voltage across electrode pair, Faraday, volts
Y(25)	=	gas pressure at (X+DX) - (design mode only)
Y(26)	=	molecular weight of the combustion gas
Y(27)	=	terminal voltage (diagonal)
Y(28)	=	open circuit voltage (diagonal)
Y(29)	=	magnetic field, Tesla
Y(30)	=	load resistance, (Faraday), ohm
Y(31)	=	load resistance (diagonal)
Y(32)	=	load current (diagonal)
Y(33)	=	internal resistance (Faraday)
Y(34)	=	internal resistance (diagonal)
Y(35)	=	gas enthalpy
Y(36)	=	electron mobility
Y(37)	=	channel width
Y(38)	=	channel height
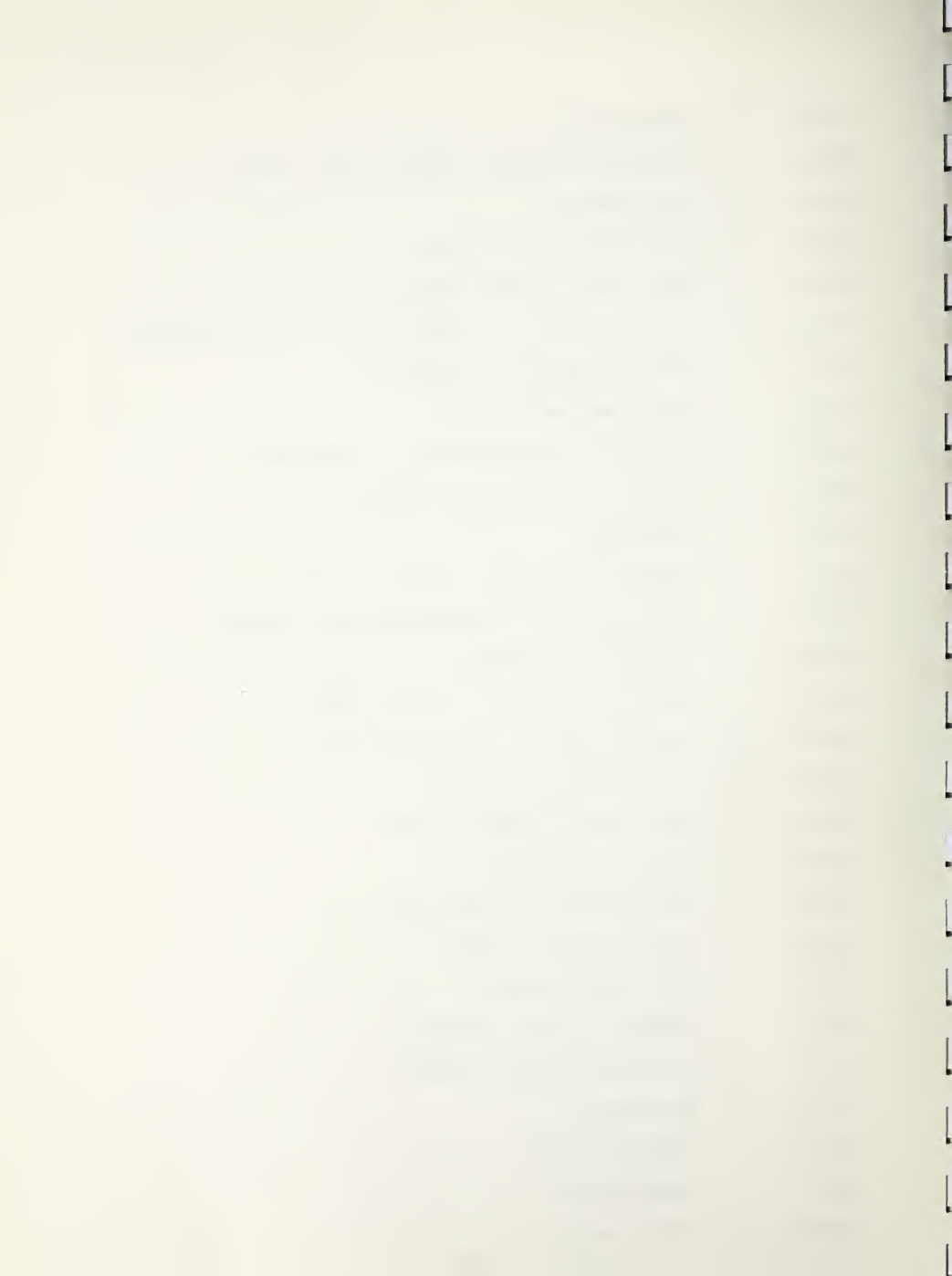
Y(39)	=	hydraulic diameter of the channel
Y(40)	=	Mach number
Y(41)	=	Reynolds number with respect to diameter
Y(42)	=	Reynolds number with respect to length
Y(43)	=	mass flow rate of the combustion gas, Kg/sec
Y(44)	=	heat loss due to electrode voltage drop
Y(45)	=	convective heat loss, watts/sq.m.
Y(46)	=	radiative heat loss, watts/sq.m.
Y(47)	=	channel aspect ratio

Data Input

The set-up of a data set for this program is illustrated below.

Card		Contents
1	=	NAME; format A8
2	=	PSI, PHI, Q, DELTA, TW1, TW2, TW3; format 7F10.4
3	=	C5, C7, C8, C9, C10, C11, C12; format 7F10.4
4	=	C13, C14, C15, XKY, AA, ALPHA, XC; format 7F10.4
5	=	XNOZ, DUCT, X, DX1, DX2, DX3, XF, FACT; format 8F10.4
6	=	A1, A2, C, S, VD, P1, T1; format 7F10.4
7	=	IDS, ISG, IA, ITYPE, IFREQN, IFREQG, IFREQD, NP, IF1, NA, NG; format 11I4
$\begin{matrix}8\\9\end{matrix}$	=	IPR(I), I = 1, 50; format 25I3
10	=	Y(1), Y(2), Y(3), Y(12), Y(21), Y(26), Y(32), Y(43); format 8F10.4
11 $\rangle$	=	IF IA ≠ 0; not needed IF IA = 0, (AR(I), I=1, NA); format 8F10.4
$\rangle$	=	IF IF1 = 0; not needed IF IF1 ≠ 0; (ERV(I), I=1, NG); format 8F10.4
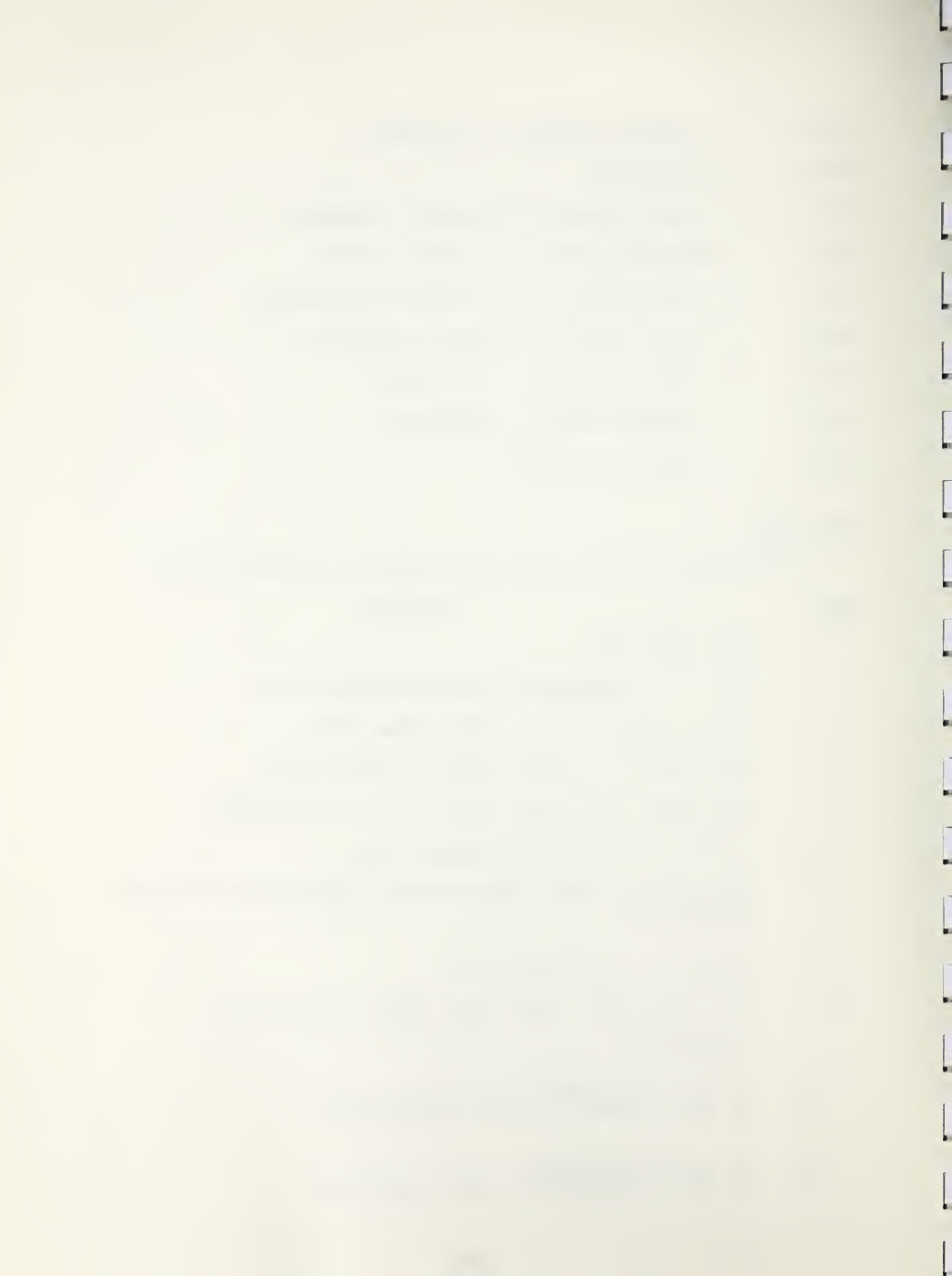
Subprograms

Function INTEGD - This subprogram employs the fourth order Runge-Kutta method with Kutta's coefficients to integrate a system of simultaneous first order ordinary differential equations, across one step of length DX in the independent variable X, subject to initial conditions. The fourth order Runge-Kutta calculation procedure used is

$$y_{i+1} = y_i + \frac{DX}{6} (k_1 + 2k_2 + 2k_3 + k_4)$$

where

$$k_1 = f(x_i, y_i)$$

$$k_2 = f(x_i + \frac{DX}{2}, y_i + 1/2 \ DX \cdot k_1)$$

$$k_3 = f(x_i + \frac{DX}{2}, y_i + 1/2 \ DX \cdot k_2)$$

$$k_4 = f(x_i + DX, y_i + DX \cdot k_3)$$

The flow diagram is shown in Figure 3.

Convergence Test

An error check may be used in function INTEGD to compare the relative increment generated during any integration step with the magnitude of the state. Preset into the main program is a default value of .001 which means the integration is judged to be non-convergent at the inequality:

Increment in state $Y(I) > (.001)$ (present value of state $Y(I)$)

is true for any state $Y(I)$. If $Y(I)$ is zero, the maximum increment allows 15 times the present estimate of the state derivatives times the present independent variable step size DX. If the inequality above is false, the integration is judged successful and the state vector is updated. If the convergence test fails, the step size DX is multiplied by FACT and integration is again attempted. If the convergence test fails 5 times, i.e. if integration is unsuccessful with a step size of DX $\cdot$ $(FACT)^5$ the least successful values of the system states will be printed and the calculation is terminated.

If integration is successful, subroutine SIDE is called to update the solution values y_i.

Subroutine STATE - This subprogram contains the differential equations (17) to (20). In the design mode, equation (17) and (18) are used and in the analysis mode, equations (19) and (20) are used.

Subroutine SIDE - This subprogram updates the solution values of the state variables y_i. It requires subroutines HGAS, ELECT and AREA. The heat transfer and friction terms are calculated in this subroutine. The flow diagram is shown in Figure 4. Additional variables used (not found in the main program) are:

CF = friction coefficient

CH = convective heat transfer coefficient on channel walls

151

EG   =   gas emissivity

EW   =   channel wall emissivity

GAMD =   empirical coefficient in turbulent heat transfer correlation
         for channel walls

HW   =   enthalpy of combustion gas at wall temperature

QR   =   radiative heat flux falling on channel walls

QW   =   convective heat flux to channel walls

RE   =   recovery factor

SK   =   Boltzmann's constant

TW   =   wall temperature

XK   =   gas thermal conductivity

XN   =   gas viscosity

S1,S2,S3,S4,S5 =   dummy variables

Subroutine HGAS - This subprogram calculates the thermodynamic (enthalpy, molecular weight and specific heats) and electrical (conductivity, electron mobility) properties of the combustion gas. The gas properties are based on the chemical equilibrium equations for carbon, oxygen, nitrogen and hydrogen mixtures.[11] The additional variables used in this subroutine are:

CP   =   specific heat, constant pressure

CT   =   specific heat, constant temperature

H   =   gas enthalpy

S   =   gas electrical conductivity

XMU =   electron mobility

XNE =   electron density

Subroutine ELEC - This subprogram calculates the electrical variables for a given MHD generator configuration (eq. 5 to 16). If segmentation effects are considered, subroutine SEG is required. If load resistances or inverter voltages, are specified, subroutine INV is needed. The magnetic field profile and the electrode voltage drops are obtained from subroutine MAG. The flow diagram is shown in Figure 5. The additional variables used are:

B1
B2
E1 } =   segmentation effects coefficients obtained from subroutine SEG
E2

AMP = dimensionless load current (diagonal)

C4 = electrode pitch to channel width (distance between opposite electrodes) ratio

$\left.\begin{array}{l} C1 \\ C2 \\ C3 \\ FACTOR \end{array}\right\} =$ correction factors due to segmentation effects

Subroutine WCOOL - This subprogram calculates the steady-state variables of the cooling system for the MHD channel. It receives from the main program the following information: the total heat loss to the channel walls, the mean temperature and pressure of the cooling water at the inlet. A data statement is required to provide the following information: average length of the cooling tubes, tube inside diameter, mass flow rate of the cooling water total water flow area, coefficient of friction inside the cooling tubes, and the outside wall surface temperature of the channel. The outputs are temperature and pressure of the cooling water at the exit.

The properties of compressed water are represented by polynomial functions ($T = f(h,p)$; $\rho = f(h,p)$) derived from the steam tables[12] using the least squares method.

List of Variables

A = total water flow area, m^2

DI = tube inside diameter, m

F = coefficient of friction inside surface of the cooling tubes

H1 = enthalpy of the water, inlet

H2 = enthalpy of the water, exit

P1 = pressure of the water, inlet

P2 = pressure of the water, exit

Q = total heat loss to the channel walls

RHO1 = mass density of the water, inlet

RHO2 = mass density of the water, exit

TWO = wall temperature, channel outside surface

T1 = temperature of the water, inlet

T2 = temperature of the water, exit

V1 = velocity of the water, inlet

V2 = velocity of the water, exit
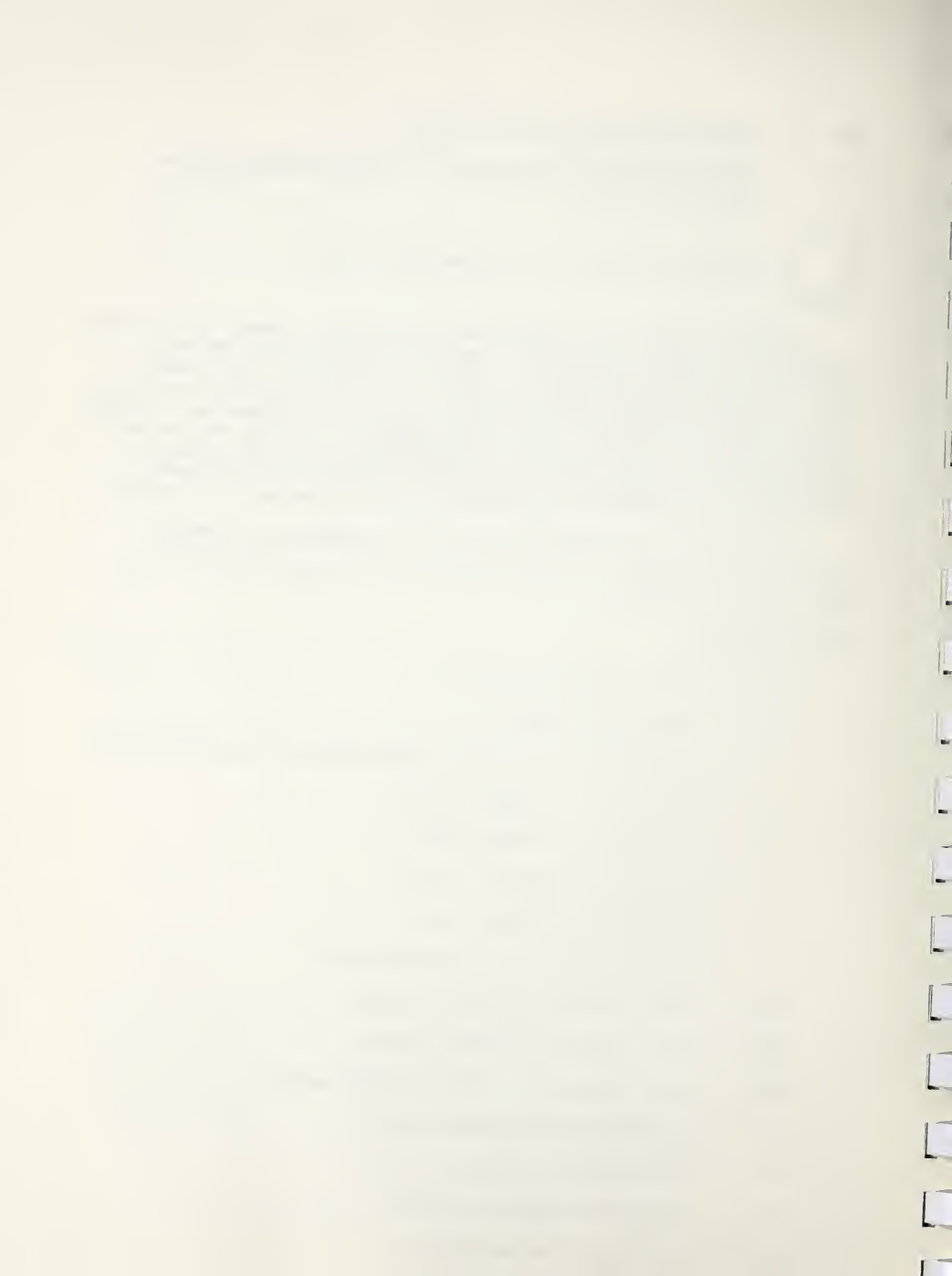
W   =   mass flow rate of the water

Y   =   average water flow length

User-Supplied Subroutines

Subroutine AREA - This subprogram supplies the area and dimensions (width, height, hydraulic diameter) of the MHD channel as a function of channel axial distance. The information from this subprogram is communicated to subprogram SIDE using the parameter list (Y,X,DX).

Subroutine SEG - This subprogram calculates the segmentation effects in the MHD generator based on the work of Dzung and Witalis[3]. The listing included in this report is for a generator with an electrode width to electrode pitch ratio of .75. The user may modify this subprogram to conform with a given electrode design. The parameter list must be (BETA, B1, B2, E1, E2) where

BETA   =   Hall parameter, obtained from subroutine ELEC

B1
B2
E1   } =   segmentation effects coefficients communicated
E2   to subroutine ELEC

Subroutine INV - This subprogram supplies the inverter voltages or load resistances across each electrode pair. The parameter list must be (X, RL, VY), where

RL   =   load resistance across an electrode pair at location X

VY   =   load voltage (inverter voltage) across an electrode pair at location X.

Subroutine MAG - This subprogram supplies the magnetic field, electrode voltage drop (includes voltage drop across the boundary layer), and the generator cross-connection parameter at the location X. The parameter list must be (X, BN, VDR, XKZ) where

BN   =   magnetic field at location X

VDR =   voltage drop at location X

XKZ =   cross-connection parameter at location X

II. Program MHDTD

A.   This program calculates the properties of non-steady-state flow in the MHD channel. The MHD equations in conservation law form are:
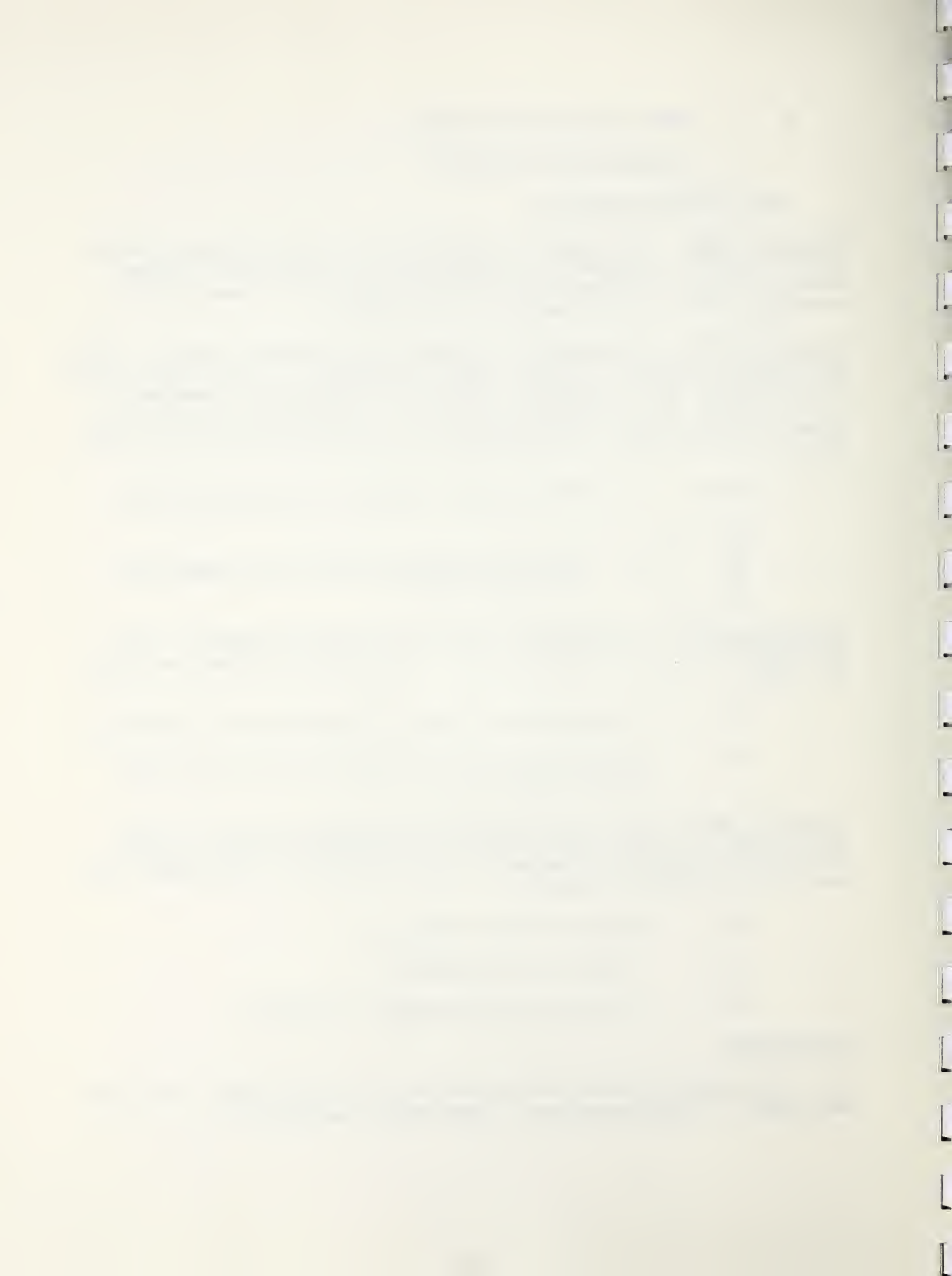
$$\frac{\partial}{\partial t}\begin{vmatrix} \rho \\ m \\ \varepsilon \end{vmatrix} = \frac{\partial}{\partial x}\begin{vmatrix} m \\ m^2/\rho + p \\ m(\varepsilon + p)/\rho \end{vmatrix} + \begin{vmatrix} \dfrac{-m}{A}\dfrac{dA}{dx} \\ (JxB)_x - F - \dfrac{m^2}{\rho A}\dfrac{dA}{dx} \\ (J\cdot E) - Q - \dfrac{m}{\rho A}(\varepsilon + p)\dfrac{dA}{dx} \end{vmatrix}$$

or may be represented by the form

$$\frac{\partial U}{\partial t} + \frac{\partial F(U)}{\partial x} + G(U) = 0$$

where

m = momentum density,

ε = $\rho(e + u^2/2)$ - stagnation internal energy density,

e = internal energy of the fluid,

Q = heat transfer per unit volume,

t = time.

Other variables are defined in Section I.

The MHD equations were solved by employing the modified two-step Lax-Wendroff method.[8,9] This method, based on the system of conservation equations (mass density, momentum density, and stagnation internal energy density as dependent variables), enables one to integrate across a flow discontinuity.

The values of U (the dependent variables defined in the above equations) are computed for the temporary points at half-time and half-space increments $(n + 1/2, j + 1/2)$ in the first step of the calculation. The second step is employed to determine the value of U at the final point $(n + 1, j)$. The finite difference calculation procedure is summarized as follows:

Step One:

$$U_{j + 1/2}^{n + 1/2} = (U_{j+1}^n + U_j^n)/2 - \frac{\Delta t}{\Delta x}(F_{j+1}^n - F_j^n) - \frac{\Delta t}{2}(G_{j+1}^n + G_j^n)$$

$$U_{j - 1/2}^{n + 1/2} = (U_{j-1}^n + U_j^n)/2 + \frac{\Delta t}{\Delta x}(F_{j-1}^n - F_j^n) - \frac{\Delta t}{2}(G_{j-1}^n + G_j^n)$$

Step Two:

$$U_j^{n+1} = U_j^n - \frac{\Delta t}{\Delta x}(F_{j+1/2}^{n+1/2} - F_{j-1/2}^{n+1/2}) - \frac{\Delta t}{2}(G_{j+1/2}^{n+1/2} + G_{j-1/2}^{n+1/2})$$

The stability limitation is given by the Courant, Friedrick, and Lewy stability criterion[10]

$$(|u| + a)\frac{\Delta t}{\Delta x} \leq 1.$$
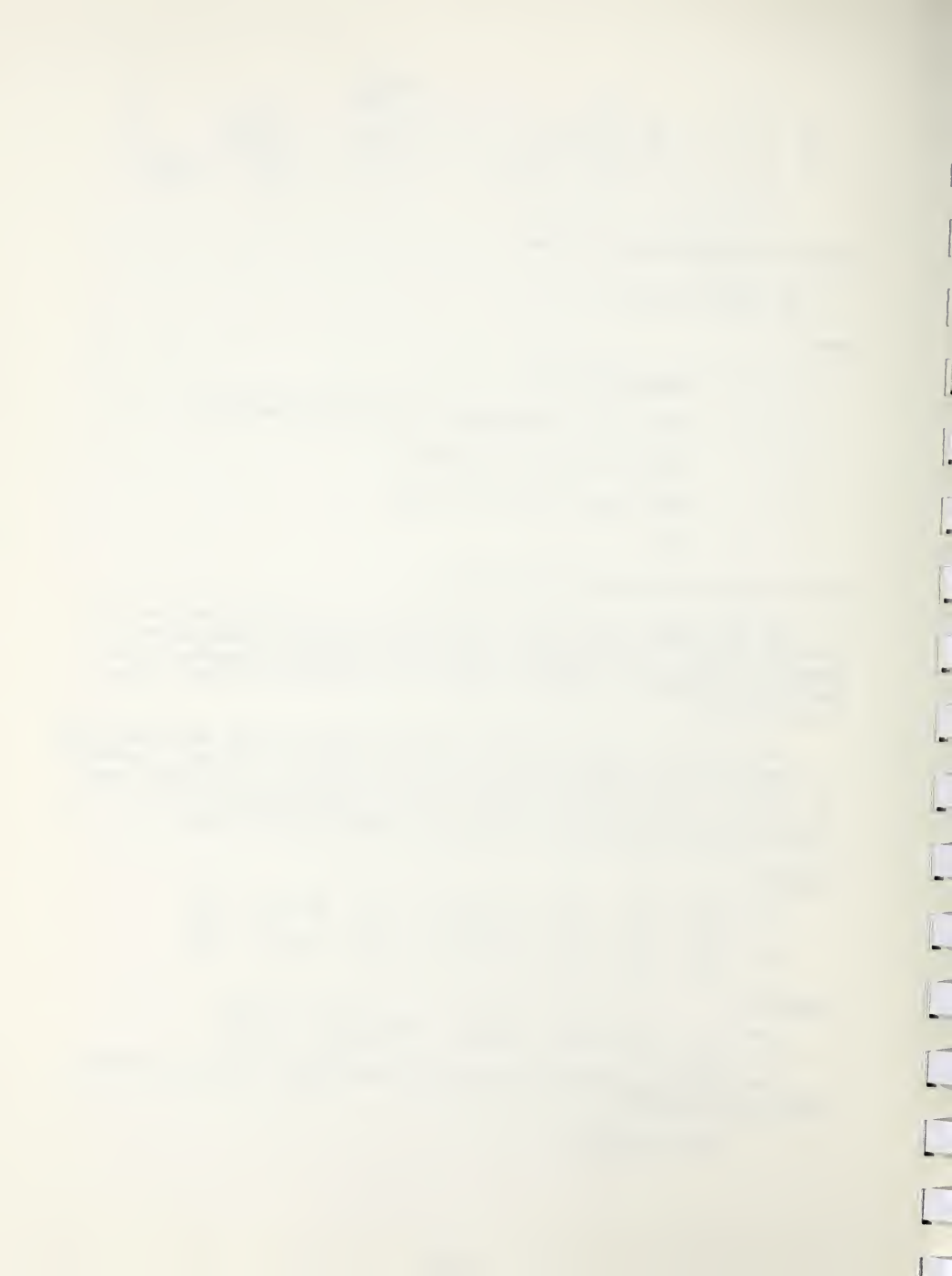
An initial condition is assumed such that a steady-state flow exists in the channel with a known distribution of the gas dynamic, thermodynamic, and electrical variables. The distribution is obtained from the numerical solution of a system of differential equations describing the steady-state flow of the working fluid (Program MHDAV). This set of variables is then introduced as initial conditions for the system of conservative nonsteady-state MHD flow equations.

The boundary conditions are

$$p_o = p_{10} = \text{constant, if } x = 0 \quad (\text{nozzle inlet}),$$

$$T_{so} = T_{s10} = \text{constant, if } x = 0, \text{ and}$$

$$p = p_2 = \text{constant, if } x = L \quad (\text{diffuser exit})$$

where p_{10}, T_{s10}, and p_2 are the corresponding stagnation parameters of the working fluid.

B.   Computer Program

The computer program was written in Fortran IV language for processing in a SEL/55 computer. It consists of a main program and six subroutine subprograms (4 are user supplied subprograms). The interconnection flow chart is shown in Figure 6. The main program provides input/output functions and the numerical solution of the conservation equations. The solution for the MHD channel is divided into two sections. The first section considers the solution to the nonsteady-state flow in the nozzle and the second section considers the solution to the nonsteady-state flow in the generator and diffuser. The nozzle requires smaller step sizes (Δt, Δx) because of the rapid changes in the fluid variables (velocity, pressure, temperature, etc.).

The flow diagram is shown in Figure 7.

Control Variables

    ITYPE -- generator type control variable
            0 -- diagonal or cross-connected generator
            1 -- Faraday generator

    ISG -- segmentation effects control variable
            0 -- segmentation effects are included
            1 -- segmentation effects are neglected

   IF1 -- Load control variable
            0 -- load factor is specified
            1 -- terminal voltages are specified
            2 -- load resistances are specified

    IFREQ -- frequency of intermediate printout. Solutions are printed
   at t=0 and after every IFREQ step.
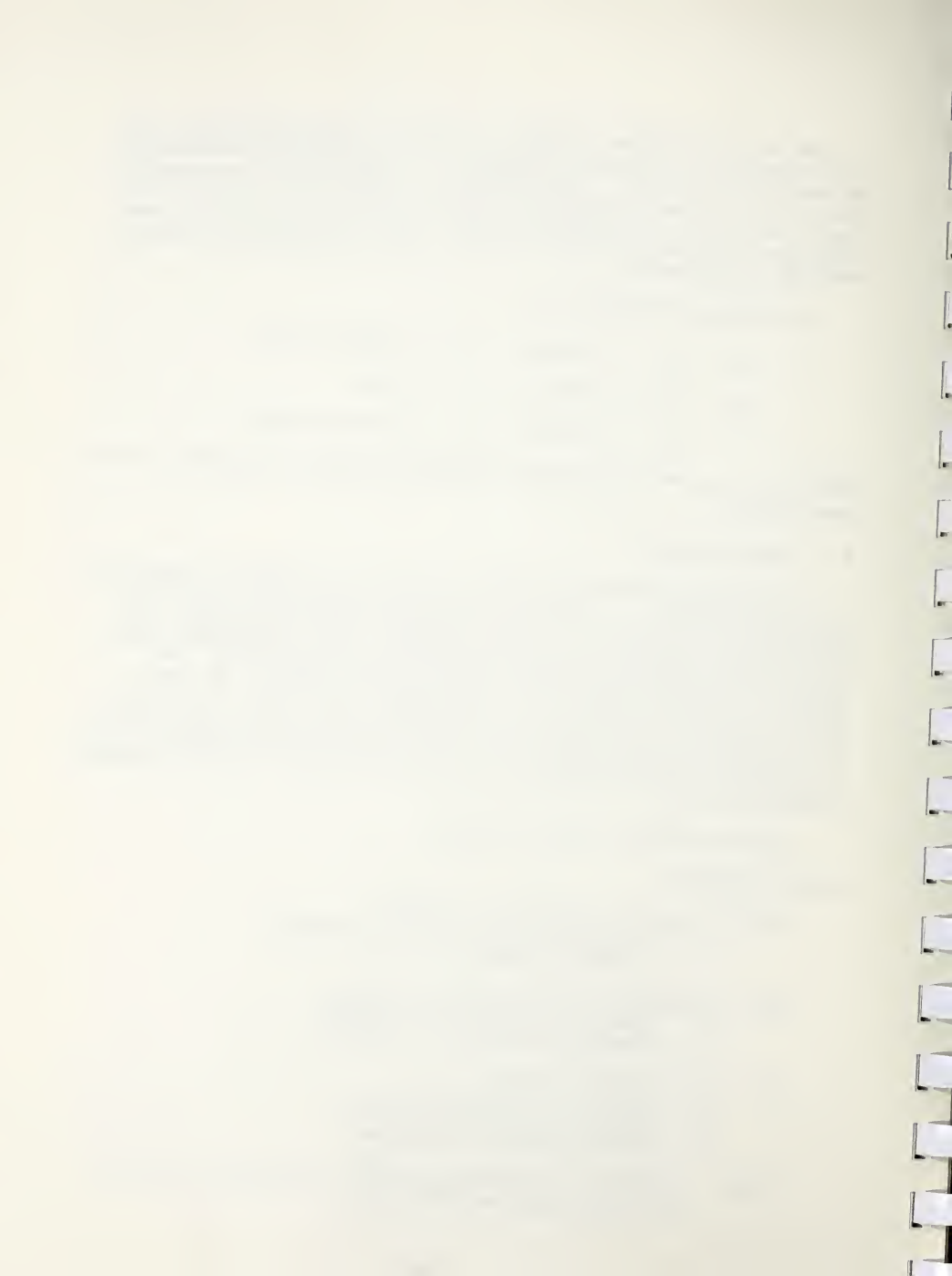
List of Variables -- Main Program

A = channel cross-sectional area

AA = channel aspect ratio, channel width/channel height

AMP1 = load current, diagonally connected generator

BN = magnetic field

C5 = electrode pitch

C7 = friction coefficient nozzle

C8 = friction coefficient generator

C9 = friction coefficient diffuser

C10
C11 $\rangle$ = empirical coefficients in turbulent heat transfer correlation
C12 for channel walls (nozzle, generator and diffuser respectively)

C13 = wall emissivity, nozzle

C14 = wall emissivity, generator

C15 = wall emissivity, diffuser

DELTA = carbon/hydrogen mole ratio of the fuel

DTAU = time step size

DUCT = generator length

DX = x-step size

DX1 = x-step size, nozzle

DX2 = x-step size, generator and diffuser

E = stagnation internal energy density at t=n

ELC = electrode current (Faraday)

ELV = terminal voltage (Faraday)

EN = stagnation internal energy density at t=n+1

EN1 = stagnation internal energy density at t=n, x=j+1/2

EN2 = stagnation internal energy density at t=n, x=j-1/2

ERV = load resistance, if IF1=2; terminal voltage if IF1=1; Faraday

157
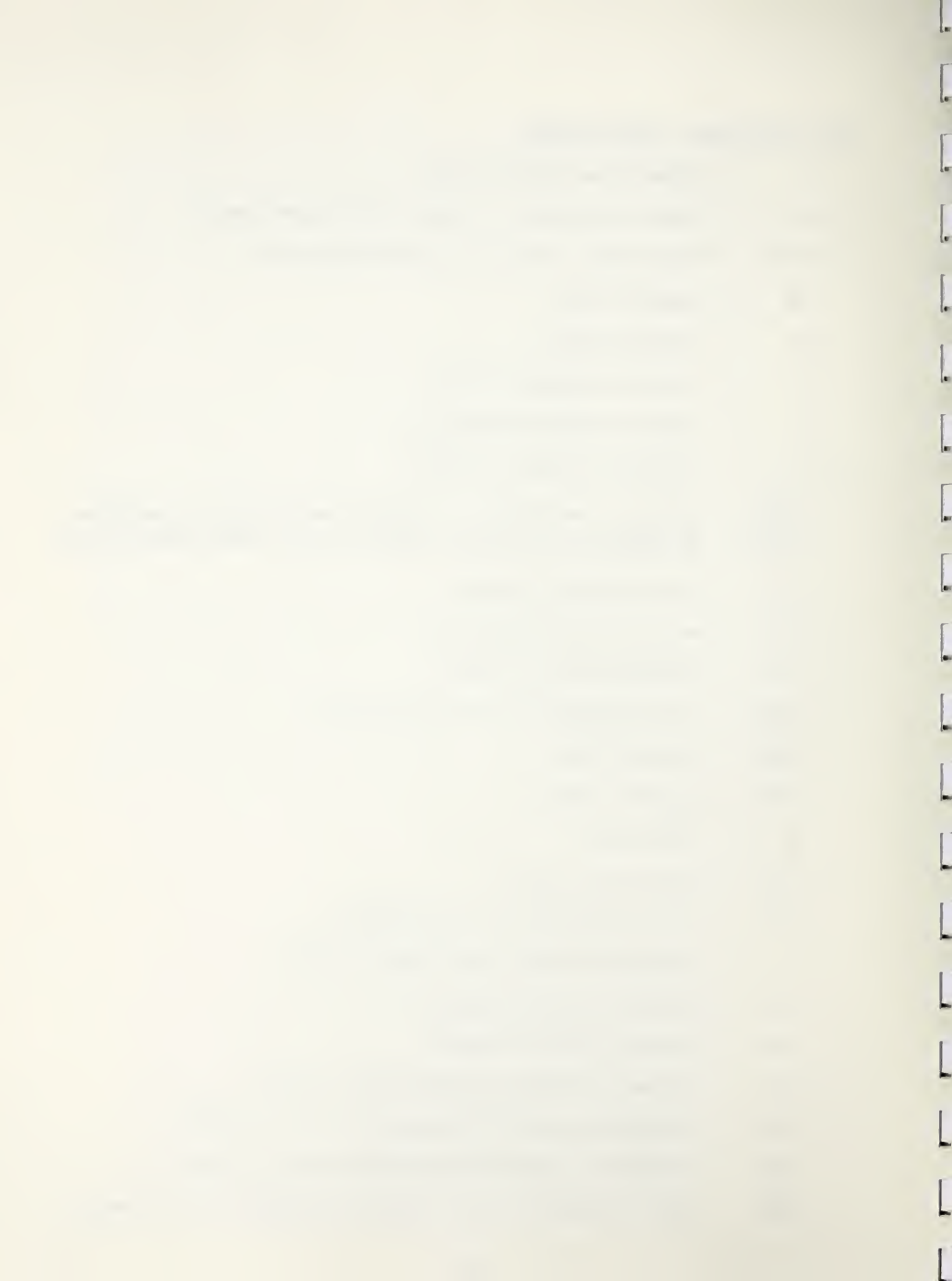
EX	=	axial electric field
EY	=	transverse electric field
F	=	friction term at t=n, x=j+1/2 or t=n+1, x=j
F2	=	friction term at t=n, x=j-1/2
G	=	heat transfer term at t=n, x=j+1/2 or t=n+1, x=j
G2	=	heat transfer term at t=n, x=j-1/2
HS	=	stagnation enthalpy at nozzle inlet
ICT	=	integration step counter
K	=	size of array, nozzle
KL	=	counter
L	=	size of array, nozzle + generator + diffuser
M	=	size of array, nozzle + generator
NAME	=	generator identification (Faraday or diagonal)
P	=	pressure at t=n, x=j+1/2; or t=n+1, x=j
P2	=	pressure at t=n, x=j-1/2
PHI	=	actual fuel mixture ratio/stoichiometric ratio
PMHD	=	MHD generator electrical power output
PR	=	stagnation pressure at diffuser exit
PSI	=	nitrogen/oxygen mole ratio
Q	=	seed concentration, mole % K
QMHD	=	heat loss to the generator walls
QNOZ	=	heat loss to the nozzle walls
QDIFF	=	heat loss to the diffuser walls
R	=	load resistance
RI	=	internal resistance
RHO	=	mass density at t=n
RHON	=	mass density at t=n+1
RHON1	=	mass density at t=n, x=j+1/2
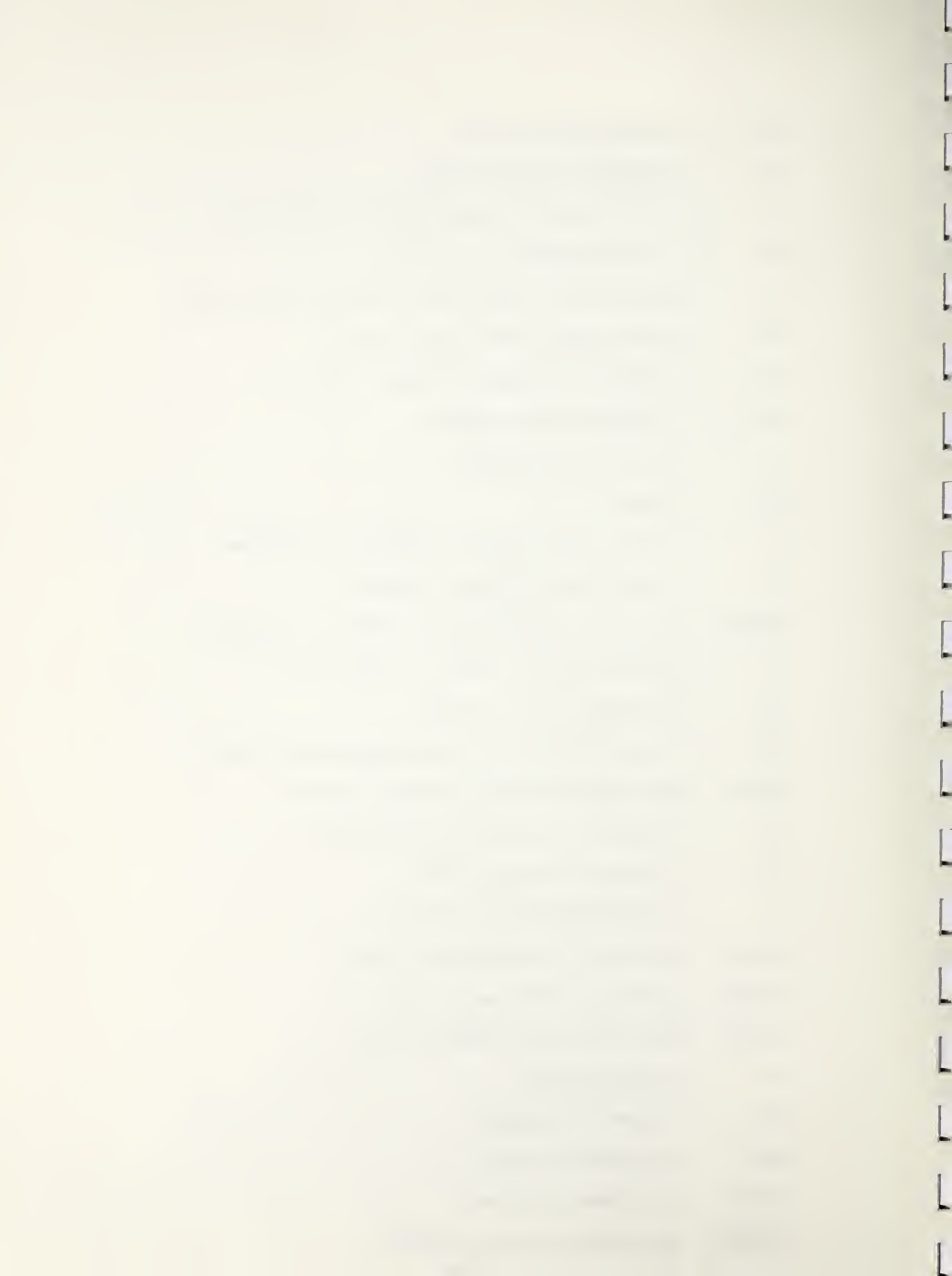
RHON2 = mass density at t=n, x=j-1/2

S1
S2
S3 } = dummy constants
S4
S5

T = temperature

TAU = time

TAU1 = time

TF = time step ratio (generator/nozzle)

TW1 = wall temperature, nozzle

TW2 = wall temperature, generator

TW3 = wall temperature, diffuser

TAUMAX = upper time limit of integration

V = gas velocity

VD = voltage drop across the electrodes and boundary layer

VDC = terminal voltage, diagonal generator

VOC = open circuit voltage, diagonal generator

W = momentum density at t=n

WM = mass flow rate

WN = momentum density at t=n+1

WN1 = momentum density at t=n, x=j+1/2

WN2 = momentum density at t=n, x=j-1/2

XC = combustor length

XI = $4 \cdot DELTA/(4 \cdot DELTA + 1)$

XJB = Lorentz force at t=n, x=j+1/2 or t=n+1, x=j

XJB2 = Lorentz force at t=n, x=j-1/2

XJE = electric power density at t=n, x=j+1/2 or t=n+1, x=j

XJE2 = electric power density at t=n, x=j-1/2

XKC = load factor (Faraday)
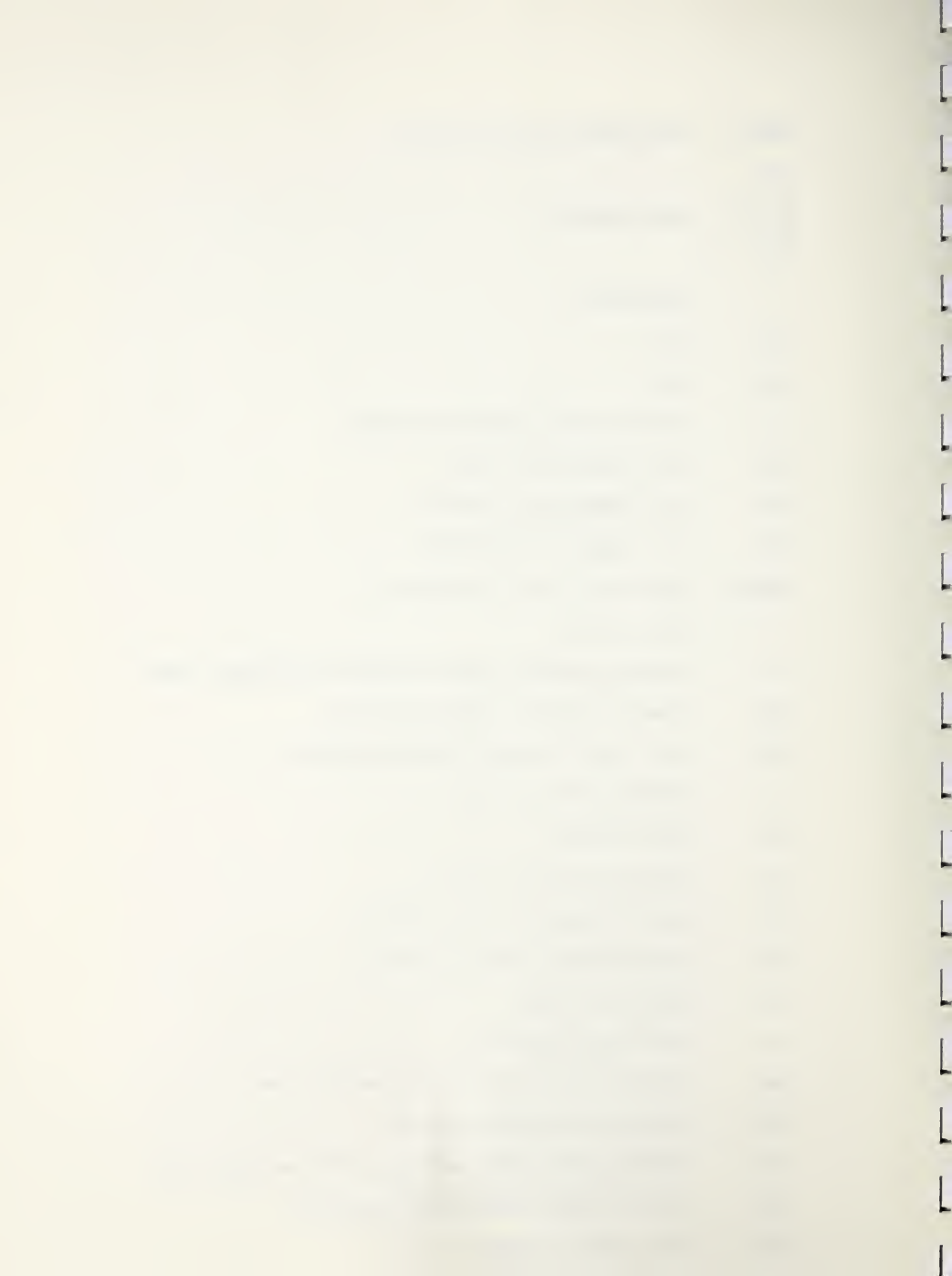
XKCD = average load factor (diagonal)

XKY   = cross-connection angle, inlet (diagonal generator)

XKZ   = cross-connection parameter (diagonal generator)

XM   = gas molecular weight

XNOZ = length of nozzle

Data Input

The set-up of a data set for this program is illustrated below.

Card	Contents
1	Name (type of generator, diagonal or Faraday; or channel section, nozzle of diffuser); format A8
2	PSI, PHI, Q, DELTA, TW1, TW2, TW3, XC; format 8F10.4
3	C5, C7, C8, C9, C10, C11, C12, C13; format 8F10.4
4	C14, C15, XKY, AMP1, VD, XKC, XM; format 7F10.4
5	DX1, DX2, DTAU, TAU, TAUMAX, WM, TF; format 7F10.4
6	K, L, M, IFREQ, ITYPE, ISG, IF1, IA; format 8I4
7	E(I), I=1, L; format 5E13.7
	P(I), I=1, L; format 5E13.7
	W(I), I=1, L; format 5E13.7
	RHO(I), I=1, L; format 8F10.4
	A(I), I=1, L; format 8F10.4
	AX(I), I=1, L; format 8F10.4

$$\left.\begin{array}{c} . \\ . \\ . \end{array}\right\rangle \qquad BX(I), \; I=1, \; L; \; format \; 8F10.4$$

$$\left.\begin{array}{c} . \\ . \\ . \end{array}\right\rangle \qquad DADX(I), \; I=1, \; L; \; format \; 8F10.4$$

$$\left.\begin{array}{c} . \\ . \\ . \end{array}\right\rangle \qquad \begin{array}{l} If \; IF1 \neq 0; \; ERV(I), \; I=1, \; MN \\ If \; IF1 = 0; \; not \; needed \end{array}$$

Subprogram

Subroutine UPDATE -- this subprogram updates the solution values (F, G, XJE, XJB, etc.). It requires subroutines HGAST and ELECT. The heat transfer and friction terms are calculated in this subroutine. The flow diagram is shown in Figure 8. Additional variables used (not found in the main program) are:

AX   =   channel width

BX   =   channel height

CF   =   coefficient of friction

CH   =   convective heat transfer coefficient

CP   =   specific heat, constant pressure

D   =   hydraulic diameter of the channel

EFF =   isotropic efficiency

EG   =   gas emissivity

EW   =   wall emissivity

GAMD =   empirical coefficient in turbulent heat transfer correlation
         for channel walls

H   =   gas enthalpy

QR   =   radiative heat loss

QW   =   convective heat loss

RE   =   recovery factor, cube root of the Prandtl number

RED =   Reynolds number with respect to diameter

REX =   Reynolds number with respect to length

SK   =   Boltzmann's constant

TW	=	wall temperature
XL	=	distance into the channel
XK	=	gas thermal conductivity
XN	=	gas emissivity

Subroutine ELECT

This subprogram calculates the electrical variables for a given MHD generator configuration. If segmentation effects are considered subroutine SEG is required. If load resistances or inverter voltages are specified, subroutine INVT is needed. The magnetic field profile and the electrode voltage drops are obtained from subroutine MAGT. The flow diagram is similar to that of subroutine ELEC (Figure 5).

The additional variables used are:

AMP	=	nondimensional load current
BETA	=	Hall parameter
B1 B2 E1 E2	=	correction coefficients due to segmentation effects
C1 C2 C3	=	correction factors due to segmentation effects, diagonal
EFF	=	isotropic efficiency
EXO	=	open circuit voltage, diagonal
FACTOR	=	correction factor due to segmentation effect, Faraday
RL	=	load resistance
VY	=	terminal voltage, Faraday
XMU	=	electron mobility

User-Supplied Subroutines

Subroutine HGAST -- This subprogram calculates the thermodynamic (temperature, specific heat, pressure) and electrical (conductivity, electron mobility) properties of the combustion gas.

The temperature enthalpy is expressed as a function of the mass density and enthalpy ($T=f(h,\rho)$). The equations for temperature and specific heat given in this program are for a specific fuel/air mixture, i.e. PSI=3.76 and PHI=1.0. Ths user may modify this program without affecting the structure

of the main program. The parameter list must be (T, P, RHO, H, XMU, SIGMA, CP, XM) where RHO and H are supplied by the main program.

Subroutine SEGT -- similar to subroutine SEG in part 1.

Subroutine INVT -- similar to subroutine INV in part 1 except for the parameter list which should be (N, RL, VY).

Subroutine MAGT -- similar to subroutine MAG in part 1 except for the parameter list which should be (N, BN, VDR, XKZ).
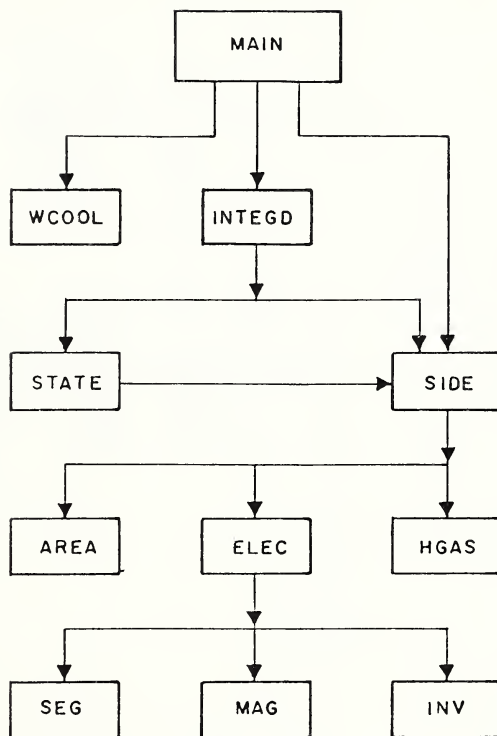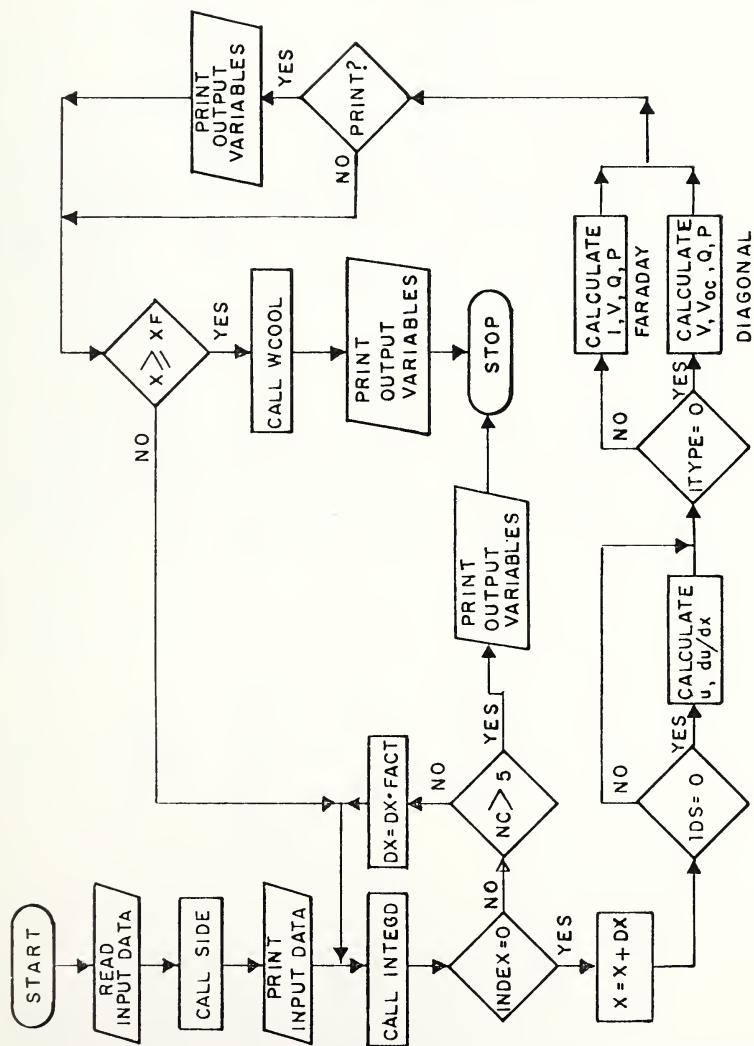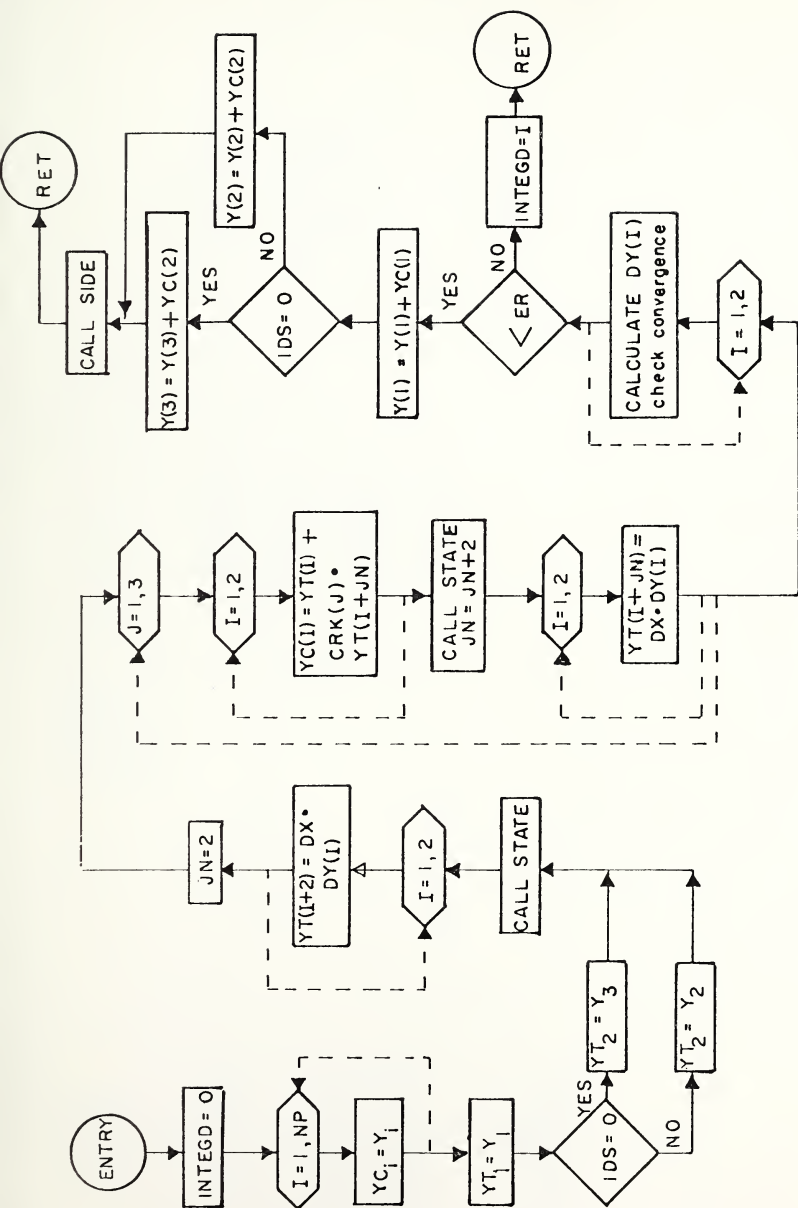
FIG. I. INTERCONNECTION FLOW CHART — MHDAV

FIG. 2. FLOW DIAGRAM FOR MAIN PROGRAM — MHDAV

165

FIG. 3. FLOW DIAGRAM — FUNCTION INTEGD
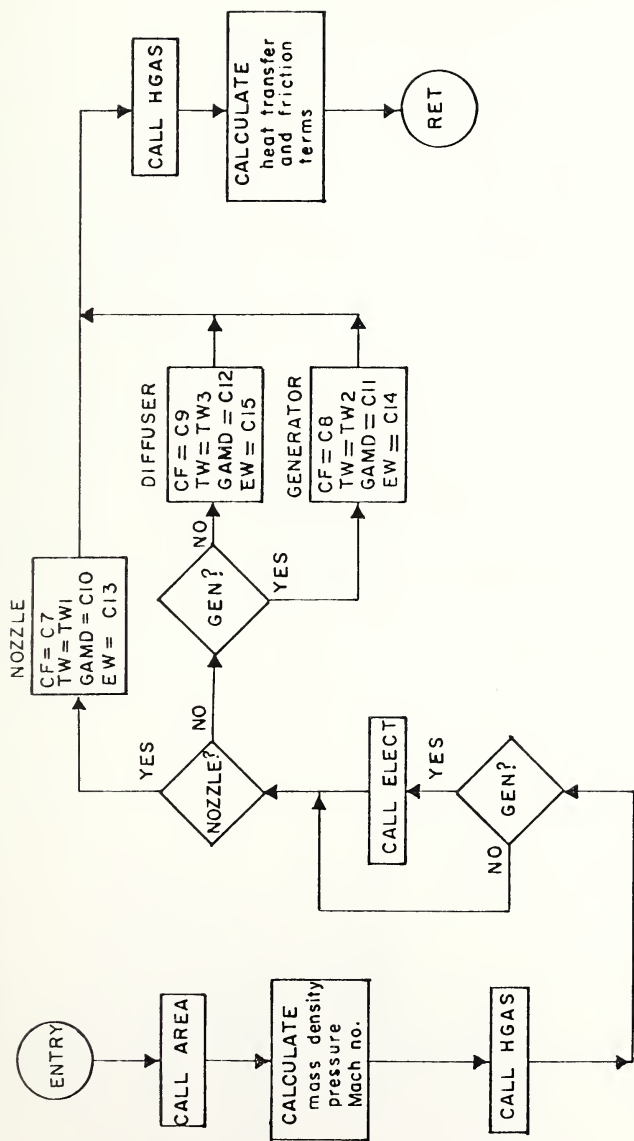
FIG. 4. FLOW DIAGRAM — SUBROUTINE SIDE

167
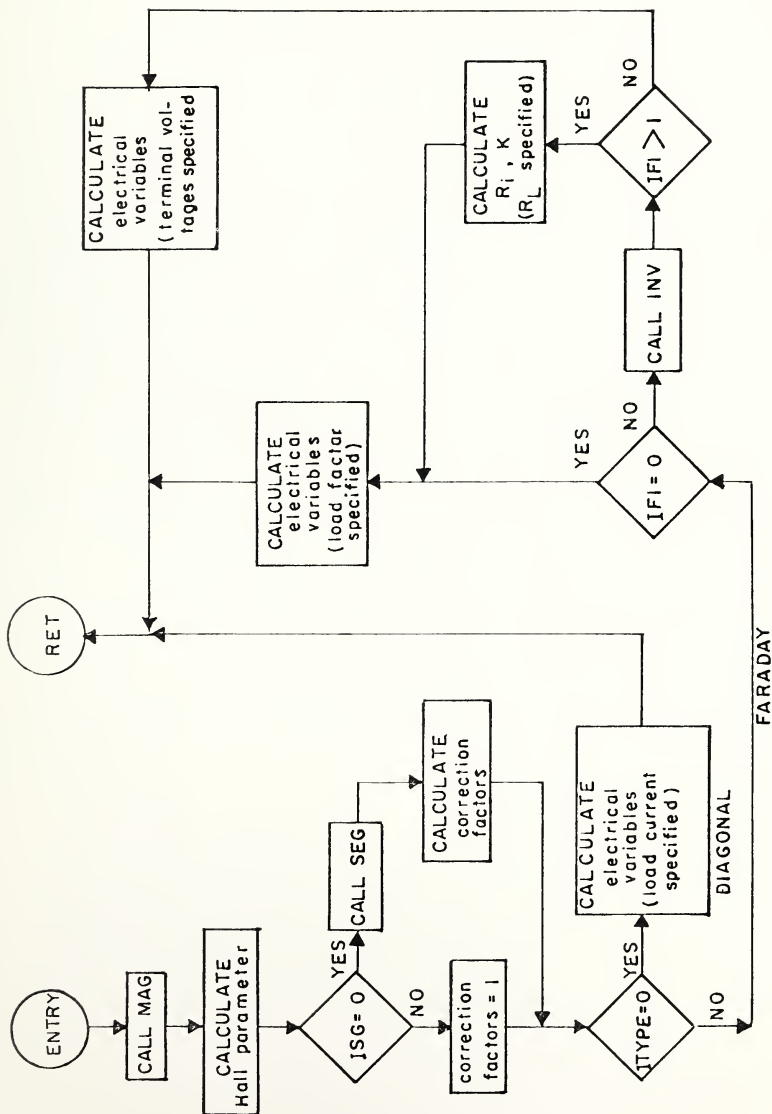
FIG. 5. FLOW DIAGRAM — SUBROUTINE ELEC

168
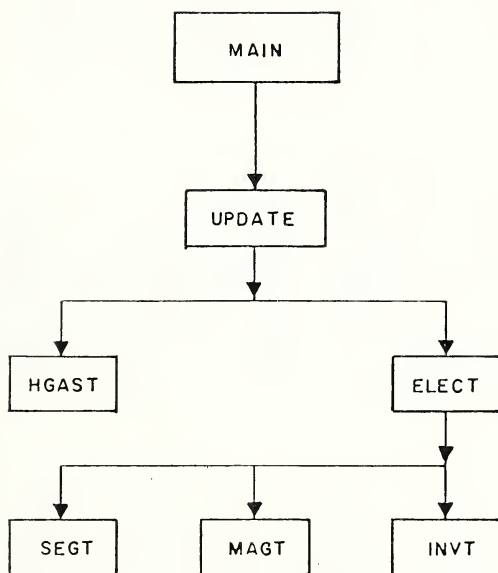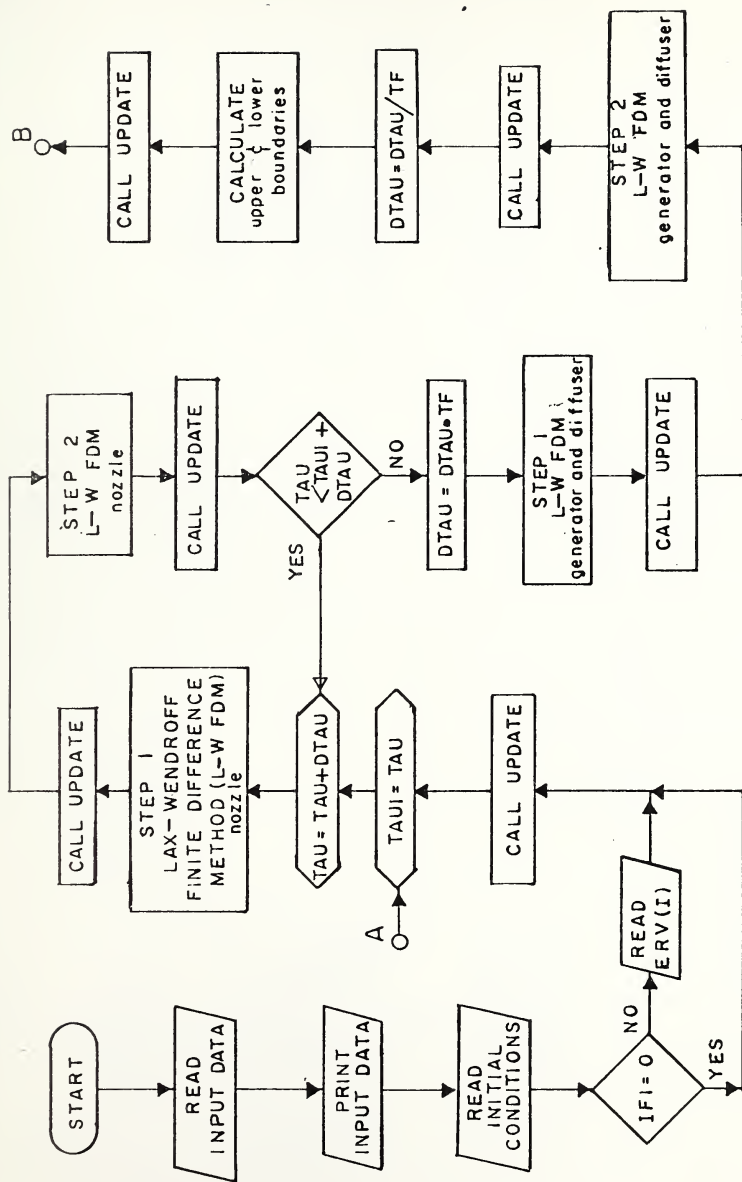
FIG. 6. INTERCONNECTION FLOW CHART — MHDTD
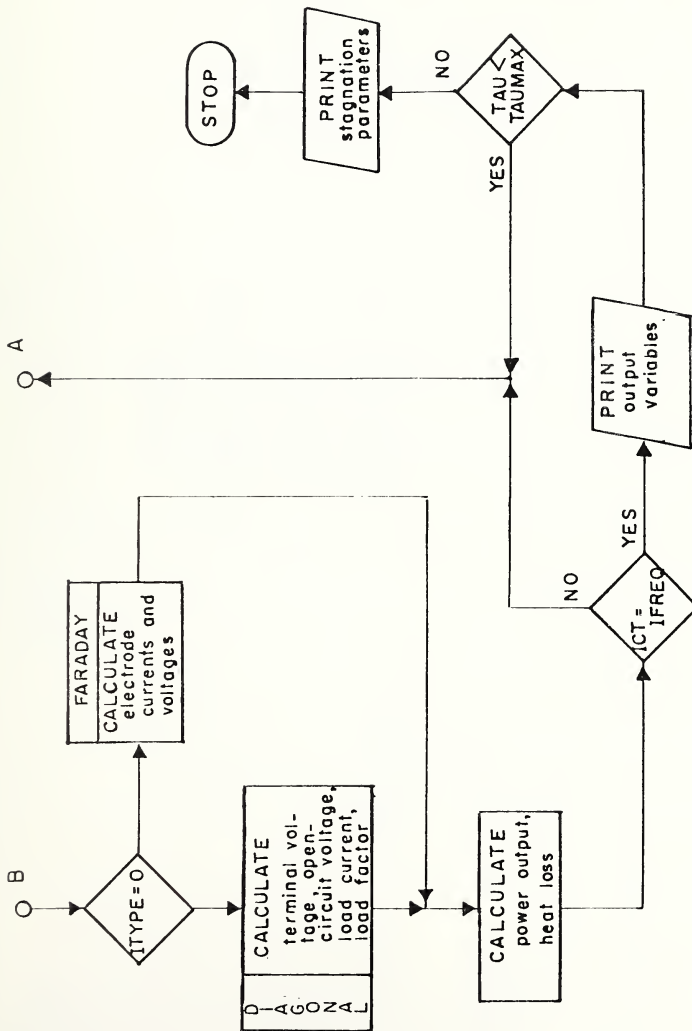
169

FIG. 7. FLOW DIAGRAM FOR MAIN PROGRAM — M H D T D
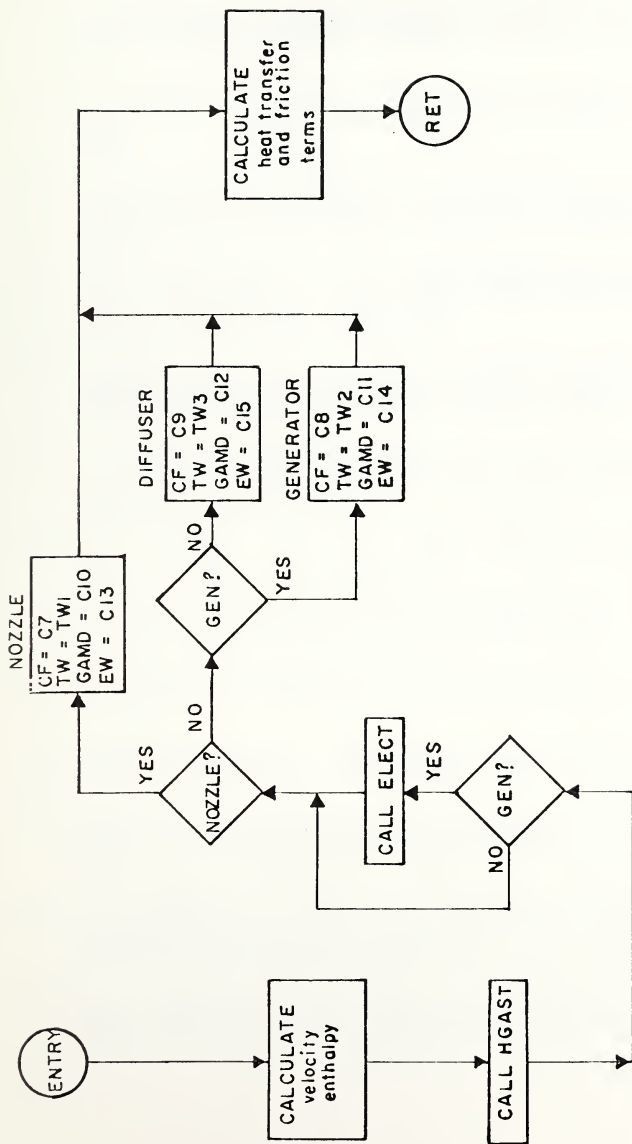
170

FIG. 7. (continuation)

171

FIG. 8. FLOW DIAGRAM — SUBROUTINE UPDATE

REFERENCES

1. T. C. Robles, <u>A Simulation Approach to a Magnetohydrodynamic/Steam Electrical Power Generation System</u>, a doctoral dissertation, Montana State University, August 1975.

2. L. S. Dzung, "Favourable Configuration of Segmented Electrodes for MHD Generators," <u>The Brown Boveri Review</u>, Vol. 53, No. 3, 1966, pp. 238-250.

3. E. A. Witalis, "Performance of a Segmented Electrode MHD Generator for Various Electrode-Insulator Length Ratio," <u>Plasma Physics</u>, <u>Journal of Nuclear Energy</u>, Part C, Vol. 7, 1965, pp. 235-244.

4. J. G. Knudsen and D. L. Katz, <u>Fluid Dynamics and Heat Transfer</u>, Research Bulletin No. 37, September, 1953, Engineering Research Institute, University of Michigan.

5. J. Teno, C. Liu and T. R. Brogan, "Boundary Layers in MHD Generators," <u>10th Symposium on the Engineering Aspects of MHD</u>, <u>Proceedings</u>, MIT, Cambridge, Massachusetts, March 1969, pp. 15-22.

6. D. R. Bartz, "Turbulent Boundary Layer Heat Transfer from Rapidly Accelerating Flow of Rocket Combustion Gas and of Heated Air," <u>Advances in Heat Transfer</u>, Vol. 2, Academic Press, New York.

7. T. C. Tsu, W. E. Young and S. Way, "Optimization Studies of MHD Steam Plants," <u>Electricity from MHD</u>, Vol. 3, 1966, pp. 899-910.

8. P. Lax and B. Wendroff, "System of Conservation Laws," <u>Communications in Pure and Applied Mathematics</u>, Vol. 13, 1960, p. 217.

9. P. J. Roache, <u>Computational Fluid Dynamics</u>, Hermoza Press, 1972, pp. 228-230.

10. F. K. Courant and H. Lewey, "On the Partial Differential Equations of Mathematical Physics," <u>IBM Journal</u>, March 1967, pp. 215-234.

11. J. A. Baylis, C. Carter, M. W. E. Coney and J. B. Heywood, "Duct Physics," in <u>Open Cycle MHD Power Generation</u>, J. B. Heywood and G. J. Womack (Eds), Pergamon Press, 1969, pp. 393-462.

12. J. H. Keenan, F. G. Keyes, P. G. Hill and J. G. More, <u>Steam Tables--Thermodynamic Properties of Water Including Vapor, Liquid and Solid Mass</u>, John Wiley and Sons, New York, 1969.

13. T. C. Robles and R. M. Johnson, "A Heat Capacitor for MHD Electric Power Generation System," 16th Symposium on the Engineering Aspects of MHD, University of Pittsburgh, Pennsylvania, May 16-18, 1977.

TASK H3
Cycle Analysis and Control
D. Pierre, D. Rudberg, C. Dudding, and N. Du

ABSTRACT

Combined-cycle MHD/steam power systems are being modeled
by digital computer simulation. Methods of providing efficient
control of such systems are being investigated to insure stable
modes of response and to obtain coordinated control of many
interdependent subsystems. During the quarter, a paper[1] was
presented at the 16th Symposium on Engineering Aspects of MHD;
control system design results were presented that were obtained
from a combined-cycle simulation called System Model III. Efforts
are directed now at expanding the number of variables included
in the control system model to determine the interaction effects
of control strategies devised for particular subsystems. Primary
manipulated variables include coal-feed rate, air-feed rate,
seed rate, channel loading, steam turbine valve area, boiler
feedwater rate, and spray for superheat steam attemperation. A
subsystem of particular interest is the coal combustor. A plug-
flow combustor model having both one-stage and two-stage capa-
bility was completed during the quarter; the code for the model
was delivered to MERDI.

I. OBJECTIVE AND SCOPE OF WORK

The objectives of the MHD systems cycle analysis and control project
are twofold: 1) to provide accurate and reliable control system analysis
of the behavior of MHD topping and steam bottoming plant combinations, and
2) to establish desirable control configurations and parameters for a given
MHD generator-bottoming plant configuration, taking into account the effects
of measurement errors and input disturbances.

In open-cycle MHD systems, a bottoming plant is required to use the
considerable quantity of heat rejected when the working plasma conductivity
drops to a level unusable for MHD generation. Although many different
cycles have been proposed, systems that have MHD topping and steam bottoming
are currently the most plausible combination. Thus, research is directed
at MHD/steam combined cycles.

To meet the first objective of understanding and evaluating the com-
bined cycle mentioned above, it is necessary to computer model the MHD
generator cycle and bottoming plant in a coupled form. This includes a
high-order, state-variable characterization of the bottoming plant so that
it can be included in a model of the overall system. This equation set
contains nonlinear algebraic relations, coupled ordinary differential
equations, and also differential-difference equations. Included in the
characterization are appropriate control variables, state variables, set-
point inputs, disturbance inputs, and a physically measurable set of output
variables.

During the FY76 contract period, our most detailed simulation of such a combined-cycle plant was a dynamic power flow simulation having two major PID controllers and two feedforward control blocks. The digital computer simulation to be developed in the current contract period will expand the number of dynamically controlled variables in the system to obtain a high-order and more accurate simulation which can be used to study the effect of alternative system control strategies on the system outputs.

Several general control philosophies will be considered, ranging from basic proportional rate and reset control through state variable formulations that are extensions of standard single-input, single-output frequency domain controls to complete optimal control strategies based on quadratic cost functions. Time invariant optimal control has been used previously on a steam turbine generator plant.

The validity and usefulness of a combined-cycle dynamic simulation depends on the accuracy with which major subsystems are characterized. In particular, the detail in combustor modeling must be increased; both a high temperature equilibrium subprogram and a pulverized coal combustor simulation are to be developed on the basis of recent experimental and theoretical results. Also, the number of independent time-variable inputs to the combustor/nozzle/channel/diffuser (CNCD) subsystem must be increased; the electrical loading parameter will be included in this category. As for the bottoming plant, additional control loops will be introduced for feedwater control, superheat attemperator control, and turbine speed. To accomplish these objectives, many dynamic models for boiler-turbine combinations and related topics will be evaluated.

II. SUMMARY OF PROGRESS TO DATE

The cycle analysis and control efforts have been directed to several related areas. First, work continued on the overall combined-cycle dynamic simulation models; a paper[1] was presented at the 16th Symposium on Engineering Aspects of MHD; and design values for 16 controller parameters were obtained on the basis of the combined-cycle simulation of System Model III. A comprehensive dynamic steam-bottoming plant model is being developed for System Model IV. Investigation continued into ways of incorporating compressor control, boiler feedwater control, and superheat attemperation in the combined-cycle simulation.

Both principal investigators attended the 16th Symposium on Engineering Aspects of MHD. Contacts were made with scientific and engineering personnel from Avco, General Electric, and Westinghouse. As system components are advanced in form and are realized in hardware, these people will be consulted with regard to the control aspects of the components. Discussions were held with MHD channel modellers from MIT and Argonne National Laboratory; from these discussions, we have a better understanding of the relative accuracy of quasi one-dimensional models in comparison to the accuracy of three-dimensional models of channel phenomena. At this time, it appears that the tradeoff of added accuracy versus increased computational cost does not favor the use of three-dimensional models in establishing overall control system models for combined-cycle plants.

During this quarter, a detailed two-stage combustor model was made operational, and the source cards and code were delivered to MERDI. Updates will be delivered as they are made. The model was constructed to fill needs related to control policy generation; a large family of input-output models can be produced from this single, detailed parent combustor model, and a wide range of output variable sensitivities can be evaluated as a function of input variable variations and system parameter variations. For example, the sensitivities of combustion gas enthalpies, conductivity, or composition can be evaluated as functions of oxidant preheat temperature and composition, of coal composition, of combustor geometry, etc.

Features of the combustor model are listed below:

One-stage or two-stage operation;

Thermal inputs from about 5 Mw to 4000 Mw;

Variable geometry (lengths, diameters, seed injection point);

Variable oxidant preheat and composition, combustion pressure (1-8 atm), and stoichiometric ratios; and

Axial profiles of temperature, velocity, gas density, heat loss, char particle burnout, electrical conductivity, gas composition, and gas enthalpy.

Emissivity calculations constitute an important part of combustor modeling. In the last quarter, an accurate model of gas emissivities was developed and implemented in the overall combustor program.

III. DETAILED DESCRIPTION OF TECHNICAL PROGRESS

The model for the steam bottoming plant is being expanded from the one developed previously. In the previous model,[1,2,3] controllers were incorporated for fuel feed and turbine valve area; these controlled values influenced throttle pressure, steam flow, and electrical power output. The new control model will make use of other important physical parameters (steam temperature, feedwater flow rate, superheater pressure and temperature, and turbine speed) as feedback and feedforward signals.

The overall control model is a coordinated type with control loops for air-fuel, feedwater, superheat attemperator, and turbine valve area. To accomplish these objectives, many dynamic models for boiler-turbine and related topics have been studied and compared. In forming the combined-cycle control system simulation of System Model IV, we are deviating from the GE ECAS study[4] in the following way: In the ECAS system, the high-pressure boiler feed pump supplies high-pressure water/steam (at 4800 PSIA) to the combustor and to the MHD channel for cooling. Unfortunately, with present and foreseeably available technology, the transporting of this high-pressure fluid through the combustor cannot be accomplished while maintaining the electrical isolation of the combustor and channel at the same time. Instead, the current simulation is based on the assumption that low-pressure water direct from the condenser hot-well will be used to cool

both combustor and channel; the resulting fluid gains additional heat from the economizer and only then is pumped by the high-pressure boiler feed pump to the diffuser and radiant boiler.

The simulation of System Model IV will contain dynamic control characteristics of the air compressor and the boiler feed pumps. Static characteristics of compressors and boiler feed pumps are well-documented in engineering handbooks, but dynamic characteristics are not. The high-pressure, high-volume compressor (either centrifugal or axial) must supply air at about ten times the mass flow rate of the coal and at pressures from five to nine atmospheres. The dynamic operating range of these units is limited by surge phenomena: flow must be maintained above limiting values (typically 75 percent of design flows) in order to avoid unstable pulsating flow; therefore, the method of controlling flow is a matter of concern. In general, flow control by throttling the inlet air stream is not advisable. More reliable control is obtained by using a variable speed drive, such as an auxilliary steam turbine drive. In System Model IV, coupled dynamics of a steam turbine driving an associated air compressor will be included.

From the standpoint of reliability, large MHD plants undoubtedly will employ a bank of compressors operating in parallel. When reduced load operation is required, some of the units will be shut down and isolated from the remainder by appropriate valves. The active compressor units will be operated well above respective surge lines. Maintenance and repair work will be performed on out-of-service units without requiring plant shutdown. For the same reason, a battery of high-pressure boiler feed pumps will operate in parallel to supply the radiant boiler.

A key subsystem of System Model IV is a new input-output model of the combustor/nozzle/channel/diffuser (CNCD). This model will be produced on the basis of the latest results in coal-combustor modeling, and a quasi one-dimensional channel model will be used. Variable inputs will include fuel feed, air feed, seed feed, preheat air temperature, and channel loading parameters. Outputs will include feedwater enthalpy, exit gas enthalpy, and electrical power output. Distinct dynamic controllers will be modeled for each of the feed systems. The seed feed controller will be implemented as a ratio controller, with air feed as the basis variable. Air and coal feed controllers will be coordinated on the basis of megawatt load demand and boiler pressure.

More effort is required to extract a simplified but relatively accurate combustor model to be included in System Model IV. The available detailed combustor models will be used for this purpose. The combustor subsystem of System Model IV should be completed next quarter.

Some typical results for the combustor models are shown in Figures 1 and 2. Figure 1 shows a single stage without seed injection. (Seed injection is an operational part of the model, but it was not used in Figures 1 and 2.) The results generally are as expected, with temperature showing a broad maximum and char burnout progressing smoothly toward complete conversion. The slightly higher temperature for $\phi=.95$ also is expected.

Figure 2 shows operation of a gasifier first stage in a two-stage system. The second stage behavior is not shown. The sharp, immediate peak of the temperature curve is very arresting but has a logical explanation. At the outset, volatiles are combusted in what is, for their concentration, an oxidant providing all oxygen necessary for complete and immediate combustion. This gives the high initial temperature near 2700 K. Following the assumed instant devolatilization, char particle burnout begins and progresses rapidly while oxygen is still available, causing a still higher temperature rise. Some of the steepness of this rise is attributable to the relatively low mass of essentially non-reacting oxidant constituents (principally nitrogen and argon) which thereby require proportionally smaller heat values to raise their temperature. The effect is that for the same heat release, the moderate mass rises quickly to about 2860 K. This compares with the near stoichiometric case in which a larger mass increases more slowly in temperature. Oxygen starvation begins at the peak, and temperature falls as a result of two factors: 1) heat loss to the walls, and 2) conversion of CO_2 back to CO as more char is burned and the accompanying loss of heats of formation. These are -94.054 Kcal/g-mole for CO_2 and -26.417 Kcal/g-mole for CO, a loss of 72 percent of the heating value. Of course, this heating is regained through complete oxidation in the second stage.

Discussion with representives of Argonne National Laboratory held at the 16th Symposium on MHD in Pittsburgh revealed that they had achieved very similar results independently. They had made some different assumptions regarding devolatilization and char burnout, but it appears that gasifier temperature profiles are not highly sensitive to such assumptions. Arrangements have been made to exchange codes and to run some identical check problems on each code.

Because of the very high temperatures in MHD combustors, most of the heat lost is the result of radiation. This makes the accurate calculation of emissivities very important. In the last quarter, an accurate model of the gas emissivities was developed and implemented in the overall combustor program. The calculation of emissivity from large particles proved to be more difficult. Correlation of experimental and analytical treatments has not been good, with measured emissivities being higher than those predicted.[5] The simple model in Reference 5 is being used now. However, in the first stage of the combustor, the combustion product has such a high temperature and contains such a large amount of unburned coal particles that the emissivity is close to 1. It would be simpler, and probably as accurate, to assign the emissivity of the first stage as 1. This possibility requires further study. The second stage ideally will contain few particles, and a complete calculation will be required.

Present heat loss calculations for radiation assume an isothermal gray gas radiating to an isothermal gray enclosure. Because of the high emissivity of the gas in the first stage, these assumptions will give reasonable results even though the gas is not isothermal. Using these same assumptions for the second stage would give a larger error in total heat loss because temperature gradients in the gas are unaccounted for. At this time, the feasibility of using a more complex model for the second stage is being considered. It will account for temperature gradients in the axial direction of the combustor.

The dynamics of each component of the steam bottoming plant are governed by the conservation equations of mass, momentum, and energy.[6,7] For illustration, the lumped equations that characterize the dynamics of the economizer are as follows (symbols used are defined in Table 1):

Mass Conservation

$$\dot{\rho}_{eo} = \frac{1}{V_e} (W_{ei} - W_{eo}) \tag{1}$$

Momentum Conservation

$$\dot{P}_{eo} = P_{ei} - f_e \frac{W_{ei}^2}{\rho_{ei}} \tag{2}$$

Energy Conservation

$$\dot{h}_{eo} = \frac{1}{\rho_{eo}} [-h_{eo}\dot{\rho}_{eo} + \frac{1}{V_e} (W_{ei}h_{ei} - W_{eo}h_{eo} + Q_e)] \tag{3}$$

In addition, equations of state and of heat transfer are

$$\dot{T}_{em} = \frac{1}{W_e C_e} (Q_{ge} - Q_e) \tag{4}$$

$$Q_e = \text{constant} \cdot (W_{ei})^{0.8} (T_{em} - T_{eo}) \tag{5}$$

$$P_{steam} = P(\rho,h) \tag{6}$$

$$T_{steam} = T(\rho,h) \tag{7}$$

$$Q_{ge} = \text{constant} \cdot (W_g)^{0.6} (T_{gal} - T_{em}) \tag{8}$$

and

$$T_{ge} = T_{gal} - \frac{Q_{ge}}{C_{ge}W_g} \tag{9}$$

The heat transfer process is illustrated in Figure 3.

A more accurate model may be obtained if one divides each component into four subdivisions (see Figure 4) and applies the above equations (1 through 9) to each subdivision. Again, using the economizer as an illustration, the equation of mass conservation becomes

$$\frac{d\rho_1}{dt} = \frac{W_{ei} - W_{e1}}{V_{e1}} \tag{1-a}$$

$$\frac{d\rho_2}{dt} = \frac{W_{e1} - W_{e2}}{V_{e2}} \tag{1-b}$$

179

$$\frac{d\rho_3}{dt} = \frac{W_{e2} - W_{e3}}{V_{e3}} \tag{1-c}$$

$$\frac{d\rho_4}{dt} = \frac{W_{e3} - W_{e4}}{V_{e4}} \tag{1-d}$$

Similarly, the momentum equation is expanded to the following:

$$\dot{P}_{e1} = P_{ei} - f_{e1} \frac{(W_{e1})^2}{\rho_{ei}} \tag{2-a}$$

$$\dot{P}_{e2} = P_{e1} - f_{e2} \frac{(W_{e2})^2}{\rho_{e1}} \tag{2-b}$$

$$\dot{P}_{e3} = P_{e2} - f_{e3} \frac{(W_{e3})^2}{\rho_{e2}} \tag{2-c}$$

$$\dot{P}_{e4} = P_{e3} - f_{e4} \frac{(W_{e4})^2}{\rho_{e3}} \tag{2-d}$$

The energy conservation equation may be shown as

$$\dot{h}_{e1} = [-h_{e1}\rho_{e1} + (W_{ei}h_{ei} - W_{e1}h_{e1} + Q_{e1}) \frac{1}{V_{e1}}] \frac{1}{\rho_{e1}} \tag{3-a}$$

$$\dot{h}_{e2} = [-h_{e2}\rho_{e2} + (W_{e1}h_{e1} - W_{e2}h_{e2} + Q_{e2}) \frac{1}{V_{e2}}] \frac{1}{\rho_{e2}} \tag{3-b}$$

$$\dot{h}_{e3} = [-h_{e3}\rho_{e3} + (W_{e2}h_{e2} - W_{e3}h_{e3} + Q_{e3}) \frac{1}{V_{e3}}] \frac{1}{\rho_{e3}} \tag{3-c}$$

$$\dot{h}_{e4} = [-h_{e4}\rho_{e4} + (W_{e3}h_{e3} - W_{e4}h_{e4} + Q_{e4}) \frac{1}{V_{e4}}] \frac{1}{\rho_{e4}} \tag{3-d}$$

Equation 4 becomes

$$\dot{T}_{em1} = \frac{1}{W_{e1}C_{e1}} (Q_{ge4} - Q_{e1}) \tag{4-a}$$

$$\dot{T}_{em2} = \frac{1}{W_{e2}C_{e2}} (Q_{ge3} - Q_{e2}) \tag{4-b}$$

$$\dot{T}_{em3} = \frac{1}{W_{e3}C_{e3}} (Q_{ge2} - Q_{e3}) \tag{4-c}$$

$$\dot{T}_{em4} = \frac{1}{W_{e4}C_{e4}} (Q_{ge1} - Q_{e4}) \tag{4-d}$$

Finally, the heat transfer equation expands to

$$Q_{e1} = (\text{constant}) \ (W_{ei})^{0.8} (T_{e1} - T_{ei}) \tag{5-a}$$

$$Q_{e2} = (\text{constant}) \ (W_{ei})^{0.8} (T_{e2} - T_{e1}) \tag{5-b}$$

$$Q_{e3} = (\text{constant}) \ (W_{ei})^{0.8} (T_{e3} - T_{e2}) \tag{5-c}$$

$$Q_{e4} = (\text{constant}) \ (W_{ei})^{0.8} (T_{e4} - T_{e3}) \tag{5-d}$$

The equations for all other components are formulated in the same manner. The scheme for computer programming is to regroup the equations as follows:

* State variable equations (equations involving $\dot{\rho}_{steam}$, $\dot{h}_{steam}$, T_{steam}, etc.).

* Steam properties and air properties (equations involving T_{steam} and P_{steam} where both T and P are functions of h and ρ, and T_{air} and P_{air} where T and P are functions of h and ρ).

* Heat transfer equations (equations involving Q_{gas}, T_{gas}, Q_{steam}, and P_{steam}).

Even though System Model IV represents a significant advance over System Model III, System Model III still is being used to develop design criteria. During the past quarter, the computer code for System Model III was modified to conform to the FORTRAN of the SEL computer; simulation runs are being conducted to determine the effect that a heat capacitor[8] will have on the electrical output. Without such a unit or other control to smooth temperature fluctuations in the preheated air, a significant ripple (10 Mw peak-to-peak on a basis of 1560 Mw) occurs in the electrical output of a particular combined-cycle plant.[1] This occurs despite the fact that the loading parameter for the MHD generator is assumed to be maintained constant.

IV. CONCLUSIONS

Many components must be modeled to obtain dynamic simulation of combined-cycle power plants for system control studies. The most desirable form of such simulations is one in which the simulation produces output that correspond to measurable outputs of the actual system, and simulated control actions are based on the available outputs and command signals. During the past quarter, advances have been made in modeling key components of the overall system. A detailed two-stage combustor model was completed,

and the computer program was delivered to MERDI. Steam bottoming plant equations have been formulated. Channel design and analysis routines are ready for use in obtaining input-output models of the combustor/nozzle/channel/diffuser.

During the next quarter, improvements will be made in the heat-loss calculations and char-burnout calculations for the detailed combustor model. An input-output model of the combustor, suitable for on-line control policies, will be generated. Computer code for steam bottoming plant equations will be produced, and controller configurations for System Model IV will be established.

CONTRACT/PROJECT
CDIF Project Management Support and Related MHD Dev. Effort

CONTRACT NO. EF-77-C-01-2524

VENDOR Montana State University

FOSSIL ENERGY

77-002 SCHEDULE

Task H3 - Cycle Analysis and Control

| | YEAR MONTH | O N D J F M A M J J A S |

TASK H3

MAJOR MILESTONES AND DECISION POINTS

CONTINUE REFINEMENTS IN THE STEAM MODEL

DEVELOP A TWO-STAGE COMBUSTOR MODEL FOR THE CDIF

a. Stage 1, air-coal gasification with slag rejection

b. Stage 2, above plus added air and/or oxygen and seed

c. Plug analysis but with residence time as a function of particle size to simulate swirl

DEVELOP LONG RANGE PLAN FOR EXPANDING DYNAMICS IN COMBUSTION MODEL

STATUS DATE

SCHEDULE PLAN

PROGRESS

STATUS DATE

VARIANCE OR PROBLEM FLAG IN RIGHT COLUMN

CONTRACT/PROJECT

CDIF Project Management Support and Related MHD Dev. Effort

CONTRACT NO. EF-77-C-01-2524

VENDOR Montana State University

FOSSIL ENERGY

77-002   SCHEDULE

Task H3 - cont. Page 2

YEAR
MONTH   O N D J F M A M J J A S

TASK H3

MAJOR MILESTONES AND DECISION POINTS

EXPAND THE COMBUSTOR MODEL TO INCLUDE MULTIPLE PLUGS AND GAS DYNAMICS.

DOCUMENTATION OF CODE UNDER DEVELOP A TWO-STAGE COMBUSTOR MODEL FOR THE CDIF BY JULY 1

COMPLETE EXTENSIONS TO THE CNCD SYSTEM

EXAMINE ALTERNATIVE SYSTEM CONTROL METHODS

STATUS DATE

SCHEDULE PLAN

PROGRESS

STATUS DATE

ADMINISTRATIVELY CONFIDENTIAL

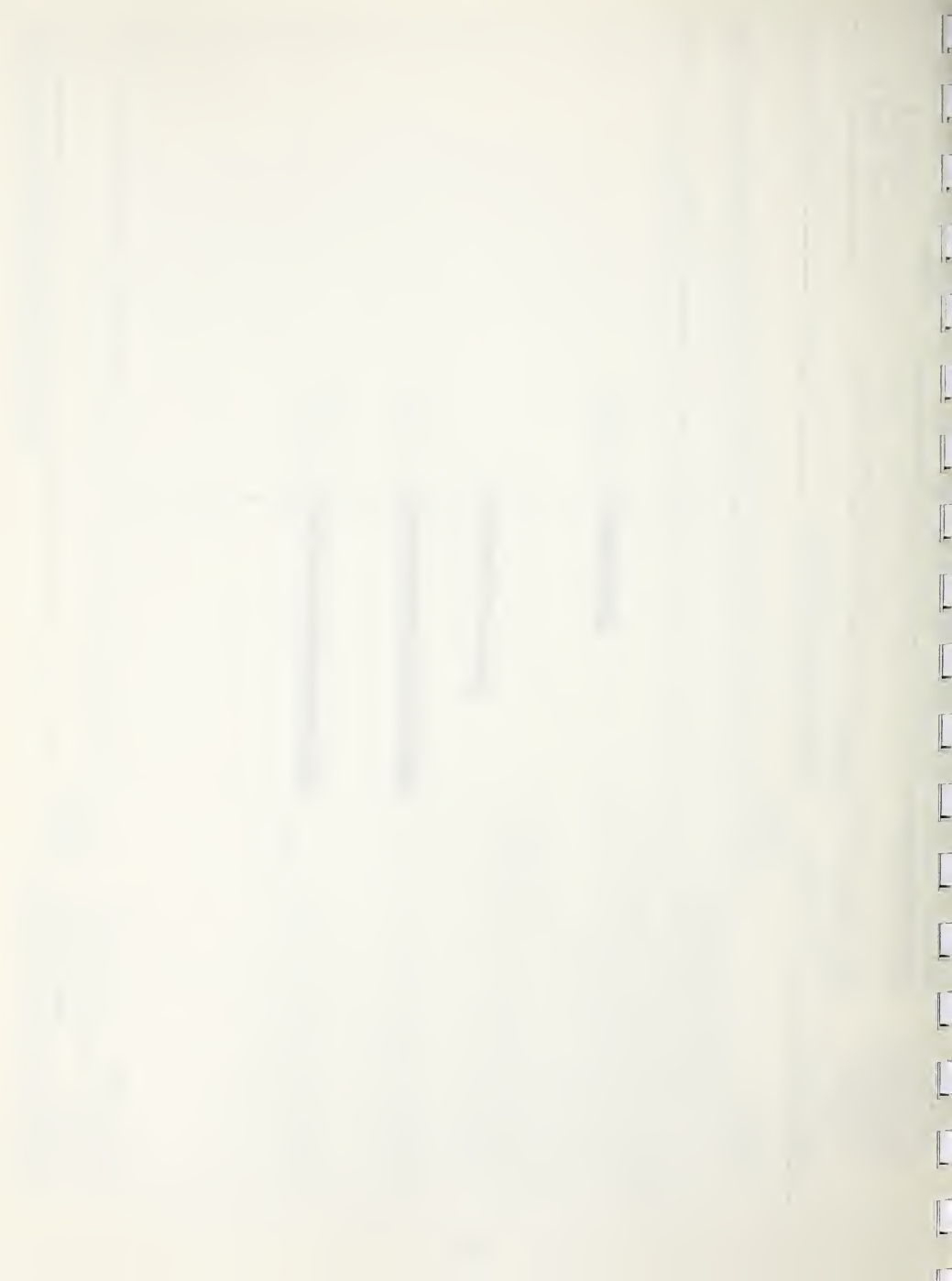VARIANCE OR PROBLEM FLAG IN RIGHT COLUMN

184

TABLE I.--Notations Used for Bottoming Plant Equations

Symbols

- h: enthalpy (Joules/Kg)
- P: pressure (Newton/m^2)
- T: temperature (K)
- W: mass flow rate (Kg/sec.)
- ρ: mass density (Kg/m^3)
- Q: heat transfer
- V: volume
- C: specific heat (Joules/Kg degree K)
- f: friction factor

Subscripts

- e: economizer
- g: gas
- i: inlet
- o: outlet
- ei: high temperature economizer inlet (steam side)
- eo: high temperature economizer exit (steam side)
- em: high temperature economizer metal
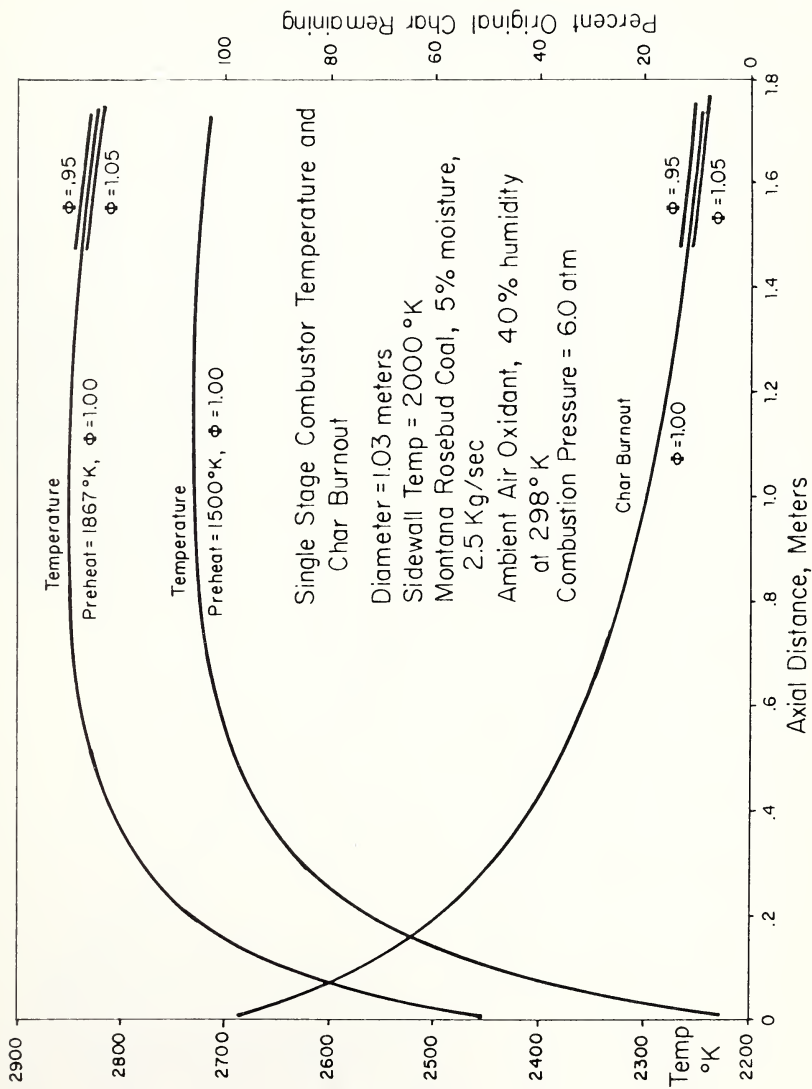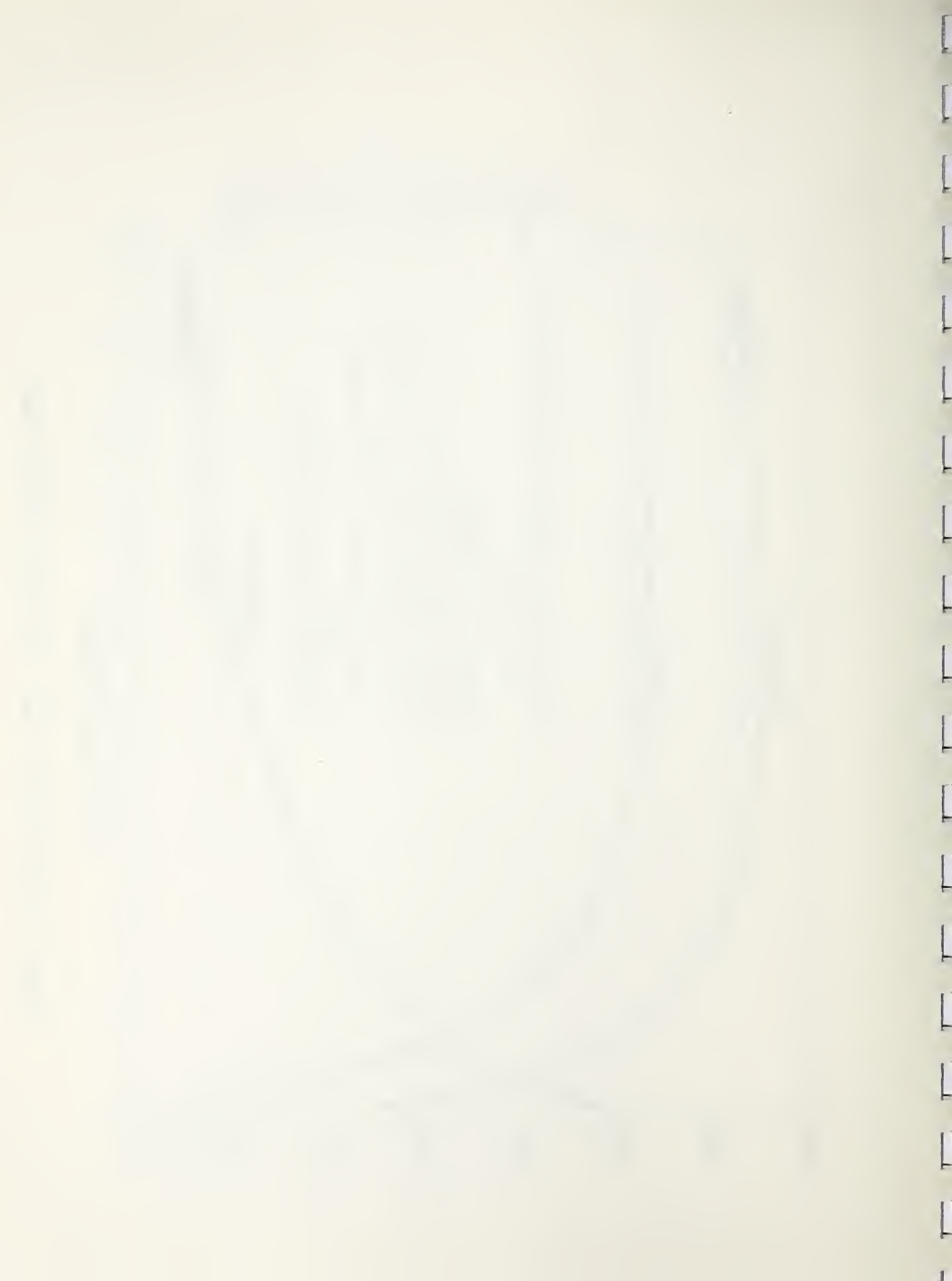- ge: high temperature economizer exit (gas side)
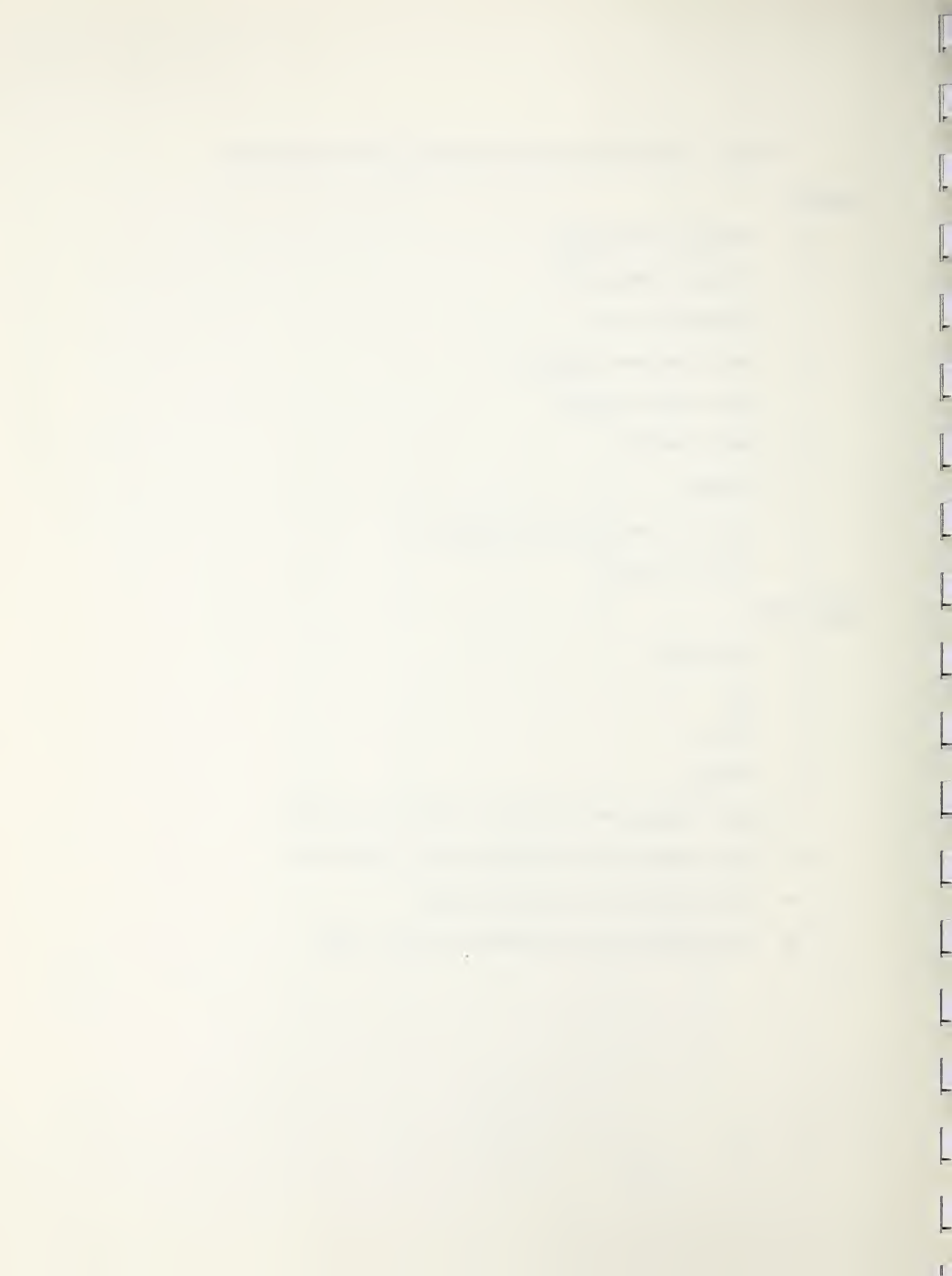
Figure 1.--Typical results from a single-stage combustor model
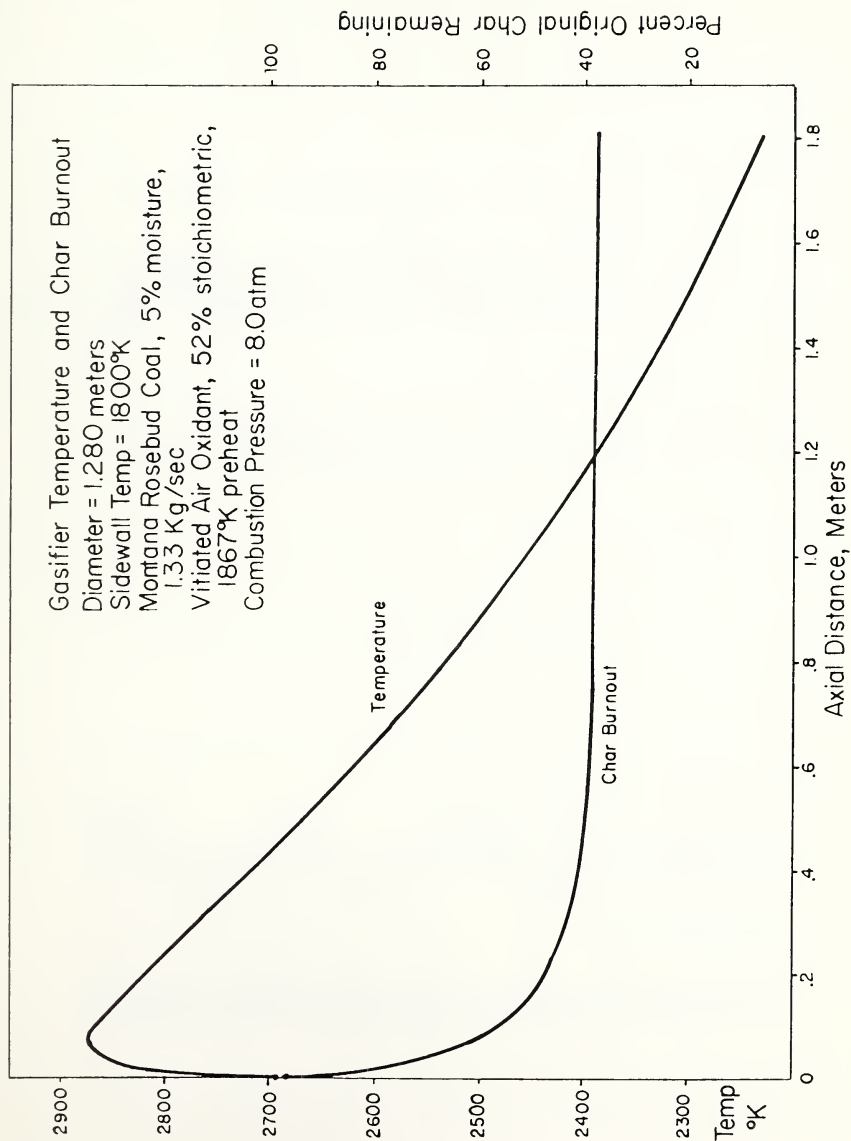
Figure 2.--Typical results from the first stage gasifier of a two-stage combustor model

Gasifier Temperature and Char Burnout
Diameter = 1.280 meters
Sidewall Temp = 1800°K
Montana Rosebud Coal, 5% moisture,
1.33 Kg/sec
Vitiated Air Oxidant, 52% stoichiometric,
1867°K preheat
Combustion Pressure = 8.0 atm

Percent Original Char Remaining

Temperature

Char Burnout

Axial Distance, Meters

Temp
°K

Figure 3.--Basis for economizer equations

Figure 4.--Lumped model for the economizer

REFERENCES

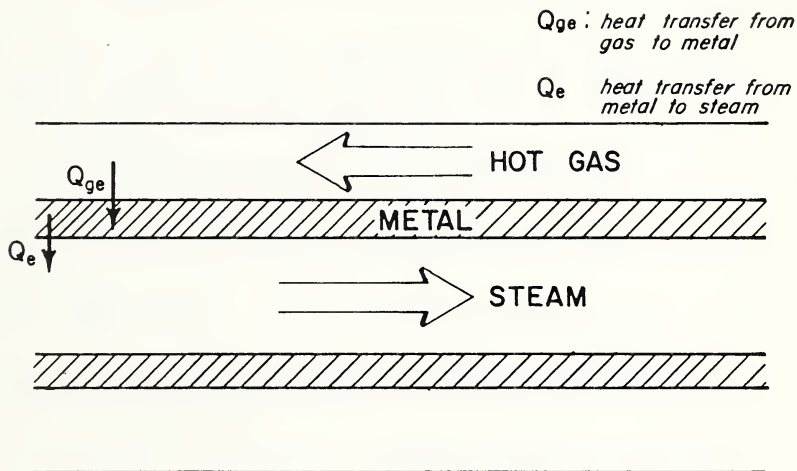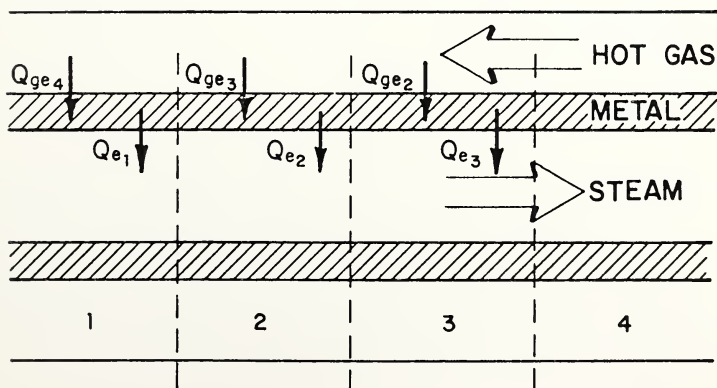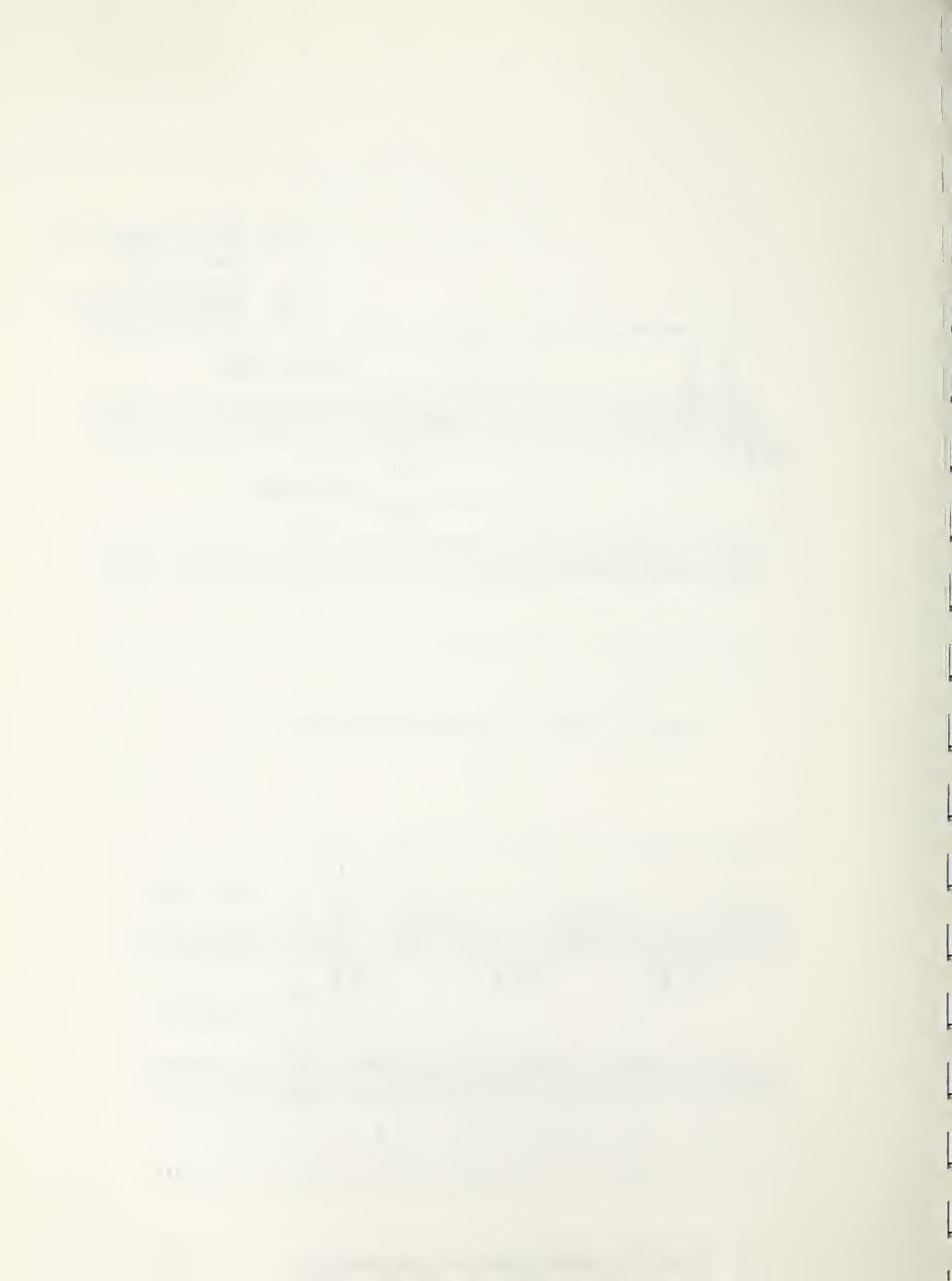1. J. Aspnes and D. A. Pierre, "Dynamic Modeling and Control of MHD/Steam Electrical Power Generating Plants," 16th Symposium on Engineering Aspects of MHD, May 1977.

2. J. Aspnes and D. A. Pierre, "Dynamic Modeling and Control of Magneto-hydrodynamic/Steam Systems," IEEE Power Engineering Society, Winter Meeting, February 1977, paper published in IEEE special publication 77CH1215-3-PWR, Energy Development III.

3. J. Aspnes, Magnetohydrodynamic/Steam System Dynamic Modeling and Control, Ph.D. Thesis, Montana State University, Bozeman, August 1976.

4. G. R. Seikel and L. P. Harris, A Summary of the ECAS MHD Power Plant Results, NASA Technical Memorandum X-73491, October 1976.

5. H. C. Hottel and A. F. Sarofim, Radiative Transfer, McGraw-Hill, New York, 1967.

6. T. C. Robles, A Simulation Approach to a Magnetohydrodynamic-Steam Electrical Power Generation System, Ph.D. Thesis, Montana State University, Bozeman, August 1975.

7. H. W. Kwan and J. H. Anderson, "A Mathematical Model of a 200 MW Boiler," Int. J. of Control, Vol. 12, June 1970, pp. 977-998.

8. T. C. Robles and R. M. Johnson, "A Heat Capacitor for MHD Electric Power Generation Systems," Proc. 16th Symposium on Engineering Aspects of MHD, May 1977.
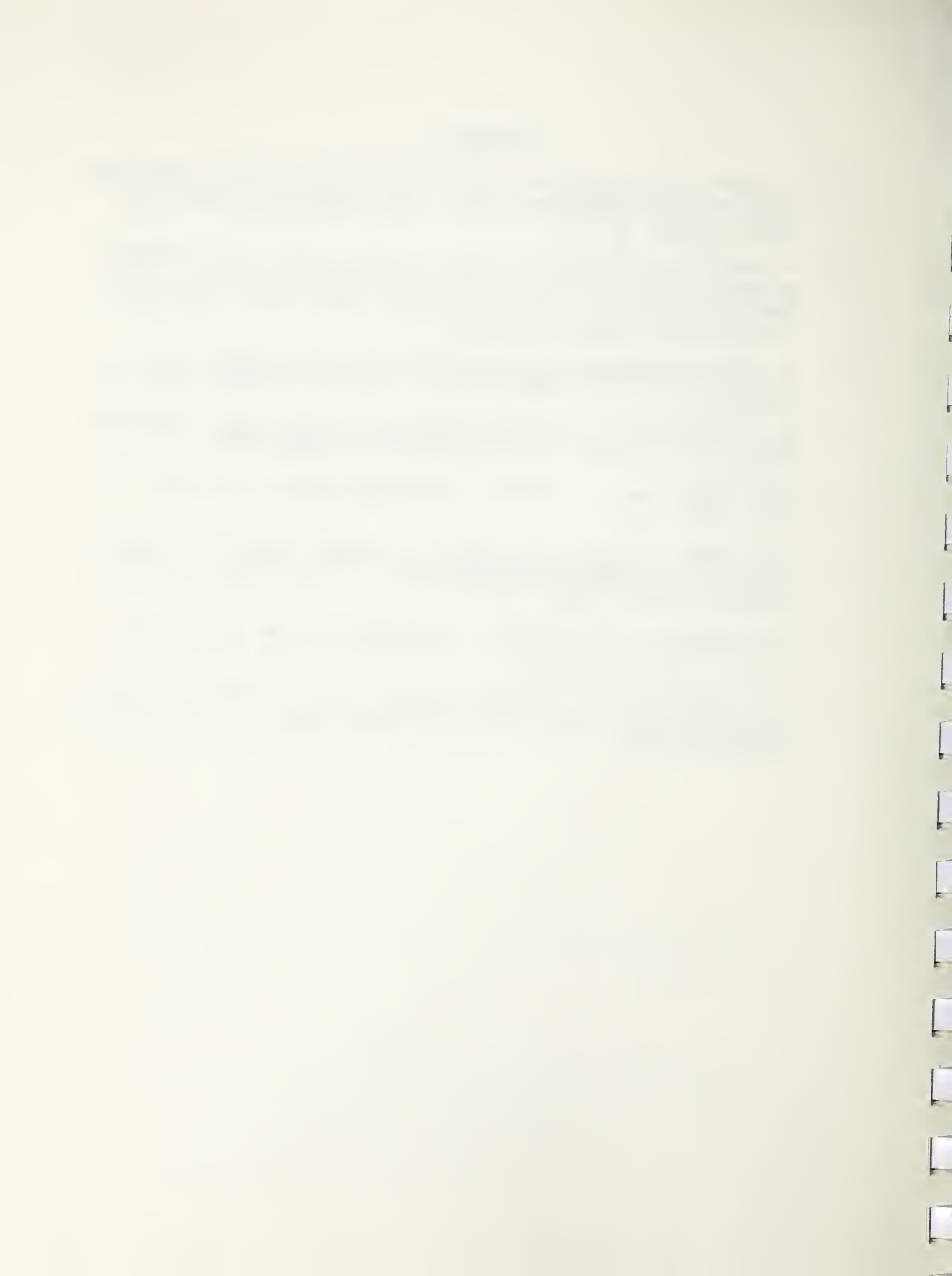
TASK M
Preliminary ETF Environmental Analysis and Site Study
D. L. Brelsford

ABSTRACT

The identification of potential power plant sites requires
the evaluation of engineering, environmental, social, and economic
attributes related to the region of interest. On this project,
a four-phase site selection process is being carried out to iden-
tify a specific site in Montana for the MHD engineering test
facility (ETF).

Based on Phase II analysis, five candidate site areas were
determined: Billings, Butte, Glasgow Air Force Base, Great
Falls, and Livingston.

I. OBJECTIVE AND SCOPE OF WORK

Public Law 93-404, Section 107, requires that ERDA construct an MHD
engineering test facility (ETF) in the state of Montana. The purpose of
this preliminary environmental impact analysis of the MHD-ETF at candidate
sites in Montana are as follows:

1. Determine what effects effluents and residuals from the MHD-ETF
    plant construction and operation may have on the ecosystem of the
    selected candidate sites;

2. Determine whether these effects may be of positive or negative
    significance at particular candidate sites; and

3. Select several specific sites for the MHD-ETF where the environ-
    mental impact effects are expected to be minimal.

A current program recently initiated by ERDA-FE-MHD is directed toward
the definition and conceptual design of a pilot-scale ETF which is a com-
bined coal-fired, open-cycle MHD steam power plant.

The overall research and development program goals of the ETF are to
1) test a combined MHD steam system on an integrated basis, 2) provide
design data for scale-up to a commercial-sized demonstration plant, 3)
evaluate component interfacing and control characteristics, endurance, and
performance and resolve critical problem areas, 4) provide basic performance
and parametric data for analytical and design improvements, and 5) define
other major problem areas requiring further development. The ETF also will
be utilized to sequentially test individual components and systems as they
become available. Thus, the ETF will include the necessary flexibility to
accommodate testing different component designs and subsystems as well as
different system configurations.
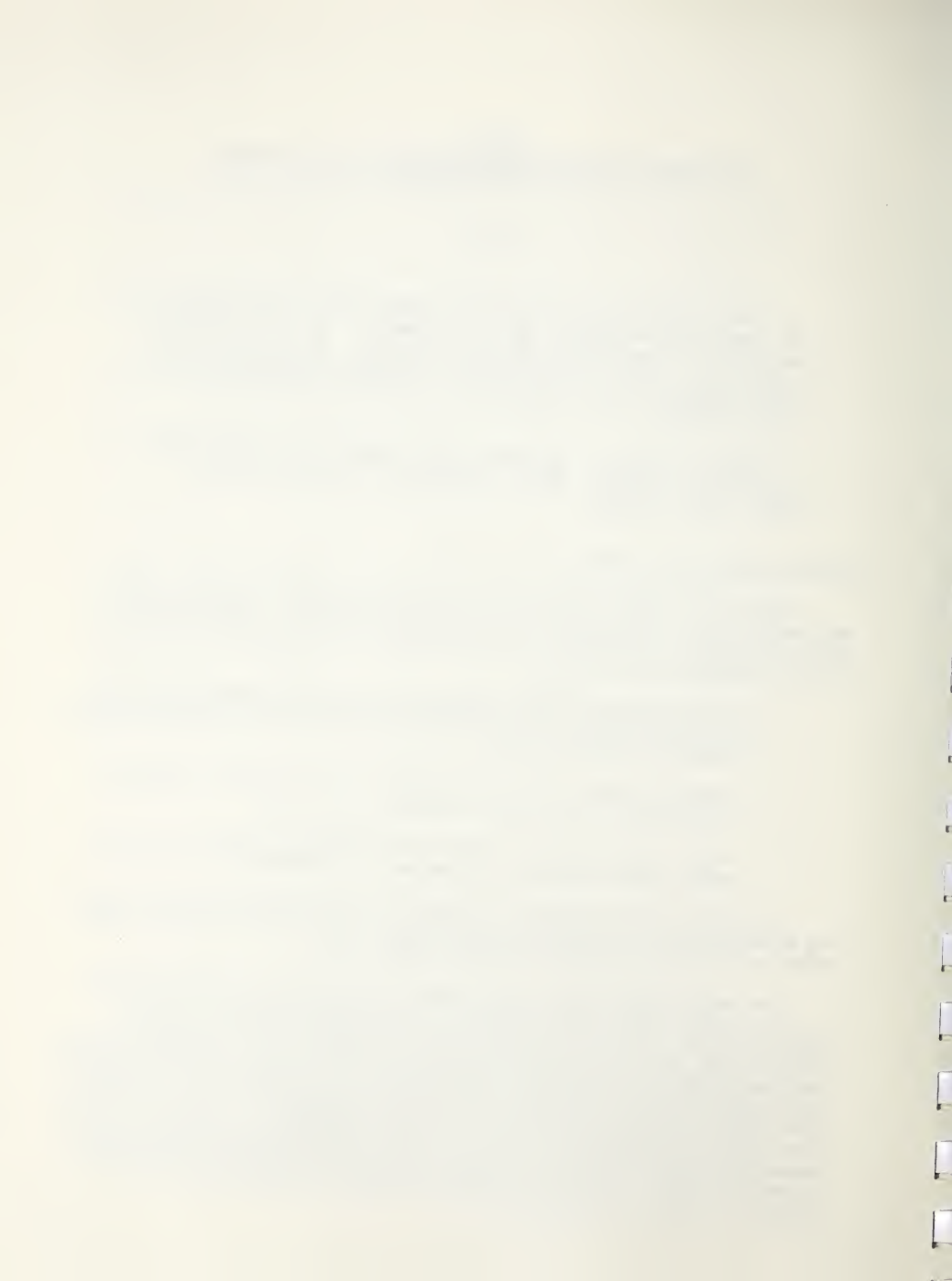
II. SUMMARY OF PROGRESS TO DATE

Phase I and the first portion of Phase II of the ETF site selection
process were completed in the second quarter of FY 77. This analysis of
the physical constraint maps yielded a total of 15 candidate site areas
(CSA) as highly suitable.

During the past quarter, the second portion of Phase II was completed.
This consisted of identifying five additional potential candidate site
areas (CSA) on the basis of the following constraints: 1) ability of the
local community to absorb the socioeconomic impact of the proposed facility
and to provide an available labor force; 2) utilization of existing ERDA or
government sites; 3) accessibility to utility networks; and 4) the acces-
sibility to transportation networks.

Completion of Phase II entailed evaluating the 20 CSA on the basis of
the most critical criteria: 1) any existing government or ERDA site would
be considered; 2) the site must be located in an area with a population
density of 15,000 within a 20-mile radius; and 3) the site must be near a
161 KV line. All CSA had available water, rail, and highway service. The
resulting documented report, Selection of Tentative MHD-ETF Candidate Site
Areas, Second Draft Interim Report, was submitted to ERDA in April 1977.

Five Montana CSA emerged for evaluation under Phase III: Billings,
Butte, Glasgow Air Force Base, Great Falls, and Livingston (Figure 1).
Initial progress was made in evaluating these CSA on the basis of 1) re-
source availability; 2) demographic and infrastructure characteristics;
3) land requirements and configurations; 4) economic cost of site develop-
ment; and 5) employment profiles.

III. DETAILED DESCRIPTION OF TECHNICAL PROGRESS

A.   Phase II--Portion II

The second portion of Phase II involved evaluating considerations not
included in the physical constraint mapping process.

A measure of the ability of local communities to absorb the socio-
economic impact of the ETF and their ability to provide ample selectivity
of the labor force had to be determined. A review of major facility siting
studies as well as testimony concerning Industrial Location Policy before
the U.S. House of Representatives Ad Hoc Subcommittee on urban growth resul-
ted in utilizing the following guideline. To minimize impact, the full-
time operational labor force should not require more than two percent of
the people available in a 20-mile radius. The range of full-time employees
for the ETF is between 500-1200 persons. The wide variation is due to lack
of information available on the design criteria for the ETF. To have a con-
servative analysis and not eliminate potential areas of lower population,
the lower figure was used. Thus, a population density of 25,000 within a
20-mile radius was required to support the ETF. Since only 1970 population
data was available, we lowered the minimum density to 15,000. Population
densities of 15,000 or more are shown in Figure 2. Areas not considered
highly suitable by the physical constraint mapping process, while providing
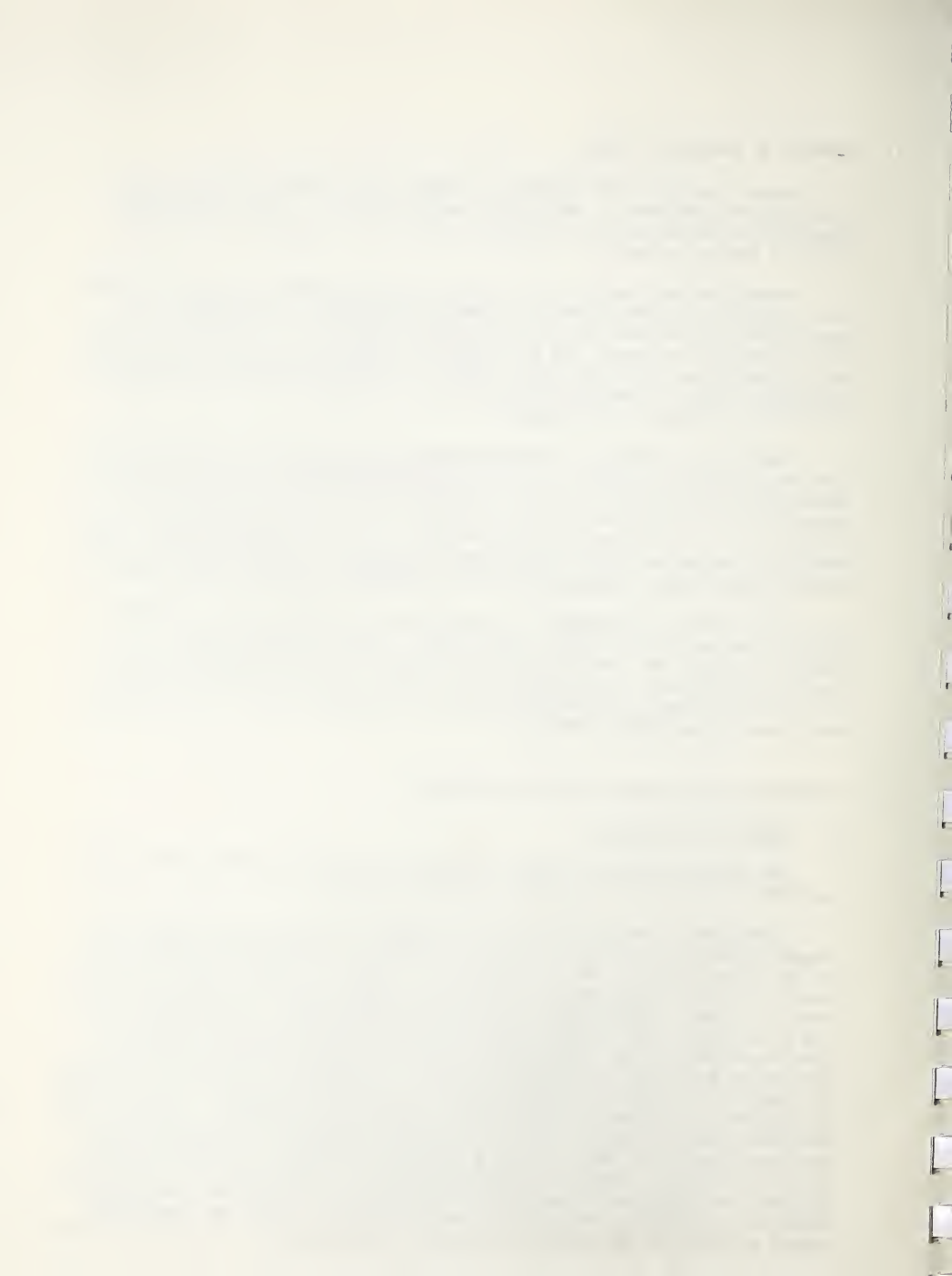
a substantial labor force or located in the vicinity of existing government or ERDA sites, thus were included for further analysis. Candidate site area inclusions were Butte, Glasgow Air Force Base, Great Falls, Livingston, and Helena.

Discussion with representatives from the Montana Power Company establsihed that the 161 KV electrical transmission line was the minimum size required to transport the output of a 250 MW_t MHD generating plant. Inquiries were made with the Montana Power Company, Montana-Dakota Utilities, and the U.S. Bureau of Reclamation to obtain maps of existing lines. The proximity of proposed CSA was noted in relation to the electrical grid system (see Figure 3).

Transportation netowrks including highways, railroads, and major airports were mapped in a similar manner. All potential CSA were serviced by both major roads and rail lines. As a secondary criteria, proximity to air service was noted (see Figure 4).

B.   Phase II--General Screening Criteria

The final screening process consisted of determining the most critical siting criteria as stated in Section II.

Existing unused facilities with the ability to provide needed support services such as housing, water and sewer systems, hospitals, schools, etc. would minimize certain environmental costs by eliminating the need for new non-renewable and renewable resources utilized in building and construction. There would be an accompanying economic advantage to utilizing such facilities; thus, the utilization of existing government sites was chosen as a major siting criteria.

In areas of stable economy based on agricultural productivity, large-scale industrial development may prove to be socially and politically disruptive to the local populas due to massive immigration of "outsiders" and large-scale population increases. Thus, it was felt that the MHD direct labor force should represent only a small portion of the existing force and that the local labor supply be able to provide a substantial portion of the construction and operational labor force of semi-skilled, skilled, and technical personnel. The population of the CSA provided a good measure of the communities' ability to withstand this socioeconomic impact and thus was selected as a decision criteria.

Within the framework of the national MHD program, a specific MHD-ETF objective is that it be designed to deliver power to an interconnected grid system while operating at conditions that are similar to base-loaded plants. In the event that the 250 MW_t ETF includes the steam electric bottoming cycle, a minimum output of 100 MW_E must be designed for. Existing Montana electrical transmission grids must be able to receive this power. Thus, the proximity to existing transmission lines was selected as the final decision criteria.

All 20 CSA were evaluated on the three above decision criteria as well as on the secondary criteria of physical constraint suitability and proximity to airline service. The results, in matrix form, are presented in
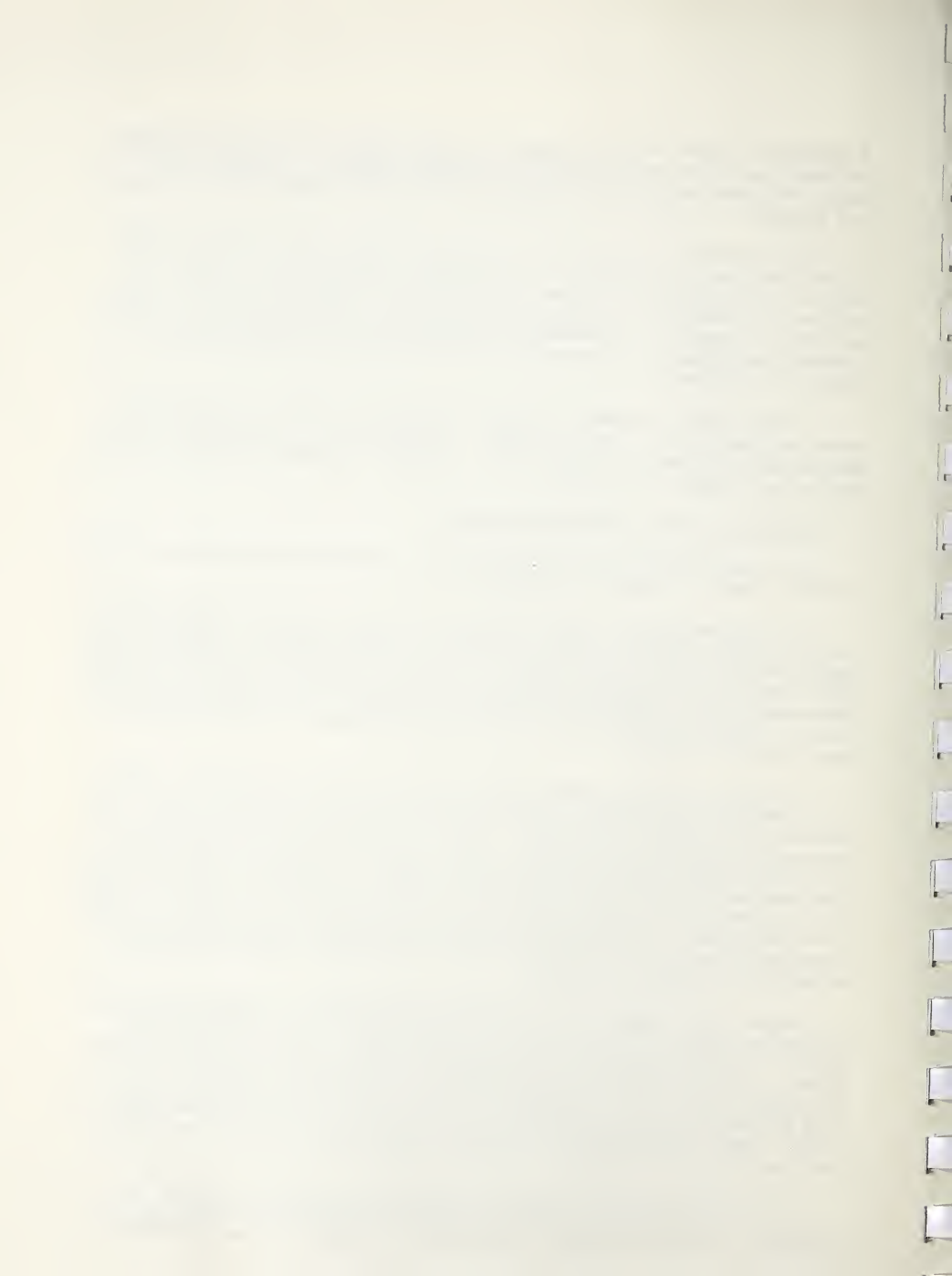
Table I. From this final Phase II analysis, five CSA were selected: 1) Billings, 2) Butte, 3) Glasgow Air Force Base, 4) Great Falls, and 5) Livingston.

C. Phase III

Considerations for Phase III analysis of the five CSA are presented in Table II. A contract to conduct consideration one, Baseline Environmental Survey, was awarded to the consulting firm of Sawyer-Waring and Associates in May 1977. Their progress report of June 30, 1977 reported completion of approximately one-third of thier effort consisting of literature reviews, map studies, and interviews with resource personnel. Field work will be conducted during the first part of next quarter, and the entire contract will be completed by August 15, 1977.

Collection of basic data by MERDI staff concerning demographic, employment, infrastructure, land use, resource availability, and economic considerations commenced in June.

D. Work Forecast

Continuation of Phase III analysis will proceed into the final quarter of FY 77. Baseline meteorological and climatological data will be collected as well as data on ambient noise levels, groundwater flow, environmental assessment of ETF impact on CSA and adjacent lands, MHD program requirements and continuity, and social acceptability. Although preliminary ETF design criteria were received in the latter part of June, specific site selection will not be made until the receipt of the final design criteria. Changes in design which significantly alter water usage, electrical output, or fuel requirements have sufficient impact on the site requirements that selection cannot be made until the final design is concurred upon.

IV. CONCLUSIONS

Pending receipt of final ETF design criteria documents, several specific candidate sites will be recommended at the completion of Phase III. An environmental impact evaluation will be initiated on each of these candidate sites under Phase IV of the siting process.

TASK ___ M

MAJOR MILESTONES

PROGRESS
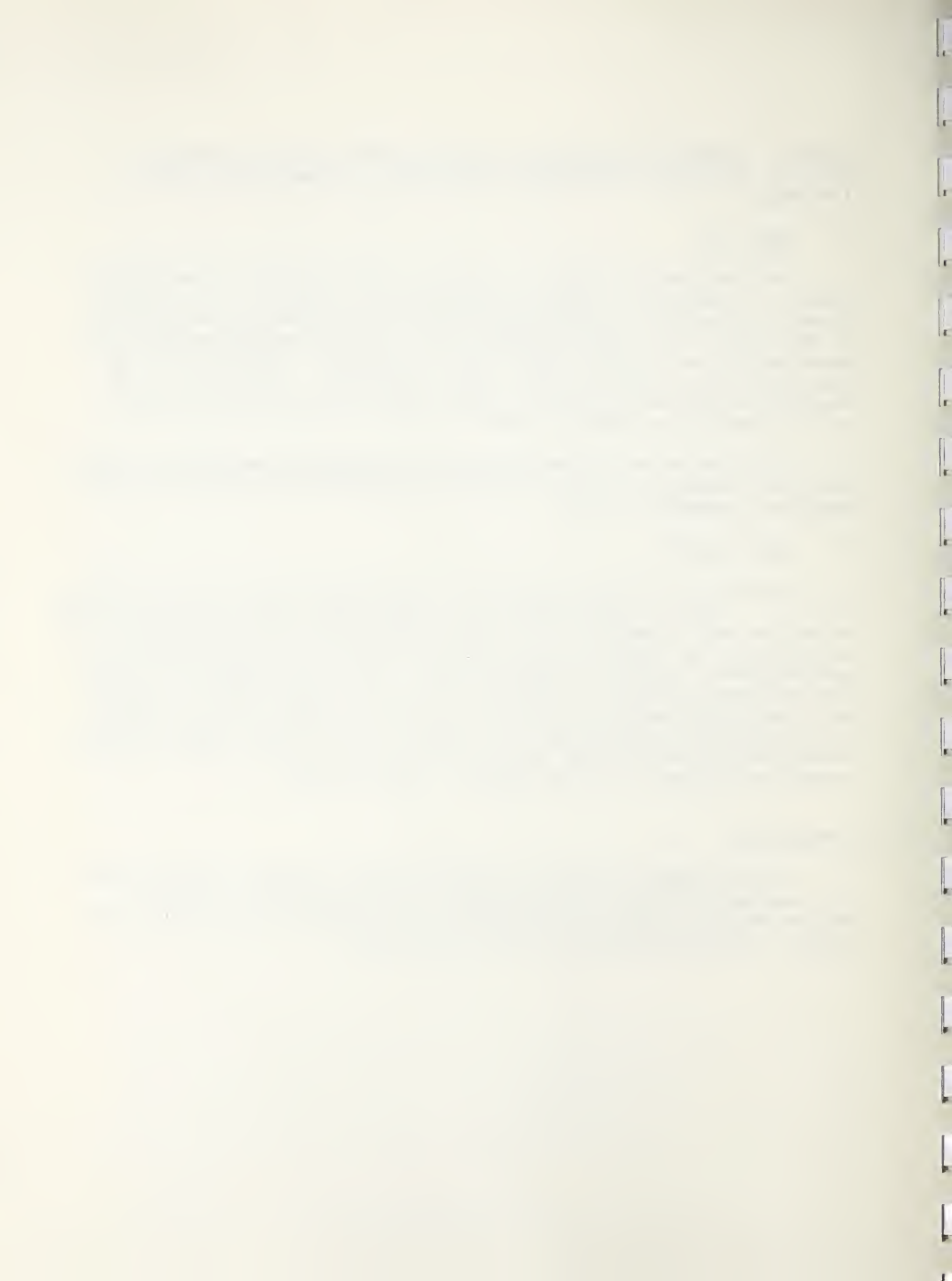
1977

O N D J F M A M J J A S

1. Determination of Search Regions

2. Identification & Evaluation of Candidate Areas

3. Identification of Candidate Site Areas

4. Evaluation of Candidate Site Areas

5. Identification of Specific Site(s)

6. Environmental Impact Analysis Plan

7. Baseline Environmental Analysis at Candidate Site Areas

8. Baseline Environmental Analysis at Specific Sites

194
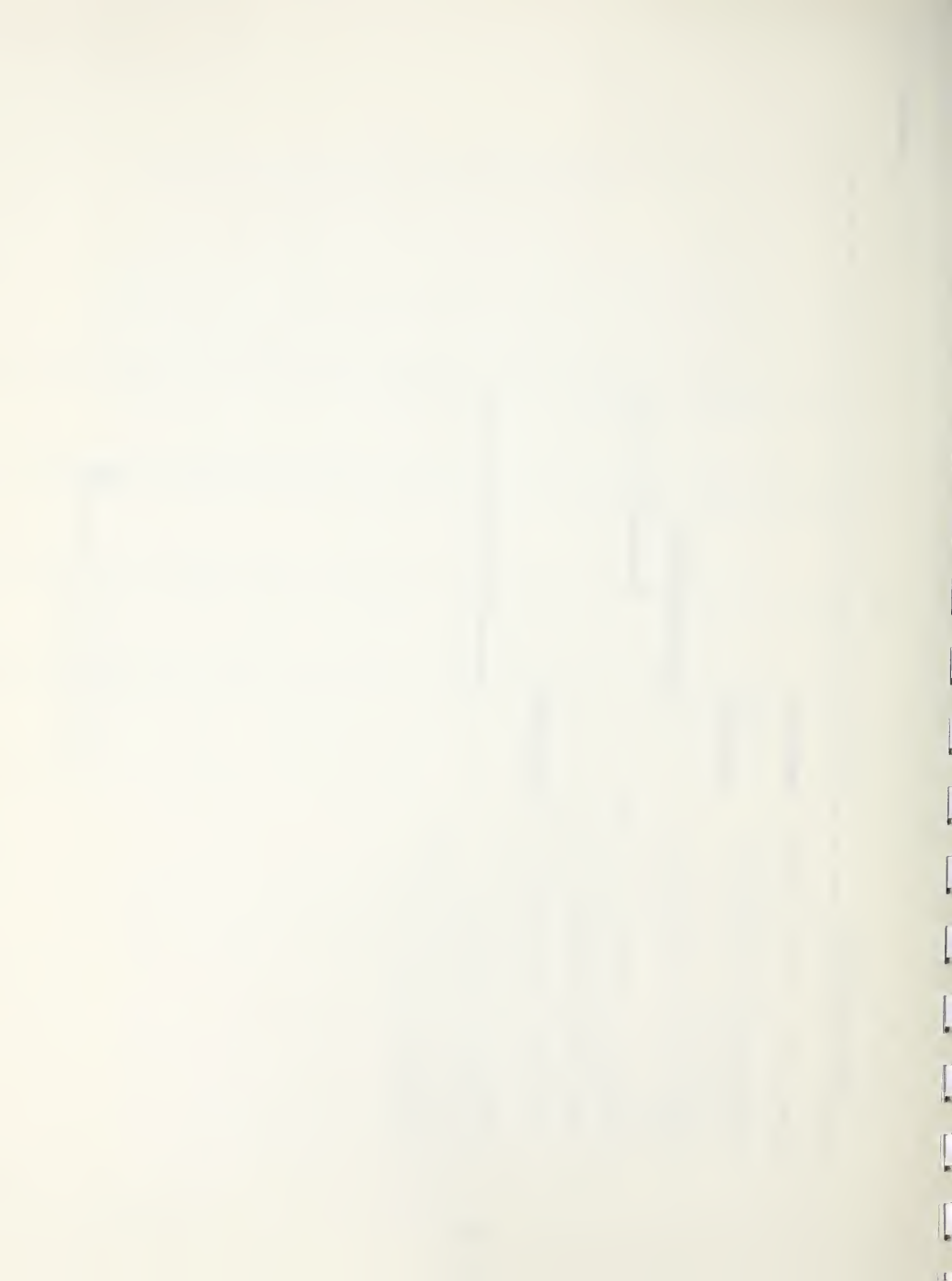
Figure 1.--Tentative Selection of MHD-ETF Candidate Site Areas

Areas With Populations of 15,000 or More
Within a 20-Mile Radius-1970 Census

MERDI, Butte, MT, E-(49-18)-1811, Task M

Figure 2 .--Map of Montana Socioeconomic Considerations

Figure 3.--Map of Montana Electrical Utilities Lines 161 KV and Larger

Figure 4.--Map of Montana Railroads and Airports

198

Table I.—General Screening Criteria

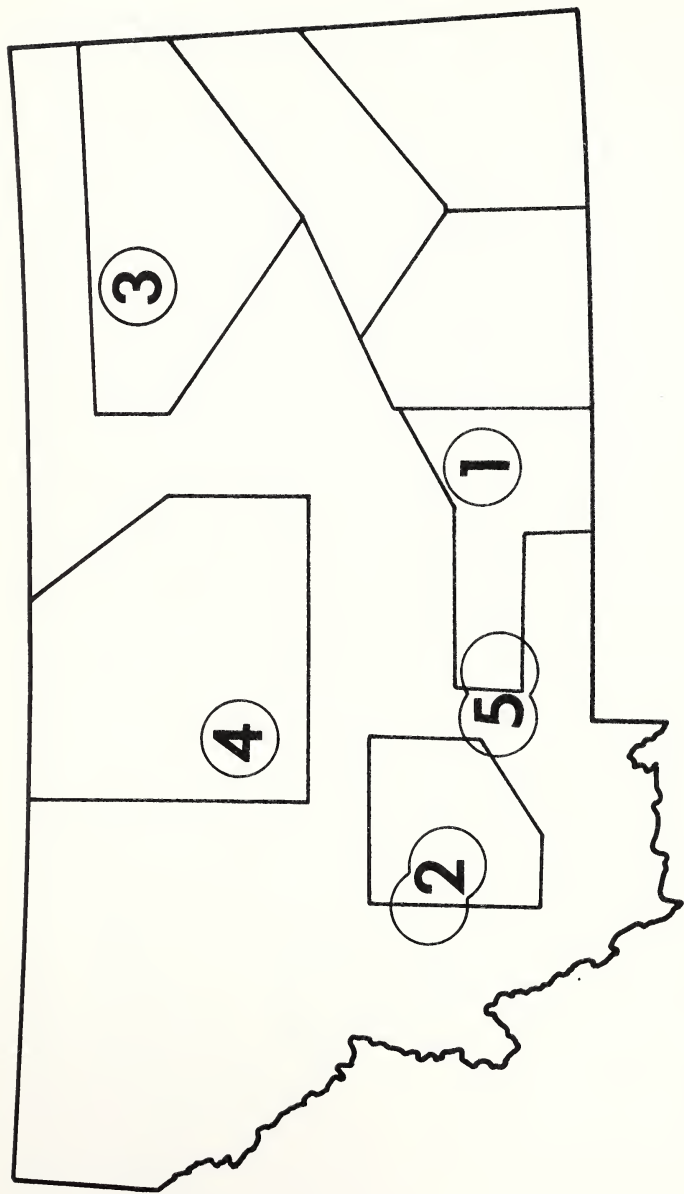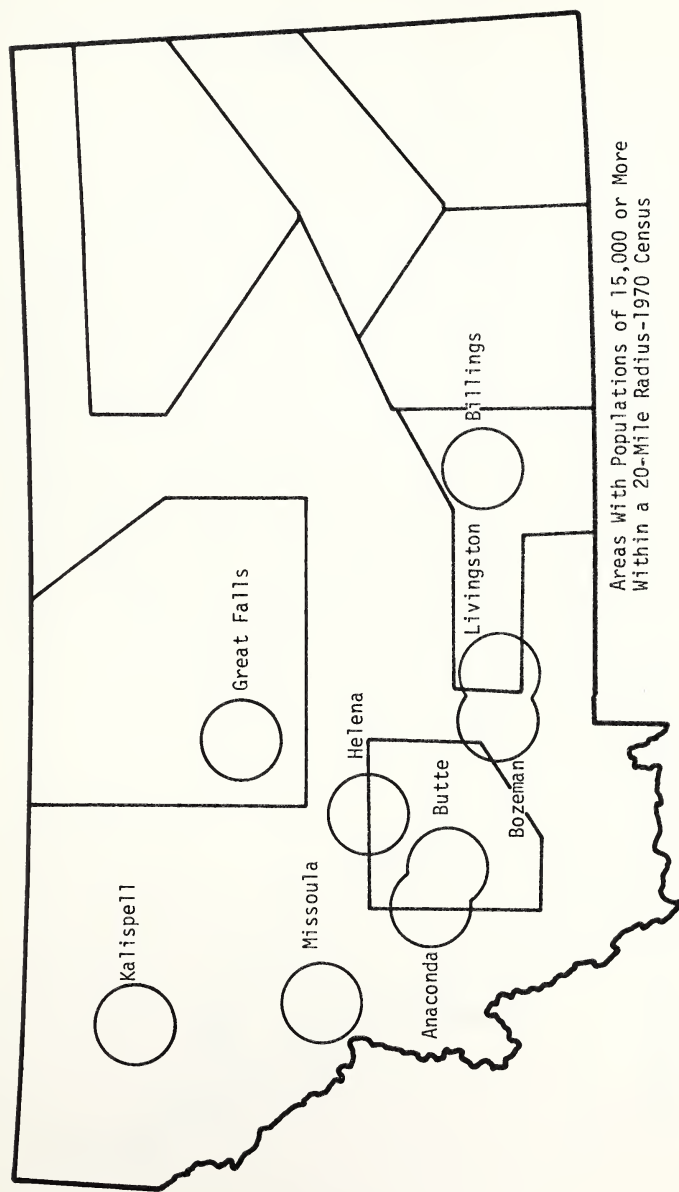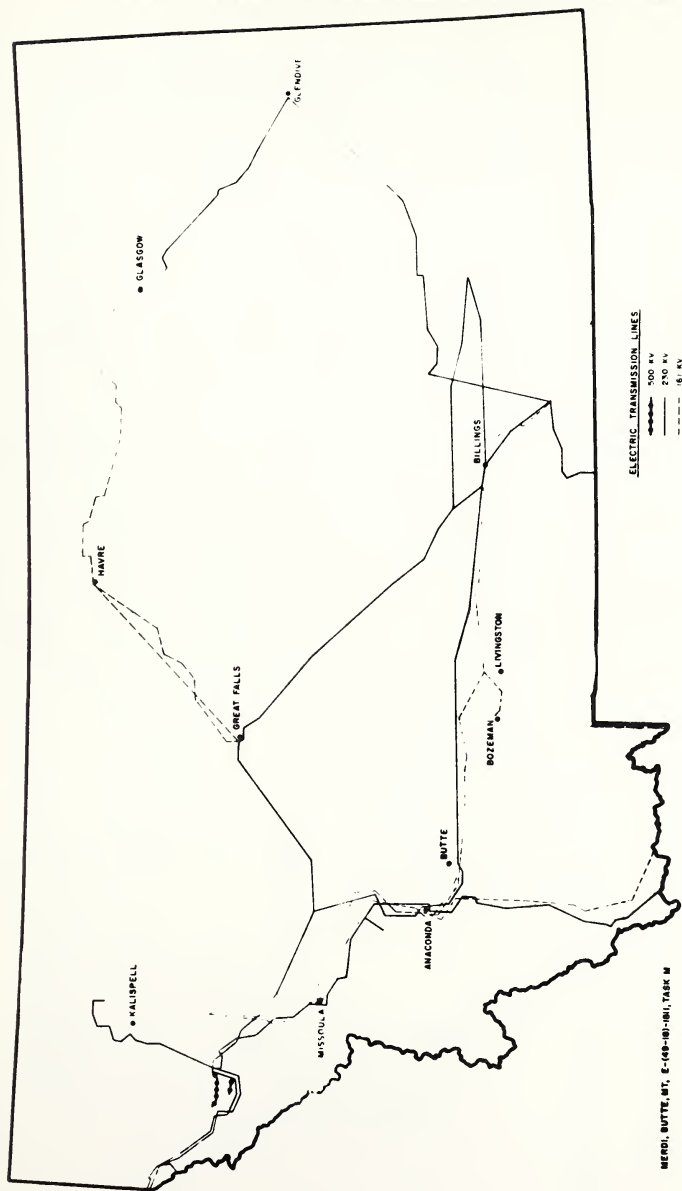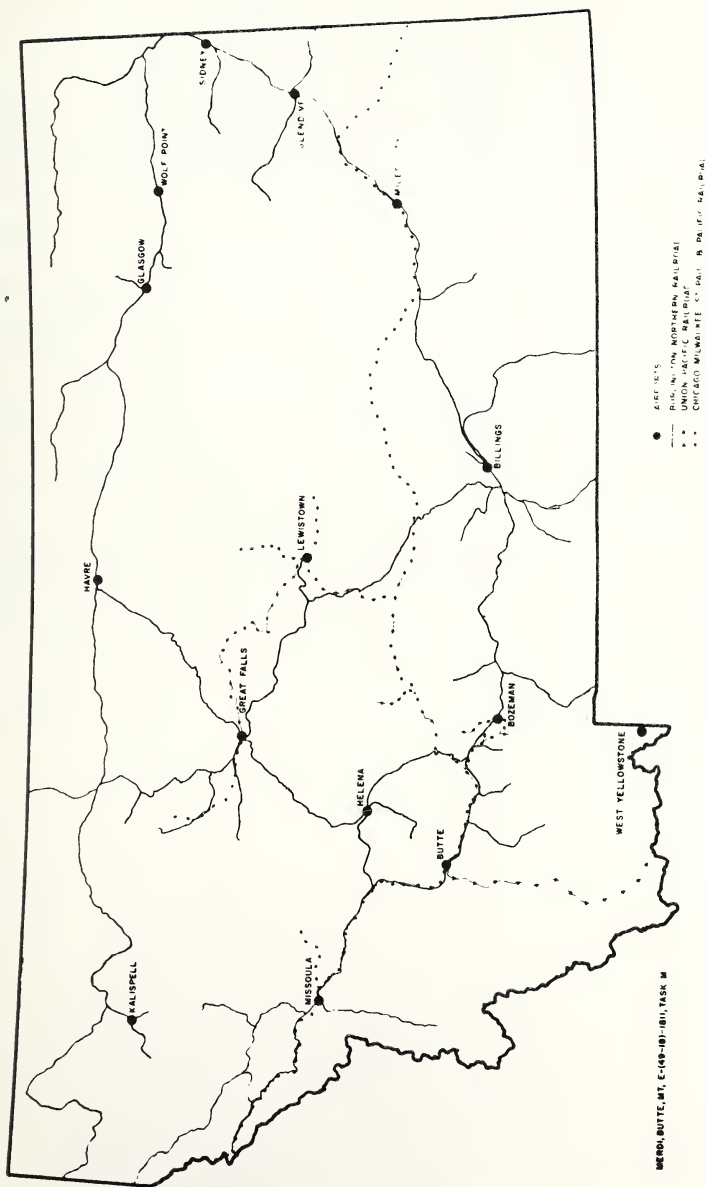| Candidate Site Area	Government or ERDA Site	Labor Force-Population base of 15,000 persons in 20 miles radius	Proximity to 161 KV Transmission Line	Suitability from Physical Constraint Maps	Water Availability	Railroad Service	Highway Service	Airport Service	1970 Population Census of Major City in Site Proximity
Ballantine			✓	✓	✓	✓	✓	20 miles Billings	350
Big Timber			NO	✓	✓	✓	✓	NO	1,592
Billings	✓	✓	✓	✓	✓	✓	✓	✓	61,581
Brockton			NO	✓	✓	✓	✓	NO	401
Butte	✓	✓	✓		✓	✓	✓	✓	23,368
Chester			NO	coal unsuitable	✓	✓	✓	NO	936
Custer			✓	✓	✓	✓	✓	NO	300
Forsyth			10 miles	✓	✓	✓	✓	NO	1,873
Fort Benton			2 miles	coal unsuitable	✓	✓	✓	NO	1,863
Glasgow Air Force Base	✓		17 miles		✓	✓	✓	8 miles Glasgow	4,700
Glendive			3 miles	✓	✓	✓	✓	✓	6,305
Great Falls	✓	✓	✓		✓	✓	✓	✓	60,091
Hardin			5 miles	✓	✓	✓	✓	NO	2,733
Helena		✓	NO		✓	✓	✓	✓	22,730
Laurel			NO	✓	✓	✓	✓	20 miles Billings	4,454
Livingston		✓	15 miles		✓	✓	✓	20 miles Bozeman	6,883
Miles City			7 miles	✓	✓	✓	✓	✓	9,023
Poplar			NO	✓	✓	✓	✓	20 miles	1,389
Sidney			NO	✓	✓	✓	✓	✓	4,543
Wolf Point			48 miles	✓	✓	✓	✓	✓	3,095

✓ Service is available.
NO Service is unavailable.
(20 miles) Service is available at specified distance.
(blank) Site does not fulfill criteria.

TABLE II.--Phase III Evaluation Criteria

1. Baseline Environmental Survey

    · wildlife
    · vegetation
    · geology
    · soils
    · hydrology/aquatic biology

2. Meteorological and Climatological Studies

    · air currents
    · background quality

3. Ambient Noise Level Studies

    · signal/noise ratio

4. Resource Availability and Costs of Fuel Feedstocks and Power

5. Statutory Requirements

6. Demography/Employment/Infrastructure

    · in-migration/out-migration
    · diversity of labor force
    · unemployment--chronic/seasonal
    · available services--hospitals, schools, housing, sewer and water
      systems, police and fire departments, and recreational facilities

7. Land Use

    · city/county zoning ordinances
    · land productivity
    · land ownership
    · existence of historical, archaeological, or cultural sites
    · existence of wilderness and primitive areas and wild rivers

8. Economic Considerations

    · property taxes
    · land acquisition costs
    · labor costs

9. Social Acceptability

    . attitudes of local interest groups
    · accumulative impact of other developments

10. MHD Program Requirements and Continuity

11. Environmental Assessment of ETF Impact on Candidate Site Areas
    and Adjacent Lands

TASK N
Materials Evaluation and Management of University and MERDI
Supporting Science and Technology
J. J. Rasmussen

ABSTRACT

The laser-flash thermal diffusivity equipment has been used to obtain thermal transport properties for a variety of materials which will provide a data base for the effective characterization of MHD materials. A detailed analysis of the heat-loss corrections required during high-temperature thermal diffusivity measurements was carried out. Recirculating water heat-exchange cooling systems are being added to the high-temperature furnaces to solve problems with uncontrolled furnace shut-downs because of plugged filters and low water pressure.

I. OBJECTIVE AND SCOPE OF WORK

The objective of Task N is to supply the technical manpower and facilities required to serve as a principal MHD materials evaluation and development capability for ERDA in conjunction with the MHD Component Development and Integration Facility (CDIF) in Butte, Montana. As directed by ERDA, this task will evaluate and develop the materials and materials' systems used in MHD power generator components including combustors, heat-exchangers, channels, electrodes and insulators, seed-recovery systems, pollution systems, and waste-disposal systems. This task also will provide the technical and administrative management of MHD supporting science and technology efforts at units of the Montana university system.

The MERDI in-house research program will include the following subtasks:

- . Selection, evaluation, and characterization of MHD materials, including testing under simulated MHD conditions;

- . Pre-and post-test analysis of MHD materials and components; and

- . Materials and specimen fabrication facilities and analytical service to assist the experimental investigators in obtaining data on well-characterized materials.

Specific activities which are being initiated to meet these objectives include the following:

- . Studies of the thermal conductivity and diffusivity of MHD materials;

- . Development and fabrication of controlled-structure MHD materials; and

- . Studies of wettability of MHD materials by slag-seed mixtures.

II.   SUMMARY OF PROGRESS TO DATE

Additional government surplus equipment has been obtained and recondi-
tioned for use in materials-characterization work at MERDI and at the univer-
sity subcontractors. Metallographic evaluation of materials has been enhanced
with the addition of in-house microscopes and additional polishing materials.

The laser-flash thermal diffusivity equipment has been used to obtain
thermal transport properties for a variety of materials. This data will pro-
vide a base for the effective characterization of MHD materials. A detailed
analysis of the heat-loss corrections required for the evaluation of high-
temperature thermal diffusivity measurements was carried out. A typical eval-
uation of alumina and alumina/barium mica composites showed that the thermal
diffusivity values were reduced about 2 percent at room temperature and 11
percent at 800°C when the heat-loss corrections were applied.

Substrate materials of high-purity, high-density alumina and magnesium
aluminate spinel have been prepared to use with the evaluation of slag wet-
tability and surface tension measurements. Representative slags being used
by other MHD investigators have been obtained also. A professor from Montana
College of Mineral Science and Technology has been hired for the summer to
initiate the experimental work on slag wettability and surface tension.

III.   DETAILED DESCRIPTION OF TECHNICAL PROGRESS

A.   Thermal Conductivity and Diffusivity of MHD Materials

During this quarter, emphasis has been placed on evaluating the thermal
transport properties of a variety of materials which will provide a data base
necessary to characterize MHD materials more effectively. At the same time,
a detailed analysis of heat-loss corrections, necessary during high-temper-
ature measurements of the thermal diffusivity by the laser-flash diffusivity
technique, was carried out.

If the thermal transport is one-dimensional and no heat-losses occur,
the thermal diffusivity (α) is calculated from the time (t_{1_2}) required for
the temperature (T) of the back-face of the disc-shaped specimen to reach
half of its maximum value (T max) from

$$\alpha = AL^2 t_{1_2} \tag{1}$$

where L is the specimen thickness and A is a dimensionless constant equal to
0.1388. When heat-losses occur, the value of A is reduced in a manner de-
scribed by Heckman[2] and others.[3] The normal procedure for determining $\alpha(T)$
consists of firing the laser at least three times at each temperature in
order to get a statistical average value for α. The heat-losses are esti-
mated at each temperature by firing one additional laser pulse and record-
ing the transient temperature change with a slower sweep time. The one-
dimensional temperature rise $(\Delta T/\Delta Tmax)$ of the back surface is compared
for times up to $10t_{1_2}$ with tabulated values given by Heckman.[2] The con-
stant A then is estimated from these tables.

Figure 1 shows a family of straight lines which gives the value of A
at different temperatures for three different materials. Basically, these
materials (all ceramic materials) can be classified as good, intermediate,

or poor thermal conductors; hence the straight lines were fit by a least squares analysis of data for materials which have room temperature values of thermal diffusivity of 0.060, 0.023 and 0.014 cm^2/sec, respectively.

The method for making heat-loss corrections has been applied successfully to an analytical study of the thermal diffusivity temperature dependence of a series of alumina/barium mica composites. These results are compared with those obtained from dense polycrystalline alumina. The data shown in Figure 2 include the heat-loss corrections. The magnitudes of the corrected thermal diffusivities are about 2 percent lower at room temperature and 11 percent lower at 800°C.

For the case reported in Figure 1 where temperature values are measured using a thermocouple, heat-loss was due primarily to radiation from the higher temperature front surface of the sample and heat conduction down the thermocouple wire itself. Another family of curves will be developed for the case when the infrared detector is used to monitor the temperature transient and only radiation losses are significant.

During the equipment check-out and heat-loss studies, the thermal diffusivity (conductivity) has been measured (calculated) from 283°k to $\sim$ 1100k for dense polycrystalline alumina, a series of Ba-mica/alumina composites, a series of heat-treated glass ceramics, and a series of microcracked $AlNbO_4$'s. These materials have been tested and the data analyzed as part of a non-MHD program; however, the results of these tests will be of significant value for the MHD characterization program. For instance, thermal transport in solid coal slag should be quite similar to that in a glass-ceramic. Arrangements have been made with cooperating researchers at Montana State University and Montana Tech to obtain a series of coal slags of various compositions. The thermal diffusivity data obtained at higher temperatures ($500-1200^{\circ}$C) will be correlated with thermal conductivity data obtained over a lower temperature range ($20-1000^{\circ}$C). It then should be possible to extend the thermal diffusivity measurements into the temperature range where slag softens and melts. This information is necessary for estimating thermal transport properties in slag-coated MHD components such as electrodes, insulators, channel walls, and pre-heater type refractories and thus for optimum engineering design of these components.

An experiment was conducted to determine the effect of thermocouple response time on thermal diffusivity measurements. Specifically, 3 mil and 5 mil chromel-constantan thermocouples were utilized. Theoretically, a 60-65 percent faster response time for the smaller diameter is expected. However, an analysis of Al_2O_3 ($t_{1_2} \sim$ .08 sec.) and C9606 glass ($t_{1_2} \sim$ .55 sec.) using 3 mil-and 5 mil-diameter thermocouple wires on the same sample specimen showed that the response time was only 15 percent faster on Al_2O_3 and 8 percent faster on C9606, which indicates that the smaller diameter wire should be used for greater accuracy, but that the effect is not as large as predicted.

In order to accommodate the use of smaller-diameter thermocouple wires, the sample holder in the Astro furnace was redesigned. This was accomplished by cutting it into two approximately equal interlocking halves so that the

sample may be placed on top of the lower half. This increases the accuracy of sample orientation and decreases the possibility of breaking the thermo-couple-sample bond.

In addition, a pump and heat-exchanger have been purchased this quarter to fabricate a recirculating water-cooling system for the Astro furnace. This system is presently under construction. Lack of sufficient city water pressure during the summer months and problems with algae contamination have made this modification of the cooling system necessary.

B.   MHD Materials Development and Fabrication

The materials-processing facility at MERDI is being established because of the well-known fact that the properties of most classes of engineering materials are controlled by many variables at the microstructural level such as grain size, porosity, impurities and their distribution, second-phase in-clusions, and the presence of alloying agents. Even minor changes in these variables can bring about major differences in the engineering behavior. By controlling or modifying these variables, engineering materials can be tai-lored to a wide variety of specific engineering conditions.

Tooling and equipment have been manufactured and purchased for the fabri-cation of ceramic materials having controlled microstructural variables. Parts currently can be formed by dry-pressing wafers, isostatic pressing of rods up to 6 inches long, or slip casting.

Additional equipment ordered through government surplus has arrived, and procedures have been taken to recondition it. As with all surplus equipment, considerable cleaning, adjusting, and repairing is usually necessary, and many items have been damaged in shipment. Major items of surplus equipment acquir-ed this quarter include an American Optical Company metallograph and a fume hood. The metallograph required some extensive cleaning and repairing of parts that were packed loosely and consequently had suffered much damage. The unit is now operable and working well to benefit the materials-polishing operation. Of great importance to the ceramic fabrication lab was the fume hood which only required thorough cleaning and installation. The hood is in operation.

A severe problem developed with the city water supply being used to cool the high-temperature furnace used for sample sintering. Particulate matter consistently plugged the furnace filter system very rapidly (often within 2-4 hours of operation) and endangered the safety of the furnaces. It be-came necessary to design and install an independent circulating and cooling system using a heat-exchanger in conjunction with the city water supply. The heat-exchangers have been received, and the new system is being install-ed on the high-temperature furnace and should be in operation in the near future.

The curtailment of the use of the high-temperature furnace has im-paired the scheduled progress of ceramic test parts. However, the time has been used well to install and repair the government surplus equipment. This will enable us to speed up production in the next quarter.

Progress is well underway with the fabrication of stoichiometric magnesium aluminate spinel, $MgAl_2O_4$, and magnesia-rich spinel and with tests to determine the fabrication reproducibility of high-purity, high-density alumina, Al_2O_3. The samples which are being fabricated will be used for tasks in-house at Montana College of Mineral Science and Technology and at Montana State University. The sintering schedule for the fabrication of the ceramics has been delayed because of the problems with maintaining a flow of cooling water for the high-temperature furnace.

The quality and rate of sample preparation has been improved significantly in the ceramigraphic evaluation of the fabricated test materials with the addition of the in-house microscopes and additional polishing materials.

C.   Wettability

The wettability of MHD materials by slag-seed mixtures will be determined using the sessile-drop method. In this technique, the wetting angle of small drops of slag and slag-seed mixtures on appropriate MHD materials such as electrodes, insulators, sidewalls, and preheater materials will be determined as a function of slag-seed composition and temperature. The wetting angle will be measured from photographs taken of the slag-seed meniscus. Surface tension values of the molten slag will be calculated from the shape of the meniscus which forms.

The computer program, which will be used to calculate the surface tension and wettability data, has been modified for operation on the MERDI computer system. The program has been tested to verify proper operation utilizing previously evaluated data. A mercury-on-glass sessile drop is being evaluated currently to assure that the data-collection techniques being developed will produce accurate surface tension values.

Substrate materials of high-purity, high-density alumina, stoichiometric magnesium aluminate spinel have been prepared. Slag samples, representing slag compositions being used in the MHD research at the Montana College of Mineral Science and Technology and the Montana State University, have been obtained for surface tension and wettability testing. A professor from Montana Tech will be working on Task N during the summer utilizing these materials to obtain data required for the computer evaluations.

IV.   CONCLUSIONS

None
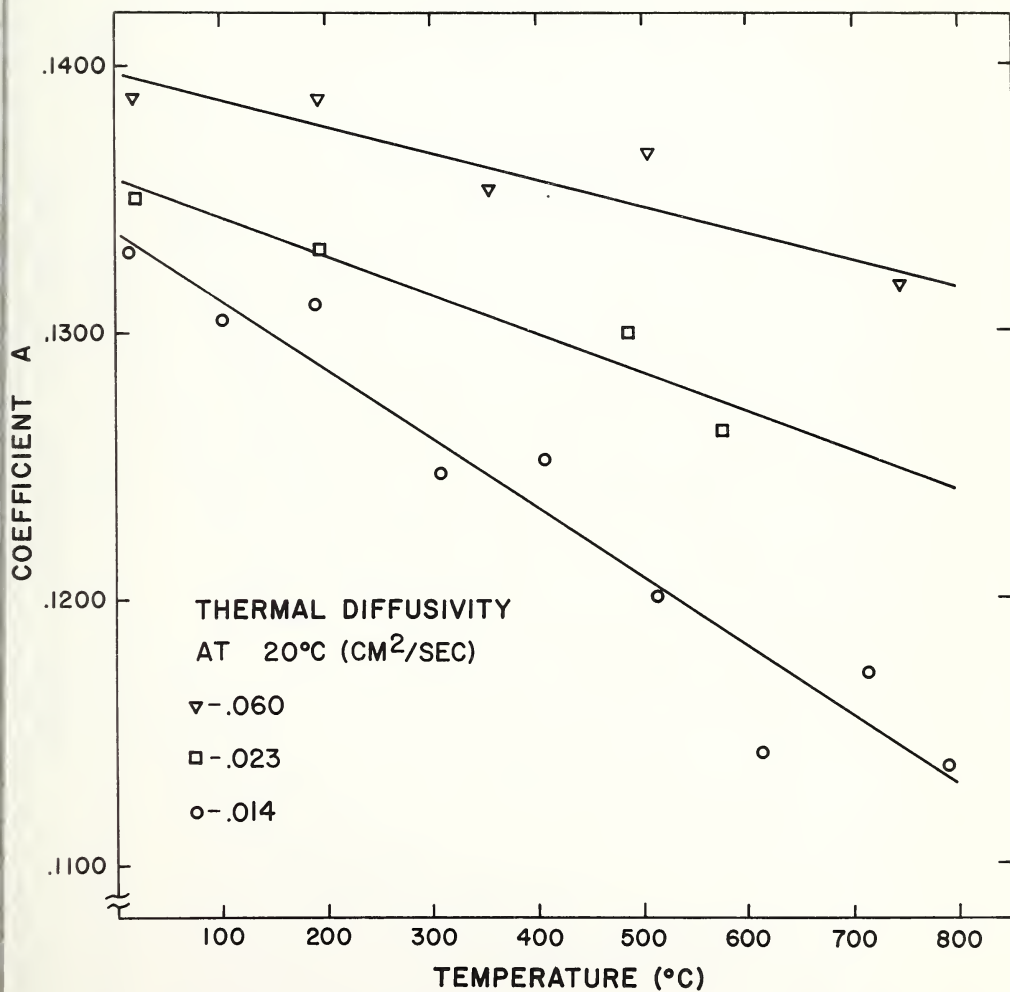
FIG. I   HEAT LOSS CORRECTIONS (THERMOCOUPLE MONITORING)
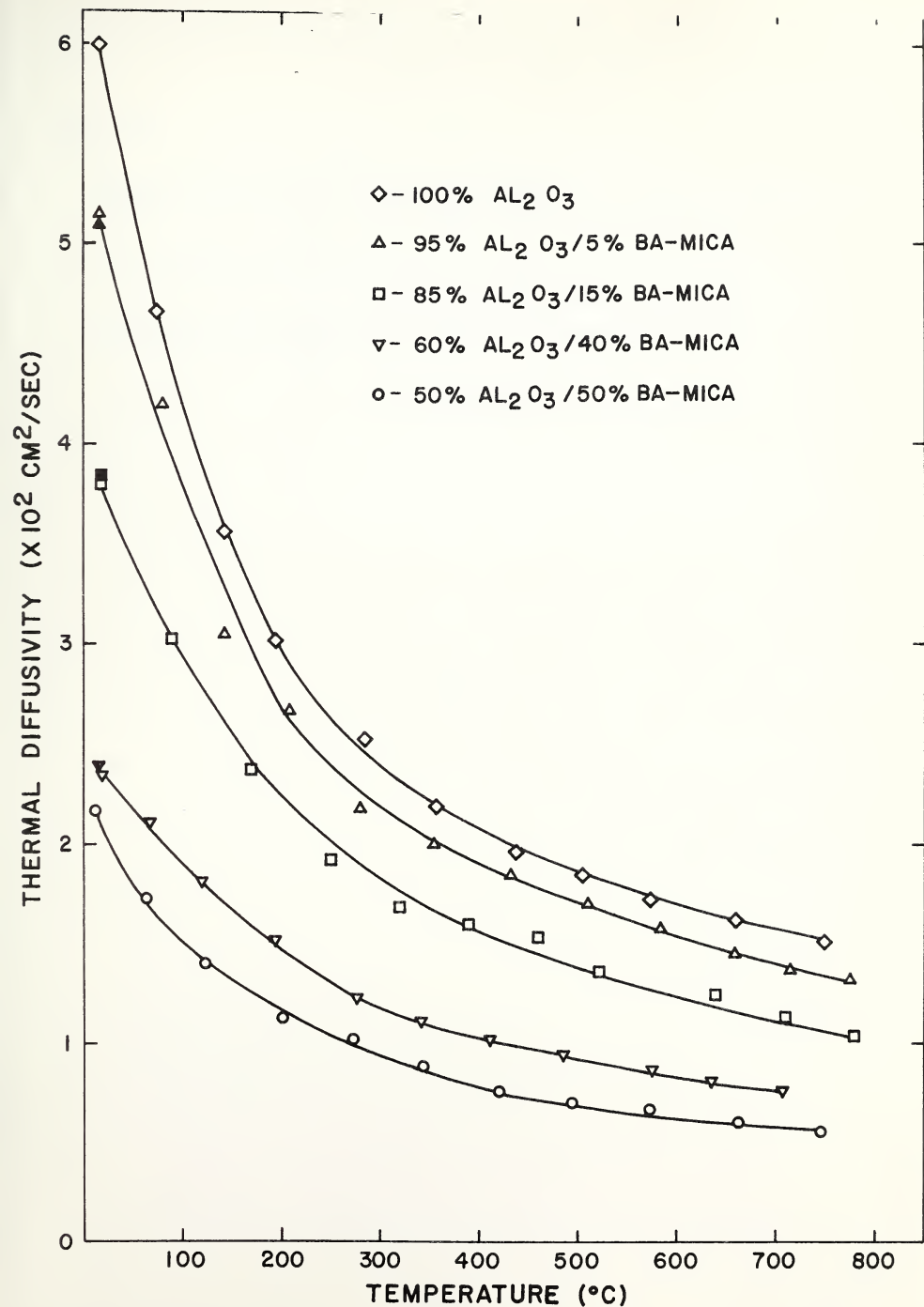
FIG. 2 THERMAL DIFFUSIVITY OF ALUMINA & ALUMINA/BA MICA COMPOSITES

References

1. W. J. Parker, R. J. Jenkins, C. P. Butler, and G. L. Abott, "Flash Method for Determining Thermal Diffusivity, Heat Capacity, and Thermal Conductivity," J. Appl. Phys., 33 (9) 1579 (1961).

2. R. C. Heckman, "Finite Pulse-Time and Heat-Loss Efforts in Pulse Thermal Diffusivity Measurements," J. Appl. Phys. 44 (4) 1455 (1973).

3. R. D. Cowan, "Pulse Method of Measuring Thermal Diffusivity at High Temperatures," J. Appl. Phys. 34 (4) 926 (1963).

CDIF Environmental Monitoring and Evaluation
D. L. Brelsford

ABSTRACT

Major milestones under Task Q are on schedule for the second
quarter. The operation of one permanent meteorological station
and two are quality stations will be about two months behind
schedule. The delay is attributable to instrument procurement
and delivery dates. Final status, however, will be completed for
work forecasts and deliverables under Task Q for FY 77.

The installation of wind and temperature sensors at 10 meters
and 40 meters on the main tower will have considerable impact in
defining the wind characteristics near the CDIF. Data from the two
   levels, together with air quality data, will be used to evaluate
the pollution potentials and environmental impacts of the Montana
MHD-CDIF.

The establishment of a meteorological/air quality station at
Terra Verde Heights will provide additional input needed to under-
stand the wind patterns in the South Butte District.

I. OBJECTIVE AND SCOPE OF WORK

The objective of this program is to ensure that the design, construction,
and operation of the MHD component development and integration facility
(CDIF) complies with the applicable environmental protection standards con-
cerning air pollution, water pollution, solid waste disposal, and noise.

In-plant environmental monitoring for air quality, noise safety, stack
gas emission, and solid/liquid waste treatment and disposal is in the
planning stage. Evaluations and recommendations will be provided to the
CDIF A and E contractors and ERDA project management as deemed appropriate.

Meteorological and air quality investigations will be performed for
the CDIF site and the surrounding area to determine the potential for air
quality degradation associated with the CDIF operation. Baseline air qual-
ity data and climatological data can be used to assess the effects of the
CDIF on the environment. Investigations will be implemented by designing
and constructing a fixed meteorological station and several air quality
monitoring stations. The system will be adequate for investigating the
impact of the engineering test facility (ETF), provided Butte is chosen as
a potential site.

II. SUMMARY OF PROGRESS TO DATE

A daily weather log (visual observations) has been pursued since the
summer of 1976. Five major sources of air pollution have been noted:

1. The Anaconda Company open pit mining operations;

2. Gilman Excavation operation approximately half a mile south-
   southeast of the pit;

3. Silver Bow County asphalt plant and rock crusher about one mile
   south of Gilman's operation;

4. The Montana Pole and Treatment Plant along the west edge of
   Butte; and

5. Transportation influences.

Analysis of the wind data obtained at the meteorological/air quality
site and the acoustic radar data was completed and submitted to ERDA in
June 1977.

Aerial infrared photography will continue of eleven control areas sur-
rounding the CDIF until September 1, 1977, inclusive. Bi-monthly fly-overs
are scheduled.

Construction of the meteorological/air quality station will begin
during the first week of July 1977. Installation of instrumentation should
coincide with delivery dates during the third week of July. Arrangements
are underway to establish the Paxson residence, Terra Verde, as the new
site of the mobile unit.

III. DETAILED DESCRIPTION OF TECHNICAL PROGRESS

A. Meteorology/Climatology

1. Daily Weather Log (Visual Observations)

The daily weather log, which was begun during the summer of 1976,
documents the existence of a haze layer embedded within the nocturnal
temperature inversion at Butte. During the year, several different
sources of pollution were noted. A seasonal dependence for some of
the sources was discovered. The major sources of pollution within the
Butte valley are listed below.

1) The Anaconda Company open pit mining operations--These
   operations are continuous throughout the year and result
   in a bluish-black haze hovering over and near the pit.
   Normally, the bluish-black haze produced by the haulage
   vehicles does not visibly extend to the CDIF area.

2) Gilman Excavation and Silver Bow County rock crushers--
   The Gilman rock crusher lies about half a mile south-
   southeast of the pit and frequently operates during summer
   and fall mornings. Little wintertime activity was seen.
   This crusher produces a visible cloud of particulates.
   Frequently, particulates from this crusher pervade the

4.   Correlation of Acoustic Radar and CDIF Wind Data

     Analysis of the wind data obtained at the CDIF Meteorological
site and the acoustic radar data was completed. A definite corre-
lation was found to exist between the temperature inversion formation
and destruction times and the character of the wind during those
periods. It was found that when no inversion formed during the night,
there was no particular wind direction or speed which consistently
occurred from one episode to the next. The wind speed and direction
reflected the general airflow pattern over the region. When a night-
time inversion did form, airflow generally was from the southwest at 2
to 3 m sec^{-1}. Prior to inversion formation after sunset, the after-
noon winds frequently were from a specific direction and often exceeded
4 m sec^{-1}. After the inversion formed, however, the wind shifted to a
southwesterly direction and decreased to a speed of 2 to 3 m sec^{-1}.
They normally remained at this speed throughout the night when an
inversion layer was present. When the nocturnal inversion was destroyed
during the morning, the wind speed normally increased from 2 to 3 m
sec^{-1} to greater than 4 m sec^{-1}, provided the general atmospheric cir-
culation was of sufficient magnitude to warrant surface wind speeds of
that strength. Frequently, a wind shift accompanied the speed increase
because the general circulation pattern no longer was decoupled from
surface airflow by the inversion's presence. The direction became
quite consistent following the destruction. During the daytime when
the convective motions were insufficient to destroy the upper portion
of the inversion, surface winds remained light. A local circulation
pattern within the valley dominated the airflow features at such times.
Frequently, wind speeds were less than 1 m sec^{-1}, and the direction
was quite variable. If the inversion happened to break during late
afternoon, the speed generally increased and the direction became
fairly consistent.

B.   Air Quality

    1.   Infrared Aerial Photography

     A total of eleven sites have been selected which will constitute
the vegetation control points for the CDIF utilizing infrared photo-
graphy. Documentation will consist of "real" color and "false" color
photographs taken from these areas approximately every two weeks
(weather permitting). The FY 77 series started May 13, 1977 and will
continue through September 1, 1977. Inclement weather and cloud
cover prevented flyovers during June 1, 1977. The selected sites are
listed below:

    a.   CDIF (looking east)

         .   Sand Creek/Little Basin Creek

    b.   East Ridge (looking east)

         .   Columbia Gardens
         .   Butte/I90 Interchange
         .   Northern Pacific Railroad Trestle

eastern portion of the valley until the nocturnal inversion is destroyed and good atmospheric mixing disperses the particulates. This plant seems to produce the greatest visual air quality deterioration when it operates. The county rock crusher lies about half a mile south of Gilman's and is much smaller. Summer and fall operations are much more intermittent but still produce a visible particulate cloud. Little winter activity was noticed.

3) A pole treatment plant at the west edge of the city--This plant operates all year and produces a yellowish-brown haze. Normally, this haze seems restricted to the western portion of the valley and was not seen at the southern portion where the CDIF is located.

4) Transportation--The effects of automobile emissions seem most pronouned during the winter. Frequently during winter, a bluish haze with a top 100m above ground at most was seen during the warmer months, possibly because during morning rush hour there was a greater degree of atmospheric mixing during warmer months than during winter when the inversion was strongest and no vertical mixing occurred during rush hour.

Other minor sources of visual pollution are no doubt present, but their contribution to the overall visual pollution at Butte is minimal. The haze layer seems worse during fall and summer mornings when all the sources are operating. During winter, the haze seems less obvious since the rock crushers do not operate at that time.

2. Aircraft Soundings

A program is continuing which was begun during August 1976 to determine the strength and height of the nocturnal temperature inversion. Aircraft soundings during this quarter (April through June) were not as frequent as those earlier in the program, mainly due to inclement weather. The frequency of inversions during April and May was less than during the fall and winter months due to the greater frequency of weather systems passing through the region. A thermocouple and digital readout system was utilized on several cases; however, radio frequency noise and static electricity in the atmosphere produced erroneous data. Various manipulations with the system to eliminate the noise have failed thus far. Therefore, data still are being collected with a mercurial thermometer placed in the cabin air vent. Results with this method are usable.

3. Acoustic Radar Data

Data continues to be collected using the acoustic radar to probe temperature inversion characteristics. During the period, numerous cases of early inversion destruction were noticed in comparison with destruction times during the fall and winter. One explanation for this may be that the general atmospheric circulation was more vigorous during the spring months than during the fall and winter months. Increased wind speeds at levels a few thousand feet above ground may be responsible for the relatively early breakup time.

c. Highlands (looking south)

            . Ueland Ranch (Little Blacktail Creek-looking east)
            . Terra Verde Heights/Chicago, Milwaukee, St. Paul, and
               Pacific Railroad
            . Girl Scout Camp

        d. West of CDIF (looking west)

            . Middle Fork Little Basin Creek

        e. North of CDIF (looking north)

            . Timber Butte
            . Mountain View Cemetery
            . Evel Knievel Residence/Country Club

Inspection of the infrared slide taken on May 13, 1977, of the
Girl Scout Camp shows an area of possible deterioration approxi-
mately 1/4 mile southeast of the camp. The typical magenta color
grades into a very light pink in the questionable area. Arrange-
ments are in progress between MERDI, the Silver Bow County Re-
source Conservation and Development Committee (RC & D), and the
Girl Scout Organization to conduct a field inspection of this area.

2. Meteorological/Air Quality Stations

        Design and specifications for the Meteorological/Air Quality
Station were completed. Approval by board members from the Montana
Tech Alumni Foundation (MTAF) and the Butte Local Development Corpor-
ation (BLDC) also were obtained regarding both the building design and
lease agreement between MERDI and the MTAF. Construction will start
during the first week of July and will be complete enough to allow
installation of instruments which are expected to arrive during the
third week of July 1977.

        Arrangements are in progress for establishing a second station
which will be located at Paxson's residence, Terra Verde. Final plans
will coincide with the completion of the meteorological station so
that a minimum of time will be lost during relocation of the mobile
unit.

3. Communication Measurements

        Western Telecomputing Corporation from Bozeman, Montana, com-
pleted a communications quality survey at eleven locations relative
to the CDIF. Density plots were made of the electro magnetic spectrum
from 10 KHz to 1000 MHz. Results from the preliminary survey support
the conclusion that the CDIF can generate a relatively large amount of
high frequency radio interference without degrading nearby communica-
tions. Distant AM radio reception, however, could be degraded because
of the presently low noise level in the AM spectrum.

4. Computer Data Base

All environmental data that has been and will be collected must be stored in an efficient and easily retrievable form for the generation of reports and for correlation of various categories of data necessary for simulation and predictive purposes. MERDI's Engineering Division will plan, design, document, and implement the environmental data base through cooperative efforts with MERDI's Computer Support Division. Implementation will begin as soon as the Data General Eclipse C-330 System is stabilized. Project format will be as follows:

a.   Define a justification for the data base;

b.   Define the general content, structure content, and structure of the data base and computer system;

c.   Perform a preliminary design of each of the computer systems giving a general description of how the data is to be collected, what type of equipment is to be used to gather and store the data, what needs to be input into the system, and what type of output can be expected from the system;

d.   Do a detailed design of each of the systems giving the structure of the system and data files, program flow charts, data flow charts, program interaction, and file interaction;

e.   Code the programs that comprise each section;

f.   Obtain concurrence from Manager, Computer Support Division;

g.   Test each program in the system;

h.   Implement the system; and

i.   Provide a user's manual for each program so that any authorized person can enter data, edit data, and generate reports as required.

Documentation will define exactly what is to be accomplished and how it is to be accomplished.

The Meteorological Data Handling System (MDHS) will be addressed first because of the preliminary work done on Montana Tech's PDP 11/70 system. Compatibility between Montana Tech's system and MERDI's system is in progress. The Air Quality Data Handling System (AQDHS) will be worked on simultaneously to the extent of designing data forms. This will enable raw data from air quality parameters to be processed for eventual computer input.

C.   Water Quality

The water quality monitoring has been assigned to the CDIF Biological Baseline Surveillance Project under the Environmental and Socioeconomic Program of ERDA-Office of Fossil Energy.

D. Work Forecast

Testing of the thermocouple-digital display system for aircraft tem-
perature soundings will continue. Until data noise elimination is accom-
plished the thermometer method presently used will be employed. Acoustic
radar data will be analyzed and compiled as it is collected. A program
to study upper level airflow within the inversion utilizing balloons
may be implemented.

The permanent meteorology/air quality station will be completed with
minimum delay as soon as instrumentation is received. Delivery is ex-
pected during the third week of July 1977. Total system checkout will be
necessary before the mobile unit can be relocated to the Paxson residence,
Terra Verde Heights.

A sample and calibration procedure manual relative to the CDIF moni-
toring program is being prepared. The analytical section will be prepared
by Mineral Research Center (MRC) personnel. Both manuals will be completed
during the fourth quarter of FY 77. Updates and/or modifications will be
introduced as new procedures are available or old ones are refined.

The meteorological/air quality data base project will be completed
during the fourth quarter of FY 77. System interaction between meteo-
rological and air quality parameters may require additional time.

An in-plant environment monitoring program will be initiated during
the last quarter of FY 77 for the CDIF facility.

CONCLUSIONS

The water quality monitoring program has been assigned to the CDIF
Biological Baseline Surveillance Project under the Environmental and Socio-
economic Program of ERDA-Office of Fossil Energy.

A computer base data work plan has been formulated and will be imple-
mented during the fourth quarter of FY 77. Documentation and a user's manual
will be provided for all meteorology and air quality data.

A user's sampling, calibrating, and analyzing procedure manual will be
provided for the CDIF Enviornmental and Evaluation Program under Task Q.
The manual will provide MERDI personnel with uniformity in sample collection
and a continuity between sampling methods, sample preparation, and sample
analysis.

Construction of the meteorological/air quality station is underway and
should be ready as instrumentation arrives during the third week of July.
Wind and temperature sensors will be located at 10 meters and 40 meters.

MAJOR MILESTONES

1977

PROGRESS

1. Collation of Existing Environmental Data

2. Operate Permanent Meteorological Station

3. Operate Mobile Air Quality Monitoring Unit

4. Operate Two Permanent Air Quality Monitoring Stations

5. Complete Plan for Total Ambient Environmental Surveillance Program (TAESP)

6. Carryout TAESP for CDIF

7. Carryout Regulatory Consultation and Liaison